

Final

Contract Report HMA-2 (TFA5)

**APPROPRIATE MODELS FOR ESTIMATING
STRESSES AND STRAINS IN ASPHALT
LAYERS**

FJ JOOSTE
JP LOURENS

PREPARED FOR

SABITA Ltd
PO Box
ROGGEBAAI
8012
Tel: +27 21 421 2577
Fax: +27 21 25 1279

PREPARED BY

CSIR Transportek
P O Box 395
PRETORIA
0001
Tel: +27 12 841 2905
Fax: +27 12 841 3232

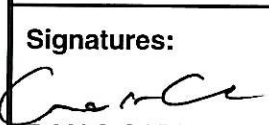



Release limitations : Privileged Document : This report, not released for publication, is furnished only for review to members or participants in the work of the "SA Hotmix Asphalt Design Programme". It is regarded as fully privileged and dissemination of the information contained herein must be approved by the Steering Committee of the SA Hotmix Asphalt Design Programme.

HMA DEVELOPMENT PROGRAMME : LIST OF REPORTS

Number	Title	Author/s	Date	CSIR Reg No
HMA-1 (TFA4)	Synthesis of construction problems	GP Rutland	June 1998	CR 99-035
HMA-2 (TFA5)	Appropriate models for estimating stresses and strains in asphalt layers	FJ Jooste JP Lourens	Sept 1998	CR 98-059
HMA-3 (TFA1)	Test methods, procedures and equipment for the determination of the effect of fillers on binder rheology and for quantifying the sorption potential of aggregates	AC Edler CM Mac Carron	Nov 1998	CR 98-074
HMA-4 (TFA1)	Test procedures for durability and stiffness quantification of bituminous binders	EJ van Assen	Nov 1998	CR 99-019
HMA-5 (TFA3)	A survey of laboratory methods for evaluating rutting and fatigue of asphalt mixes	FJ Jooste	Jan 1999	CR 98-075
HMA-6 (TFA3)	Fatigue properties of an SMA mix	S Jooste BMJA Verhaeghe A Crawford	Jan 1999	CR 99-002
HMA-7 (TFA2)	Conditioning and compaction of asphalt specimens in the laboratory : survey of recent studies	FJ Jooste BMJA Verhaeghe	Jan 1999	CR 99-006
HMA-8 (TFA2)	Conceptualisation of spatial composition	MFC van de Ven KJ Jenkins A de F Smit	Feb 1999	CR 99-059
HMA-9 (TFA2)	Effect of laboratory compaction method on dynamic properties of asphalt mixes	CJ Semmelink	Mar 1999	CR 99-022

HMA DEVELOPMENT PROGRAMME : LIST OF REPORTS

Number	Title	Author/s	Date	CSIR Reg No
HMA-1 (TFA4)	Synthesis of construction problems	GP Rutland	June 1998	CR 99-035
HMA-2 (TFA5)	Appropriate models for estimating stresses and strains in asphalt layers	FJ Jooste JP Lourens	Sept 1998	CR 98-059
HMA-3 (TFA1)	Test methods, procedures and equipment for the determination of the effect of fillers on binder rheology and for quantifying the sorption potential of aggregates	AC Edler CM Mac Carron	Nov 1998	CR 98-074
HMA-4 (TFA1)	Test procedures for durability and stiffness quantification of bituminous binders	EJ van Assen	Nov 1998	CR 99-019
HMA-5 (TFA3)	A survey of laboratory methods for evaluating rutting and fatigue of asphalt mixes	FJ Jooste	Jan 1999	CR 98-075
HMA-6 (TFA3)	Fatigue properties of an SMA mix	S Jooste BMJA Verhaeghe A Crawford	Jan 1999	CR 99-002
HMA-7 (TFA2)	Conditioning and compaction of asphalt specimens in the laboratory : survey of recent studies	FJ Jooste BMJA Verhaeghe	Jan 1999	CR 99-006
HMA-8 (TFA2)	Conceptualisation of spatial composition	MFC van de Ven KJ Jenkins A de F Smit	Feb 1999	

DOCUMENT RETRIEVAL PAGE		Report No: HMA-2 (TFA5)	
Title: Appropriate Models for Estimating Stresses and Strains in Asphalt Layers			
Authors: FJ JOOSTE and JP LOURENS			
Client: SABITA	Client Report No: CR 98-060	Date: September 1998	CSIR Registry No: CR 98-059
Project No: TRS11	OE2: Asphalt Technology		ISBN:
<p>Abstract: The study consisted of a systematic evaluation of the suitability of multi-layer elastic theory models for estimating the stress and strain response of asphalt layers. Complex response modes such as three-dimensional dynamic finite element models and viscoelastic models were used to simulate the following effects: dynamics, non-uniform tyre pressures, viscoelasticity, non-linear support effects, temperature gradients and shear forces generated on inclines. Results obtained with the more complex and accurate models were compared with the results obtained from conventional layered elastic models.</p> <p>It was found that, because of the simplifications in multi-layer elastic theory models, these models could not provide an accurate estimate of stresses and strains in asphalt layers. Neglect to take account of dynamic effects, for example, can lead to differences in excess of 50 per cent between multi-layer elastic and dynamic finite element model results. Complex models, however, are also not appropriate for use in routine mix design situations, since results can be highly sensitive to input parameters which are often unknown at the mix/pavement design stage, or are too expensive to measure for rehabilitation design purposes. Absolute and accurate prediction of performance is therefore not considered to be a viable and cost-effective endeavour if it is to be rationally pursued.</p> <p>It is recommended that, for the purposes of routine mix design, a simplified rational system be developed to assist designers in designing the most cost-effective asphalt pavements. The system should be coarse and robust and should be based only on those principles which have been well-validated through research and experience.</p>			
Keywords: Asphalt, Dynamics, Non-uniform tyre pressures, Performance Prediction			
<p>Proposals for implementation: The study results will be used as part of the HMA project. Proposals for implementation will be considered after peer reviewing.</p>			
<p>Related documents (e.g. software, interim or other reports, working drawings etc): None</p>			
Signatures:			
 C MAC CARRON Language editor	 M DE BEER Technical Reviewer	 BMJA VERHAEGHE Programme Manager	 A VD MERWE Info Centre

ACKNOWLEDGEMENT

This work is sponsored by the Southern Africa Bitumen Association (SABITA) and was conducted in the SA Hotmix Asphalt Design Programme, a joint programme initiated by SA DoT, SABITA and CSIR Transportek, guided by an industry represented steering group and administered by the Pavement Management Group.

DISCLAIMER

This copy is an uncorrected draft as submitted by the research agency. A decision concerning acceptance by the Steering Committee of the SA Hotmix Asphalt (HMA) Design Programme will not be made until the document has been completely reviewed and discussed with the researchers. The opinions and views expressed in this report are those of the authors and do not necessarily represent those of the research agency, the SA Department of Transport, the Southern Africa Bitumen Association, Committee of Land Transport Officials, SA National Road Agency or of the individual organizations or persons participating or cooperating in the SA HMA Design Programme.

This report was prepared as part of the HMA development process and publication of this report does not necessarily indicate approval or endorsement by the SA HMA Design Programme or by any of the organizations or persons participating in its work, of any of the findings or recommendations inferred or specifically expressed in this report.

Neither the research agency, the SA HMA Design Programme nor any of the organizations or persons participating in its work accept any liability for the consequences of application of the findings expressed in this report.

EXECUTIVE SUMMARY

1. Introduction

Over the past decade, multi-layer linear elastic computer programs have become accepted as a key component of routine mechanistic pavement design methods. Multi-layer elastic programs offer a fast and convenient way of estimating the stresses and strains generated in pavement systems under typical wheel loads. In recent years, however, research and experience have indicated that the use of multi-layer elastic theory may not be appropriate in some design situations. In particular, there are some doubts as to the applicability of multi-layer elastic theory to take account of dynamic effects, non-uniform tyre pressure distributions, viscoelastic effects etc.

This study was therefore undertaken to systematically evaluate the suitability of conventional layered elastic theory (LET) programs for estimating the stress and strain responses in asphalt layers. The general approach followed was to investigate several effects which cannot be adequately accounted for in conventional layered elastic models. More complex response models, in which these effects could be included, were also used to evaluate responses in the asphalt layer. These responses were then compared with those which had been calculated with the simplified layered elastic model. Specific effects investigated in the study were:

- i) Effects of dynamic loading;
- ii) Effects of non-uniform tyre pressures;
- ii) Horizontal shear force effects;
- iv) Effects of non-uniform support systems;
- v) Effects of temperature and stiffness gradients in asphalt layers, and
- vi) Viscoelastic effects.

It should be noted that the results of this study cannot be viewed as a comprehensive analysis of all the above effects. Flexible pavement behaviour is often non-linear, and the relative importance of certain effects is therefore bound to vary for different values of input parameters such as stiffness, vehicle speed, layer thickness etc. Within the constraints of this project, only a limited set of structure types and input variables could be studied. However, it is believed that the input variables and pavement structures that were analysed are representative of many of the most frequently occurring situations in South Africa. The conclusions that follow are therefore regarded as valid for many pavement design situations and provide a meaningful indication of effects that can be considered as vital for an accurate representation of asphalt layer response.

2. Conclusions for Selected Effects

2.1 Dynamic Effects (influence of vehicle speed)

Analysis of dynamic effects led to the following conclusions:

Fatigue-related issues:

Static response models such as conventional layered elastic models overestimate the tensile strains in the asphalt layer by 50 per cent or more. This was found to be the case for both pavement structures and for both of the simulated vehicle speeds (20 and 80 km/h). The modelled

effects of dynamic loading on tensile strains at the bottom of the asphalt layers generally agree with published results and field measurements. *The analysis results therefore suggest that the more approximate LET model will grossly overestimate the tensile strains of asphalt layers and will therefore also tend to underestimate the fatigue life of asphalt layers if that fatigue life estimate is based on an absolute estimate of tensile strains.* The very low strains estimated by the dynamic finite element model also suggest that the mechanism which causes fatigue cracking may not be properly understood at present.

Rutting-related issues:

In the case of the rutting parameter (octahedral shear stress), large differences between static and dynamic model results were noted. The effects of dynamic loading on octahedral shear stresses are not as clear as those for tensile strains. In general, the dynamic response model predicts higher vertical stresses and lower horizontal stresses than the static model. The relative differences between the results from the static and dynamic models depend on the evaluation position. In all cases the maximum octahedral shear stress was predicted by the static LET model. This result was generally higher than the corresponding value predicted by the dynamic model. *The analysis results thus suggest that static models will tend to overestimate the rutting potential of asphalt mixes for pavement sections on which vehicle speeds are likely to exceed 20 km/h.*

It should be noted that only the effects of dynamic loading on the induced stresses and strains were investigated in the analysis of dynamic effects. Dynamic effects are also likely to play a role in determining the resistance of asphalt mixes to fatigue and rutting at a specified applied stress state. This is especially relevant in the case of rutting, where the rate of loading not only affects the applied stress, but also affects the amount of flow induced in the asphalt mix.

2.2 Non-uniform Tyre Pressure Distributions

Analysis of non-uniform tyre pressure distributions prompted the following conclusions:

Fatigue implications: The results indicate that, for thin asphalt surfacings on granular support layers, non-uniform contact stress distributions can have a significant effect on the maximum horizontal tensile strains. Conventional LET models in which a uniform, circular contact stress is assumed can underestimate the maximum horizontal tensile strain in the asphalt surfacing (differences of 100 per cent and larger were observed). The effects of contact pressure shape and distribution on horizontal tensile strains diminish with depth. Consequently the effects of non-uniform tyre pressure distributions are not as great for asphalt bases as for thin asphalt surfacings (differences were less than 10 per cent).

Implications for rutting: As expected, the analysis indicated that non-uniform contact stress distributions led to higher octahedral shear stresses than those calculated with conventional layered elastic models. The layered elastic model with a uniform circular contact stress generally underestimated the maximum octahedral shear stress in the asphalt layer by more than 20 per cent. This difference is caused partly by the shape of the load contact area, which is rectangular rather than circular.

It should be noted that the load and tyre pressure combination on which the analysis of non-uniform tyre pressures was based led to a somewhat extreme variation in contact stresses. The

effects of non-uniform tyre pressures are thus likely to decrease under smaller wheel loads and at tyre pressures that conform to manufacturers' specifications. Despite this observation, the results indicate that neglect to take account of the shape of the load contact area as well as of non-uniform tyre pressures can lead to underestimation of the rutting and fatigue potential of asphalt layers. Differences between the results obtained with different models suggest that non-uniform tyre pressure effects should be included in design calculations, or at the very least, that they warrant further investigation.

2.3 Horizontal Shear Force Effects

Analysis of the horizontal shear force effects indicates that horizontal shear forces such as those induced by heavy vehicles moving on steep inclines do not significantly affect the response parameters that are related to fatigue and rutting. Differences between results of models in which shear force effects were simulated and those in which zero horizontal shear was assumed were generally below 10 per cent. These differences are not viewed as significant if they are considered relative to random errors which may occur because of variations in support conditions, material properties etc. It should, however, be noted that, as far as rutting potential is concerned, this conclusion applies only to the stress state induced in the asphalt layer. The duration of loading, which is greater for slow moving traffic on inclines than for fast moving traffic on level surfaces, is bound to lead to an increased flow of the binder and may therefore lead to a greater potential for rutting.

2.4 Effects of Non-uniform Support Layers

Analysis of the effects of non-uniform support layers indicates that the presence of a non-uniform support layer does not have a significant effect on the critical stress and strain parameters calculated in the asphalt surface. The results suggest that the simplified LET model, which does not take into account the change in support stiffness with increasing depth and increased offset from the load, can provide a reasonably accurate estimate (i.e. within 5 per cent of the more rigorous FE solution) of the most critical stress and strain parameters, *provided that the support stiffness is representative of the average stiffness of the support layer under the loaded area.*

The results indicate that, in routine pavement evaluation situations, reasonably large differences (generally in the order of 20 per cent) between the simplified LET model and the more representative finite element (FE) model can occur because of the simplifications in the backcalculation model. If the stiffness of the base varies significantly with depth, the backcalculated stiffness is likely to be lower than the average base stiffness. This means that stiffness of the immediate support (i.e. the upper base) is under-estimated, resulting in over-estimation of the tensile strains and shear stresses at the bottom of the asphalt surfacing. The practical implications of this may be a gross over-estimation of the fatigue crack potential and rutting potential of thin asphalt layers.

2.5 Effects of Temperature and Stiffness Gradients in Asphalt Layers

Analysis of the temperature gradient effects indicates that temperature variations with depth in asphalt layers do not have a significant effect on calculated stresses and strains, provided that the average temperature in the asphalt layer is representative of field conditions. Differences between stresses and strains obtained with the FE model (with subdivided asphalt layer) and those obtained with the layered elastic model (with undivided asphalt layer) are generally below 5 per cent for thin asphalt surfacings. For thick asphalt bases, however, somewhat larger differences were noted.

In general, it can be concluded from the analysis results that variations in temperature and stiffness with depth do not lead to large modelling errors. However, total neglect to take account of the fluctuation of asphalt stiffness with temperature can lead to large errors for some performance parameters. If, for example, an average asphalt stiffness obtained at 25 °C is used to represent the asphalt response for summer afternoon temperatures (when asphalt temperatures may reach 50°C or higher), differences in excess of 50 per cent may occur. In effect, this suggests that asphalt stiffness is an important input parameter and emphasises the importance of obtaining a measurement of asphalt stiffness over a range of temperatures. Most current design methods use only a single stiffness value to represent asphalt response over all seasons and temperatures. The findings of this analysis indicate that this may not be sufficient and that a cumulative damage approach in which the damage is estimated and added for different seasons may have to be considered.

2.6 Viscoelastic Effects

The overall conclusion drawn from the analysis is that viscoelastic effects are not critical for vehicle speeds of more than 20 km/h. It should be emphasized, however, that this analysis was based on only one set of assumed material parameters. Although this set of parameters is deemed to be fairly representative of material response as measured in the time domain, viscoelastic effects may become more significant for materials that exhibit a higher permanent deformation and delayed elastic response components, and also for vehicles moving at speeds of less than 20 km/h. However, in the context of the overall study reported here, and when considered relative to the effects of dynamics, non-uniform tyre pressures and random variations in stiffness, layer thickness etc., viscoelastic effects do not seem to be critical in the accurate determination of key response parameters in asphalt pavements.

3. Further Conclusions and Discussion

It was noted earlier that the analyses presented in this report were subject to limited sets of input parameters and pavement situations. In view of this, some of the conclusions noted above for certain effects can be disputed. A more rigorous and expensive study, coupled with field and laboratory measurements, may indicate that some of the effects may be more or less important than indicated by this brief study.

However, one observation that cannot be disputed is that conventional layered elastic theory cannot provide an accurate estimate of stresses and strains in asphalt layers in situations that involve moving traffic (with speeds greater than 20 km/h) over support systems of uncertain stiffness in which wheel loads and contact pressure distributions are not known.

Since serious consideration of the above statement is likely to have a profound influence on the manner in which asphalt pavements are designed, some qualification should perhaps be made of what is meant by "an accurate estimate of stresses and strains". Practitioners who are charged with the design of asphalt pavement frequently defend the use of layered elastic models by stating that the models are accurate enough, given the coarse and robust nature of pavement material behaviour. To evaluate this statement, consider a design situation in which the objective is to design a thin asphalt layer for an A-category road. Assume that the pavement design is as defined in Table 2.1 on page 2.2. If the design in terms of fatigue life is to be based on tensile strain at the bottom of the asphalt layer, the following results will be obtained for different modelling and actual scenarios:

1. Multi-layer Elastic Theory Model (current routine design)
Approximate maximum tensile strain: 250 microstrain (see Table 2.3 on page 2-3)
Approximate Expected Fatigue Life: **250,000 repetitions**
2. Three-Dimensional Dynamic Finite Element Model, Vehicle Speed 20 km/h
Approximate maximum tensile strain; 110 microstrain (see Table 2.3 on page 2-3)
Expected Fatigue Life: **18 million repetitions**
3. Three-Dimensional Dynamic Finite Element Model, Vehicle Speed 80 km/h
Approximate maximum tensile strain; 90 microstrain (see Table 2.3 on page 2-3)
Expected Fatigue Life: **50 million repetitions**

The expected fatigue life calculations are based on the transfer functions used in the South African mechanistic design method and include a shift factor of 2 to account for crack propagation¹⁸. Several observations follow from, or can be added to, this example:

- i) Differences between predictions made by the models are significant, even when considered in terms of pavement design classes. The three scenarios effectively lead to three different pavement design classes.
- ii) None of the three design calculations really conforms to the expected life for a thin asphalt surfacing on a proper granular support under typical South African environmental conditions.
- iii) Any of the three design calculations will be invalid if the fatigue resistance characteristics of the design mix differ significantly from the "generic" transfer function used for the design calculations. *This implies that the pavement design function may to a large extent be governed or even overridden by the mix design function.*

A statement that is often made in defence of the use of multi-layer elastic theory, is that it offers a convenient way of comparing the expected performance of different pavement designs. It is also frequently asserted that the current use of multi-layer elastic programs for the design of asphalt layers has been calibrated with field experience. However, these statements prompt the following questions:

- i) If the only valid use of multi-layer elastic theory is to compare different designs with one another, and if the approach requires a large element of field calibration, why is such a complex approach chosen in which there is uncertainty regarding many of the variables that may in fact reverse the outcome of the comparison?
- ii) Does this use of the multi-layer elastic method, coupled with the findings of this study, not indicate that the method *merely provides an erroneous quantification* of pavement design principles which are already established and which have been verified through accelerated testing (examples of such principles include: the importance of pavement balance, importance of support stiffness to asphalt layer performance, etc.)?
- iii) Is a simpler, more robust approach, such as the use of the method of equivalent thicknesses¹⁹, which can be performed on a hand-held calculator, or the DCP design method²⁰ not more pertinent and cost-effective and even more rational for use in routine asphalt pavement design situations?

A further issue that should enter this discussion is that, even for the more accurate dynamic response model, differences in the estimated tensile strains are significant for small changes in

input values (speed being the input value for the example illustrated above). If the estimation of fatigue life is based on tensile strain, then this also implies a sensitivity of fatigue life estimates to input values. This sensitivity is likely to be even greater when variations in other parameters such as layer thickness, material stiffness, load magnitude etc. are considered at the same time. This means that, for performance models based on tensile strain, the three-dimensional finite element program will also not provide an accurate estimate of design life unless the vehicle speed, layer thicknesses, material stiffnesses etc. are known.

While it is conceivable that all of these parameters may be measurable (at considerable cost) at a specific point in a road, what cannot be avoided is the variation of these parameters over a given length of road. Thus an accurate prediction of asphalt performance may be possible at a specific point in a road (if all relevant parameters are known at that point), but will vary from point to point. A comparison of the fatigue life estimates of scenarios (2) and (3) indicates to what extent such an estimate will vary. This explains why some parts of an asphalt surfacing may exhibit cracks after two years while large sections of the same road may remain intact for 12 years or more.

It is hoped that the above discussion provides enough evidence to allow the following statements to be made:

- i) The current approach to routine design of asphalt pavements using conventional layered elastic theory models cannot be expected to provide an *accurate estimate of absolute performance* of asphalt layers;
- ii) Conventional layered elastic theory models can be used to provide a qualitative assessment of pavement behaviour but their use is not necessarily the most cost-effective or even the most rational way of comparing different design situations. Simpler design methods, which contain fewer variables which can be determined with greater reliability and at reduced cost, may be more appropriate;
- iii) Precise estimates of asphalt layer responses and performance are not meaningful. In order to accommodate the full spectrum of possible values that important input parameters can take on, estimates of pavement life need to be expressed in coarse and robust terminology. Failure to do so will lead to unrealistic expectations as far as the pavement design function of asphalt design is concerned.

4. Recommendations

It should be clear from the above discussion that a new approach to the pavement design function of asphalt mix design is needed. In essence, there are two possibilities: (i) a more complex and accurate response model has to be developed for use in routine design situations; or (ii) a robust, simplified and more rational approach to the pavement design function has to be developed. It is recommended that a simplified, rational pavement design method be adopted for routine pavement design situations ^{*1}. The reasons for this have been covered to a certain degree in the preceding section, but can be summarized as follows:

- Complex response models, such as dynamic, non-linear, anisotropic, viscoelastic three-dimensional finite element programs are only as accurate as their input values. As

*1 The phrase "rational pavement design method" was coined by Mr. Hechter Theyse of Transportek CSIR, during discussions with one of the authors.

suggested in the previous discussion, accurate measurement of properties such as vehicle speed, layer thickness, density, material stiffness, Poisson's ratios and damping characteristics is vital if the model results are to be truly accurate. However, such measurements are not considered feasible for routine design purposes and may not even be possible for the design of new pavements. The use of "generic" input values such as those obtained from literature or published tables is not sufficient, since it is simply not rational to supply unreliable and inaccurate input data to a very expensive and complex response model and then claim that the resulting stresses and strains are accurate.

- Because of the nature of pavement materials and pavement construction processes, input values such as layer thicknesses, stiffnesses, Poisson's ratios, densities and damping characteristics are likely to vary significantly over even a short length of road. Thus a proper stochastic simulation of pavement response will indicate that pavement life may vary significantly over a nominally uniform section of road¹⁹. The proper use of complex response models is thus likely to result in a wide range of estimates of asphalt layer performance, even for a short section of road. Such imprecise estimates can also be obtained (at significantly reduced cost) by the use of simplified methods.

Although the above statements may seem to suggest that complex response models do not have a place in asphalt pavement design, this is not the case. Complex response models are vital to the development of an understanding of material behaviour and performance because they provide insight into failure mechanisms and assist in determining the most important parameters that affect material performance. The maximum horizontal tensile strains obtained with the dynamic three-dimensional finite element model, for example, suggest that an asphalt layer may not fail because of the (very low) induced tensile strain but may in fact crack for other reasons. It is therefore possible that a new mechanism for fatigue failure needs to be investigated.

Complex models are therefore vital for obtaining increased understanding of pavement behaviour and performance. However, the use of these models should be restricted to the research domain where input parameters can be accurately determined and where the model results can be interpreted in a methodical and critical manner.

Knowledge gained in this manner should then be implemented in the routine mix and pavement design functions. The manner in which this knowledge is implemented in routine design situations, however, should be in the form of a relatively simple and robust method that is not prone to misuse or over-interpretation.

It is recognized that the proposal for developing a simplified, robust approach to the pavement design function of mix design is at variance with the more fundamental and complex approach currently being pursued in the United States and Europe. However, it is believed that the approach proposed here is based on sound reasoning and on a holistic approach to pavement design. The analyses presented in this report include many aspects of complexity and fundamentals. However, a proper interpretation of these analyses, coupled with knowledge of the variability and uncertainty of pavement construction processes, suggest that a complex and refined approach is not the most **cost-effective** approach for routine design purposes.

The above discussions outline the principal reasons for the selection of a simplified, rational approach to the pavement design function of asphalt mix design. In the following section the most important characteristics of the proposed system are discussed.

Proposed Approach to the Pavement Design Function of Routine Asphalt Mix Design

The method proposed for the evaluation of the pavement design component of mix design should have the following characteristics:

- The system would follow a comparative approach and would contain a large element of knowledge-based calibration; performance would not be predicted in absolute terms, but the system would ensure that the pavement design conforms to the principles set out in the TRH4 document and design catalogue²⁰.
- The essence of the method should consist of an expert system in which only those design principles which have been well tested and validated are embodied. Such a system could be computerized or represented in a graphical format. The system would typically require only first order input values such as (i) the thickness and stiffness of the asphalt layer (ii) maximum expected asphalt temperature, (iii) stiffness of the support layer, (iv) number of heavy vehicles expected over the design period, (v) probability of overloading and (vi) number of steep inclines, (vii) selected deflection bowl parameters (for rehabilitation design purposes).

These input values should be determined using reliable and well proven methods, and should be expressed in a manner that is consistent with the uncertainty of the measurement and the variability of the parameter in question. Stiffness of the support values should, for example, be expressed in classes such as very stiff (500 to 800 MPa), stiff (300 to 500 MPa) and weak (less than 300 MPa) and could therefore be based on coarse empirical estimates.

- The system would provide two primary outputs:
 - i) Recommended laboratory tests (with the recommended stress or strain state) to be used in the mix design phase; For example, for the evaluation of rutting potential by means of the dynamic creep test, it is essential that a confining stress be applied. The level of confinement and the magnitude of the overall stress would be dictated by the pavement system and load intensity. The expert system should therefore recommend broad classes of stress states to be used. Again, this recommendation would be imprecise and relative (e.g. "high" or "low" deviator stress).
 - ii) Expected ranges of performance for the various laboratory test methods. This would enable the designer to interpret his data and make a qualitative assessment of the expected performance of the design mix. The expected or typical ranges of performance of different test methods should be based on a data base of values and could be updated from time to time as more laboratory test experience is gained and the quantity of available test data increases.

The approach outlined above essentially limits the resources that are expended on the pavement design function and instead places emphasis on the mix design function. It should be noted that the development of the proposed approach does not require expensive model building, accelerated testing or long term performance monitoring (although these elements should be pursued as part of the research function and should ideally be used to update and refine the proposed method from time to time). In essence, the *development* of the proposed method would

require the gathering and formalizing of existing knowledge, coupled with a limited set of mechanistic design calculations using the most advanced models available.

Required Input Parameters to be Determined from Materials Testing

As already suggested by the above discussion, only one parameter is needed to serve as input into the pavement design function. This is true, regardless of whether the proposed approach is adopted or of whether the current use of multi-layer elastic theory is retained. *This parameter is the mix stiffness, or resilient modulus, at a range of test temperatures.* Although the Poisson's ratio is also needed as input into conventional multi-layer elastic models, this parameter is known to be highly variable and non-linear in behaviour, as well as to be highly dependent on test method. Sufficiently accurate measurement of this parameter during routine mix design is therefore not considered to be viable. If the use of the multi-layer elastic theory for qualitative evaluation of asphalt pavements is retained, then it is recommended that the Poisson's ratio be determined using published values such as those proposed in the South African mechanistic design method (see reference 18).

TABLE OF CONTENTS

	PAGE
1. INTRODUCTION	1-1
1.1 Terms of Reference	1-1
1.2 Background	1-1
1.3 Project Objectives	1-2
1.4 Scope	1-2
1.5 Analysis Approach	1-3
2. DYNAMIC EFFECTS	2-1
2.1 Introduction	2-1
2.2 Pavement Structures and Assumed Material Properties	2-1
2.3 Results	2-3
2.4 Discussion	2-6
2.5 Summary and Conclusions	2-7
3. INFLUENCE OF NON-UNIFORM TYRE PRESSURES	3-1
3.1 Introduction	3-1
3.2 Pavement Structures and Assumed Material Properties	3-1
3.3 Assumed Stress Distribution and Loading Conditions	3-2
3.4 Results	3-4
3.4 Discussion	3-8
3.5 Summary and Conclusions	3-9
4. EFFECT OF HORIZONTAL SHEAR FORCES	4-1
4.1 Introduction	4-1
4.2 Pavement Structures and Assumed Material Properties	4-1
4.3 Analysis Results	4-1
4.4 Discussion	4-3
4.5 Summary and Conclusions	4-3
5. THE INFLUENCE OF NON-LINEAR (STRESS SENSITIVE) SUPPORT	5-1
5.1 Introduction	5-1
5.2 Non-linear Finite Element Pavement Response Model	5-1
5.3 Layered Elastic Pavement Response Models	5-2
5.4 Summary and Conclusions	5-8
6. INFLUENCE OF TEMPERATURE AND STIFFNESS GRADIENTS	6-1
6.1 Introduction	6-1
6.2 Pavement Structures and Assumed Material Properties	6-1
6.3 Model Types, Assumed Load Conditions and Evaluation Positions	6-6
6.4 Analysis Results: Structure 1	6-7
6.5 Analysis Results: Structure 2	6-9
6.6 Summary and Conclusions	6-11

7.	VISCOELASTIC EFFECTS	7-1
7.1	Introduction	7-1
7.2	Pavement Structures and Assumed Material Properties	7-2
7.3	Layered Elastic Response Model	7-4
7.3	Results	7-5
7.4	Discussion	7-7
7.5	Summary and Conclusions	7-7
8.	CONCLUSIONS, DISCUSSION AND RECOMMENDATIONS	8-1
8.1	Summary	8-1
8.2	Conclusions for Selected Effects	8-1
8.3	Further Conclusions and Discussions	8-4
8.4	Recommendations	8-6
9.	REFERENCES	9-1

APPENDIX A: ANALYSIS RESULTS - DYNAMIC EFFECTS

APPENDIX B: ANALYSIS RESULTS - NON-UNIFORM CONTACT STRESS DISTRIBUTION

APPENDIX C: ANALYSIS RESULTS - HORIZONTAL SHEAR FORCE EFFECTS

APPENDIX D: ANALYSIS RESULTS - TEMPERATURE GRADIENT EFFECTS

LIST OF TABLES

Table 2.1	Structure 1: Assured Material Properties and Layer Thicknesses	2-2
Table 2.2	Structure 2: Assured Material Properties and Layer Thicknesses	2-2
Table 2.3	Summary of Maximum Horizontal Tensile Strain Results : Structure 1	2-4
Table 2.4	Octahedral Shear Stresses in Asphalt Surfacing: Structure 1	2-4
Table 2.5	Summary of Maximum Horizontal Tensile Strain Results : Structure 2 (Asphalt Base)	2-5
Table 2.6	Octahedral Shear Stresses in Asphalt Surfacing: Structure 2	2-5
Table 2.7	Octahedral Shear Stresses in Asphalt Base Structure 2	2-6
Table 3.1	Structure 1: Assumed Material Properties and Layer Thicknesses	3-1
Table 3.2	Structure 2: Assumed Material Properties and Layer Thicknesses	3-2
Table 3.3	Summary of Maximum Horizontal Tensile Strain Results: Structure 1	3-5
Table 3.4	Octahedral Shear Stresses in Asphalt Surfacing: Structure 1	3-6
Table 3.5	Summary of Maximum Horizontal Tensile Strain Results: Structure 2 - Asphalt Base	3-6
Table 3.6	Octahedral Shear Stresses in Asphalt Surfacing: Structure 2	3-7
Table 3.7	Octahedral Shear Stresses in Asphalt Base: Structure 2	3-7
Table 4.1	Structure 2: Assumed Material Properties and Layer Thicknesses	4-1
Table 4.2	Summary of Maximum Horizontal Tensile Strain Results: Structure 2 (Asphalt Base)	4-2
Table 4.3	Octahedral Shear Stresses in Asphalt Surfacing: Structure 2	4-2
Table 4.4	Octahedral Shear Stresses in Asphalt Base: Structure 2*	4-2
Table 5.1	Pavement System and Material Properties Considered	5-2

Table 5.2	Comparison of Model Results (Base Modulus in LET Model from Backcalculation)	5-4
Table 5.3	Comparison of Model Results (Base Modulus in LET Model equal to average stiffness of all base elements under the load plate)	5-5
Table 6.1	Structure 1: Assumed Material Properties and Layer Thicknesses	6-4
Table 6.2	Structure 2: Assumed Material Properties and Layer Thicknesses	6-4
Table 6.3	Structure 1: Refined Pavement Model with Temperature-dependent Asphalt Sub-layers (used in Finite Element model)	6-4
Table 6.4	Structure 2: Refined Pavement Model with Temperature Dependent Asphalt Sub-layers (used in the Finite Element model)	6-5
Table 6.5	Structure 1: Assumed Material Properties and Layer Thicknesses (used in the Layered Elastic Model)	6-5
Table 6.6	Structure 1: Assumed Material Properties and Layer Thicknesses (used in Layered Elastic Model)	6-6
Table 6.7	Evaluation Depths and Parameters	6-6
Table 6.8	Comparison of Model Results for Similar Input Values	6-7
Table 6.9	Comparison of Model Results for 07h00 Temperature Gradient	6-8
Table 6.10	Comparison of Model results 14h00 Temperature Gradient	6-8
Table 6.11	Comparison of Model Results when a Constant Asphalt Stiffness, Representative of 25°C Temperature is used to Represent Summer Conditions.	6-9
Table 6.12	Comparison of Model Results for Similar Input Values	6-10
Table 6.13	Comparison of Model Results for 7h00 Temperature Gradient	6-10
Table 6.14	Comparison of Model Results for 14h00 Temperature Gradient	6-11
Table 7.1	Structure 1: Assumed Material Properties and Layer Thicknesses	7-2
Table 7.2	Structure 2: Assumed Material Properties and Layer Thicknesses	7-3
Table 7.3	Burgers Model Parameters used in VEROAD	7-4
Table 7.4	Summary of Maximum Horizontal Tensile Strain Results: Structure 1	7-6
Table 7.5	Summary of Octahedral Shear Stresses: Structure 1	7-6
Table 7.6	Summary of Maximum Horizontal Tensile Strain Results: Structure 2	7-6
Table 7.7	Summary of Octahedral Shear Stresses: Structure 2	7-7

LIST OF FIGURES

Figure 3.1	Measured Vertical Contact Stress Distribution used in Finite Element Model	3-3
Figure 3.2	Measured Lateral Contact Stress Distribution used in Finite Element Model	3-3
Figure 3.3	Measured Longitudinal Contact Stress Distribution used in Finite Element Model	3-4
Figure 5.1	Pavement Structure and Stiffness Variation in the Base After Convergence	5-3
Figure 5.2	Displacements Calculated with FE Model and Backcalculated Displacements using LET	5-4
Figure 5.3	Maximum horizontal Strain at the Bottom of the Asphalt Surfacing as a Function of Load Offset as Calculated with the FE and LET models	5-6
Figure 5.4	Octahedral Shear Stress at the bottom of the Asphalt Surfacing as a Function of Load Offset as Calculated with the FE and LET models	5-6
Figure 5.5	Maximum Horizontal Strain at the Bottom of the Asphalt Surfacing as a Function of Load Offset as Calculated with the FE and LET models	5-7
Figure 5.6	Octahedral Shear Stress at the Bottom of the Asphalt Surfacing as a Function of Load Offset as Calculated with the FE and LET models	5-7
Figure 6.1	Typical Variation of Temperature with Depth: Summer (after Inge and Kim ¹)	6-2
Figure 6.2	Typical Variation of Temperature with Depth: Winter (after Inge and Kim ¹)	6-2

Figure 6.3	Analysis Methodology	6-3
Figure 7.1	Typical Behaviour of Asphalt during constant Stress Loading	7-2
Figure 7.2	Rheological Model used in VEROAD Program	7-3
Figure 7.3	Measured and Theoretical Strain Response for the Material Parameters shown in Column 2 of Table 7.3	7-5
Figure 8.1	Conceptual Model to Support the Selection of a Simplified Approach to Asphalt Mix Design	8-8



1. INTRODUCTION

1.1 Terms of Reference

The project which is documented in this report forms part of the longer term Hot Mix Asphalt (HMA) project that was launched during 1998. The aim of the HMA project is to improve mix design procedures for asphalt surfacings on heavily trafficked roads and to integrate mix design procedures with pavement design, construction and expected performance. To address these objectives, the HMA project was structured to focus on the following technical areas (referred to as Technical Focus Areas, or TFA's):

- TFA1: Mix Components;
- TFA2: Spatial Composition;
- TFA3: Performance-related Tests and Properties;
- TFA4: Construction;
- TFA5: Structural Design and Performance;

The investigation which is documented in this report resorts under TFA5: Structural Design and Performance. The broad objective of this part of the project is to make recommendations for appropriate modelling procedures to be used in the structural design of asphalt layers. Findings of this investigation are intended to be used in refining and validating existing asphalt pavement design and analysis models, or where more appropriate, to develop new models for the prediction of working stresses and strains in asphalt layers.

1.2 Background

Over the past decade, multi-layer linear elastic computer programs have become accepted as a key component of routine mechanistic pavement design methods. Multi-layer elastic programs offer a fast and convenient way of estimating the stresses and strains generated in pavement systems under typical wheel loads. In recent years, however, research and experience have indicated that the use of multi-layer elastic theory may not be appropriate in some design situations. In particular, there are some doubts as to the applicability of multi-layer elastic theory to take account of:

- dynamic effects, which may lead to a different stress and strain distribution in the asphalt layer;
- non-uniform tyre pressures which may lead to high shear stresses at the asphalt surface and may lead to fatigue cracks which initiate at the surface rather than at the bottom of the asphalt (as is currently assumed in the South African mechanistic design method);
- slow moving traffic on inclines, where vehicle speed and traction effects may have a significant influence on rutting formation, and
- temperature gradients in asphalt layers, which may affect oxidation and ageing and hence, fatigue cracking and rutting mechanisms.

While it is widely known that linear elastic models contain assumptions which are not valid for asphalt layers and dynamic loads, the consequences of these invalid assumptions in terms of

design and whole life cycle costing have not been quantified. The use of more complicated (albeit more accurate) models may be unjustified for routine design purposes if one takes into account the significant variations in material properties and layer thicknesses which make precise estimates of stresses and strains meaningless in most design situations. In order to address these uncertainties, a systematic evaluation of the suitability of multi-layer elastic theory for estimating stresses and strains in asphalt pavements was performed. This report contains the results of these investigations.

1.3 Project Objectives

The objectives of the project are:

- i) To identify situations where multi-layer elastic theory may not provide an adequate estimate of stresses and strains in asphalt layers, with specific attention being paid to stress and strain parameters that relate to fatigue cracking and rutting;
- ii) To quantify the magnitude of errors made using multi-layer elastic theory and to develop an understanding of critical stresses and strains which occur in specific design situations;
- iii) To recommend methods for compensating for inefficiencies in multi-layer elastic theory or where more appropriate, to recommend alternative models for use in specific design situations, and
- iv) To determine the input parameters required for the estimation of stresses and strains in asphalt layers.

1.4 Scope

Because of time and funding constraints, an exhaustive investigation of all possible asphalt pavement types and input parameter effects could not be performed. Instead, the focus was on a few key issues which are regarded as the most probable causes of incorrect estimation of working stresses and strains in asphalt layers when the multi-layer elastic theory is used. These issues are:

- i) Dynamic effects;
- ii) Non-uniform tyre pressures;
- iii) Effects of horizontal shear forces generated at inclines or intersections;
- iv) Effects of non-uniform (non-linear) support layers;
- v) Effects of temperature and stiffness gradients in asphalt layers, and
- vi) Viscoelastic effects.

For each of these issues, a limited set of material input parameters and load conditions was assumed. It is thus possible that, because of the complex and often non-linear behaviour of asphalt pavement systems, some of the conclusions made in this report may have been different if a wider set of material parameters and load conditions had been considered in the analyses. However, it should be noted that the general objective of this project is primarily to identify and to some extent quantify the major deficiencies of multi-layer elastic models.

The pavement systems, material parameters and load conditions assumed in the analyses are deemed to be fairly typical of more highly trafficked South African pavements. It is therefore felt that the conclusions drawn from the analysis presented are indeed valid and can be used as an indication of areas within the design and analysis function where more research is needed or where new modelling techniques are required.

1.5 Analysis Approach

1.5.1 General

In the following chapters, each of the modelling issues noted in items (i) to (vi) in section 1.4 are analysed separately. Each chapter therefore addresses a different modelling issue so that the relative effects of each issue can be evaluated separately from other modelling elements. The general approach followed in each chapter was as follows:

- i) Outline the modelling issue;
- ii) Define the pavement systems, models and material parameters that were used in the analysis;
- iii) Using advanced modelling techniques, perform an analysis in which the modelling issue is taken into account. For example, in the analysis of dynamic effects, an analysis was performed using a fully dynamic model of the load and pavement system.
- iv) Perform a similar analysis using conventional layered elastic theory. In some cases, the layered elastic model was modified to more effectively take account of the issue in question (for example, by modifying the stiffness values or load situation).
- v) Results obtained in steps (iii) and (iv) are analysed and compared and conclusions are drawn.

An attempt was made to structure the various chapters in such a manner that each chapter forms a complete section that can be read and understood without reference to other chapters. However, since some of the issues are relatively complex, the interested reader may want to consult the listed references for a more detailed explanation of some issues. The results included in the various chapters represent those results that are deemed to be most critical and conducive to the formation of sound conclusions. More comprehensive and detailed results are included in the Appendices.

All the results were analysed with two performance aspects in mind: (i) fatigue cracking and (ii) permanent deformation, or rutting. The parameters used to evaluate these two performance aspects are described in the following sections.

1.5.2 Parameter Used for the Analysis of Fatigue Cracking Potential

The parameter used for the analysis of fatigue cracking was the horizontal tensile strain. This strain parameter was in all instances evaluated at both the top and bottom of the asphalt layers.

1.5.3 Parameter Used for the Analysis of Rutting Potential

The parameter used for the analysis of rutting potential is the stress invariant which is known as the octahedral shear stress. This parameter provides an indication of the overall shear stress induced by the applied load, and is defined as follows^{1,2}:

$$\text{Octahedral Shear Stress} = \sqrt{\frac{2}{3} J_2} \dots \dots \dots \text{(eq. 1.1)}$$

where J_2 is the second invariant of the deviator stress tensor. J_2 is calculated as follows²:

$$J_2 = \left(\frac{1}{2}\right) \cdot [(\sigma_{11}^D)^2 + (\sigma_{22}^D)^2 + (\sigma_{33}^D)^2] + (\sigma_{12}^D)^2 + (\sigma_{23}^D)^2 + (\sigma_{13}^D)^2 \dots \dots \text{(eq. 1.2)}$$

where σ_{ii}^D are the normal components of the deviator stress tensor, and σ_{ij}^D are the shear stresses. The normal components of the deviator stress tensor (σ_{ii}^D) are calculated as follows:

$$\sigma_{ii}^D = \sigma_{ii} - \frac{\theta}{3} \dots \dots \dots \text{(eq. 1.3)}$$

where θ is the sum of the normal stresses. The shear components (σ_{ij}^D) are simply the shear components of the stress tensor.

The octahedral shear stress or derivatives thereof are often used in theories of strength and permanent deformation, and have also been used as an indicator of permanent deformation in asphalt³. The octahedral shear stress generally varies parabolically with depth in an asphalt layer, with a minimum at the middle of the layer and maxima occurring at the top and bottom of the layer. The pattern agrees closely with the variation of permanent deformation with depth in an asphalt layer, as measured by Brown and Bell⁴.

2. DYNAMIC EFFECTS

2.1 Introduction

When a dynamic load is applied to a structure, equilibrium conditions require that the applied external force should equal the sum of the forces generated in the structure. This summation of forces can be written as follows:

$$m.a + c.v + k.x = F(t) \dots\dots\dots (eq. 2.1)$$

where:

m	=	the mass of the structure;
c	=	the damping of the structure;
k	=	the stiffness of the structure;
a	=	acceleration;
x	=	displacement;
v	=	velocity, and
F(t)	=	the applied load, which is a function of time.

As a broad simplification it can be said that conventional multi-layer elastic models do not take into account the first two terms on the left hand side of equation 2.1, so that only the stiffness of the structure is taken into account. The load is assumed to be constant with time and the forces generated by acceleration and damping are ignored.

A wheel load moving over pavement structure imparts a dynamic force to the pavement structure and thus the forces generated by acceleration and damping should ideally be taken into account. However, dynamic pavement response models are complex and require time-consuming and sophisticated numerical techniques to provide an estimate of stresses and strains generated within the structure. Because of this, and despite the advances in computer science made over the past decade, the modelling of dynamic pavement response has been largely confined to the research domain and is seldom, if ever, taken into account during the routine design of asphalt pavements.

Although some efforts have been made to obtain an indication of the importance of dynamic effects⁵, researchers seem to disagree on the importance of taking dynamic effects into account in routine pavement design⁶. It is the objective of this chapter to obtain an indication of the importance of dynamic effects in asphalt pavement design and to evaluate the errors made when dynamic effects are ignored, as in layered elastic analysis programs.

2.2 Pavement Structures and Assumed Material Properties

Two pavement structures were considered in this investigation: the first structure was a thin (40 mm thick) asphalt surfacing on a granular base and subbase. The second structure consisted of a 40 mm thick asphalt surfacing on an asphalt base of 120 mm thickness, underlain by a granular subbase. These structures are defined in Tables 2.1 and 2.2. The load assumed in the modelling process was a 40 kN single wheel with a contact pressure of 800 kPa (contact radius of 126 mm).

Table 2.1: Structure 1: Assumed Material Properties and Layer Thicknesses

Layer	Stiffness Modulus (MPa)	Damping Factor (%) at		Poisson's Ratio	Thickness (mm)
		20 km/h	80 km/h		
Asphalt Surfacing	2500	4.7	0.9	0.45	40
Granular Base	400	6.6	2.5	0.40	150
Granular Subbase	200	10.7	5.0	0.40	150
Subgrade*	70	10.7	5.0	0.40	1660

* To ensure compatibility between models, it was assumed that the subgrade was underlain by a stiff layer.

Table 2.2: Structure 2: Assumed Material Properties and Layer Thicknesses

Layer	Stiffness Modulus (MPa)	Damping Factor (%) at		Poisson's Ratio	Thickness (mm)
		20 km/h	80 km/h		
Asphalt Surfacing	2500	4.7	0.9	0.45	40
Asphalt Base	1800	4.7	0.9	0.40	120
Granular Subbase	300	10.7	5.0	0.40	150
Subgrade*	70	10.7	5.0	0.40	1690

* To ensure compatibility between models, it was assumed that the subgrade was underlain by a stiff layer.

Modelling was performed with two analysis programs: (i) conventional layered elastic theory (LET) and (ii) a three-dimensional dynamic finite element model. Dynamic finite element analysis was performed for vehicle speeds of 20 and 80 km/h. The damping factors shown in Tables 2.1 and 2.2 were obtained from previous work by Lourens⁵, and are based on correlations between calculated and measured pavement responses.

In addition to these two analyses, a static finite element analysis was performed and the results compared with the static LET model results. This was done to obtain an indication of the differences which are due to dynamic effects and those which are due to inherent differences between the models (i.e. those caused by the coarseness of the finite element mesh and by differences in the shapes of the contact areas). The load used in the analysis was a 40 kN single wheel load with an assumed contact pressure of 800 kPa.

2.3 Results

2.3.1 General

In the following sections, the results of four modelling procedures and model types are compared. These procedures and models types are:

- i) Conventional layered elastic model with a circular load area (LET). This model assumes a static load and response condition;
- ii) Static three-dimensional finite element model with a rectangular load area;
- iii) Dynamic three-dimensional finite element model with a rectangular load area and an assumed vehicle speed of 20 km/h, and
- iv) Dynamic three-dimensional finite element model with a rectangular load area and an assumed vehicle speed of 80 km/h;

The results shown in the following tables are a summary of the influence of dynamic effects on certain responses in the asphalt layer. More details of the model results can be found in Appendix A.

It should be noted that maximum stresses and strains that are obtained by the dynamic response model do not occur directly beneath the wheel as normally happens in the case of static response models. This complicates the comparison of results from the static and dynamic response models, since a direct comparison of stresses and strains at specific locations in the pavement structure is not really meaningful. To address this problem, the following approach was adopted:

- i) For the analysis of strains (fatigue issues): the strain results shown in the following tables are the maximum tensile strains obtained with the different model types, *regardless of position*.
- ii) For the analysis of stresses (rutting issues): the stress results shown for the static models represent those stresses that occur directly beneath the load, at various depths in the asphalt layers (i.e. generally the maximum stress zone for the static model). For the dynamic model, the stresses shown in the following tables represent those stresses which were calculated directly behind the wheel at various depths in the asphalt layers (i.e. generally the maximum stress zone for the dynamic model).

2.3.2 Structure 1

The analysis results for structure 1 are summarized in Table 2.3 for the horizontal tensile strain and in Table 2.4 for the octahedral shear stress, respectively. The tables also indicate the error, or difference between LET model results and FE results. The difference between the LET and static FE results can be ascribed to the difference in load contact area (circular versus rectangular) as well as to the coarseness of the finite element mesh. In some instances this difference is quite large. For this reason the approximate dynamic effect error was also calculated. These values are indicated in brackets and were calculated as the differences between the static FE and dynamic FE results, and therefore offer a clearer indication of dynamic effects, since load shape and mesh resolution effects are not included in this error term.

Table 2.3: Summary of Maximum Horizontal Tensile Strain Results: Structure 1

Model Type*	Maximum Tensile Strain (microstrain)	% Difference †	Strain Direction and Approximate Position
LET	253	NA	Longitudinal and Transverse, bottom of asphalt layer
Static FE	230	-9.1 (0.0)	Longitudinal and Transverse, bottom of asphalt layer
Dynamic FE, 20 km/h	110	-56.5 (-52.2)	Transverse strain, bottom of asphalt layer, directly behind contact area
Dynamic FE, 80 km/h	89	-64.8 (-61.3)	Transverse strain, bottom of asphalt layer, directly behind contact area

* Note: Finite element model assumes a square contact area and LET model assumes a circular contact area;

† Errors were calculated using LET solution as base value; Values in brackets were calculated using the Static FE model results as base value.

Table 2.4: Octahedral Shear Stresses in Asphalt Surfacing: Structure 1

Model Type	Top of Asphalt Surfacing		Middle of Asphalt Surfacing		Bottom of Asphalt Surfacing	
	T-oct (kPa)	% Error†	T-oct (kPa)	% Error†	T-oct (kPa)	% Error†
LET	825	NA	71	NA	605	NA
FE Static	609	-26.2 (0.0)	51	-28.2 (0.0)	608	0.7 (0.0)
FE 20 km/h	299	-63.8 (-50.9)	237	>100 (>100)	374	-38.5 (-38.5)
FE 80 km/h	178	-78.4 (-70.8)	231	>100 (>100)	320	-47.1 (-47.4)

† Errors were calculated using LET solution as base value. Values in brackets denote error corrected for model and contact area effects. Values in brackets were calculated using the Static FE model results as base value.

2.3.3 Structure 2

In order to simplify the analysis and model used for structure 2, a relatively coarse finite element mesh was used to represent the base layer. Because of this, the stresses and strains calculated with the static finite element model in the base layer do not compare well with those which are calculated with the LET model. This means that the results calculated in the base layer cannot effectively be used to evaluate the differences between LET and dynamic FE models. However, as in the case of structure 1, the error terms shown in brackets offer an indication of the relative effects of vehicle speed on analysis results.

The calculated results for structure 2 are summarized in Tables 2.5 to 2.7 for the maximum horizontal tensile strains and octahedral shear stresses in the surfacing and base, respectively. It should be noted that the tensile strains in the asphalt surfacing were all below 40 microstrain and are therefore not considered to be significant contributors to fatigue cracking. Thus only the tensile strains in the asphalt base of structure 2 are shown in Table 2.5.

Table 2.5: Summary of Maximum Horizontal Tensile Strain Results: Structure 2 (Asphalt Base)

Model Type*	Maximum Tensile Strain (microstrain)	% Difference †	Strain Direction and Approximate Position
LET	286	NA	Longitudinal and transverse, bottom of asphalt base
Static FE	221	-22.7 (0.0)	Longitudinal and transverse, bottom of asphalt base
Dynamic FE, 20 km/h	94	-67.1 (-57.5)	Transverse strain, bottom of asphalt base, directly behind contact area
Dynamic FE, 80 km/h	67	-76.6 (-69.7)	Transverse strain, bottom of asphalt base, directly behind contact area

† Errors were calculated using LET solution as base value. Values in brackets were calculated using the Static FE model results as base value.

Table 2.6: Octahedral Shear Stresses in Asphalt Surfacing: Structure 2

Model Type	Top of Asphalt Surfacing		Middle of Asphalt Surfacing		Bottom of Asphalt Surfacing	
	T-oct (kPa)	% Error†	T-oct (kPa)	% Error†	T-oct (kPa)	% Error†
LET	438	NA	192	NA	6	NA
FE Static	320	-26.9 (0.0)	134	-30.2 (0.0)	48	>100 (0.0)
FE 20 km/h	197	-55.0 (-38.4)	198	3.1 (-47.8)	252	>100 (>100)
FE 80 km/h	108	-75.3 (-66.3)	190	-1.0 (-23.9)	275	>100 (>100)

† Errors were calculated using LET solution as base value. Values in brackets were calculated using the Static FE model results as base value.

Table 2.7: Octahedral Shear Stresses in Asphalt Base: Structure 2

Model Type	Top of Asphalt Base		Middle of Asphalt Base		Bottom of Asphalt Base	
	T-oct (kPa)	% Error†	T-oct (kPa)	% Error†	T-oct (kPa)	% Error†
LET	81.6	NA	240	NA	431	NA
FE Static	126.3	54.8	222	-7.5 (0.0)	357	-17.2 (0.0)
FE 20 km/h	205.5	>-100 (-59.5)	236	-1.7 (6.3)	292	-32.3 (-18.2)
FE 80 km/h	140.1	>-100 (-11.1)	169	-29.6 (-23.9)	188	-56.4 (-47.3)

† Errors were calculated using LET solution as base value. Values in brackets were calculated using the Static FE model results as base value.

2.4 Discussion

2.4.1 Structure 1

Tensile Strain Results

It is clear from Table 2.3 that the tensile strains in the asphalt layer are highly dependent on dynamic effects. Static models clearly over-estimate the strain in the asphalt layers. It can be noted that there is a 9 per cent difference between the static LET and static FE solution. This difference can be attributed to the shape of the loading area and other effects associated with FE mesh resolution etc. This difference is small compared to the influences of vehicle speed, which lead to differences of more than 50 per cent, even at the relatively low speed of 20 km/h. For a speed of 80 km/h, the difference between the static and dynamic model results is more than 60 per cent, almost all of which can be attributed to dynamic effects. These effects generally agree with strain measured at different vehicle speeds⁷.

Octahedral Shear Stress Results

Table 2.4 shows that there are considerable differences between the octahedral shear stresses obtained from the different model types. This is the case, even in comparisons between the LET model and the static FE model, in which differences in excess of 25 per cent are noted. It should, however, be noted that the octahedral shear stress contains terms in which the differences between stresses are squared. Small differences between the stresses calculated by the different models are therefore somewhat amplified by the octahedral shear stress calculation. For example, a more detailed analysis of the normal stresses shown in Table A1 in Appendix A shows that the differences between the normal stresses of the LET and static FE models are less than 15 per cent for the evaluation position at the top of the asphalt surfacing. The corresponding difference in octahedral shear stress, however, is much larger (26 per cent - see row 2, column 3 of Table 2.4).

In general, the dynamic effect seems to increase the vertical stress while decreasing the horizontal stresses. This leads to a more uniform stress state in which shear stresses are reduced. However, Table 2.4 indicates that the effect of dynamic loading on octahedral shear stress is dependent on

the evaluation position. At the top and bottom of the asphalt surfacing, where the octahedral shear stresses tend to be greatest, the static LET estimate of octahedral shear stress is significantly higher than the dynamic FE estimate. The differences vary from approximately 40 per cent to more than 100 per cent. The results therefore suggest that static conventional LET will overestimate the rutting potential of structures on which vehicles are likely to move at speeds of more than 20 km/h.

2.4.2 Structure 2

Tensile Strain Results

The maximum horizontal tensile strains calculated in the base layer of structure 2 again suggest that static response models over-estimate the dynamic strain response of asphalt layers by more than 50 per cent, even for vehicle speeds as low as 20 km/h. It should also be noted that, since fatigue versus strain curves are normally represented by a log-log curve, the effect of this overestimate on fatigue life is likely to be several orders of magnitude (in terms of standard axes).

Octahedral Shear Stress Results

Table 2.6 again indicates that the effect of dynamic loading on octahedral shear stresses is dependent on the evaluation position. At the top of the surfacing, the LET model again tends to overestimate the octahedral shear stresses (differences between static and dynamic model results are greater than 35 per cent) At the bottom of the layer, however, the dynamic model predicts shear effects that are more than 100 per cent greater than those of the corresponding static models (i.e. solutions of static FE or LET models).

For evaluation positions in the asphalt base, similar differences were generally noted between static and dynamic model results (as compared to evaluation positions situated in the surfacing). At the top of the asphalt base, the dynamic models predict higher octahedral shear stresses than the static models (differences of 11 to more than 100 per cent). At the bottom of the asphalt base, however, the static models predict higher shear conditions. A more detailed analysis of the stresses shown in Table A3 (Appendix A) will show that this is due to the higher tensile stresses predicted by the static models.

2.5 Summary and Conclusions

In this chapter, a comparison was made between results obtained with static and dynamic response models. Two static models were investigated: (i) a conventional layered elastic model with a static load and a circular contact area, and (ii) a finite element model with a square contact area. The results obtained with these two models were compared with those generated with a three-dimensional dynamic finite element model in which the wheel load was modelled as a moving load with a given speed. Wheel speeds of 20 and 80 km/h were investigated.

The different models were used to estimate the strains and stresses in two different pavement structures. The analysis results prompt the following conclusions:

Fatigue Related Issues: Static response models such as conventional layered elastic models overestimate the tensile strains in the asphalt layer by 50 per cent or more. This was found to be the case for both types of pavement structure and for both the simulated vehicle speeds. The modelled effects of dynamic loading on tensile strains at the bottom of the asphalt

layers generally agree with published results and field measurements. *The analysis results therefore suggest that the more approximate LET model will grossly underestimate the fatigue life of asphalt layers.*

Rutting Related Issues: In the case of the rutting parameter (octahedral shear stress) large differences between static and dynamic model results were noted. The effects of dynamic loading on octahedral shear stresses are not as clear as for tensile strains. In general, the dynamic response model predicts higher vertical stresses and lower horizontal stresses than the static model. The relative differences between static and dynamic model results depend on the evaluation position. In all cases the maximum octahedral shear stress was predicted by the static LET model. This result was generally higher than the corresponding dynamic model predicted result. *The analysis results thus suggest that static models will tend to over-estimate the rutting potential of asphalt mixes for pavement sections on which vehicle speeds are likely to exceed 20 km/h.*

Finally, it should be noted that in the above analysis only the effects of dynamic loading on the induced stresses and strains were investigated. Dynamic effects are also likely to play a role in determining the resistance of asphalt mixes to fatigue and rutting at a specified applied stress state. This is especially relevant in the case of rutting, where the rate of loading not only affects the induced stress (as shown by the analysis presented here), but also affects the amount of flow induced in the asphalt mix.

3. INFLUENCE OF NON-UNIFORM TYRE CONTACT STRESSES

3.1 Introduction

Over the past five years a vast amount of information regarding the distribution of contact stresses under pneumatic tyres has become available^{8,9}. This knowledge was largely brought about by the development of the Stress-In-Motion (SIM) measurement system⁸, which makes it possible to obtain detailed measurements of the manner in which vertical and horizontal contact stresses are distributed under pneumatic tyres.

Measurements obtained by de Beer⁸ have shown that the stresses that develop under pneumatic tyres are not uniformly distributed, as assumed in routine design calculations using layered elastic theory, but can in fact exhibit a large degree of non-uniformity. This is especially true for tyres with high loads and low inflation pressures (i.e. overloaded, under-inflated tyres).

Although some preliminary estimates have been made of the effects of non-uniform tyre contact stresses on pavement design calculations, these calculations have generally been made using simplified models of the non-uniformly distributed pressure in which an axisymmetric instead of a fully three-dimensional load condition was assumed⁹. Furthermore, the calculations did not include a thorough and systematic evaluation of the deficiencies of layered elastic theory with regard to non-uniform tyre contact stresses.

In this chapter, an analysis is documented in which a three-dimensional finite element model was used to investigate the effects of a non-uniform pressure distribution on the stresses and strains that are calculated in the asphalt layers. Stresses calculated with the finite element model are compared with those which were calculated using a conventional multi-layer elastic model in which the contact pressure was assumed to be uniformly distributed and circular in shape.

3.2 Pavement Structures and Assumed Material Properties

Two pavement structures were considered in this investigation: the first structure was a thin (40 mm thick) asphalt surfacing on a granular base and subbase. The second structure consisted of a 40 mm asphalt surfacing on an asphalt base of 120 mm thickness, underlain by a granular subbase. These structures are defined in Tables 3.1 and 3.2.

Table 3.1: Structure 1: Assumed Material Properties and Layer Thicknesses

Layer	Stiffness Modulus (MPa)	Poisson's Ratio	Thickness (mm)
Asphalt Surfacing	2500	0.45	40
Granular Base	400	0.40	150
Granular Subbase	200	0.40	150
Subgrade*	70	0.40	1660

* To ensure compatibility between models, it was assumed that the subgrade was underlain by a stiff layer.

Table 3.2: Structure 2: Assumed Material Properties and Layer Thicknesses

Layer	Stiffness Modulus (MPa)	Poisson's Ratio	Thickness (mm)
Asphalt Surfacing	2500	0.45	40
Asphalt Base	1800	0.40	120
Granular Subbase	300	0.40	150
Subgrade*	70	0.40	1690

* To ensure compatibility between models, it was assumed that the subgrade was underlain by a stiff layer.

3.3 Assumed Stress Distribution and Loading Conditions

The pressure distribution used in the three-dimensional finite element model was based on the pressure distribution measured under a 75 kN single wheel load with a 700 kPa inflation pressure. Figures 3.1 to 3.3 show the variation of the vertical, lateral and longitudinal contact stresses over the contact area. The shape and dimensions of the load contact area are illustrated in Appendix B. It should be noted that this loading and pressure configuration leads to a somewhat extreme variation of contact stresses and therefore does not represent the norm that can be expected on heavily trafficked roads. However, this load configuration was chosen since it would give a clear indication of the relative importance of taking non-uniform contact stresses into account in asphalt pavement design calculations.

To simplify the finite element model, only the vertical and transverse contact stresses were taken into account during modelling. This simplification should not have a great impact on the calculated stresses since the longitudinal stresses (which were omitted in the analysis) were significantly smaller than the vertical and transverse stresses (see Figure 3.3).

MICHELIN E-22.5 315/80 R22.5 (XZA) Tyre
 Inflation Pressure = 700 kPa
 Applied Vertical Load (HVS) = 75 kN
 Measured Vertical Load = 62.35 kN
 Temperature = 20deg. C
 Wheel speed = 0.28 m/s
 Max Stress = 1.82 MPa

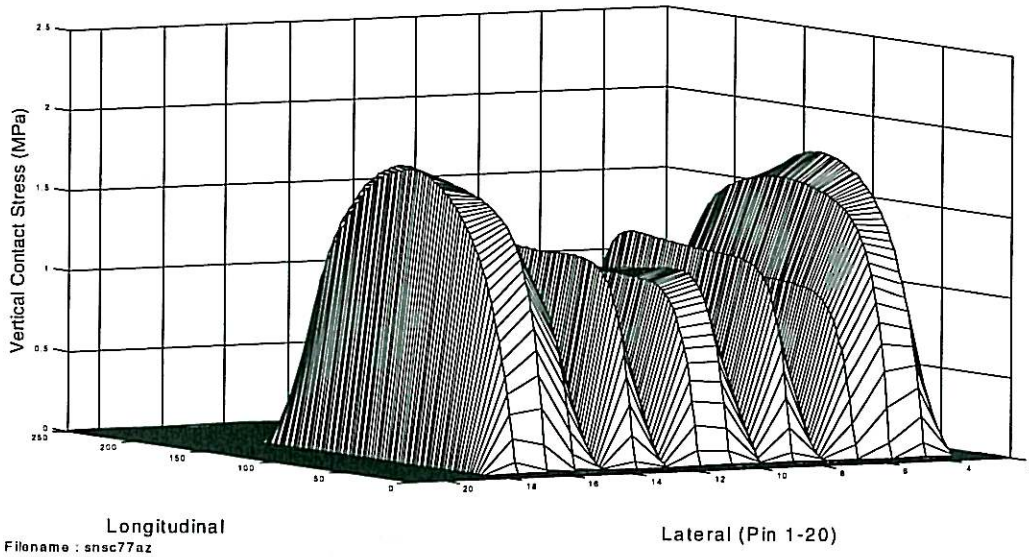


Figure 3.1: Measured Vertical Contact Stress Distribution used in Finite Element Model

MICHELIN E-22.5 315/80 R22.5 (XZA) Tyre
 Inflation Pressure = 700 kPa
 Applied Vertical Load (HVS) = 75 kN
 Measured Lateral Load = 0.1267 kN
 Temperature = 20deg. C
 Wheel speed = 0.28 m/s
 Max Stress = 0.3767 MPa
 Min Stress = -0.3704 MPa

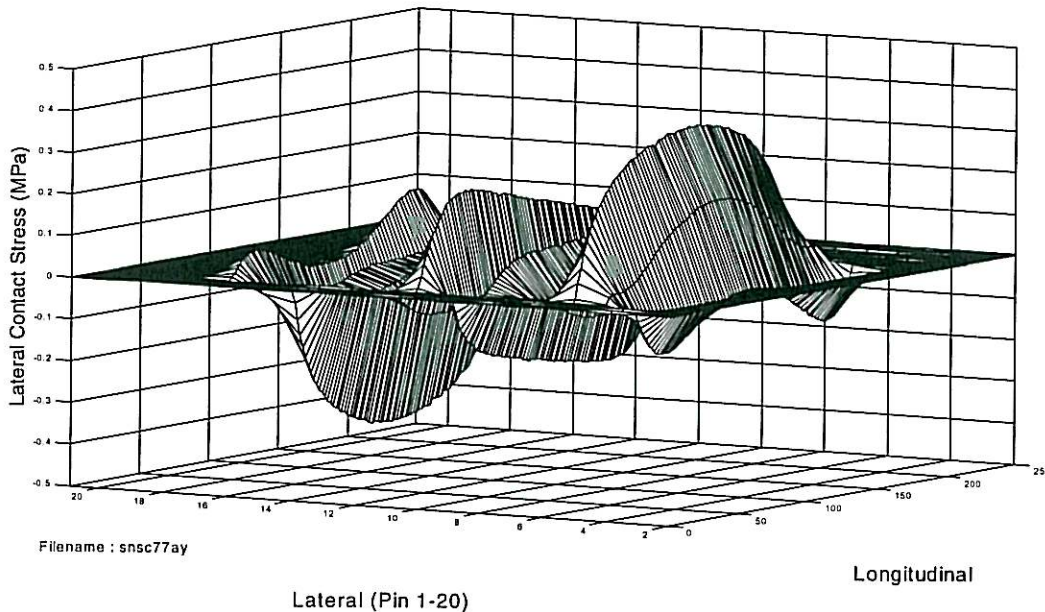


Figure 3.2: Measured Lateral Contact Stress Distribution used in Finite Element Model

MICHELIN E-22.5 315/80 R22.5 (XZA) Tyre
 Inflation Pressure = 700 kPa Temperature = 20deg. C
 Applied Vertical Load (HVS) = 75 kN Wheel speed = 0.28 m/s
 Measured Longitudinal Load = -0.3573 kN Max Stress = 0.3456 MPa
 Min Stress = -0.2274 MPa

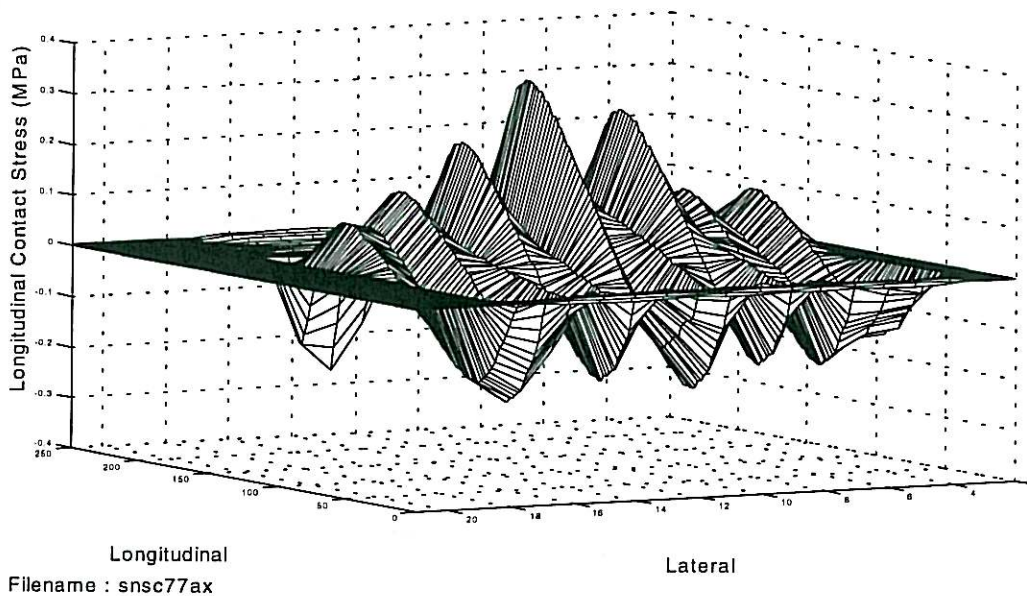


Figure 3.3: Measured Longitudinal Contact Stress Distribution used in Finite Element Model

3.4 Results

3.4.1 General

In the following sections, the results of three model types are compared. These models are:

- i) Conventional layered elastic (LET);
- ii) Three-dimensional finite element with a uniform tyre pressure distribution, but with a rectangular contact area shape that approximates the measured tyre contact area (FE Uniform), and
- iii) Three-dimensional finite element with a representative contact area and non-uniform tyre pressure distribution (FE Non-uniform)

Model (ii) was included here to provide an indication of the influence of the contact area shape and dimensions on measured results. Differences between models (i) and (ii) can also be attributed to approximations and simplifications that are inherent in the finite element model (i.e. approximations related to load definition, mesh resolution and load input resolution). By including model (ii) results in the analysis, an indication can be obtained of the differences that are due to non-uniform tyre pressure distributions as well as of those that are simply due to the shape of the load area.

The results shown in the following tables provide a concise summary of the effects of non-uniform tyre contact stresses on model results. Detailed results of the analysis are shown in Appendix B. The comparison of the LET and FE model results again poses some problems since the peak

The comparison of the LET and FE model results again poses some problems since the peak stresses and strains do not occur at the same place for the different model types. However, the results of the model in which non-uniform tyre contact stresses were taken into account indicate that a definite peak exists at the edge of the load area. This can also be surmised from the shape of the vertical contact pressure (see Figure 3.1). Thus the edge of the contact area represents an area where maximum stresses and strains generally occur. Thus, for the comparison of LET and FE model results, the following procedure was adopted:

- i) For the analysis of strains (fatigue issues): the strain results shown in the following tables are the maximum tensile strains obtained with the different model types, *regardless of position.*
- ii) For the analysis of stresses (rutting issues): for all of the models considered, the stresses were evaluated at the centre of the load axis as well as at the edge of the loaded area. These two areas represent the zones where maximum stresses occur, and therefore provide an indication of the influence of non-uniform contact stresses on rutting potential.

3.4.1 Structure 1

The analysis results for structure 1 are summarized in Tables 3.3 and 3.4 for the horizontal tensile strain and the octahedral shear stress, respectively. In order to differentiate between the differences that are due to (i) contact area shape as well as to inherent differences between the models and (ii) those which are caused by non-uniform contact stresses, a corrected error was calculated by using the difference between the FE model with a uniform contact pressure (but correct load shape) and the FE model with a non-uniform contact pressure. These differences are shown in brackets in the following tables.

Table 3.3: Summary of Maximum Horizontal Tensile Strain Results: Structure 1

Model Type*	Maximum Tensile Strain (microstrain)	% Difference †	Strain Direction and Approximate Position
LET	157	NA	Longitudinal strain, bottom of asphalt layer, approximately below edge of contact area
FE: Uniform	348 (172)‡	>100 (0.0)	Transverse strain, bottom of asphalt layer, below load centre
Fe: Non-Uniform	466	>100 (33.9)	Transverse strain, bottom of asphalt layer, below load edge

* Note: Finite element model assumes a square contact area and LET model assumes a circular contact area.

† Differences were calculated using LET solution as base value.

‡ Value in brackets is the longitudinal strain (see section 3.4.1 for discussion).

Table 3.4: Octahedral Shear Stresses in Asphalt Surfacing: Structure 1

Lateral Position	Model Type*	Top of Asphalt Surfacing		Middle of Asphalt Surfacing		Bottom of Asphalt Surfacing	
		T-oct (kPa)	% Diff.†	T-oct (kPa)	% Diff.†	T-oct (kPa)	% Diff.†
Centre of Wheel	LET	745	NA	223	NA	307	NA
	FE: Uniform	877	17.7 (0.0)	152	-31.8 (0.0)	579	88.6 (0.0)
	FE: Non-uniform	993	33.3 (13.3)	37	-83.4 (-75.7)	522	70.0 (-9.9)
Edge of Wheel	LET	488	NA	401	NA	273	NA
	FE: Uniform	477	-2.3 (0.0)	470	17.2 (0.0)	311	13.9 (0.0)
	FE: Non-uniform	717	46.9 (50.2)	562	40.1 (19.6)	807	>100 (>100)

* Note: Finite element model assumes a square contact area and LET model assumes a circular contact area.

† Differences were calculated using LET solution as base value. Differences in brackets were calculated using FE: Uniform solution as base value.

3.3.2 Structure 2

The calculated results for structure 2 are summarized in Tables 3.5 to 3.7 for the maximum horizontal tensile strains and octahedral shear stresses in the surfacing and base, respectively. It should be noted that, because of the high stiffness of the asphalt base, the horizontal strains in the asphalt surfacing were either very low (below 50 microstrain) or in compression. This was found to be the case for all the models. For this reason, only the maximum tensile strain in the asphalt base are shown in Table 3.5.

Table 3.5: Summary of Maximum Horizontal Tensile Strain Results: Structure 2 - Asphalt Base

Model Type*	Maximum Tensile Strain (microstrain)	% Difference †	Strain Direction and Approximate Position
LET	380	NA	Longitudinal and transverse strain, bottom of asphalt base, centre of contact area
FE: Uniform	389	2.4 (0.0)	Transverse strain, bottom of asphalt base, centre of contact area
Fe: Non-Uniform	354	-6.8 (-9.0)	Transverse strain, bottom of asphalt base, below load edge

* Note: Finite element model assumes a square contact area and LET model assumes a circular contact area.

† Differences were calculated using LET solution as base value. Differences in brackets were calculated using FE: Uniform solution as base value.

Table 3.6: Octahedral Shear Stresses in Asphalt Surfacing: Structure 2

Lateral Position	Model Type*	Top of Asphalt Surfacing		Middle of Asphalt Surfacing		Bottom of Asphalt Surfacing	
		T-oct (kPa)	% Diff.†	T-oct (kPa)	% Diff.†	T-oct (kPa)	% Diff.†
Centre of Wheel	LET	627	NA	399	NA	183	NA
	FE: Uniform	624	-0.5 (0.0)	300	-24.8 (0.0)	79	-56.8 (0.0)
	FE: Non-uniform	754	20.3 (20.8)	211	-47.1 (-29.7)	93	-49.2 (17.5)
Edge of Wheel	LET	460	NA	388	NA	335	NA
	FE: Uniform	420	-8.7 (0.0)	394	1.5 (0.0)	361	7.8 (0.0)
	FE: Non-uniform	267	-42.0 (-36.4)	465	19.8 (18.0)	407	21.5 (12.7)

* Note: Finite element model assumes a square contact area and LET model assumes a circular contact area.

† Differences were calculated using LET solution as base value. Differences in brackets were calculated using FE: Uniform solution as base value.

Table 3.7: Octahedral Shear Stresses in Asphalt Base: Structure 2

Lateral Position	Model Type*	Top of Asphalt Base		Middle of Asphalt Base		Bottom of Asphalt Base	
		T-oct (kPa)	% Diff.†	T-oct (kPa)	% Diff.†	T-oct (kPa)	% Diff.†
Centre of Wheel	LET	44	NA	249	NA	573	NA
	FE: Uniform	155	>100 (0.0)	306	22.9 (0.0)	485	-15.4 (0.0)
	FE: Non-uniform	93	>100 (>-40.4)	330	32.5 (7.8)	467	-18.5 (-3.7)
Edge of Wheel	LET	303	NA	294	NA	345	NA
	FE: Uniform	348	14.9 (0.0)	326	10.9 (0.0)	274	-20.3 (0.0)
	FE: Non-uniform	407	34.3 (16.9)	393	33.7 (20.5)	270	-21.7 (-1.0)

* Note: Finite element model assumes a square contact area and LET model assumes a circular contact area.

† Differences were calculated using LET solution as base value. Differences in brackets were calculated using FE: Uniform solution as base value.

3.4 Discussion

3.4.1 Structure 1

Tensile Strain Results

The results shown in Table 3.3 indicate that there are large differences between all the models considered. In the case of horizontal tensile strains, the shape and size of the contact area alone result in a difference of more than 100 per cent between the LET and FE results. Although the tensile strains obtained for the LET model may seem unreasonably low, it should be noted that, for the assumption of a circular contact area, the load radius for a 75 kN load with a tyre pressure of 700 kPa is approximately 185 mm. The asphalt surfacing, on the other hand, is only 40 mm thick. Thus the ratio of the load contact radius to the asphalt surfacing thickness is very high. This effectively deepens the neutral axis of the pavement structure, which leads to a reduction in the tensile strain at the bottom of the asphalt layer.

The rectangular load contact area which is assumed for the FE analysis has approximately the same length as the contact area diameter assumed for the LET analysis (approximately 390 mm versus 368 mm, see Appendix B for the shape and dimension of the actual load contact area). Thus, in a longitudinal direction the ratio of load length (or radius) to asphalt surfacing thickness is more comparable for the LET and FE models. This perhaps explains the relatively good correlation between the longitudinal strain calculated with the LET model and the FE model in which a uniform tyre pressure distribution was assumed (see second row of Table 3.3).

Table 3.3 also indicates that a non-uniform contact pressure distribution can lead to an increase of more than 30 per cent in the maximum horizontal tensile strains in the asphalt surfacing. If a circular and uniform contact area is assumed (as for the LET model) the horizontal tensile strains can differ by more than 100 per cent from those strains calculated using a model with a rectangular and non-uniform contact area. Furthermore, it should be noted that, in the case of the non-uniform contact stress distribution, the maximum tensile strain occurs at the edge of the load. This means that there are effectively two peaks in the maximum tensile strain (i.e. one at each edge of the load), which may also lead to an increased potential for crack initiation.

Octahedral Shear Stress Results

In general, the results shown in Table 3.4 suggest a very poor correlation between the results obtained from a conventional LET model (which assumes a circular stress contact area) and those obtained from the FE models with a rectangular contact area and a non-uniform contact stress distribution. The differences between the LET model results and those of the FE model in which a non-uniform contact stress was assumed suggest that conventional LET models may underestimate the maximum octahedral shear stress by more than 30 per cent. A large portion of this error can be attributed to the shape of the contact area.

Differences between LET and FE model results are generally the highest at the edge of the contact area, where differences of greater than 100 per cent were noted. At this position, the difference between LET and FE model results can mostly be attributed to non-uniform contact pressure distribution. Also, at the edge of the load area the LET model underestimates the octahedral shear stress at most of the depths which were analysed. At the top of the asphalt layer and at the edge of the contact area, the difference between the LET model results and the results of the FE model with non-uniform contact stress was nearly 50 per cent, almost all of which can be attributed to the non-uniformity of the contact stress distribution.

3.4.2 Structure 2

Tensile Strain Results

The results shown in Table 3.5 indicate that the effects of the contact area shape and dimensions as well as the effect of the non-uniform contact stress distribution have largely dissipated at the bottom of the base layer (also see the stress contours shown in Appendix B). The strains obtained with the different model types compare reasonably well, the maximum difference between the LET and FE model results being less than 10 per cent. The results indicate that the effect of contact area shape leads to a difference of only 2.4 per cent for strains at the bottom of the base layer.

Octahedral Shear Stress Results

The results shown in Tables 3.6 and 3.7 again indicate that the shape and size of the contact area as well as the non-uniform contact stress distribution, have a large effect on the stresses calculated by the different models. For the asphalt surfacing, the FE model with non-uniform contact pressure distribution predicted the highest octahedral shear stress. This stress was approximately 20 per cent higher than the corresponding LET model results.

It is surprising to note that, for the asphalt surfacing of structure 2, the LET model results are in many instances more conservative (i.e. octahedral shear stresses are higher for the LET model) than the corresponding FE model results. More detailed analysis of the stress results indicated that this was caused by the fact that the FE model stresses are more hydrostatic in orientation. In other words, the differences between the normal stress components are smaller, which leads to reduced shear stresses.

Although there are still large differences between the octahedral shear stress results obtained with the different models for the asphalt base, it appears that these differences can largely be attributed to the shape of the load area rather than to the non-uniform contact stress distribution. However, Table 3.7 also indicates that, for the asphalt base, the maximum octahedral shear is again calculated by the FE model with a non-uniform contact stress distribution. This maximum occurs at the top of the layer and at the edge of the load area, and is more than 30 per cent higher than the corresponding stress that was calculated with the conventional LET model. It appears that approximately half of this difference is caused by the shape of the contact area and the other half is caused by the non-uniformity of the contact stress.

3.5 Summary and Conclusions

In this chapter, the effects of non-uniform tyre contact stresses were investigated. Three models were used : (i) a conventional layered elastic model; (ii) a three-dimensional finite element model with a load area that approximates (in shape and dimension) actual measured load areas, and (iii) a three-dimensional finite element model in which both the load area and the contact stress distribution approximate actual measured values. The contact stress distribution and load shape were based on results obtained by de Beer^a. The analysis results prompt the following conclusions:

Fatigue Implications: The results indicate that, for thin asphalt surfacings on granular support layers, non-uniform contact stress distributions can have a significant effect on the maximum horizontal tensile strains. Conventional LET models in which a uniform, circular contact stress is assumed can

underestimate the maximum horizontal tensile strain in the asphalt surfacing (differences of 100 per cent and larger were observed). The effects of the shape and distribution of the contact pressure on horizontal tensile strains diminish with depth. Consequently the effects of non-uniform tyre pressure distributions are not as great for asphalt bases as for thin asphalt surfacings (differences were less than 10 per cent).

Implications for Rutting: As expected, the analysis indicated that non-uniform contact stress distributions lead to octahedral shear stresses which were greater than those calculated with conventional layered elastic models. The layered elastic model with a uniform circular contact stress generally underestimated the maximum octahedral shear stress in the asphalt layer by more than 20 per cent. This error is partly caused by the shape of the load contact area, which is rectangular rather than circular.

It should be noted that the load and tyre pressure combination on which this analysis was based lead to a somewhat extreme variation in contact stresses. The effects of non-uniform tyre contact stresses are thus likely to decrease under smaller wheel loads and at tyre pressures that conform to manufacturers' specifications. Despite this observation, the results indicate that neglect to take account of the shape of the load contact area as well as non-uniform tyre contact stresses can lead to an underestimation of the rutting and fatigue potential of asphalt layers. Differences between the results obtained with different models suggest that non-uniform tyre pressure effects should be included in design calculations, or at the very least that they warrant further investigation.

4. EFFECT OF HORIZONTAL SHEAR FORCES

4.1 Introduction

An analysis was performed to evaluate the effects of horizontal shear forces that are generated when heavy traffic moves uphill on inclines. To some extent this analysis also applies to the shear forces that are generated when traffic accelerates at intersections. For the analysis presented in this chapter, a 6 per cent incline was assumed. The horizontal shear force used in the analysis was based on the assumption of a 56 ton truck with 4 driving wheels. Thus the assumed horizontal shear force was 8.4 kN, while the normal load component was assumed to be 40 kN. Tyre contact pressure was assumed to be 800 kN. For the purposes of this analysis the shear force was assumed to be uniformly distributed over the contact area.

4.2 Pavement Structures and Assumed Material Properties

Only one pavement structure was considered in this investigation. This structure consisted of a thin (40 mm) asphalt surfacing on a 120 mm thick asphalt base with a granular support. The structure is defined in Table 4.1. The load assumed in the modelling process was a 40 kN single wheel with a contact pressure of 800 kPa (contact radius of 126 mm).

Table 4.1: Structure 2: Assumed Material Properties and Layer Thicknesses

Layer	Stiffness Modulus (MPa)	Poisson's Ratio	Thickness (mm)
Asphalt Surfacing	2500	0.45	40
Asphalt Base	1800	0.40	120
Granular Subbase	300	0.40	150
Subgrade*	70	0.40	1690

* To ensure compatibility between models, it was assumed that the subgrade was underlain by a stiff layer.

Modelling was performed with two analysis programs: (i) conventional layered elastic theory (LET) and (ii) a three-dimensional finite element model.

4.3 Analysis Results

The analysis results are summarized in Tables 4.2 and 4.3. Also shown in Tables 4.2 and 4.3 are the FE results for the case where no horizontal shear was applied. These results are included to provide an indication of the differences resulting from inherent differences between the models (including differences and errors associated with the shape of the load area, coarseness of the FE mesh, load definition etc.). It should be noted that both the FE models assumed a square load contact area while the LET model assumed a circular contact area. Values in bold denote the maximum values calculated for the evaluation position in question.

Table 4.2: Summary of Maximum Horizontal Tensile Strain Results: Structure 2 (Asphalt Base)

Model Type*	Maximum Tensile Strain (microstrain)	% Difference †	Strain Direction and Approximate Position
LET	286	NA	Longitudinal and Transverse, bottom of asphalt base
FE: No shear	221	-22.7 (0.0)	Longitudinal and Transverse, bottom of asphalt base
FE: with shear	237	-17.1 (7.2)	Longitudinal strain, bottom of asphalt base

† Differences were calculated using LET solution as base value. Values in brackets denote difference corrected for model and contact area effects (i.e difference between "FE: No shear" and "FE: with shear" model results)

Table 4.3: Octahedral Shear Stresses in Asphalt Surfacing: Structure 2

Model Type	Top of Asphalt Surfacing		Middle of Asphalt Surfacing		Bottom of Asphalt Surfacing	
	T-oct (kPa)	% Error†	T-oct (kPa)	% Error†	T-oct (kPa)	% Error†
LET	438	NA	192	NA	6	NA
FE: No shear	320	-26.9 (0.0)	134	-30.2 (0.0)	48	>100
FE: With shear	310	-29.2 (-3.1)	118	-34.9 (-6.7)	55	>100 (20.8)

* Values were calculated along the central axis of the load area

† Differences were calculated using LET solution as base value. Values in brackets denote difference corrected for model and contact area effects (i.e. difference between "FE: No shear" and "FE: with shear" model results)

Table 4.4: Octahedral Shear Stresses in Asphalt Base: Structure 2*

Model Type	Top of Asphalt Surfacing		Middle of Asphalt Surfacing		Bottom of Asphalt Surfacing	
	T-oct (kPa)	% Error†	T-oct (kPa)	% Error†	T-oct (kPa)	% Error†
LET	82	NA	240	NA	431	NA
FE: No shear	126	54.8 (0.0)	222	-7.5 (0.0)	357	-17.2 (0.0)
FE: with shear	58	-29.3 (-54.0)	241	0.4 (-8.6)	302	-29.9 (-15.4)

* Values were calculated along the central axis of the load area

† Differences were calculated using LET solution as base value. Values in brackets denote difference corrected for model and contact area effects (i.e. difference between "FE: No shear" and "FE: with shear" model results)

4.4 Discussion

The results shown in Tables 4.2 to 4.4 indicate that the effects of horizontal shear forces generated on steep inclines are not significant. Although some large differences were observed between the results obtained with the different models, the greatest part of this difference seems to be attributable to the effects of the load contact area shape and FE mesh approximations rather than to shear force effects.

This is suggested by the differences shown in brackets in Tables 4.2 to 4.4, which provide an indication of the isolated effect of shear forces (i.e. contact area shape and mesh effects are not included) on the calculated parameters. These differences show that, for the positions where octahedral shear stresses are critical, the effect of horizontal shear forces is generally below 15 per cent. For the maximum horizontal tensile strain, the difference between the results of the FE model in which horizontal shear was assumed and those of the FE model with no horizontal shear was less than 10 per cent. These differences are not viewed as significant when they are considered relative to random errors which may occur as a results of variations in support conditions, material properties etc.

It can be seen in Tables 4.3 and 4.4 that in many cases the FE model with shear forces provides lower estimates of the octahedral shear stress than the other two models. This applies particularly to the evaluation of stresses at the bottom of the asphalt base. Although this result is somewhat unexpected, it can be explained by a more detailed analysis of the stresses shown in Appendix C. These stresses show that, although some pure shear stresses are generated by the FE model with horizontal shear, the horizontal shear force also leads to reduced tension at the bottom of the base. This reduced tension effectively reduces the octahedral shear stress and overrides the shear effect that is otherwise generated.

4.5 Summary and Conclusions

In this chapter, the effect of horizontal shear forces which are generated on steep inclines was investigated. The analysis results suggest that such shear forces do not significantly affect the stresses and strains obtained by different model types. Differences that are due to mesh resolution and load contact area are generally greater than those that are caused by horizontal shear forces.

5. THE INFLUENCE OF NON-LINEAR (STRESS SENSITIVE) SUPPORT

5.1 Introduction

The objective in this chapter is to investigate the effects of non-linear support layers on the estimated stresses and strains and to determine the effects of assuming a uniformly linear support layer when the support is in fact non-uniform and stress-dependent.

The non-linear, stress sensitive behaviour of dense granular materials has been well documented^{10,11}. The phenomenon, known as stress-sensitivity, generally means that the stiffness of the material is not constant as is assumed in standard layered elastic pavement analysis programs. Instead, the stiffness of the material is dependent on the stress state at each point in the pavement layer, with the result that the stiffness of the material changes from point to point. When a thin asphalt layer is placed on a non-linear support such as a granular base, the stiffness of the immediate support changes with increasing depth and offset from the load. These effects are not taken into account in layered elastic models and have to be simulated by means of finite element (FE) models.

Several models have been proposed to describe the stress sensitive behaviour of granular materials. In recent years, the model developed by Uzan¹¹ has become one of the most widely used in the field of pavement modelling. This model has the form:

$$E = (k_1 \cdot Pa) \cdot \left(\frac{\theta}{Pa}\right)^{k_2} \cdot \left(\frac{\tau}{Pa}\right)^{k_3} \dots \dots \dots \text{(Eq. 5.1)}$$

where:

E	=	Stiffness modulus;
θ	=	First stress invariant (calculated as the sum of the normal stresses or principal stresses);
τ	=	Octahedral shear stress, as defined in chapter 1;
Pa	=	Atmospheric pressure, used to normalize stress units;
k_i	=	Material constants determined by means of laboratory testing.

The constant k_1 normally ranges from between 1000 to 10,000 MPa for dense granular materials, and k_2 and k_3 roughly range from 0.2 to 0.8 and 0.0 to -0.4, respectively¹². It can be seen from equation 5.1 that these coefficients imply that an increase in the first stress invariant (which effectively means that particles are being pushed together) will lead to an increase in stiffness. On the other hand, an increase in the octahedral shear stress (which effectively means that particles are being sheared or pulled apart), will lead to a decrease in stiffness.

5.2 Non-linear Finite Element Pavement Response Model

5.2.1 Load Conditions and Pavement Structure Considered

In order to study the effects of non-linear support layers on the stress and strain response on the asphalt, a finite element model which utilizes the model defined by equation 5.1 was used. Axisymmetric and static load conditions were assumed. The applied load was 20 kN with a contact

pressure of 690 kPa. The pavement structure that was investigated consisted of a thin asphalt on a granular support system, as defined in Table 5.1.

Table 5.1: Pavement System and Material Properties Considered

Layer	Assumed Material Behaviour	Stiffness Properties	Thickness (mm)	Poisson's Ratio
Asphalt Surfacing	Linear elastic	$E = 2500 \text{ MPa}$ (constant)	40	0.45
Granular Base	Non-linear elastic, as defined by equation 5.1	$k_1 = 2000$ $k_2 = 0.6$ $k_3 = -0.3$	150	0.40
Granular Subbase	Linear elastic	$E = 200 \text{ MPa}$ (constant)	150	0.40
Subgrade	Linear elastic	$E = 70 \text{ MPa}$ (constant)	1660*	0.40

* To ensure compatibility between models, it was assumed that the subgrade was underlain by a stiff layer

The finite element analysis of a non-linear problem type requires repeated solution of the analysis problem. After each iteration the stiffness modulus of each element is adjusted to be compatible with the stress condition at the centre of the element. This process is repeated until the modulus of each element has converged to within 5 per cent of the previous modulus value. Figure 5.1 shows the pavement structure with the stress-dependent moduli of different elements in the base, after convergence of the finite element solution had been achieved.

5.3 Layered Elastic Pavement Response Models

5.3.1 General

As noted before, the purpose of this chapter is to analyse the effects of assuming a constant linear support when the actual support stiffness varies. The objective of this section is to compare the results obtained with layered elastic theory (LET) with those obtained from the FE analysis described in the previous section.

An important consideration in this type of investigation is the selection of a stiffness value to represent the uniform support conditions. For the purposes of this analysis, two model options were considered: (i) LET model with base modulus from backcalculation, and (ii) LET model with base modulus equal to the average modulus (after conversion) of all FE model elements directly under the load. The results of these two modelling options are described in the following subsections.

5.3.2 Option 1: Base Modulus Obtained from Backcalculation

In this modelling approach the surface displacements calculated with the FE model were used as input in a backcalculation process. A backcalculation was then performed using layered elastic theory. This backcalculation was performed manually, using the BISAR multilayer elastic program. The backcalculation process was similar to that which would be followed in a routine pavement evaluation process using Falling Weight Deflectometer (FWD) results. The following differences should however be noted:

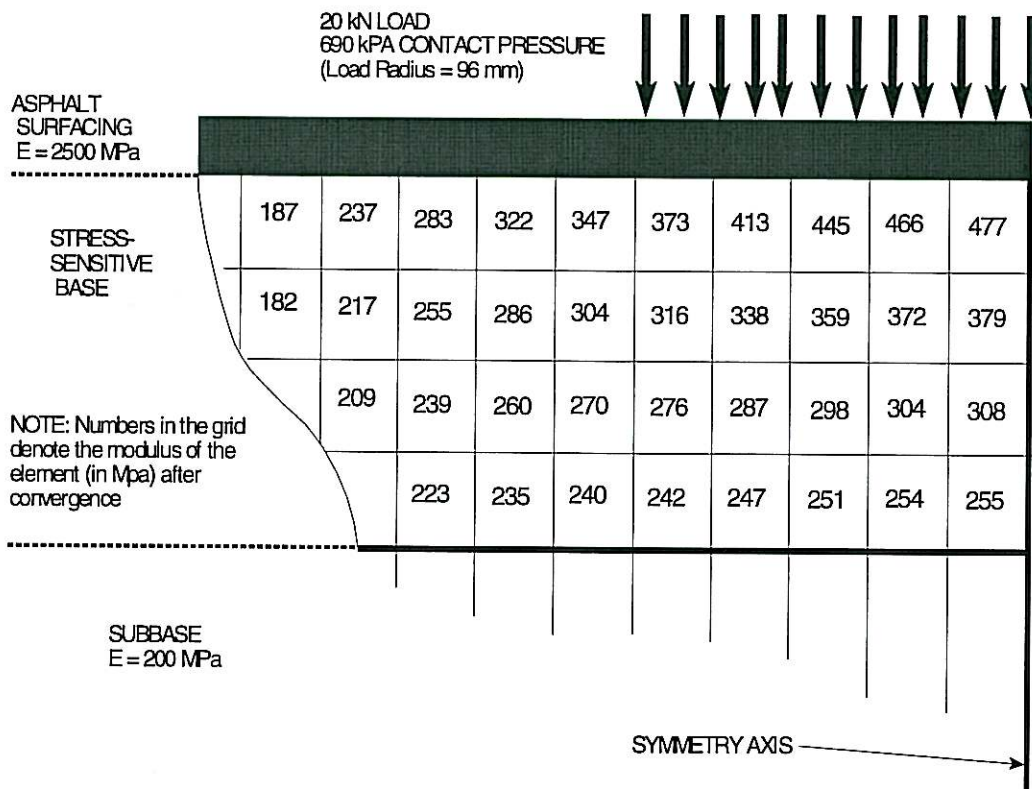


Figure 5.1: Pavement Structure and Stiffness Variation in the Base After Convergence

- i) Since the stiffness of the linear layers (i.e. the asphalt surface, subbase and subgrade) were known (see Table 5.1), these values were used as input in the backcalculation process. *Thus the only unknown to be calculated was the stiffness of the base.*
- ii) The load differed from a standard FWD load in that a 20 kN load with a contact radius of 96 mm was used in the FE calculation. This load and contact radius were therefore also used in the backcalculation process.

Figure 5.2 shows the displacements calculated with the FE model as well as those calculated with the LET model in which the base stiffness was constant. It should be noted that the FE model results are based on a non-uniform stiffness in the base, as shown in Figure 5.1. The LET model, on the other hand, assumes a constant base modulus at all depths and load offsets.

The backcalculated base modulus was **270 MPa**. This value resulted in backcalculation errors of less than 5 per cent on all except the outermost displacements. Comparison of this value with the base stiffnesses shown in Figure 5.1 will show that this value is roughly equal to the stiffness towards the bottom of the base, where compressive stresses are small.

The next step in the analysis was to use the backcalculated base stiffness in a LET model to calculate the stresses and strains in the asphalt layer. The pavement structure used in this analysis is identical to that defined in Table 5.1, except that the base is modelled as a linear elastic material with a constant stiffness (value of 270 MPa). The stresses and strains in the asphalt layer were calculated and compared with those obtained with the FE solution. The results are summarized in Table 5.2. Figures 5.3 and 5.4 show the influence lines for the strains and stresses at the most critical depths in the asphalt layer.

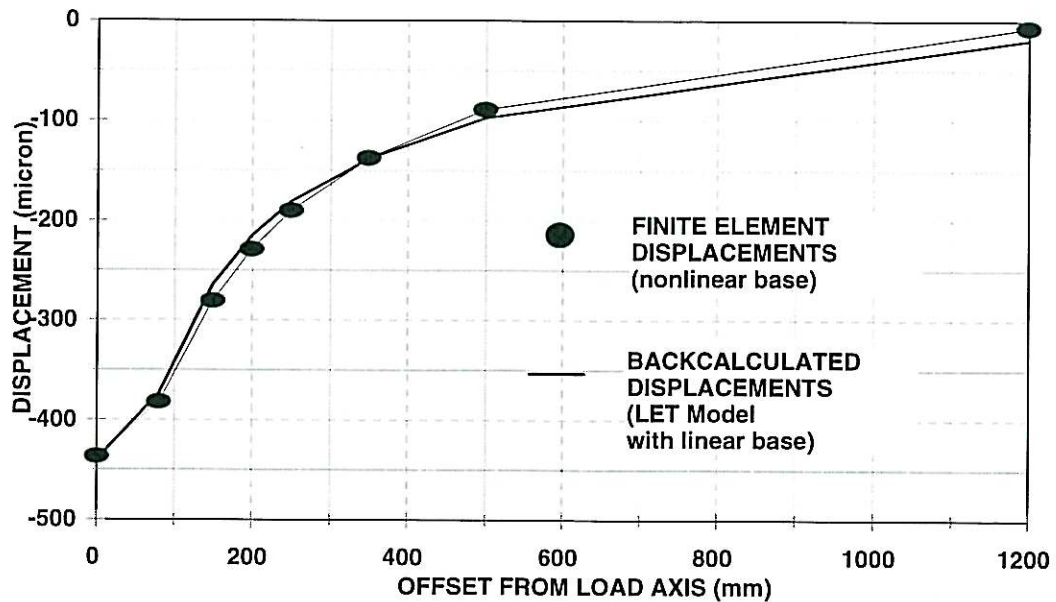


Figure 5.2: Displacements Calculated with FE Model and Backcalculated Displacements using LET

Table 5.2: Comparison of Model Results (Base Modulus in LET Model from Backcalculation)

Evaluation Position	Maximum Tensile Strain (microstrain)		% Difference†	Octahedral Shear Stress (kPa)		% Difference†
	LET	FE		LET	FE	
Top of Asphalt Surface	74	56	-24.3	597	468	-21.6
Middle of Asphalt Surface	NA	NA	NA	371	338	-8.9
Bottom of Asphalt Surface	359	287	-20.1	814	665	-18.3

* LET = Layered Elastic Theory.

** Fe = Finite Element Model.

† Differences between values were calculated using LET results as base values.

It should be noted that in Tables 5.2 and 5.3, a positive percentage difference indicates that the layered elastic theory model is less conservative than the finite element model. Critical values with their corresponding percentage differences are indicated in bold.

It is clear from the results shown in Table 5.2 and Figures 5.3 and 5.4 that the layered elastic model significantly overestimates the tensile strain and the octahedral shear stress values. However, this can be attributed more to the simplified backcalculation procedure which clearly leads to an underestimation of the base stiffness, than to the fact that the base modulus is not constant. This will be investigated in more detail in the next section.

5.3.3 Option 2: Base Modulus Equal to Average Base Stiffness Under the Load Area

In this modelling option, the base modulus used in the LET model was set equal to the average stiffness of all elements in the base that are directly under the load, as shown in Figure 5.2. The averaging of the stiffnesses of all these elements resulted in a base stiffness of **333 MPa**. This value was thus used in the LET model in which all layers were assumed to be linear elastic with constant modulus values. The results of this modelling procedure are shown in Table 5.3 and in Figures 5.5 and 5.6.

Table 5.3: Comparison of Model Results (Base Modulus in LET Model equal to average stiffness of all base elements under the load plate)

Evaluation Position	Maximum Tensile Strain (microstrain)		% Difference†	Octahedral Shear Stress (kPa)		% Difference†
	LET	FE		LET	FE	
Top of Asphalt Surface	57	56	-1.8	526	468	-11.0
Middle of Asphalt Surface	NA	NA	NA	348	338	-2.9
Bottom of Asphalt Surface	302	287	-5.0	693	665	-4.0

* LET = Layered Elastic Theory.

** FE = Finite Element Model.

† Differences between values were calculated using LET results as base values.

By comparison with the first modelling option considered, Table 5.3 and Figures 5.5 and 5.6 indicate a significantly reduced percentage difference between the FE and LET model results. As indicated by the result in Table 5.3, the LET model results are within 5 per cent of the FE model results for the most critical stress and strain parameters if the support value used in the LET model is similar to the average stiffness value that exists directly beneath the load in the base layer.

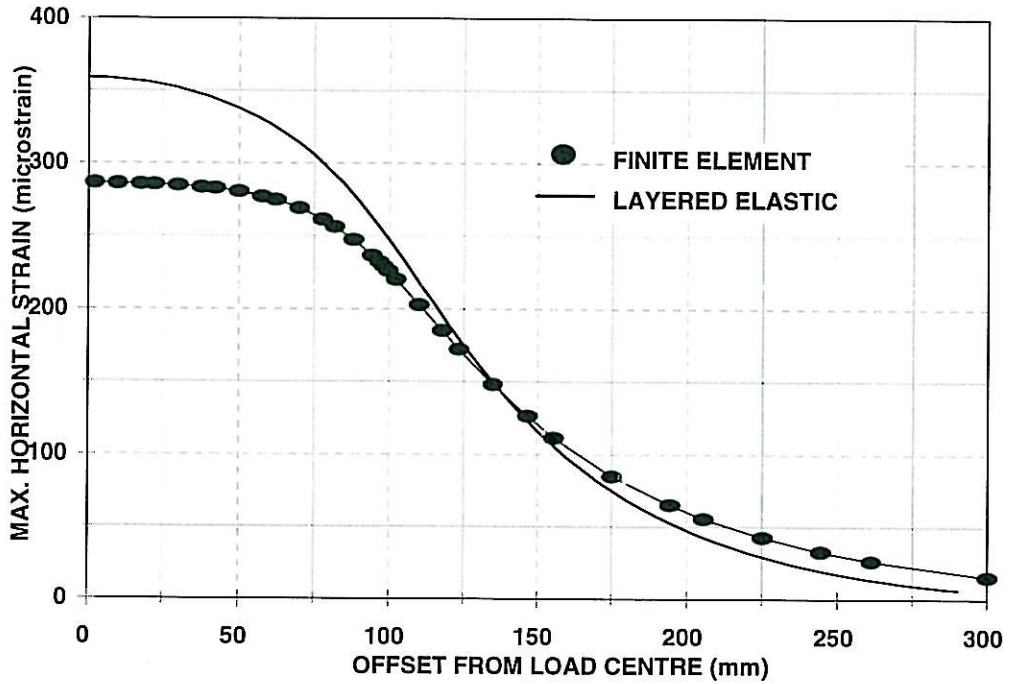


Figure 5.3: Maximum horizontal Strain at the Bottom of the Asphalt Surfacing as a Function of Load Offset as Calculated with the FE and LET models

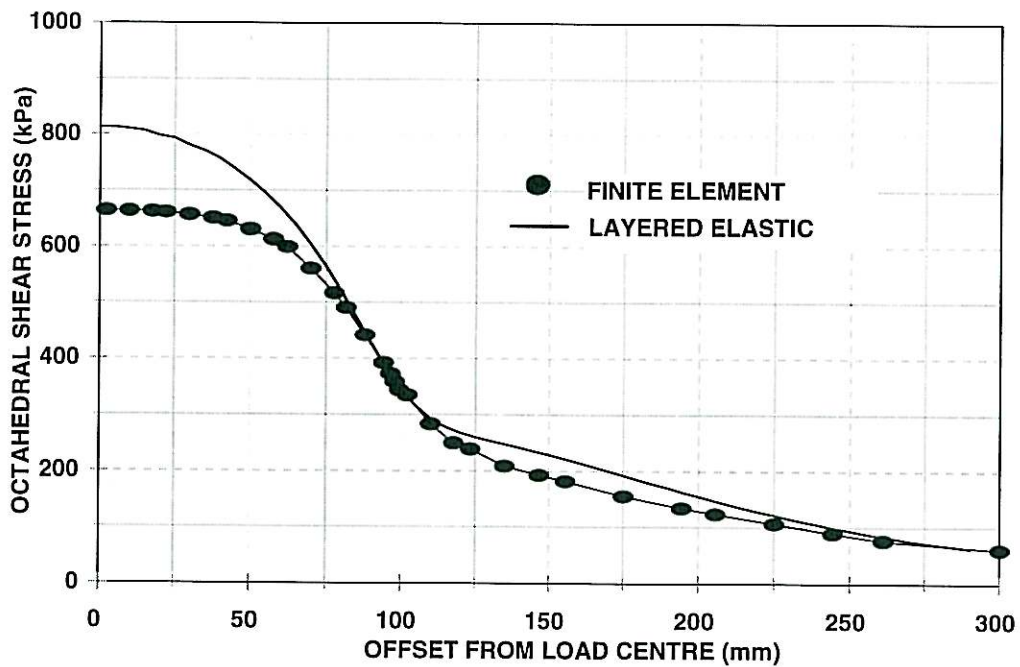


Figure 5.4: Octahedral Shear Stress at the bottom of the Asphalt Surfacing as a Function of Load Offset as Calculated with the FE and LET models

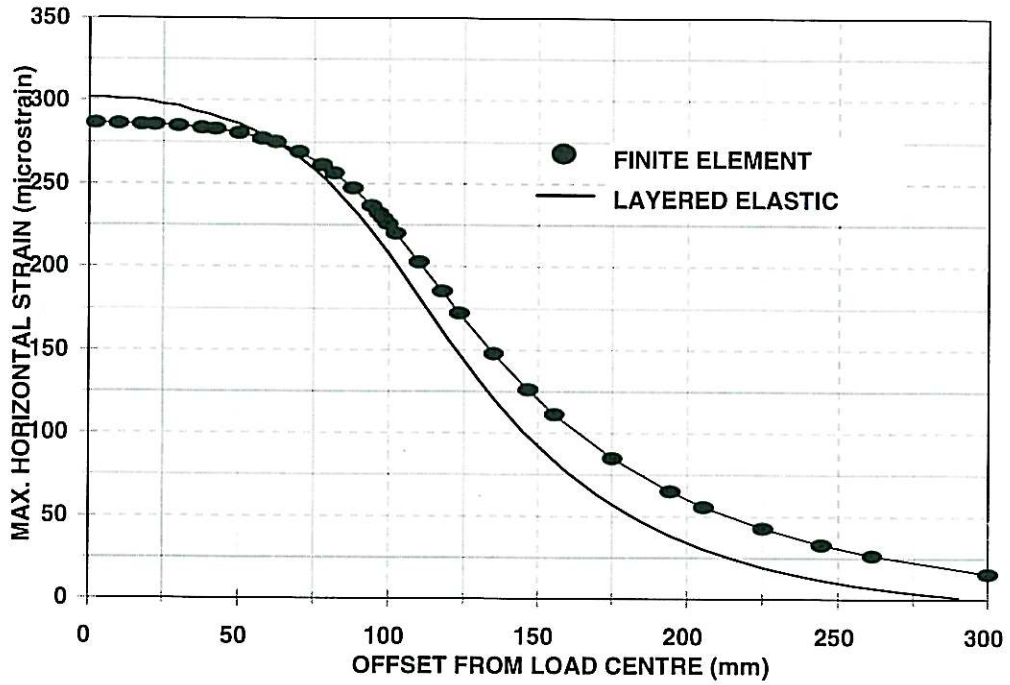


Figure 5.5: Maximum Horizontal Strain at the Bottom of the Asphalt Surfacing as a Function of Load Offset as Calculated with the FE and LET models

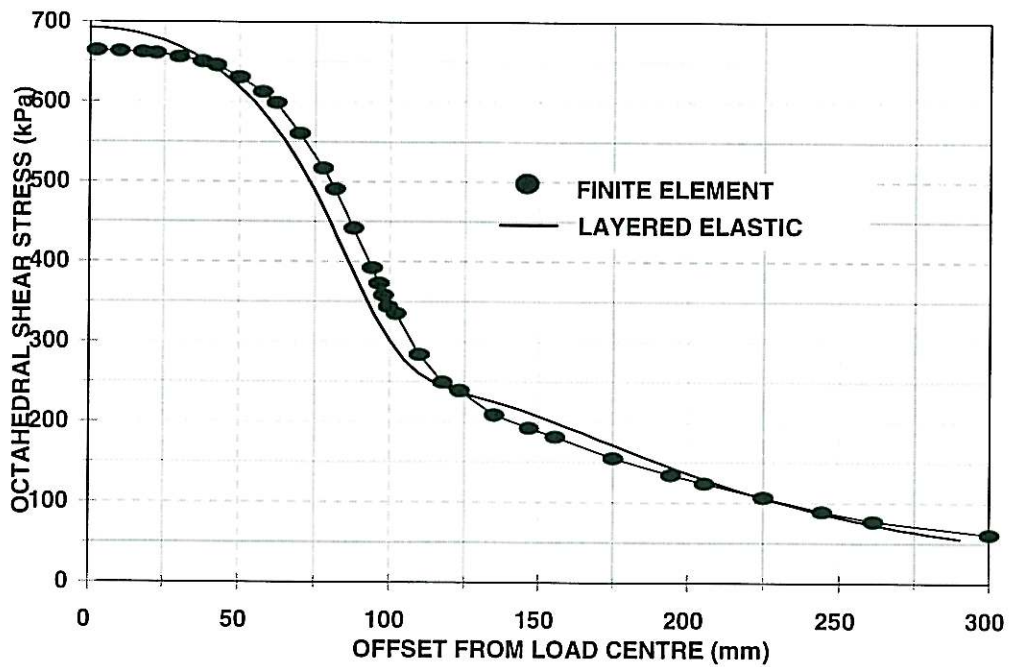


Figure 5.6: Octahedral Shear Stress at the Bottom of the Asphalt Surfacing as a Function of Load Offset as Calculated with the FE and LET models

5.4 Summary and Conclusions

In this chapter, the effects of non-linear support systems on the stress and strain response of asphalt layers were investigated. A non-linear, axisymmetric finite element program was used to obtain stresses and strains in a thin asphalt surfacing which was assumed to be supported by a stress-sensitive granular layer. The finite element results were compared with the results obtained with a conventional layered elastic model.

The analysis results presented in this section indicate that the presence of a non-uniform support layer does not have a significant effect on the critical stress and strain parameters calculated in the asphalt surface. The results suggest that the simplified LET model, which does not take into account the change in support stiffness with increasing depth and increased offset from the load, can provide a reasonably accurate estimate (i.e. within 5 per cent of the more rigorous FE solution) of the most critical stress and strain parameters, *provided that the support stiffness is representative of the average stiffness of the support layer under the loaded area.*

The results indicate, however, that in routine pavement evaluation situations large differences (generally in the order of 20 per cent) between the simplified LET model and the more representative FE model can occur because of the simplifications in the backcalculation model. The analysis presented here indicates that, if the stiffness of the base varies significantly with depth, the backcalculated stiffness is likely to be lower than the average base stiffness. This means that stiffness of the immediate support (i.e. the upper base) is underestimated, with a resulting overestimation of the tensile strains and shear stresses at the bottom of the asphalt surfacing. The practical implications of this may be a gross underestimation of the fatigue life and rutting potential of thin asphalt layers.

Finally, it should be noted that the analysis presented in this chapter applies only to thin asphalt surfacings on granular support layers. This pavement situation can be regarded as a worst case scenario as far as non-linearity effects are concerned, since the effects of stress sensitivity are likely to reduce significantly if thicker asphalt layers are used. It should also be noted that the effects of non-linearity on backcalculation and estimation of stresses and strains are likely to be further complicated by dynamic effects.

6. INFLUENCE OF TEMPERATURE AND STIFFNESS GRADIENTS

6.1 Introduction

In this chapter the purpose is to investigate the effects of temperature and stiffness gradients in asphalt layers on the modelling of stresses and strains. Figures 6.1 and 6.2 show typical temperature gradients in a thick asphalt layer as recorded by Inge and Kim¹³ during summer and winter, respectively. Because of these temperature gradients, asphalt stiffness will not be constant throughout the layer but will vary with depth in a manner that is inversely proportional to the temperature gradient. In most routine mechanistic design methods, however, this variation of asphalt stiffness with depth is not considered and the asphalt is modelled as a single layer with a constant stiffness. This stiffness is typically derived from backcalculation or laboratory tests in which the stiffness is normalized to a standard temperature (typically 20 or 25 °C).

In order to study the effects of temperature and stiffness gradients in asphalt layers on the modelling of stresses and strains, the methodology illustrated in Figure 6.3 was adopted. Two pavement structures were considered, as well as two types of temperature gradients. Thus there was a total of 4 sets of stress-strain results that had to be compared, as shown in Figure 6.3. The following sections contain more detailed information on the analysis methodology, assumed material properties and applied load conditions.

6.2 Pavement Structures and Assumed Material Properties

Two pavement structures were considered in this investigation: the first structure consisted of a thin (40 mm) asphalt surfacing on a granular base and subbase. The second structure consisted of a 40 mm thick asphalt surfacing on an asphalt base of 120 mm thickness, underlain by a granular subbase. These structures are defined in Tables 6.1 and 6.2. It should be noted that the material properties shown for the asphalt layers in Tables 6.1 and 6.2 pertain to a temperature of 25°C.

The temperature gradients selected for use in this investigation are those shown in Figure 6.1. Two types of temperature gradients were thus considered: an early morning temperature gradient in which the lower part of the asphalt layer is less stiff than the upper part, and an afternoon temperature gradient in which the lower part of the asphalt layer is stiffer than the upper part. These two gradients represent a typical fluctuation of temperature with depth during a warm summer month and are deemed to be fairly representative of South African conditions.

Tables 6.3 and 6.4 show the material properties used in the refined pavement model in which the asphalt layers were subdivided into several layers. The stiffnesses shown for each sub-layer were obtained by converting the stiffness at 25°C (i.e. the asphalt stiffnesses shown in Tables 6.1 and 6.2) to equivalent stiffnesses using the estimated mid-depth temperature for the sub-layer (read from Figure 6.1) and the temperature-stiffness conversion factors derived by Park and Kim¹⁴.

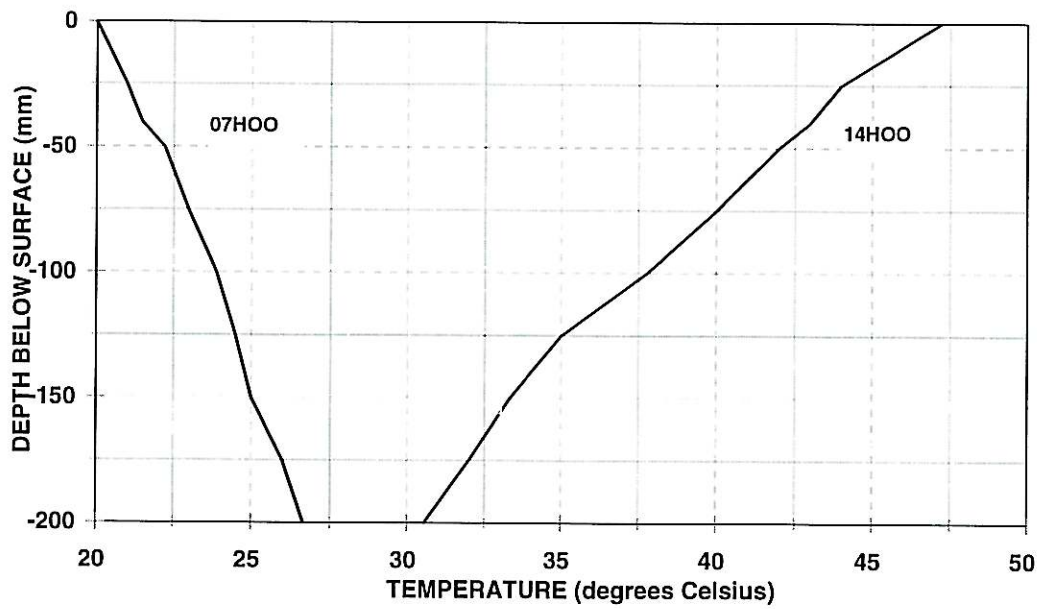


Figure 6.1: Typical Variation of Temperature with Depth: Summer (after Inge and Kim ¹⁾)

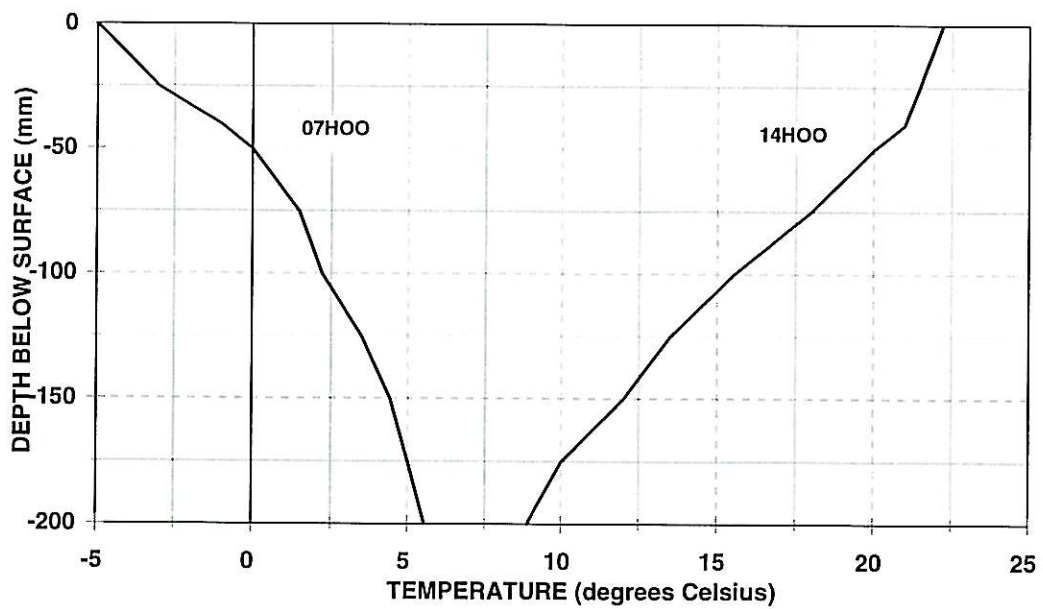


Figure 6.2: Typical Variation of Temperature with Depth: Winter (after Inge and Kim ¹⁾)

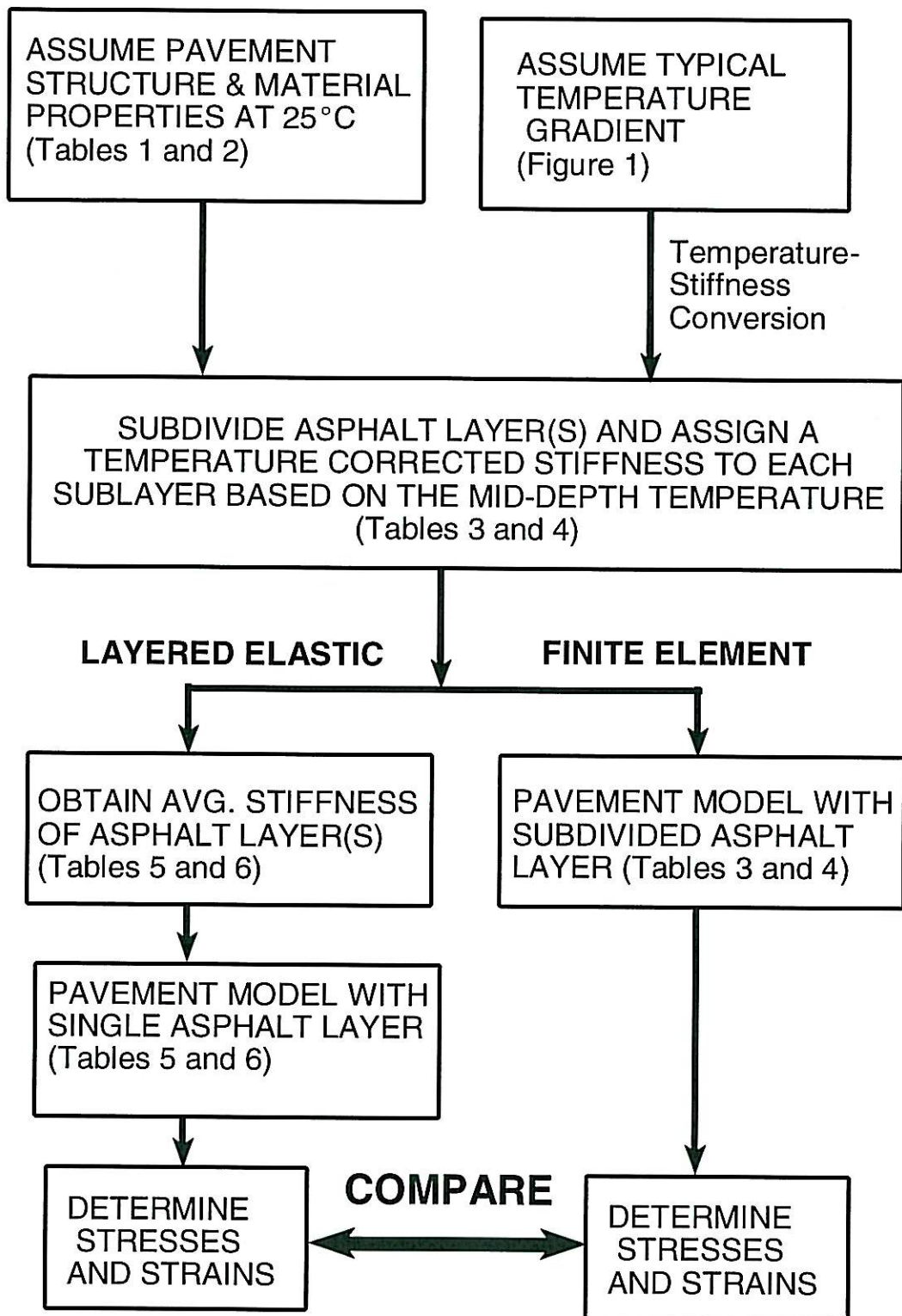


Figure 6.3: Analysis Methodology

Table 6.1: Structure 1: Assumed Material Properties and Layer Thicknesses

Layer	Stiffness Modulus (MPa)	Poisson's Ratio	Thickness (mm)
Asphalt Surfacing	2500*	0.45	40
Granular Base	400	0.40	150
Granular Subbase	200	0.40	150
Subgrade**	70	0.40	1660

* Stiffness at 25°C.

** To ensure compatibility between models, it was assumed that the subgrade was underlain by a stiff layer.

Table 6.2: Structure 2: Assumed Material Properties and Layer Thicknesses

Layer	Stiffness Modulus (MPa)	Poisson's Ratio	Thickness (mm)
Asphalt Surfacing	2500*	0.45	40
Asphalt Base	1800*	0.40	120
Granular Subbase	300	0.40	150
Subgrade**	70	0.40	1690

* Stiffness at 25°C.

** To ensure compatibility between models, it was assumed that the subgrade was underlain by a stiff layer.

The next step in the analysis was to determine - for each of the temperature gradients considered - the representative stiffness of the undivided asphalt layers that was to be used in the layered elastic pavement model. This was done by calculating the average stiffness of the asphalt surfacing and base layers, using the sub-layer stiffnesses shown in Tables 6.3 and 6.4. These average stiffnesses were used in the layered elastic pavement model and are shown in Tables 6.5 and 6.6.

Table 6.3 Structure 1: Refined Pavement Model with Temperature-dependent Asphalt Sub-Layers (used in the Finite Element model)

Layer and Sub-layer Properties		Thickness (mm)	Poisson's Ratio	Stiffness at 07h00 (MPa)	Stiffness at 14h00 (MPa)
Asphalt Surfacing	Sub-layer 1	10	0.45	3392	636
	Sub-layer 2	10	0.45	3314	683
	Sub-layer 3	10	0.45	3236	730
	Sub-layer 4	10	0.45	3159	777
Granular Base		150	0.40	400	
Granular Subbase		150	0.40	200	
Subgrade**		1660	0.40	70	

* Based on a stiffness of 2500 MPa at 25°C (see Table 6.1) and the temperature gradient shown in Figure 6.1.

Table 6.4: Structure 2: Refined Pavement Model with Temperature Dependent Asphalt Sub-layers (used in the Finite Element model)

Layer and Sub-layer Properties		Thickness (mm)	Poisson's Ratio	Stiffness at 07h00 (MPa)	Stiffness at 14h00 (MPa)
Asphalt Surfacing	Sub-layer 1	10	0.45	3392	636
	Sub-layer 2	10	0.45	3314	683
	Sub-layer 3	10	0.45	3236	730
	Sub-layer 4	10	0.45	3159	777
Asphalt Base	Sub-layer 1	20	0.40	2146	613
	Sub-layer 2	20	0.40	2076	700
	Sub-layer 3	20	0.40	2005	787
	Sub-layer 4	20	0.40	1935	874
	Sub-layer 5	20	0.40	1865	961
	Sub-layer 6	20	0.40	1795	1048
Granular Base		150	0.40	300	
Subgrade**		1690	0.40	70	

* Based on a stiffness of 2500 MPa at 25°C (see Table 6.1) and the temperature gradient shown in Figure 6.1.

Table 6.5: Structure 1: Assumed Material Properties and Layer Thicknesses (used in the Layered Elastic Model)

Layer	Avg. Stiffness at 14h00 (MPa)	Avg. Stiffness at 07h00 (MPa)	Poisson's Ratio	Thickness (mm)
Asphalt Surfacing	3275	707	0.45	40
Granular Base	400		0.40	120
Granular Subbase	200		0.40	150
Subgrade**	70		0.40	1660

Table 6.6: Structure 2: Assumed Material Properties and Layer Thicknesses (used in the Layered Elastic Model)

Layer	Avg. Stiffness at 14h00 (MPa)	Avg. Stiffness at 07h00 (MPa)	Poisson's Ratio	Thickness (mm)
Asphalt Surfacing	3275	707	0.45	40
Asphalt Base	1970	830	0.40	120
Granular Subbase	300		0.40	150
Subgrade**	70		0.40	1690

6.3 Model Types, Assumed Load Conditions and Evaluation Positions

Two models were used: a standard multi-layer elastic model and an axisymmetric finite element model. The multi-layer elastic model represented a more routine design approach in which a single asphalt layer is used. The structures used as input to the multilayer elastic model are shown in Tables 6.5 and 6.6. The finite element model was used to analyse the pavement structures in which the asphalt layers were subdivided (i.e. the pavement structures defined in Tables 6.3 and 6.4). A single 20 kN load with an assumed contact pressure of 690 kPa was used. For both model types, the stresses and strains were calculated under the assumption of static load conditions.

In order to facilitate an assessment of the effect of temperature gradients on the analysis of cracking and rutting potential, the evaluation positions and parameters shown in Table 6.7 were investigated. It should be noted that, for each depth position, the stresses and strains were calculated at various offsets from the load centre so that a complete stress and strain influence line was obtained.

Table 6.7. Evaluation Depths and Parameters

Structure	Performance Aspect	Evaluation Depths	Evaluation Parameter
1	Fatigue Cracking	Near top and bottom of asphalt surfacing	Maximum horizontal strain
	Rutting Potential	Top, middle and bottom of asphalt surfacing	Octahedral shear stress
2	Fatigue Cracking	Bottom of asphalt base	Maximum horizontal strain
	Rutting Potential	Top, middle and bottom of asphalt base	Octahedral shear stress

6.4 Analysis Results: Structure 1

6.4.1 Comparison of Models for Identical Input Values

In order to ensure that differences between the calculated stresses and strains were due to temperature variation in the asphalt rather than to differences between the models themselves, benchmarking was first performed in which identical input values for the asphalt were used in both models. In the case of the layered elastic model, the pavement structure shown in Table 6.1 was used to define input values. For the finite element model, the layer thicknesses and Poisson's ratios shown in Table 6.3 were used, but the asphalt stiffness of each sub-layer was set to 2500 MPa (i.e. all sub-layers had the same stiffness). The results of the benchmarking are summarized in Table 6.8.

It can be seen from the results given in Table 6.8 that the values obtained with the two types of models compare very well. The values suggest that differences in stresses and strains that are larger than 4 per cent can be attributed to temperature gradient effects rather than to inherent differences between the finite element and layered elastic models.

Table 6.8: Comparison of Model Results for Similar Input Values

Evaluation Position	Maximum Tensile Strain (microstrain)		% Difference†	Octahedral Shear Stress (kPa)		% Difference†
	LET	FE		LET	FE	
Top of Asphalt Surface	42	42	0.0	469	473	0.9
Middle of Asphalt Surface	NA	NA	NA	330	342	3.6
Bottom of Asphalt Surface	256	256	0.0	595	595	0.0

* LET = Layered Elastic Theory.

** Fe = Finite Element Model.

† Differences between values were calculated using LET results as base values.

6.4.2 Comparison of Model Results for 07h00 Temperature Gradient

The results of the finite element (FE) and layered elastic theory (LET) models for the early morning (07h00) temperature gradient are summarized in Table 6.9. Detailed results in the form of influence lines are shown in Appendix D. It should be noted that, for the FE analysis, the asphalt surfacing was subdivided as shown in Table 6.3. For the LET analysis, the asphalt was not subdivided and only a single stiffness was used to represent the asphalt layer. The pavement structure used in the LET model is defined in Table 6.5 (07h00 temperature gradient).

It should be noted that, in Tables 6.9 to 6.14, a positive percentage difference indicates that the layered elastic theory model is less conservative than the finite element model. Critical values with their corresponding percentage differences are indicated in bold.

Table 6.9. Comparison of Model Results for 07h00 Temperature Gradient

Evaluation Position	Maximum Tensile Strain (microstrain)		% Difference†	Octahedral Shear Stress (kPa)		% Difference†
	LET	FE		LET	FE	
Top of Asphalt Surface	43	41	-4.7	592	607	2.5
Middle of Asphalt Surface	NA	NA	NA	364	376	3.3
Bottom of Asphalt Surface	249	253	1.6	742	728	0.6

6.4.3 Comparison of Model Results for 14h00 Temperature Gradient

The results of the finite element (FE) and layered elastic theory (LET) models for the early afternoon (14h00) temperature gradient are summarized in Table 6.10. Detailed results in the form of influence lines are shown in Appendix D.

Table 6.10: Comparison of Model Results for 14h00 Temperature Gradient

Evaluation Position	Maximum Tensile Strain (microstrain)		% Difference†	Octahedral Shear Stress (kPa)		% Difference†
	LET	FE		LET	FE	
Top of Asphalt Surface	53	11	-79.0	194	202	4.1
Middle of Asphalt Surface	NA	NA	NA	213	222	4.2
Bottom of Asphalt Surface	234	231	-1.3	209	217	3.8

6.4.4 Conclusions: Structure 1

The results shown in Tables 6.9 and 6.10 indicate that a temperature gradient and its corresponding effect on asphalt stiffness does not have a significant influence on the estimated stresses and strains. This observation is supported by the results shown in Appendix D, which indicate that the stress and strain values at different offsets from the load generally exhibit similar patterns for the two models, despite the differences in absolute values.

Differences between model results were in all cases less than 5 per cent for the critical stress and strain values. This observation can, to a certain extent, be ascribed to the fact that the response of a thin asphalt layer is to a large degree governed by the supporting structure and the applied load. Because of its thinness, any changes in the stiffness of a thin asphalt layer are slow to be reflected in the calculated stresses and strains of the structure.

It should, however, be noted that the above results merely indicate that the effect of a varying stiffness with depth in a thin asphalt layer is not significant. Efforts should still be made to ensure that the stiffness values used in the analysis are representative of the prevailing temperature

conditions. If, for example, the effects of temperature are ignored altogether and a stiffness of 2500 MPa, as measured at 25°C, is used to represent afternoon conditions in warm summer months, then the results will be as shown in Table 6.11.

As can be seen from Table 6.11, large differences (as high as 63 per cent for some critical values) between the FE and more simplified LET model results occur if seasonal fluctuations in temperature and stiffness are not taken into account. Tables 6.9 and 6.10, however, indicate that, in the case of thin asphalt layers, it is not critical that the asphalt stiffness be varied with depth, provided that the layer stiffness is fairly representative of the average stiffness of the layer.

Table 6.11: Comparison of Model Results when a Constant Asphalt Stiffness Representative of 25°C Temperature is Used to Represent Afternoon Summer Conditions

Evaluation Position	Maximum Tensile Strain (microstrain)		% Difference†	Octahedral Shear Stress (kPa)		% Difference†
	LET	FE		LET	FE	
Top of Asphalt Surface	42	11	-73.8	469	202	-56.9
Middle of Asphalt Surface	NA	NA	NA	330	222	-32.7
Bottom of Asphalt Surface	256	231	-9.8	595	217	-63.5

6.5 Analysis Results: Structure 2

6.5.1 Comparison of Models for Identical Input Values

As in the case of structure 1, benchmarking was performed to ensure that the differences between the calculated stresses and strains were due to temperature variation in the asphalt rather than to differences between the models themselves. For the finite element model, the layer thicknesses and Poisson's ratios shown in Table 6.4 were used, but the asphalt stiffness of each sub-layer was set to 2500 MPa. The LET model input values used in the benchmarking were as shown in Table 6.2. The benchmarking results are shown in Table 6.12.

The results shown in Table 6.12 show that the values obtained with the two models compare very well. The values suggest that differences in stresses and strains that are larger than 2 per cent may be attributed to temperature gradient effects rather than to inherent differences between the finite element and layered elastic models.

Table 6.12: Comparison of Model Results for Similar Input Values

Evaluation Position	Maximum Tensile Strain (microstrain)		% Difference†	Octahedral Shear Stress (kPa)		% Difference†
	LET	FE		LET	FE	
Top of Asphalt Base	30	30	0.0	201	201	0.0
Middle of Asphalt Base	NA	NA	NA	177	177	0.0
Bottom of Asphalt Base	167	167	0.0	253	250	-1.2

* LET = Layered Elastic Theory.

** Fe = Finite Element Model.

† Differences between values were calculated using LET results as base values.

6.5.2 Comparison of Model Results for 07h00 Temperature Gradient

The results of the finite element (FE) and layered elastic theory (LET) models for the early morning (07h00) temperature gradient are summarized in Table 6.13. Detailed results in the form of influence lines are shown in Appendix D. It should be noted that for the FE analysis, the asphalt surfacing was subdivided as shown in Table 6.4. For the LET analysis, the asphalt was not subdivided and only a single stiffness was used to represent the asphalt layer. The pavement structure used in the LET model is defined in Table 6.6 (07h00 temperature gradient).

Table 6.13: Comparison of Model Results for 07h00 Temperature Gradient

Evaluation Position	Maximum Tensile Strain (microstrain)		% Difference†	Octahedral Shear Stress (kPa)		% Difference†
	LET	FE		LET	FE	
Top of Asphalt Surface	31	28	-9.7	202	209	3.5
Middle of Asphalt Surface	NA	NA	NA	179	183	2.2
Bottom of Asphalt Surface	157	159	1.3	259	238	-8.1

6.5.3 Comparison of Model Results for 14h00 Temperature Gradient

The results of the finite element (FE) and layered elastic theory (LET) models for the early afternoon (14h00) temperature gradient in structure 2 are summarized in Table 6.14. Detailed results in the form of influence lines are shown in Appendix D.

Table 6.14: Comparison of Model Results for 14h00 Temperature Gradient

Evaluation Position	Maximum Tensile Strain (microstrain)		% Difference†	Octahedral Shear Stress (kPa)		% Difference†
	LET	FE		LET	FE	
Top of Asphalt Surface	77	119	54.5	194	183	-5.7
Middle of Asphalt Surface	NA	NA	NA	166	157	-5.4
Bottom of Asphalt Surface	242	233	-3.7	183	216	18.0

6.5.4 Conclusions: Structure 2

As in the case of the thin asphalt surfacing, the results shown in Tables 6.13 and 6.14 indicate that a temperature gradient and its corresponding effect on asphalt stiffness does not have a very large effect on the estimated stresses and strains in the asphalt base. Although a difference as high as 18 per cent was noted in the case of the 14h00 temperature gradient, this value - when considered in the context of the general pattern that emerges in Tables 6.13 and 6.14 - is not considered to be unacceptably high.

6.6 Summary and Conclusions

In this chapter, the effects of temperature and stiffness variations in asphalt layers on estimated stresses and strains were evaluated. The temperature variation used in the analysis was based on measured data¹³, and represented early morning and afternoon temperatures for warm summer months. Two types of models were studied. In the more rigorous FE model the asphalt layer was subdivided into several sub-layers, and each layer was assigned a different stiffness based on the temperature at the mid-depth of the layer. The results obtained with this model were compared with those of the conventional layered elastic model, in which the asphalt was modelled as a single layer with a constant stiffness.

The results of the analysis indicate that temperature variations with depth in asphalt layers do not have a significant effect on calculated stresses and strains, provided that the average temperature in the asphalt layer is representative of field conditions. The differences between stresses and strains obtained with the FE model (with subdivided asphalt layer) and layered elastic model (with undivided asphalt layer) are generally less than 5 per cent for thin asphalt surfacings. For thick asphalt bases, somewhat larger differences (up to 18 per cent in isolated cases) were noted.

In general, it can be concluded from the analysis results that variations in temperature and stiffness with depth do not lead to large modelling differences. However, total neglect to take account of the fluctuation of asphalt stiffness with temperature can lead to large differences for some performance parameters. If, for example, an average asphalt stiffness obtained at 25 °C is used to represent the asphalt response for summer afternoon temperatures (where temperatures may reach 50°C or higher), differences in excess of 50 per cent may occur. In effect, this suggests that asphalt stiffness is an important input parameter and emphasises the importance of obtaining a measurement of asphalt stiffness over a range of temperatures. Most

current design methods use only a single stiffness value to represent the asphalt response over all seasons and temperatures. The findings of this analysis indicate that this may not be sufficient and that a cumulative damage approach, in which the damage is estimated and added for different seasons, may have to be considered.

7. VISCOELASTIC EFFECTS

7.1 Introduction

Laboratory experiments and practical experience^{15,16,17} show that asphalt response is dependent not only on temperature but also on the rate and duration of loading. A typical asphalt response to a constant load would be an immediate strain at the instant that the load is applied, followed by a slow and continuous increase of strain - at a decreasing rate - for as long as the load is applied. This is called viscoelastic behaviour and is illustrated in Figure 7.1. This figure shows that the total strain response consists of three components: (i) an immediate elastic strain (ii) a permanent, or viscous strain and (iii) a viscoelastic strain which is time-dependent but recoverable. The first is independent of loading time and is also fully recoverable and the latter two are dependent on the duration of loading,

Because the stresses and strains in a viscoelastic material are dependent on the duration of loading, it follows that the stresses and strains in an asphalt layer subjected to dynamic wheel loading will also be dependent on the speed of loading. It also means that the response of an asphalt layer to a stationary vehicle will change with time.

Although viscoelastic effects in asphalt pavement analysis are also concerned with the speed of at which the load moves, viscoelastic effects should not be confused with dynamic effects. Dynamic effects, as discussed in Chapter 2, deal with the forces that are generated by acceleration and damping of the structure as a whole. Although viscoelasticity can also be considered as a form of damping, it only describes the relation between the stress and the strain of the asphalt (or of any other viscoelastic material in the structure). It is therefore only concerned with the constitutive behaviour of the asphalt under a given stress condition.

As a broad simplification, it can be said that viscoelastic models of asphalt pavement behaviour - like conventional layered elastic models - do not take account of the first two terms in equation 2.1. However, unlike conventional layered elastic models, viscoelastic models of asphalt pavement behaviour consider a time-dependent stiffness. In other words, the stiffness term k in equation 2.1 is not constant but is a function of the time of loading. It should be noted that this is a considerable simplification, offered merely to illustrate the difference in emphasis between viscoelastic and fully dynamic models. The actual mechanics of viscoelastic models involve considerably more than mere adjustment of the stiffness of the material as a function of loading time.

In recent years, viscoelastic constitutive models of asphalt have been implemented in multi-layer pavement analysis models. Results obtained by Hopmann¹⁶ suggest that viscoelastic pavement models can more accurately match the strain response as measured under a slowly moving wheel load than conventional layered elastic models. Strain influence lines obtained with viscoelastic models differ in shape and magnitude from those obtained when conventional layered elastic theory (LET) models are used.

Although the results published by Hopmann¹⁶ indicate that it is important to take viscoelastic effects into account, the consequences of ignoring such effects (as is done in conventional LET models) during routine asphalt pavement design have not been adequately investigated. In this chapter, aspects of viscoelastic modelling are investigated in order to obtain an indication of the relative importance of viscoelastic effects in asphalt pavement design and analysis.

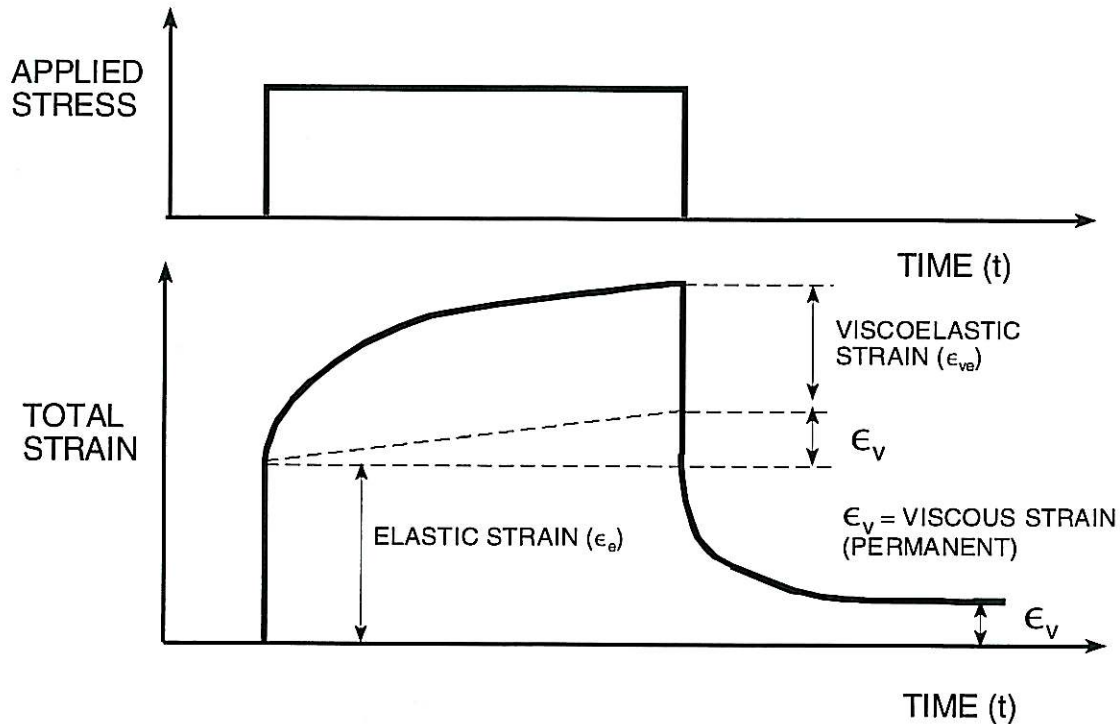


Figure 7.1: Typical Behaviour of Asphalt during constant Stress Loading

7.2 Pavement Structures and Assumed Material Properties

Two pavement structures were considered in this investigation: the first structure consisted of a thin (40 mm thick) asphalt surfacing on a granular base and subbase. The second structure consisted of a 40 mm thick asphalt surfacing on an asphalt base of 120 mm thickness, underlain by a granular subbase. These structures are defined in Tables 7.1 and 7.2. The load assumed in the modelling process was a 20 kN single wheel with a contact pressure of 650 kPa (contact radius of 99 mm).

Table 7.1: Structure 1: Assumed Material Properties and Layer Thicknesses

Layer	Stiffness Modulus (MPa)	Poisson's Ratio	Thickness (mm)
Asphalt Surfacing	Viscoelastic (time-dependent)	0.40	40
Granular Base	400	0.40	150
Granular Subbase	200	0.40	150
Subgrade*	70	0.40	2000

* To ensure compatibility between models, it was assumed that the subgrade was underlain by a stiff layer.

Table 7.2: Structure 2: Assumed Material Properties and Layer Thicknesses

Layer	Stiffness Modulus (MPa)	Poisson's Ratio	Thickness (mm)
Asphalt Surfacing	Viscoelastic (time dependent)	0.40	40
Asphalt Base	Viscoelastic (time dependent)	0.40	120
Granular Subbase	300	0.40	150
Subgrade*	70	0.40	1690

* To ensure compatibility between models, it was assumed that the subgrade was underlain by a stiff layer.

The approach adopted was to use a viscoelastic pavement analysis model to determine the responses under wheel loads moving at two different speeds (20 and 80 km/h). The results obtained with the viscoelastic model were then compared with those obtained by layered elastic theory (LET). The viscoelastic model used was that developed by Hopmann (called VEROAD). Viscoelastic modelling was performed under the guidance of Dr. Piet Hopmann by Netherlands Pavement Consultants (NPC).

The viscoelastic model used in the VEROAD computer program is illustrated in Figure 7.2. This model is referred to as the Burgers model, and can fairly accurately simulate the type of response shown in Figure 7.1. It can be seen from Figure 7.2 that the Burgers model requires four material parameters to characterize the asphalt response. The parameters assumed for the purposes of this analysis for structures 1 and 2 are summarized in Table 7.3.

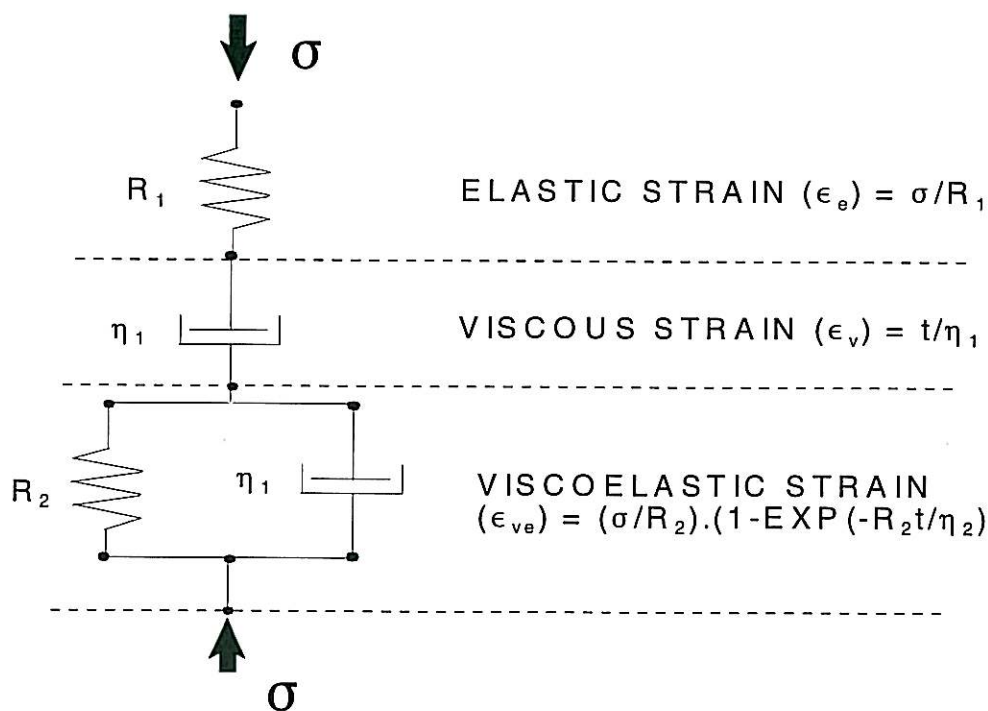


Figure 7.2 Rheological Model used in VEROAD program

Table 7.3 Burgers Model Parameters used in VEROAD

Parameter related to:	Asphalt Surfacing for Structures 1 and 2	Asphalt Base for Structure 2
Immediate Elastic Strain (spring in series) (R_1 in Figure 7.2)	3 500	2 300
Delayed Elastic Strain (spring in parallel) (R_2 in Figure 7.2)	5 000	3 500
Permanent Strain (viscous damper, η_1 in Figure 7.2)	10 000	10 000
Delayed Elastic Strain (damper in parallel) η_2 in Figure 7.2)	500	400

The model parameters assumed for the analysis are roughly based on laboratory test results measured at short loading times under constant loading conditions. The parameters were thus chosen to be fairly representative of the observed asphalt response, specifically with regard to (i) the ratio between the delayed and immediate strain components, and (ii) the ratio between the permanent strain and the total strain.

Figure 7.3 shows the theoretical strain response for the material parameters assumed for the asphalt surfacing of structures 1 and 2 (i.e. the values shown in column 2 of Table 7.3), together with the laboratory-measured strain response for a continuously graded asphalt mix. It can be seen that there is a good agreement between the measured and theoretical strain responses. It should, however, be noted that the measured response shown in Figure 7.3 was scaled to have the same maximum value as the theoretical strain response. There was thus some difference between the absolute values of the theoretical and measured strains. However, the most important point to note is that the theoretical model matches the measured response in shape as well as in the amount of permanent deformation present after loading.

7.3 Layered Elastic Response Model

In order to ensure that the layered elastic response model results approximate those of the viscoelastic response model, a judicious choice has to be made of the asphalt stiffness to be used in the layered elastic response calculations. One approach, discussed by Huang¹⁵, is to use the inverse of the Burgers model compliance, calculated at a loading time that is similar to the time needed for a vehicle to pass over a point in the pavement system at a given speed. This method is discussed in detail by Huang¹⁵ and will not be described here. Other details of the method, such as the definition of Burgers model compliance can also be found in Findley et al.¹⁷.

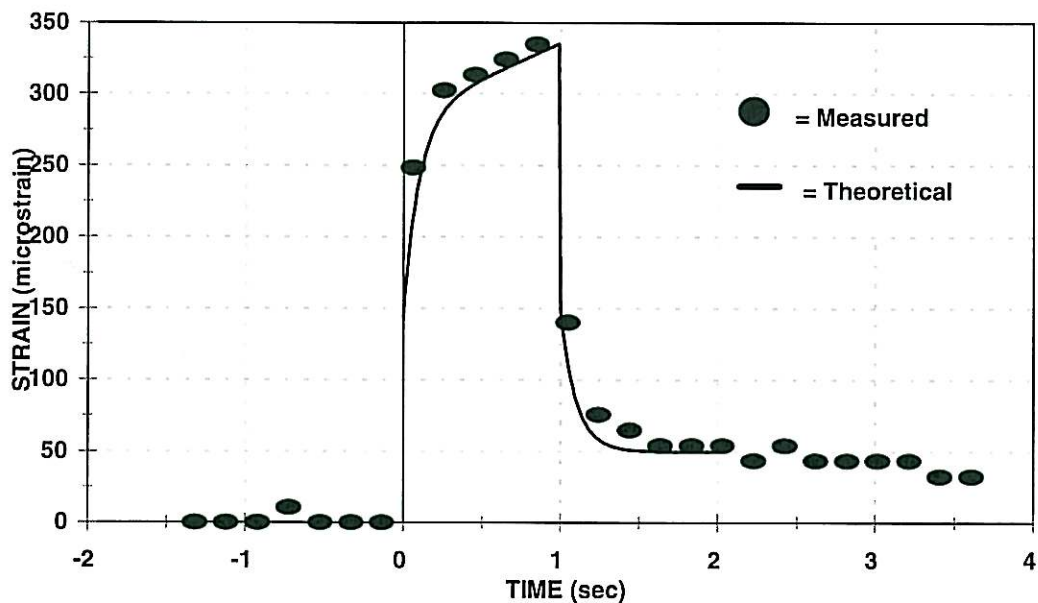


Figure 7.3 Measured and Theoretical Strain Response for the Material Parameters shown in Column 2 of Table 7.3

The method of using the inverse of the Burgers model compliance was not used in this analysis. Instead, the asphalt stiffness was simply assumed to be equal to the stiffness of the series-spring (R_1 in Figure 7.2) in the Burgers model. *Thus, for the simplified layered elastic model the stiffness of the asphalt surfacing of structures 1 and 2 was assumed to be 3500 MPa, and the stiffness of the base for structure 2 was assumed to be 2300 MPa.* This assumption is based on the fact that, for speeds of more than 20 km/h, the time taken for the induced stress pulse to reach a peak is likely to be well below 0.2 seconds for points in the upper part of the pavement structure. For speeds of 80 km/h and greater, this time is likely to be below 0.05 seconds. It can be seen from Figure 7.3 that, at such short loading times, the immediate elastic strain component is far greater than either the delayed elastic or permanent strain components. It can therefore be assumed that the total strain response will be represented fairly accurately by the immediate "stiffness" represented by the series spring in Figure 7.2.

7.3 Results

7.3.1 Structure 1

The results of the viscoelastic (VEROAD) and conventional layered elastic theory (LET) models for structure 1 are summarized in Tables 7.4 and 7.5. It should be noted that the tensile strains shown in Table 7.4 were calculated at the bottom of the surfacing. Neither of the two models calculated large tensile strains at the top of the surfacing. Values shown in bold in Tables 7.4 and 7.5 represent the most critical values. It should be noted that the differences in Tables 7.4 and 7.5, as well as in other tables that follow were calculated using the VEROAD results as base value. Thus a positive error indicates that the LET model is more conservative (i.e. predicts higher stresses or strains) than the viscoelastic model.

Table 7.4: Summary of Maximum Horizontal Tensile Strain Results: Structure 1

Position in Surfacing	LET Strain (microstrain)	VEROAD Results for 20 km/h		VEROAD Results for 80 km/h	
		Strain (microstrain)	% Diff. in LET*	Strain (microstrain)	%Diff. in LET*
Bottom	228	237	-3.8	236	-3.4

* Errors were calculated using VEROAD results as base values

Table 7.5: Summary of Octahedral Shear Stresses: Structure 1

Position in Surfacing	LET Stress (kPa)	VEROAD Results for 20 km/h		VEROAD Results for 80 km/h	
		Stress (kPa)	% Diff. in LET*	Stress (kPa)	%Diff. in LET*
Top	745	648	15.0	716	4.1
Middle	8	33	-75.8	27	-70.4
Bottom	706	671	-5.2	706	0.0

* Differences were calculated using VEROAD results as base values

7.3.2 Structure 2

The calculated results for structure 2 are summarized in Tables 7.6 and 7.7 for the maximum horizontal tensile strains and octahedral shear stresses, respectively.

Table 7.6: Summary of Maximum Horizontal Tensile Strain Results: Structure 2

Layer	Position in Layer	LET Strain ($\mu\epsilon$)	VEROAD Results for 20 km/h		VEROAD Results for 80 km/h	
			Strain ($\mu\epsilon$)	% Diff. in LET*	Strain ($\mu\epsilon$)	% Diff. in LET*
Surfacing	Bottom	Strains were all negligible (less than 10 microstrain)				
Base	Bottom	150	162	-7.4	153	-2.0

* Differences were calculated using VEROAD results as base values

Table 7.7: Summary of Octahedral Shear Stresses: Structure 2

Layer	Position in Surfacing	LET Stress (kPa)	VEROAD Results for 20 km/h		VEROAD Results for 80 km/h	
			Stress (kPa)	% Diff. in LET*	Stress (kPa)	% Diff. in LET*
Surfacing	Top	264	235	12.3	238	10.9
	Middle	58	38	52.6	44	-13.6
	Bottom	106	112	-5.4	110	-3.6
Base	Top	100	111	-9.9	111	-9.9
	Middle	171	163	4.9	167	2.4
	Bottom	285	256	11.3	267	6.7

* Differences were calculated using VEROAD results as base values

7.4 Discussion

The results shown in Tables 7.4 to 7.7 indicate that, for the material properties and vehicle speeds assumed for this analysis, viscoelastic effects do not have a significant influence on the most critical predicted response. As can be expected from the nature of viscoelastic responses, the VEROAD model predicts that strains tend to increase at lower speeds while stresses tend to decrease. These effects are due to the effective "softening" of the asphalt at longer loading times (i.e. slower speeds) which lead to reduced stress and increased strain. It can also be expected that the agreement between the viscoelastic and conventional linear elastic (LET) models will improve at higher speeds when the immediate elastic strain dominates the overall strain response.

In the case of structure 1, the largest tensile strain was calculated with the viscoelastic model for the 20 km/h speed. This strain was only 3.8 per cent higher than the corresponding elastic solution. The octahedral shear stresses calculated with the LET and viscoelastic models also agreed fairly well, the difference between the most critical values being 4.1 per cent. However, the octahedral stress results indicate that larger differences can be expected at lower speeds. Except for the low octahedral stresses in the middle of the layer, all the differences between model predictions were less than 20 per cent.

The results for structure 2 also indicated that the differences between the two models are likely to be less than 20 per cent. For the most critical strain values, the largest difference was -7.4 per cent. For the most critical octahedral shear stress values, the largest difference was 10.9 per cent.

7.5 Summary and Conclusions

In this chapter, an analysis was presented in which asphalt response was estimated with a conventional layered elastic and a viscoelastic response model. The viscoelastic response model is capable of taking account of delayed elastic and permanent strains which are a function of vehicle speed.

The overall conclusion drawn from this analysis is that viscoelastic effects are not critical for vehicle speeds of more than 20 km/h. It should be emphasized, however, that this analysis was based on only one set of assumed material parameters. Although this set of parameters is deemed to be fairly representative of material response as measured in the time domain (see Figure 7.3), viscoelastic effects may become more significant for materials that exhibit higher permanent deformation and delayed elastic response components, and also for vehicles moving at speeds of less than 20 km/h. However, in the context of the overall study reported here, and when considered relative to the effects of dynamics, non-uniform tyre pressures and random variations in stiffness, layer thicknesses etc., viscoelastic effects do not seem to be critical for accurate determination of key response parameters in asphalt pavements.

8. CONCLUSIONS, DISCUSSION AND RECOMMENDATIONS

8.1 Summary

This study consisted of an evaluation of the suitability of conventional layered elastic theory (LET) programs for evaluating the stress and strain responses in asphalt layers. The general approach followed was to investigate several effects (such as dynamics, viscoelasticity and non-uniform tyre pressures) which cannot be adequately accounted for in conventional layered elastic models. More complex response models in which these effects could be included were used to evaluate responses in the asphalt layer. These responses were then compared with those which had been calculated with the simplified layered elastic model. Specific effects investigated in the study were:

- i) Effects of dynamic loading;
- ii) Effects of non-uniform tyre pressures;
- ii) Horizontal shear force effects;
- iv) Effects of non-uniform support systems;
- v) Effects of temperature and stiffness gradients in asphalt layers, and
- vi) Viscoelastic effects.

It should be noted that the results of this study cannot be viewed as a comprehensive analysis of all of the above effects. Flexible pavement response is highly non-linear, and the relative importance of certain effects is therefore bound to vary for different values of input parameters such as stiffness, vehicle speed, layer thickness etc. Within the constraints of this project, only a limited set of structure types and input variables could be studied. However, it is believed that the input variables and pavement structures that were analysed are representative of many of the most frequently occurring situations in South Africa. The conclusions that follow are therefore regarded as valid for many pavement design situations and provide a meaningful indication of effects that can be considered as vital for an accurate representation of asphalt layer response.

8.2 Conclusions for Selected Effects

8.2.1 Dynamic Effects (influence of vehicle speed)

The analysis of dynamic effects lead to the following conclusions:

Fatigue-related Issues:

Static response models such as conventional layered elastic models overestimate the tensile strains in the asphalt layer by 50 per cent or more. This was found to be the case for both pavement structures and for both the simulated vehicle speeds (20 and 80 km/h). The modelled effects of dynamic loading on tensile strains at the bottom of the asphalt layers generally agree with published results and field measurements. *The analysis results therefore suggest that the more approximate LET model will grossly overestimate the tensile strains of asphalt layers and will therefore also tend to underestimate the fatigue life of asphalt layers if that fatigue life estimate is based on an absolute estimate of tensile strains.* The very low strains estimated by the dynamic finite element model also suggest that the mechanism which causes fatigue cracking may not be properly understood at present.

Rutting-related Issues:

In the case of the rutting parameter (octahedral shear stress), large differences between static and dynamic model results were noted. The effects of dynamic loading on octahedral shear stresses are not as clear as for tensile strains. In general, the dynamic response model predicts higher vertical stresses and lower horizontal stresses than the static model. The relative differences between the static and dynamic model results depend on the evaluation position. In all cases the maximum octahedral shear stress was predicted by the static LET model. This result was generally higher than the corresponding value predicted by the dynamic model. *The analysis results thus suggest that static models will tend to overestimate the rutting potential of asphalt mixes for pavement sections on which vehicle speeds are likely to exceed 20 km/h.*

It should be noted that only the effects of dynamic loading on the induced stresses and strains were investigated in the analysis of dynamic effects. Dynamic effects are also likely to play a role in determining the resistance of asphalt mixes to fatigue and rutting at a specified applied stress state. This is especially relevant in the case of rutting, where the rate of loading not only affects the applied stress, but also affects the amount of flow induced in the asphalt mix.

8.2.2 Non-uniform Tyre Pressure Distributions

The analysis of non-uniform tyre pressure distributions prompted the following conclusions:

Fatigue Implications: The results indicate that, for thin asphalt surfacings on granular support layers, non-uniform contact stress distributions can have a significant effect on the maximum horizontal tensile strains. Conventional LET models in which a uniform, circular contact stress is assumed can underestimate the maximum horizontal tensile strain in the asphalt surfacing (differences of 100 per cent and larger were observed). The effect of contact pressure shape and distribution on horizontal tensile strains diminish with depth. Consequently the effects of non-uniform tyre pressure distributions are not as great for asphalt bases as for thin asphalt surfacings (differences were less than 10 per cent).

Implications for Rutting: As expected, the analysis indicated that non-uniform contact stress distributions led to higher octahedral shear stresses than those calculated with conventional layered elastic models. The layered elastic model with a uniform circular contact stress generally underestimated the maximum octahedral shear stress in the asphalt layer by more than 20 per cent. This difference is caused partly by the shape of the load contact area, which is rectangular rather than circular.

It should be noted that the load and tyre pressure combination on which the analysis of non-uniform tyre pressures was based led to a somewhat extreme variation in contact stresses. The effects of non-uniform tyre pressures are thus likely to decrease under smaller wheel loads and tyre pressures that conform to manufacturers' specifications. Despite this observation, the results indicate that neglect to take account of the shape of the load contact area as well as of non-uniform tyre pressures can lead to underestimation of the rutting and fatigue potential of asphalt layers. Differences between the results obtained with different models suggest that non-uniform tyre pressure effects should be included in design calculations, or at the very least, that they warrant further investigation.

8.2.3 Horizontal Shear Force Effects

The analysis of horizontal shear force effects indicates that horizontal shear forces such as those that are induced by heavy vehicles moving on steep inclines do not significantly affect the response parameters that are related to fatigue and rutting. Differences between results of models in which shear force effects were simulated and those in which zero horizontal shear was assumed were generally below 10 per cent. These differences are not viewed as significant if they are considered relative to random errors which may occur due to variations in support conditions, material properties etc. It should, however, be noted that, as far as rutting potential is concerned, this conclusion applies only to the stress state induced in the asphalt layer. The duration of loading, which is greater for slowly moving traffic on inclines than for fast moving traffic on level surfaces, is bound to lead to an increased flow of the binder, and may therefore lead to a greater potential for rutting.

8.2.4 Effects of Non-uniform Support Layers

The analysis of the effects of non-uniform support layers indicate that the presence of a non-uniform support layer does not have a significant effect on the critical stress and strain parameters calculated in the asphalt surface. The results suggest that the simplified LET model, which does not take into account the change in support stiffness with increasing depth and increased offset from the load, can provide a reasonably accurate estimate (i.e. within 5 per cent of the more rigorous FE solution) of the most critical stress and strain parameters, *provided that the support stiffness is representative of the average stiffness of the support layer under the loaded area.*

The results indicate that, in routine pavement evaluation situations, reasonably large differences (generally in the order of 20 per cent) between the simplified LET model and the more representative finite element (FE) model can occur because of the simplifications in the backcalculation model. If the stiffness of the base varies significantly with depth, the backcalculated stiffness is likely to be lower than the average base stiffness. This means that stiffness of the immediate support (i.e. the upper base) is underestimated, resulting in overestimation of the tensile strains and shear stresses at the bottom of the asphalt surfacing. The practical implications of this may be a gross overestimation of the fatigue crack potential and rutting potential of thin asphalt layers.

8.2.5 Effects of Temperature and Stiffness Gradients in Asphalt Layers

The analysis of temperature gradient effects indicates that temperature variations with depth in asphalt layers do not have a significant effect on calculated stresses and strains, provided that the average temperature in the asphalt layer is representative of field conditions. The differences between stresses and strains obtained with the FE model (with subdivided asphalt layer) and those obtained with the layered elastic model (with undivided asphalt layer) are generally less than 5 per cent for thin asphalt surfacings. For thick asphalt bases, however, somewhat larger differences were noted.

In general, it can be concluded from the analysis results that variations in temperature and stiffness with depth do not lead to large modelling errors. However, total neglect to take account of the fluctuation of asphalt stiffness with temperature can lead to large errors for some performance parameters. If, for example, an average asphalt stiffness obtained at 25 °C is used to represent the asphalt response for summer afternoon temperatures (where asphalt temperatures may reach 50°C or higher), differences in excess of 50 per cent may occur. In effect, this suggests that asphalt stiffness is an important input parameter and emphasises the

importance of obtaining a measurement of asphalt stiffness over a range of temperatures. Most current design methods use only a single stiffness value to represent asphalt response over all seasons and temperatures. The findings of this analysis indicate that this may not be sufficient and that a cumulative damage approach in which the damage is estimated and added for different seasons may have to be considered.

8.2.6 Viscoelastic Effects

The overall conclusion drawn from the analysis is that viscoelastic effects are not critical for vehicle speeds of more than 20 km/h. It should be emphasized, however, that this analysis was based on only one set of assumed material parameters. Although this set of parameters is deemed to be fairly representative of material response as measured in the time domain, viscoelastic effects may become more significant for materials that exhibit a higher permanent deformation and delayed elastic response components, and also for vehicles moving at speeds of less than 20 km/h. However, in the context of the overall study reported here, and when considered relative to the effects of dynamics, non-uniform tyre pressures and random variations in stiffness, layer thickness etc., viscoelastic effects do not seem to be critical in the accurate determination of key response parameters in asphalt pavements.

8.3 Further Conclusions and Discussion

It was noted in section 8.2 as well as in the introductory chapter that the analyses presented in this report were subject to limited sets of input parameters and pavement situations. In view of this, some of the conclusions noted above for certain effects could be disputed. A more rigorous and expensive study coupled with field and laboratory measurements may indicate that some of the effects may be more or less important than indicated by this brief study.

However, one observation that cannot be disputed is that conventional layered elastic theory cannot provide an accurate estimate of stresses and strains in asphalt layers in situations that involve moving traffic (with speeds greater than 20 km/h) over support systems of uncertain stiffness in which wheel loads and contact pressure distributions are not known.

Since serious consideration of the above statement is likely to have a profound influence on the manner in which asphalt pavements are designed, some qualification should perhaps be made of what is meant by "an accurate estimate of stresses and strains". Practitioners who are charged with the design of asphalt pavement frequently defend the use of layered elastic models by stating that the models are accurate enough, given the coarse and robust nature of pavement material behaviour. To evaluate this statement, consider a design situation in which the objective is to design a thin asphalt layer for an A-category road. Assume that the pavement design is as defined in Table 2.1. If the design in terms of fatigue life is to be based on tensile strain at the bottom of the asphalt layer, the following results will be obtained for different modelling and actual scenarios:

1. Multi-layer Elastic Theory Model (current routine design)
Approximate maximum tensile strain: 250 microstrain (see Table 2.3 on page 2-3)
Approximate Expected Fatigue Life: **250 000 repetitions**
2. Three-Dimensional Dynamic Finite Element Model, Vehicle Speed 20 km/h
Approximate maximum tensile strain; 110 microstrain (see Table 2.3 on page 2-3)
Expected Fatigue Life: **18 million repetitions**

3. Three-Dimensional Dynamic Finite Element Model, Vehicle Speed 80 km/h
Approximate maximum tensile strain; 90 microstrain (see Table 2.3 on page 2-3)
Expected Fatigue Life: **50 million repetitions**

The expected fatigue life calculations are based on the transfer functions used in the South African mechanistic design method and include a shift factor of 2 to account for crack propagation¹⁸. Several observations follow from, or can be added to, this example:

- i) Differences between predictions made by the models are significant, even when considered in terms of pavement design classes. The three scenarios effectively lead to three different pavement design classes.
- ii) None of the three design calculations really conforms to the expected life for a thin asphalt surfacing on a proper granular support.
- iii) Any of the three design calculations will be invalid if the fatigue resistance characteristics of the design mix differ significantly from the "generic" transfer function used for the design calculations. *This implies that the pavement design function may to a large extent be governed or even overridden by the materials design function.*

A statement that is also often made in defence of the use of multi-layer elastic theory, is that it offers a convenient way of comparing the expected performance of different pavement designs. It is also frequently asserted that the current use of multi-layer elastic programs for the design of asphalt layers has been calibrated with field experience. However, these statements prompt the following questions:

- i) If the only valid use of multi-layer elastic theory is to compare different designs with one another, and if the approach requires a large element of field calibration, why is such a complex approach chosen in which there is uncertainty regarding many of the variables that may in fact reverse the outcome of the comparison?
- ii) Does this use of the multi-layer elastic method, coupled with the findings of this study, not indicate that the method *merely provides an erroneous quantification* of pavement design principles which are already established and have been verified through accelerated testing (examples of such principles include: the importance of pavement balance, importance of support stiffness to asphalt layer performance, etc.)?
- iii) Is a simpler, more robust approach, such as the use of the method of equivalent thicknesses¹⁹, which can be performed on a hand-held calculator, or the DCP design method²⁰ not more pertinent and cost-effective and even more rational for use in routine asphalt pavement design situations?

A further issue that should enter this discussion is that, even for the more accurate dynamic response model, differences in the estimated tensile strains are significant for small changes in input values (speed being the input value for the example illustrated above). If the estimation of fatigue life is based on tensile strain, then this also implies a sensitivity of fatigue life estimates to input values. This sensitivity is likely to be even greater when variations in other parameters such as layer thickness, material stiffness, load magnitude etc. are considered at the same time. This means that, for performance models based on tensile strain, the three-dimensional finite element program will also not provide an accurate estimate of design life unless the vehicle speed, layer thicknesses, material stiffnesses etc. are known.

While it is conceivable that all of these parameters may be measurable (at considerable cost) at a specific point in a road, what cannot be avoided is the variation of these parameters over a given

length of road. Thus an accurate prediction of asphalt performance may be possible at a specific point in a road (if all relevant parameters are known at that point), but this will vary from point to point. A comparison of the fatigue life estimates of scenarios (2) and (3) indicates to what extent such an estimate will vary. This explains why some parts of an asphalt surfacing may exhibit cracks after two years while large sections of the same road may remain intact for 12 years or more.

It is hoped that the above discussion provides enough evidence for the following statements to be made:

- i) The current approach to routine design of asphalt pavements using conventional layered elastic theory models cannot be expected to provide an *accurate estimate of absolute performance* of asphalt layers;
- ii) Conventional layered elastic theory models can be used to provide a qualitative assessment of pavement behaviour but their use is not necessarily the most cost-effective or even the most rational way of comparing different design situations. Simpler design methods, which contain fewer variables which can be determined with greater reliability and at reduced cost, may be more appropriate;
- iii) Precise estimates of asphalt layer responses and performance are not meaningful. In order to accommodate the full spectrum of possible values that important input parameters can take on, estimates of pavement life need to be expressed in coarse and robust terminology. Failure to do so will lead to unrealistic expectations as far as the pavement design function of asphalt design is concerned.

8.4 Recommendations

It should be clear from the above discussion that a new approach to the structural design function of asphalt mix design is needed. In essence, there are two possibilities: (i) a more complex and accurate response model has to be developed for use in routine design situations; or (ii) a robust, simplified and more rational approach to the pavement design function has to be developed. It is recommended that a simplified, rational pavement design method be adopted for routine pavement design situations*². The reasons for this have been covered to a certain degree in the preceding section, but can be summarized as follows:

- Complex response models, such as dynamic, non-linear, anisotropic, viscoelastic three-dimensional finite element programs are only as accurate as their input values. As suggested in the previous discussion, an accurate measurement of properties such as vehicle speed, layer thickness, density, material stiffness, Poisson's ratio's and damping characteristics is vital if the estimates of stresses and strains are to be truly accurate. However, such measurements are not considered feasible for routine design purposes and may not even be possible for the design of new pavements. The use of "generic" input values such as those obtained from literature or published tables is not sufficient, since it is simply not rational to supply unreliable and inaccurate input data to a very

*1 The phrase "rational pavement design method" was coined by Mr. Hechter Theyse of Transportek CSIR, during discussions with the one of the authors.

expensive and complex response model and then claim that the resulting stresses and strains are accurate.

- Because of the nature of pavement materials and pavement construction processes, input values such as layer thicknesses, stiffnesses, Poisson's ratios, densities and damping characteristics are likely to vary significantly over even a short length of road. Thus a proper stochastic simulation of pavement response will indicate that pavement life may vary significantly over a nominally uniform section of road¹⁹. The proper use of complex response models is thus likely to result in a wide range of estimates of asphalt layer performance, even for a short section of road. Such imprecise estimates can also be obtained (at significantly reduced cost) by the use of simplified methods.

Although the above statements may seem to suggest that complex response models do not have a place in asphalt pavement design, this is not the case. Complex response models are vital to the development of an understanding of material behaviour and performance because they provide insight into failure mechanisms and assist in determining the most important parameters that affect material performance. The maximum horizontal tensile strains obtained with the dynamic three-dimensional finite element model, for example, suggest that an asphalt layer may not fail because of the (very low) induced tensile strain but may in fact crack for other reasons. It is therefore possible that a new mechanism for fatigue failure needs to be investigated.

Complex models are therefore vital for obtaining an increased understanding of pavement behaviour and performance. However, the use of these models should be restricted to the research domain where input parameters can be accurately determined and where the model results can be interpreted in a methodical and critical manner.

Knowledge gained in this manner should then be implemented in the routine mix and pavement design functions. The manner in which this knowledge is implemented in routine design situations, however, should be in the form of a relatively simple and robust method that is not prone to misuse or over-interpretation.

It is recognized that the proposal for developing a simplified, robust approach to the pavement design function of mix design is at variance with the more fundamental and complex approach that is being pursued in the United States and Europe. However, it is believed that the approach proposed here is based on sound reasoning and on a holistic approach to pavement design. The analyses presented in this report include many aspects of complexity and fundamentals. However, proper interpretation of these analyses, coupled with knowledge of the variability and uncertainty of pavement construction processes, suggest that a complex and refined approach is not the most **cost-effective** approach for routine design purposes. To a certain extent, therefore, the process followed in this study can be characterized by Figure 8.1 (the concept illustrated by Figure 8.1 was first suggested to one of the authors by Mr. Larry Schofield of the Arizona State Department of Transport).

The above discussions outline the principal reasons for the selection of a simplified, rational approach to the pavement design function of asphalt mix design. In the following paragraphs the most important characteristics of the proposed system are discussed.

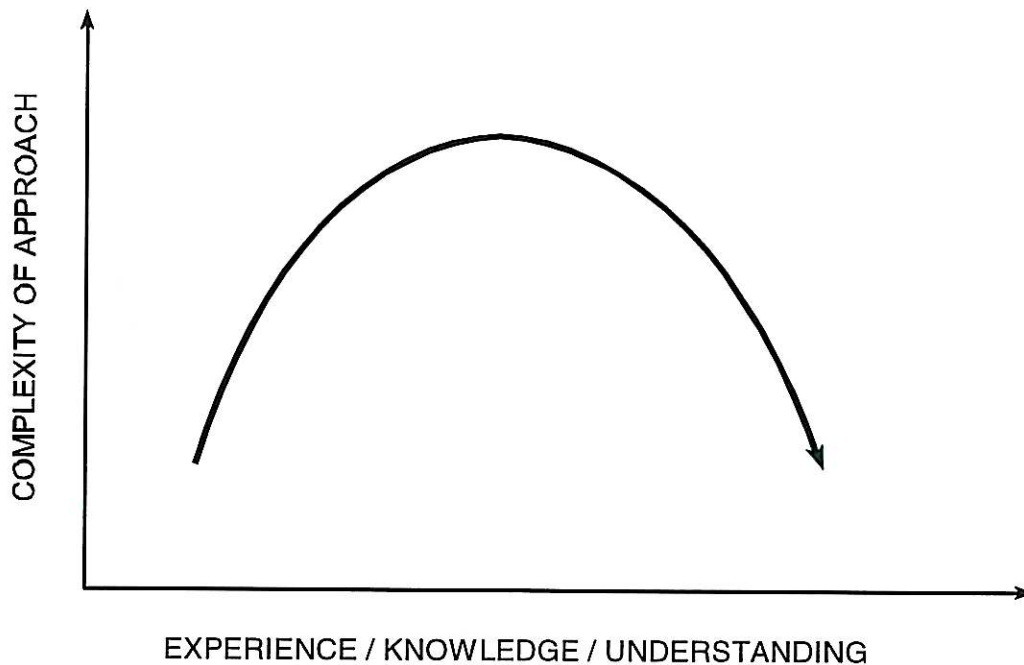


Figure 8.1 Conceptual Model to Support the Selection of a Simplified Approach to Asphalt Mix Design

Proposed Approach to the Pavement Design Function of Routine Asphalt Mix Design

The method proposed for the evaluation of the pavement design component of mix design should have the following characteristics:

- The system would follow a comparative approach and would contain a large element of knowledge-based calibration; Performance would not be predicted in absolute terms, but the system would ensure that the pavement design conforms to the principles set out in the TRH4 document and design catalogue²⁰.
- The essence of the method should consist of an expert system in which only those design principles which have been thoroughly tested and validated are embodied. Such a system could be computerized or represented in a graphical format. The system would typically require only first order input values such as (i) the thickness and stiffness of the asphalt layer (ii) maximum expected asphalt temperature, (iii) stiffness of the support layer, (iv) number of heavy vehicles expected over the design period, (v) probability of overloading and (vi) number of steep inclines, (vii) selected deflection bowl parameters (for rehabilitation design purposes).

These input values should be determined using reliable and well proven methods, and should be expressed in a manner that is consistent with the uncertainty of the measurement and the variability of the parameter in question. Stiffness of the support values should, for example, be expressed in classes such as very stiff (500 to 800 kPa), stiff (300 to 500 MPa) and weak (less than 300 MPa) and could therefore be based on coarse empirical estimates.

- The system would provide two primary outputs:
 - i) Recommended laboratory tests (with the recommended stress or strain state) to be used in the mix design phase; For example, for the evaluation of rutting potential by means of the dynamic creep test, it is essential that a confining stress be applied. The level of confinement and the magnitude of the overall stress would be dictated by the pavement system and load intensity. The expert system should therefore recommend broad classes of stress states to be used. Again, this recommendation would be imprecise and relative (e.g. "high" or "low" deviator stress).
 - ii) Expected ranges of performance for the various laboratory test methods. This would enable the designer to interpret his data and make a qualitative assessment of the expected performance of the design mix. The expected or typical ranges of performance of different test methods should be based on a data base of values and could be updated from time to time as experience and the quantity of available test data increases.

The approach outlined above essentially limits the resources that are expended on the pavement design function and places emphasis on the materials design function instead. It should be noted that the development of the proposed approach does not require expensive model building, accelerated testing or long term performance monitoring (although these elements should be pursued as part of the research function and should ideally be used to update and refine the proposed method from time to time). In essence, the *development* of the proposed method would require the gathering and formalizing of existing knowledge, coupled with a limited set of mechanistic design calculations using the most advanced models available.

Required Input Parameters to be Determined from Materials Testing

As already suggested by the above discussion, only one parameter is needed to serve as input into the structural design function. This is true, regardless of whether the proposed approach is adopted or of whether the current use of multi-layer elastic theory is retained. *This parameter is the mix stiffness, or resilient modulus, at a range of test temperatures.* Although the Poisson's ratio is also needed as input into conventional multi-layer elastic models, this parameter is known to be highly variable and non-linear in behaviour, as well as to be highly dependent on the test method. Sufficiently accurate measurement of this parameter during routine mix design is therefore not considered to be viable. If the use of the multi-layer elastic theory for qualitative evaluation of asphalt pavements is retained, then it is recommended that the Poisson's ratio be determined using published values such as those proposed in the South African mechanistic design method.

9. References

1. OWEN, D.R.J. and Hinton E. 1980. **Finite Elements in Plasticity. Theory and Practice**, Pineridge Press, Swansea, United Kingdom.
2. HOFFMAN O. and Sachs, G. 1953. **Introduction to the theory of plasticity for engineers**. New York: McGraw-Hill Book Company Inc.
3. LITTLE, D.N. and Youssef, H.A. 1992. **Improved ACP mixture design: development and verification**. College Station, Texas: Texas Transportation Institute. (Research Study No. 2-9-88-1170).
4. BROWN, S.F. and Bell, C.A. 1977. The validity of design procedures for the permanent deformation of asphalt pavements. In: **Fourth International conference on the structural design of asphalt pavements**, Vol I, Ann Arbor, pp. 467-482.
5. LOURENS, J.P. 1991. **Nonlinear dynamic analysis and design of road pavements**. Pretoria: Department of Transport: National Roads. South African Roads Board (Interim Report IR 90/030/1).
6. HARDY, M.S.A. and Cebon, D. 1994. Importance of speed and frequency in flexible pavement response. **Journal of Engineering Mechanics, ASCE**, Vol 120, No. 3.
7. SEBAALY, Peter E. and Tabatabaee, Nader. 1993. Influence of vehicle speed on dynamic loads and pavement response. In: **Pavement design, management, and performance; pavement monitoring and evaluation**. Washington, DC: Transportation Research Board, National Research Council. (Transportation Research Record; No. 1410), pp. 107-114.
8. De BEER, M. 1994. Measurement of tyre/pavement interface stresses under moving wheel loads. **Vehicle-Road and Vehicle-Bridge Interaction Conference**, June 5-10, Noordwijkerhout, The Netherlands.
9. De BEER, M., Fisher, C and Jooste, F.J. 1997. Determination of pneumatic tyre/pavement interface contact stresses under moving loads and some effects on pavements with thin asphalt surfacings. In: **Proceedings of the 8th International Conference on Asphalt Pavements**, August 10-14, Seattle, Washington.
10. HICKS, R.G. and Monismith, C.L. 1971. Factors influencing the resilient response of granular materials. In: **Highway Soils Engineering**, Washington, D.C.: Transportation Research Board, National Research Council. (Highway Research Record; 345), pp. 123-131.
11. UZAN, J. 1985. Characterization of granular Material. In **Analysis and testing of granular bases and subbases**. Washington, DC: Transportation Research Board, National Research Council. (Transportation Research Record; 1022).
12. JOOSTE, F.J. 1995. **Modeling flexible pavement response under superheavy load vehicles**. Ph.D. dissertation. Texas A&M University, College Station, Texas.

13. INGE, E.H. and Kim, Y.R. 1995. Prediction of effective asphalt layer temperature. In: **Strength and deformation characteristics of pavement sections and pavement rehabilitation**. Washington, D.C.: Transportation Research Board, National Research Council. (Transportation Research Record; No. 1473), pp. 93..100.
14. PARK, S.W. and Kim, Y.R. 1997. Temperature corrections of backcalculated moduli and deflections using linear viscoelasticity and time-temperature superposition.. In: **Pavement research issues**. Washington, D.C.: Transportation Research Board, National Research Council. (Transportation Research Record; No. 1570), pp. 108..117.
15. HUANG, Y.H. 1993. **Pavement analysis and design**. Englewood Cliffs, New Jersey: Prentice Hall, Inc.
16. HOPMANN, P.C. 1996. VEROAD: A Viscoelastic Multilayer Computer Program. In: **Flexible Pavement Design and Rehabilitation Issues**. Washington, D.C.: Transportation Research Board, National Research Council, (Transportation Research Record; No. 1539), pp. 72-80.
17. FINDLEY, William N., Lai James S. and Onaran, Kassif. 1976. **Creep and relaxation of nonlinear viscoelastic materials**. Amsterdam: North Holland Publishing Company. (North Holland Series in Applied Mathematics and Mechanics: Vol. 18), pp. 367.
18. THEYSE, H.L., de Beer M. and Rust F.C. 1996. **Overview of the South African mechanistic pavement design analysis method**. Pretoria: Division of Roads and Transport Technology, CSIR. (Divisional Publication; DP-96/005; Preprint of paper no. 961294 - 75th TRB 1996 meeting)).
19. ULLIDTZ, P. 1987. **Pavement Analysis**. Elsevier: Amsterdam.
20. DE BEER, M. 1991. Use of the Dynamic Cone Penetrometer (DCP) in the design of road structures. **Proceedings of the tenth regional conference for Africa on Soil Mechanics & Foundation Engineering and the third International Conference on Tropical and Residual Soils**, Maseru, 23-27 September.
21. JOOSTE, F.J. 1997. **Probabilistic pavement analysis and design**. Pretoria: Division of Roads and Transport Technology, CSIR. (Internal report TR-97/035).
22. **Structural design of inter-urban and rural road pavements**. 1985. Pretoria: Department of Transport. (Technical recommendations for highways; TRH4).

NOTE TO APPENDICES A TO C

Appendices A,B and C contain the results of the dynamic effects, non-uniform tyre contact stress effects and horizontal shear force effects, respectively. The following sign and orientation conventions apply to Appendices A to C:

- Compressive stresses and strains are negative; tensile stresses and strains are positive.
- The yy-axis denote the vertical direction;
- The xx-axis denote the transverse direction;
- The zz-axis denote the longitudinal direction (i.e the direction in which the wheel is moving, in the case of the dynamic analysis);

APPENDIX A
ANALYSIS RESULTS: DYNAMIC EFFECTS

RESULTS FROM LET AND FE MODELS FOR DYNAMIC ANALYSIS

TABLE A1: STRESS RESULTS FOR STRUCTURE 1: ASPHALT SURFACING

DEPTH IN AC	MODEL	VERTIC SIG-YY	TRANSV SIG-XX	LONGI SIG-ZZ	SIG-XY	TAU-OCT
TOP	LET	-800	-2550	-2550	0	825.0
	FE STAT	-879	-2170	-2170	0	608.6
	FE 20	-890	-1580	-1387	-86	299.0
	FE 80	-1025	-1420	-1254	-89	177.5
MIDDLE	LET	-777	-928	-928	0	71.2
	FE STAT	-759	-868	-868	0	51.4
	FE 20	-788	-790	-694	-286	237.8
	FE 80	-923	-796	-752	-268	230.5
BOTTOM	LET	-722	561	561	0	604.8
	FE STAT	-703	586	586	0	607.6
	FE 20	-689	31	-120	-257	374.4
	FE 80	-820	-284	-376	-268	320.4

TABLE A2. STRESS RESULTS FOR STRUCTURE 2: ASPHALT SURFACING

DEPTH IN AC	MODEL	VERTIC SIG-YY	TRANSV SIG-XX	LONGI SIG-ZZ	SIG-XY	TAU-OCT
TOP	LET	-800	-1730	-1730	0	438.4
	FE STAT	-850	-1528	-1528	0	319.6
	FE 20	-879	-1330	-1208	-61	196.9
	FE 80	-1016	-1245	-1143	-66	108.1
MIDDLE	LET	-783	-1190	-1190	0	191.9
	FE STAT	-791	-1077	-1077	0	134.8
	FE 20	-809	-944	-918	-232	198.2
	FE 80	-945	-946	-914	-232	190.0
BOTTOM	LET	-725	-711	-711	0	6.6
	FE STAT	-717	-615	-615	0	48.1
	FE 20	-673	-600	-628	-306	251.7
	FE 80	-804	-679	-702	-331	275.7

TABLE A3. STRESS RESULTS FOR STRUCTURE 2: ASPHALT BASE

DEPTH IN AC	MODEL	VERTIC SIG-YY	TRANSV SIG-XX	LONGI SIG-ZZ	SIG-XY	TAU-OCT
TOP	LET	-721	-548	-548	0	81.6
	FE STAT	-695	-427	-427	0	126.3
	FE 20	-537	-435	-440	-245	205.5
	FE 80	-406	-332	-329	-166	140.1
MIDDLE	LET	-410	99	99	0	239.9
	FE STAT	-425	46	46	0	222.0
	FE 20	-369	0	0	-196	236.4
	FE 80	-284	-62	-80	-166	168.8
BOTTOM	LET	-169	746	746	0	431.3
	FE STAT	-183	575	575	0	357.3
	FE 20	-211	408	332	-116	291.5
	FE 80	-179	232	166	-66	188.1

**FINITE ELEMENT RESULTS
STRUCTURE 1: STATIC ANALYSIS**

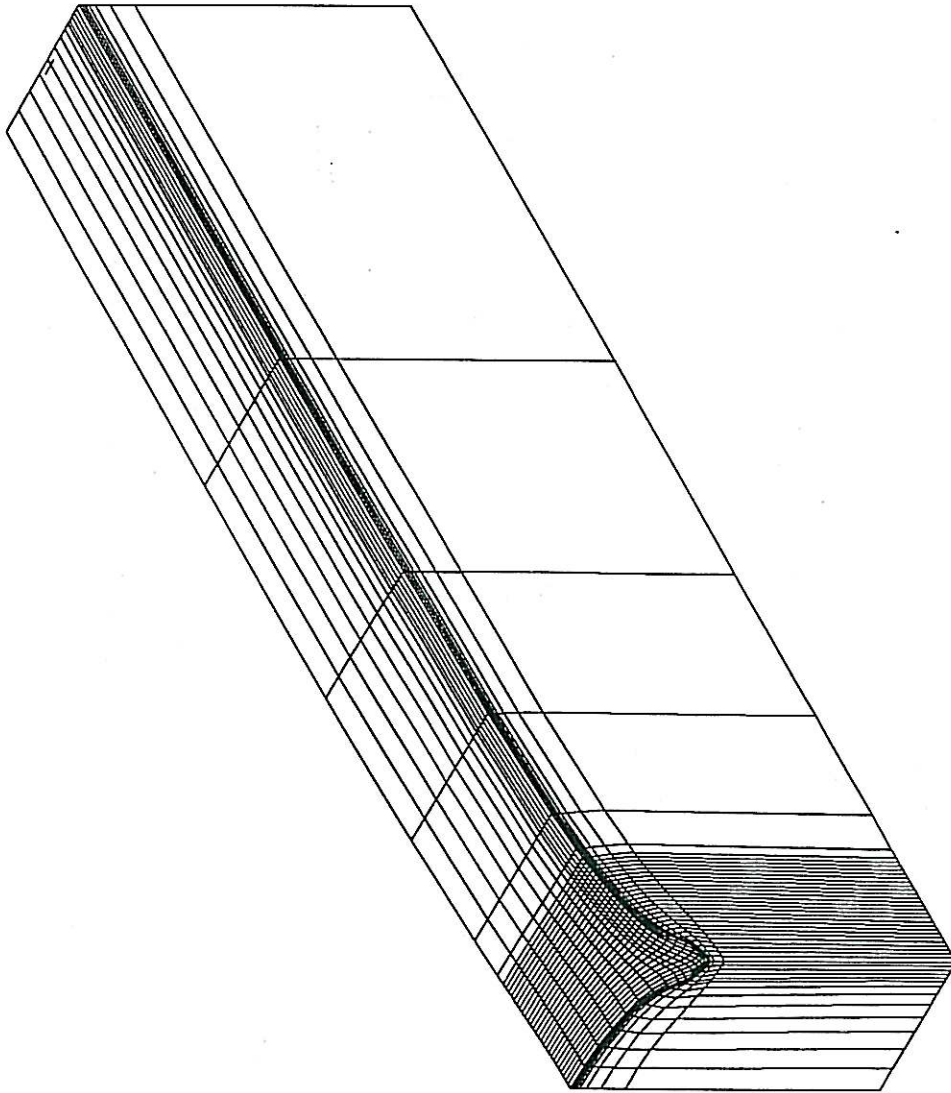
SCALE: 1/10

LENGTH
X #=31.283cm
Y #=31.283cm
Z #=31.283cm

DISPLACEMENT
X #=0.038689cm
Y #=0.038689cm
Z #=0.038689cm

LOAD-STEP:
LS=2

PRESENTATION:
DEFORMED MESH



DESIGN BY SGG/901-Lopez 14.51.13
1998-7-17
geofe model HV 20.00-08

STRUCTURE 1, MAX. DEFLECTION=0.58mm

ROLS
DISS
PROS

HMA PROJECT		TFAS/A/1
STATIC TYRE; 40kN, 800kPa		BKS (Pty) Ltd. Dr JP Laurens BOX 3173 PRETORIA FAX 012 4213501
FIG. 1: Deflection Bowl		

Dyn 1 Sted

SCALE: 1:1

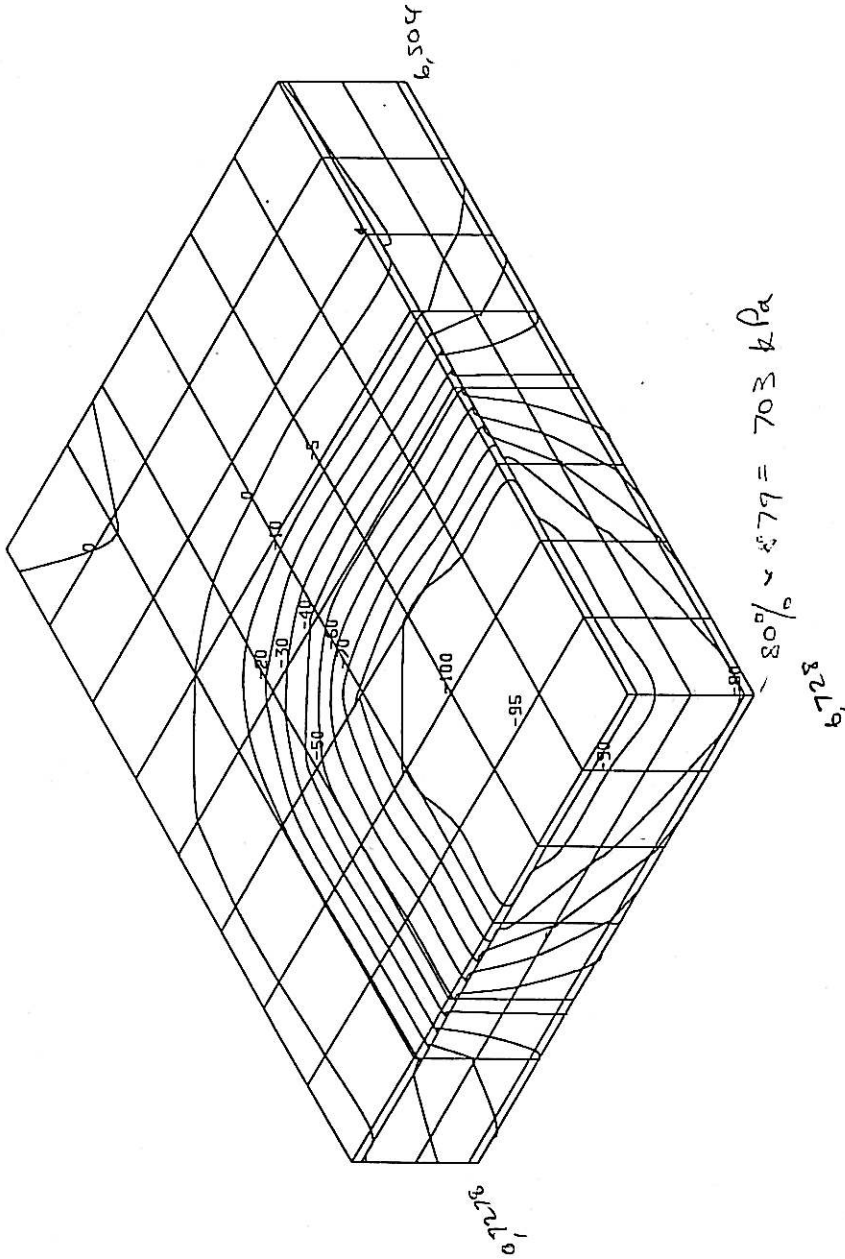
LENGTH
X #=1.6508cm
Y #=1.6508cm
Z #=1.6508cm

LOAD-STEP:
LS=2-1

PRESENTATION:
UNDEFORMED MESH
DETAIL

ARGUMENT:

STRESS
Y - COMPONENT
SIGN CONSIDERED
100% =
879.081542kN/m²



STRUCTURE 1, MAX. DEFLECTION=0.58mm

DESIGN BY SGG/901-Lopez 14.54.23
1998-7-17 geofe model NU 20.00-08

HMA PROJECT	TFAS/A/1
STATIC TYRE; 40kN, 800kPa	BKS (Pty) Ltd. Dr JP Laurens BOX 3173 PRETORIA FAX 012 4213501
FIG. 2: Vertical Stress; Sigma Y	

Dyn I Stat

SCALE: 1/20

LENGTH

X #=1.6508cm
Y #=1.6508cm
Z #=1.6508cm

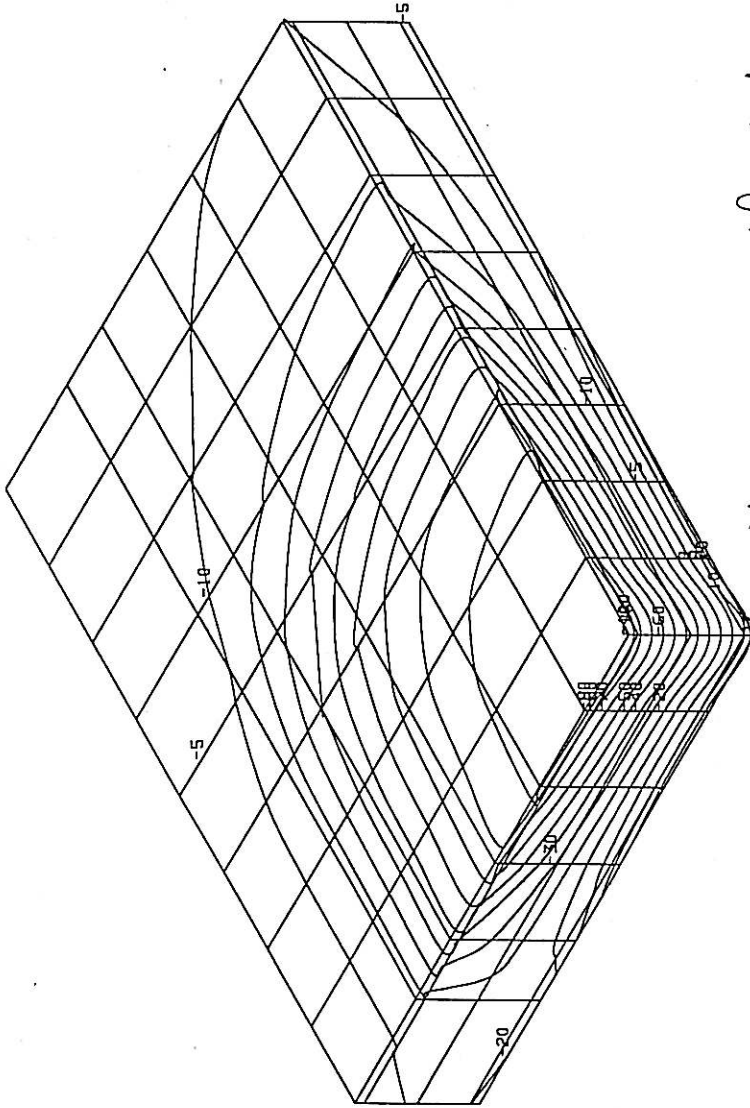
LOAD-STEP:

LS=2-1

PRESENTATION:
UNDEFORMED MESH
DETAIL

ARGUMENT:

STRESS
X-COMPONENT
SIGN CONSIDERED
100% =
2170.293457kN/m2



27 1/2 x 2170 = 586 kPa - track

STRUCTURE 1, MAX. DEFLECTION=0.58mm

DESIGN BY SGG/901-Lopez geofe model HU 20.00-08
1998-2-12 14:57:14

TFAS/A/1

BKS (Pty) Ltd.
Dr JP Laurens
BOX 3173 PRETORIA
FAX 012 4213501

HMA PROJECT

STATIC TYRE; 40kN, 800kPa
FIG. 3: Hor. Stress; Sigma X

Dyn I Steel

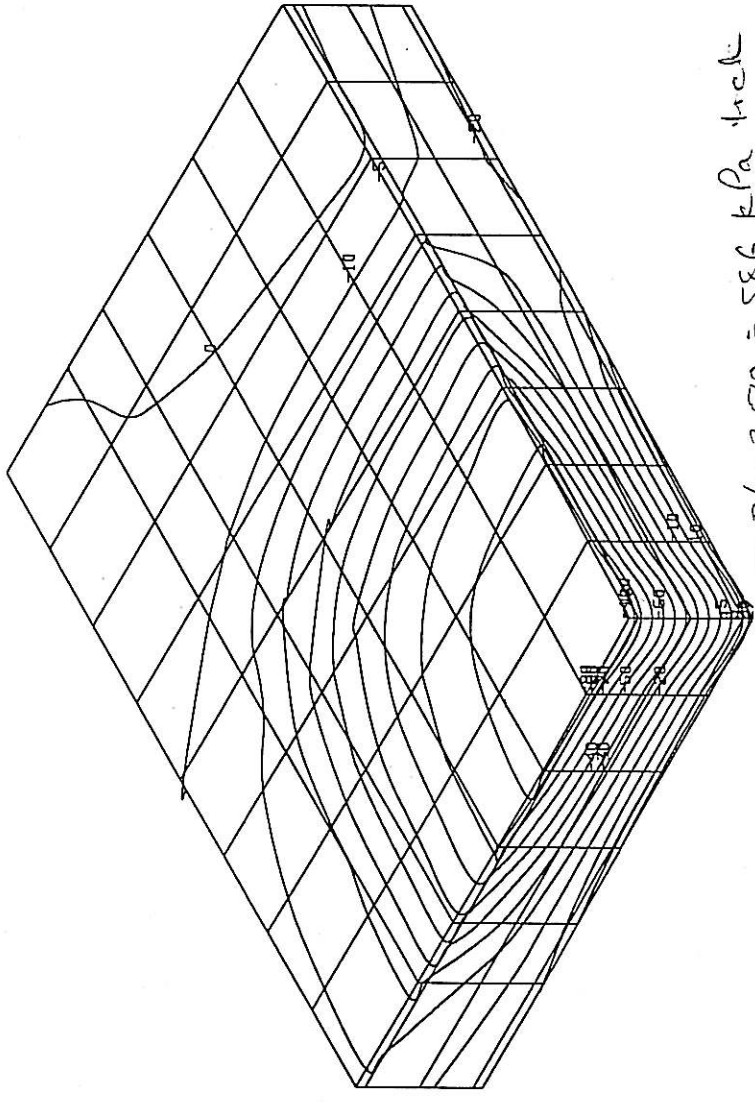
SCALE: 1:1

LENGTH
X #=1.6508cm
Y #=1.6508cm
Z #=1.6508cm

LOAD-STEP:
LS=2-1

PRESENTATION:
UNDEFORMED MESH
DETAIL

ARGUMENT:
STRESS
Z -COMPONENT
SIGN CONSIDERED
100% =
2170.135986kN/m2



STRUCTURE 1, MAX. DEFLECTION=0.58mm

DESIGN BY SGG/901-Lopez 15/11/57
1998-7-12
geofe model HU 20.00-08

TFAS/A/1	HMA PROJECT	
BKS (Pty) Ltd. Dr JP Laurens BOX 3173 PRETORIA FAX 012 4213501	STATIC TYRE; 40kN, 800kPa FIG. 4; Hor. Stress; Sigma Z	

Dyn I Start

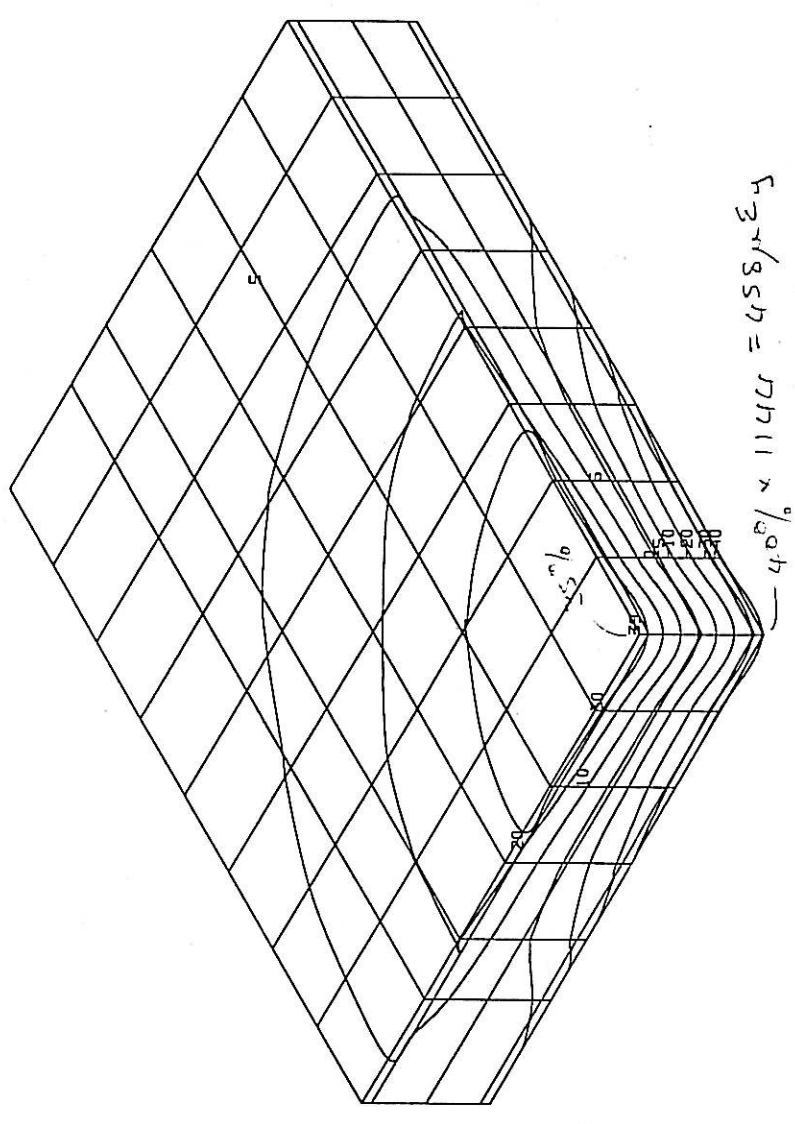
SCALE: 1:100

LENGTH
 X #=1.6508cm
 Y #=1.6508cm
 Z #=1.6508cm

LOAD-STEP:
 LS=2-1

PRESENTATION:
 UNDEFORMED MESH
 DETAIL

ARGUMENT:
 STRAIN
 Y -COMPONENT
 SIGN CONSIDERED
 100% =
 0.001144



STRUCTURE 1, MAX. DEFLECTION=0.58mm

DESIGN BY SGG/901-Lopez geofe model MV 20.00-08
 1998-2-12 15:12:41

HMA PROJECT	TFAS/A/1
STATIC TYRE; 40kN, 800kPa	BKS (Pty) Ltd. Dr JP Laurens BOX 3173 PRETORIA FAX 012 4213501
FIG. 5: Vert. Strain; Eps. Y	

Dyn I Stat

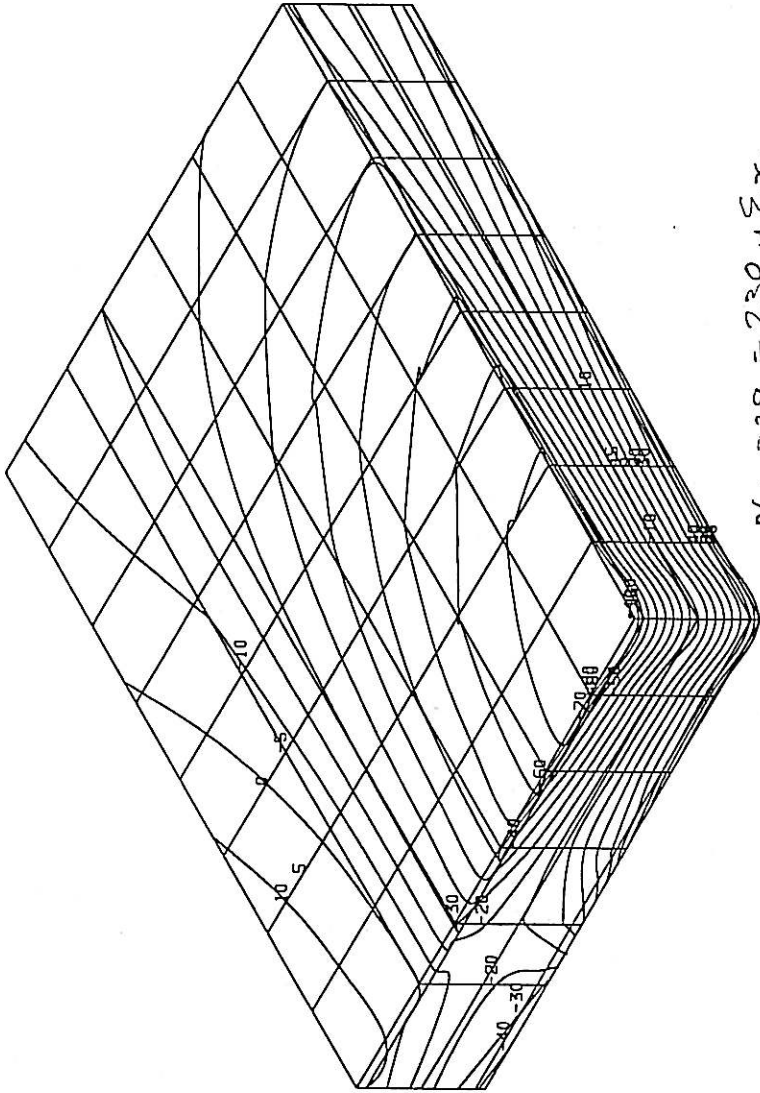
SCALE: 1# = 1

LENGTH
X # = 1.6508cm
Y # = 1.6508cm
Z # = 1.6508cm

LOAD-STEP:
LS=2-1

PRESENTATION:
UNDEFORMED MESH
DETAIL

ARGUMENT:
STRAIN
X -COMPONENT
SIGN CONSIDERED
100% =
0.000329



*DESIGN BY SGG/901-1cpaz 15/2016
1998-7-17 geofe model MV 20.00-08

STRUCTURE 1, MAX. DEFLECTION=0.58mm

TFAS/A/1

HMA PROJECT

STATIC TYRE, 40kN, 800kPa

FIG. 6: Hor. Strain; Eps. X

BKS (Pty) Ltd.
Jr JP Laurens
BOX 3173 PRETORIA
FAX 012 4213501

Dyn I Stat

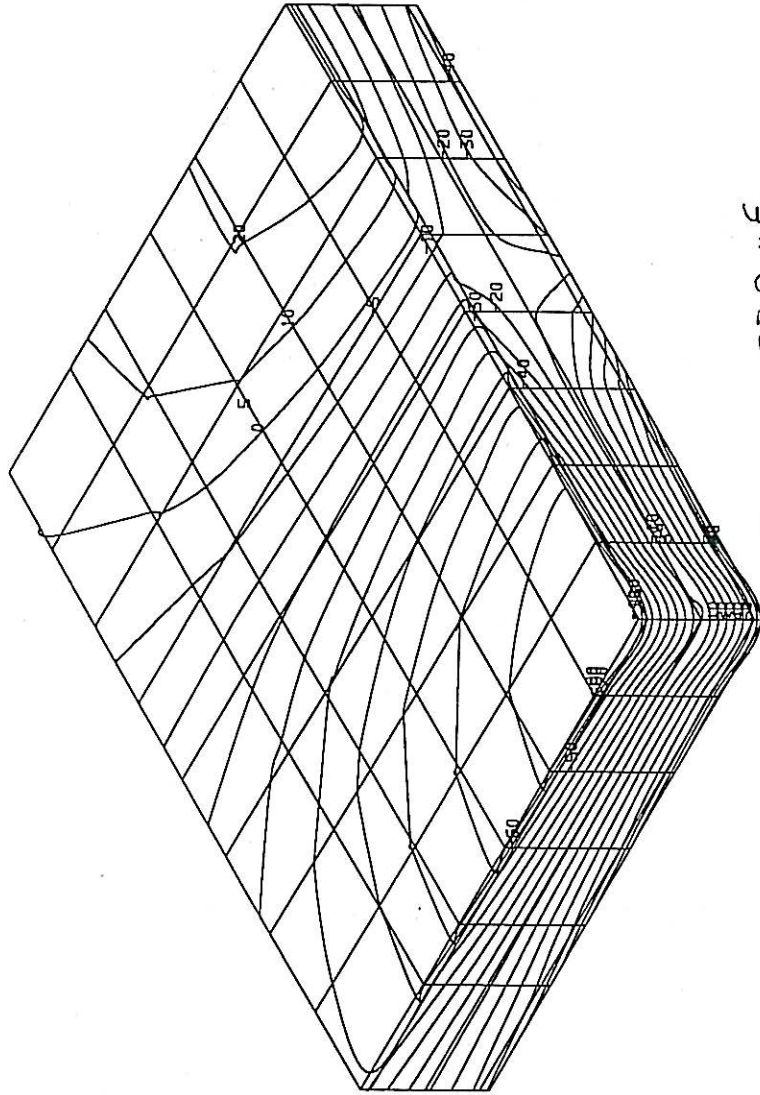
SCALE: 1# = 1

LENGTH
 X # = 1.6508cm
 Y # = 1.6508cm
 Z # = 1.6508cm

LOAD-STEP:
 LS=2-1

PRESENTATION:
 UNDEFORMED MESH
 DETAIL

ARGUMENT:
 STRAIN
 Z - COMPONENT
 SIGN CONSIDERED
 100% =
 0.000329



STRUCTURE 1, MAX. DEFLECTION=0.58mm

DESIGN BY SGG/901-Lopez 15:22:33
 1998-7-17 GeofE model MU 20.00-08

TFAS/A/1	HMA PROJECT	
BKS (Pty) Ltd. Dr JP Laurens BOX 3173 PRETORIA FAX 012 4213501	STATIC TYRE; 40kN, 800kPa FIG. 7: Hor. Strain; Eps. Z	

Dym I Stat

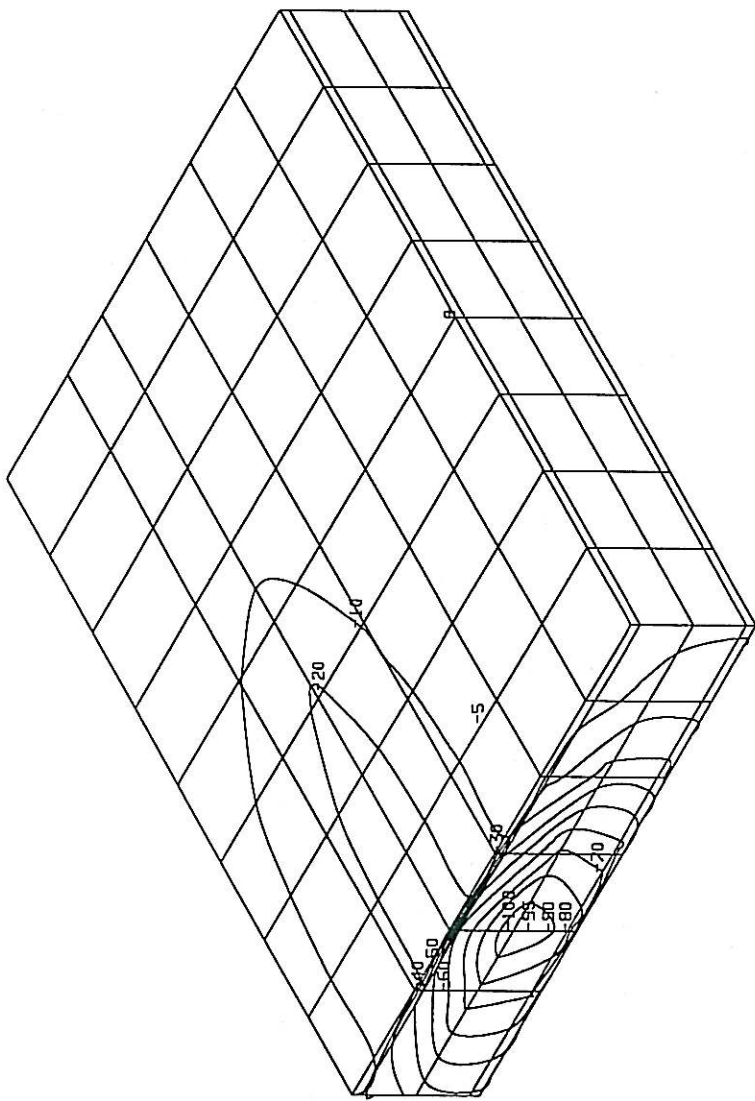
SCALE: 1# = 1

LENGTH
X # = 1.6508cm
Y # = 1.6508cm
Z # = 1.6508cm

LOAD-STEP:
LS=2-1

PRESENTATION:
UNDEFORMED MESH
DETAIL

ARGUMENT:
STRESS
Tau-XY
SIGN CONSIDERED
100% =
370.888427kN/m²



*DESIGN BY SGG/901-Lopez 15.25.8
1998-7-17 geofe model HV 20.00-08

STRUCTURE 1, MAX. DEFLECTION=0.58mm

HMA PROJECT	TFAS/A/1
STATIC TYRE; 40kN, 800kPa	BKS (Pty) Ltd. Dr JP Laurens BOX 3173 PRETORIA FAX 012 4213501
FIG. 8: Shear Stress; Tau XY	

Dyn I Start

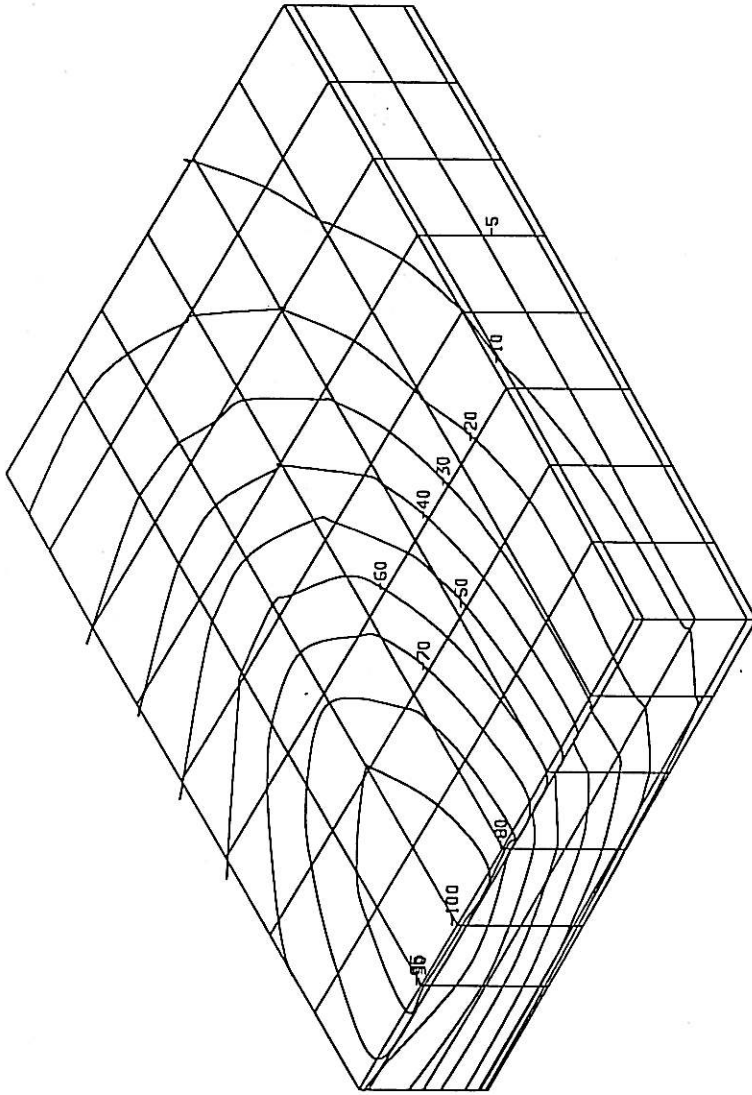
SCALE: 1:1

LENGTH H=1.6508cm
X
Y H=1.6508cm
Z H=1.6508cm

LOAD-STEP:
LS=2-1

PRESENTATION:
UNDEFORMED MESH
DETAIL

ARGUMENT:
STRAIN
Gamma-XY
SIGN CONSIDERED
100% =
0.001232



STRUCTURE 1, MAX. DEFLECTION=0.58mm

DESIGN BY SGG/901-lopaz geofe model nu 20.00-08
1998-7-17 15:28:10

TFAS/A/1
BKS (Pty) Ltd.
Dr JP Lourens
BOX 3173 PRETORIA
FAX 012 4213501

HMA PROJECT
STATIC TYRE; 40kN, 800kPa
FIG. 9: Shear Strain; Gamma XY

Dyn 1 Stat

FINITE ELEMENT RESULTS
STRUCTURE 1: 20 KM/H

SCALE: 1/10

LENGTH

X = 20.343cm

Y = 20.343cm

Z = 20.343cm

DISPLACEMENT

X = 0.0225555cm

Y = 0.0225555cm

Z = 0.0225555cm

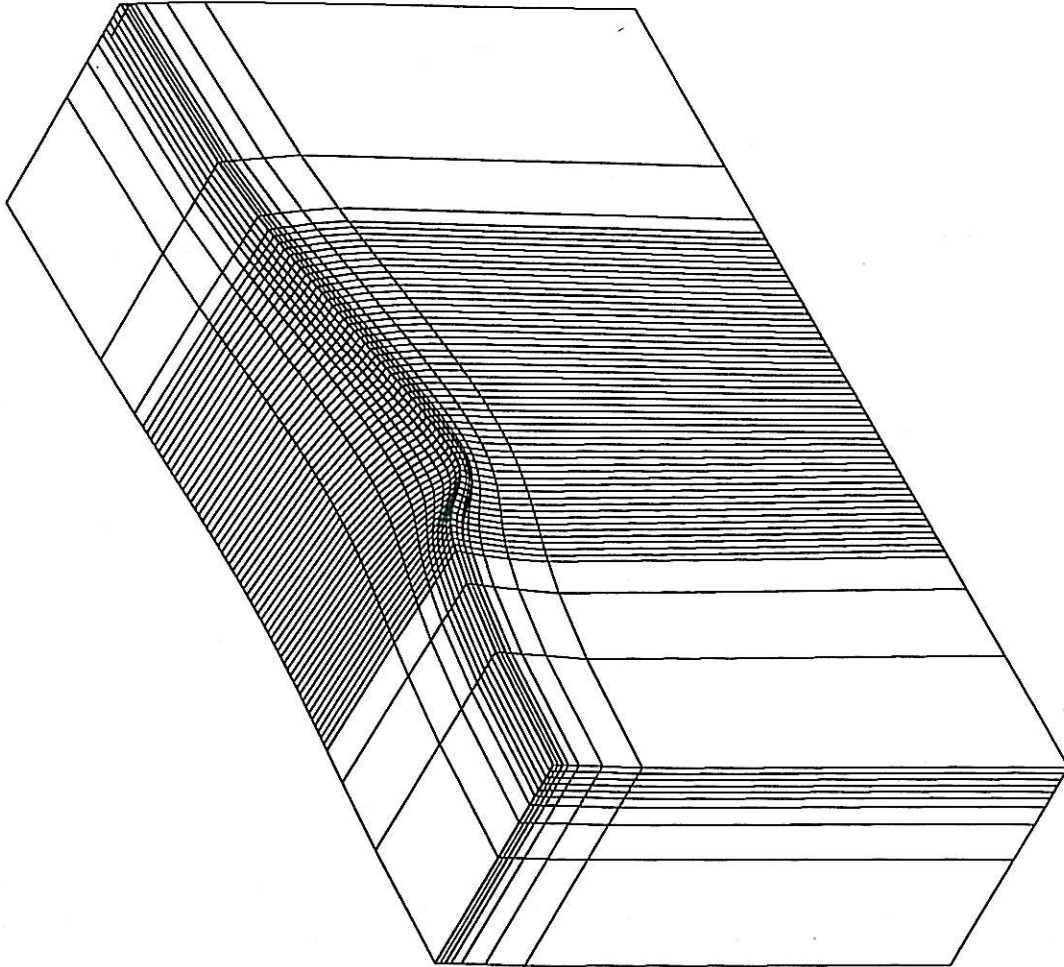
LOAD-STEP:

LS=40

PRESENTATION:

DEFORMED MESH

DETAIL



STRUCTURE 1, MAX. DEFLECTION=0.34mm

DESIGN BY SGG/901-Lopez BGE model NU 20.00-08
1998-8-13 8:57

DYN1

DISJA REFS

Dyn I 20

HMA PROJECT		TFAS/A/1
TYRE @ 20km/hour; 40kN, 800kPa		BKS (Pty) Ltd. Dr JP Lourens BOX 3173 PRETORIA FAX 012 4213501
FIG. 1: Deflection Bowl		

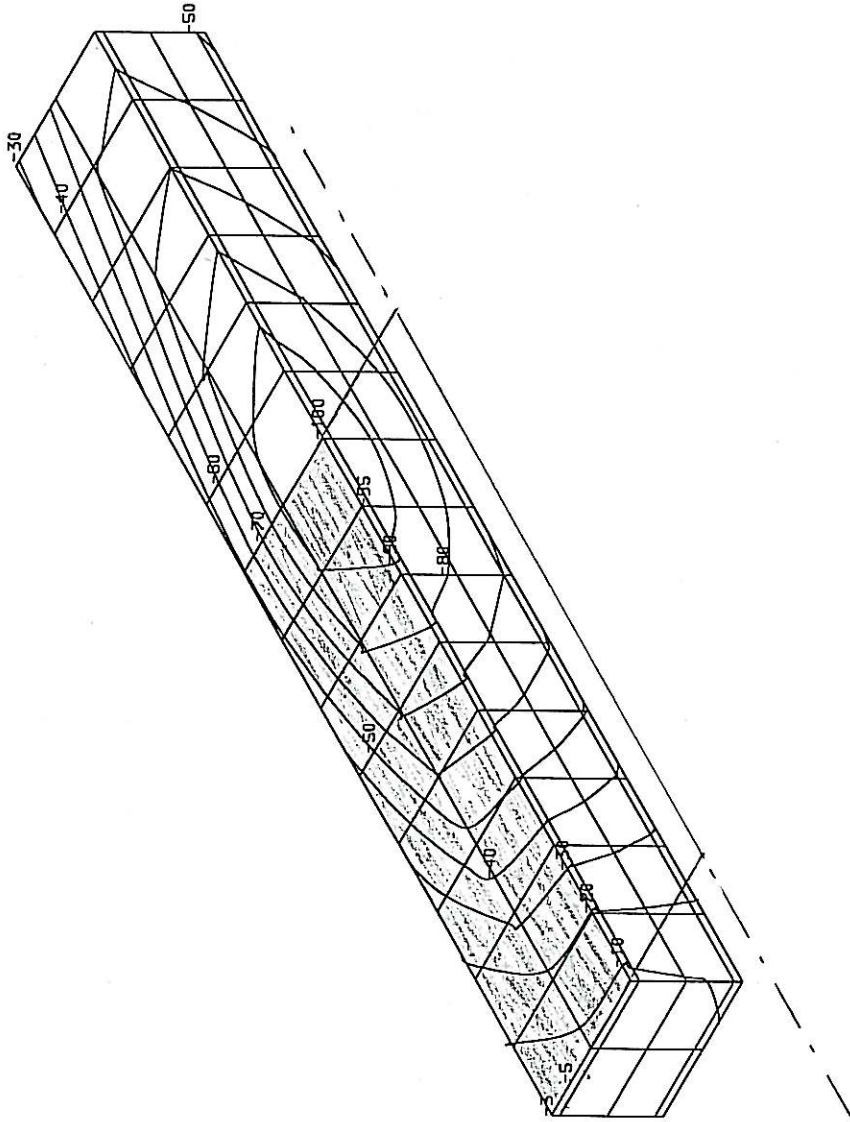
SCALE: 1/10

LENGTH
X #=1.8666cm
Y #=1.8666cm
Z #=1.8666cm

LOAD-STEP:
LS=40-1

PRESENTATION:
UNDEFORMED MESH
DETAIL

ARGUMENT:
STRESS
Y -COMPONENT
SIGN CONSIDERED
100% =
890.922668kN/m2



DESIGN BY SGG/901-Lopez 8/16/45
1998-8-13
• 20.00-08 HU model geofe

STRUCTURE 1, MAX. DEFLECTION=0.34mm

Dyn I 20

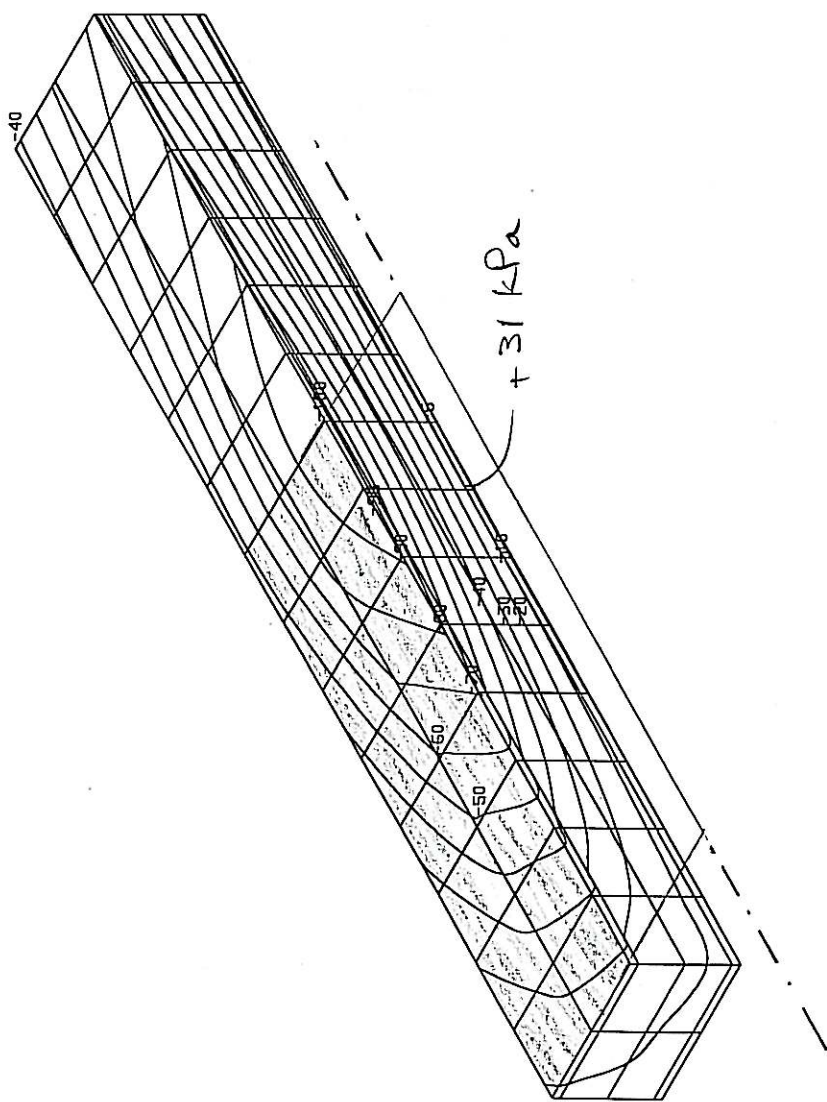
SCALE: 1# = 1

LENGTH
 X # = 1.8666cm
 Y # = 1.8666cm
 Z # = 1.8666cm

LOAD-STEP:
 LS=40-1

PRESENTATION:
 UNDEFORMED MESH
 DETAIL

ARGUMENT:
 STRESS
 X -COMPONENT
 SIGN CONSIDERED
 100% = 1579.654296kN/m2



DESIGN BY SGG/901-Lopez geofe model1 MV 20.00-08
 1998-8-13 8.19.53

STRUCTURE 1, MAX. DEFLECTION=0.34mm

Dyn 1 20

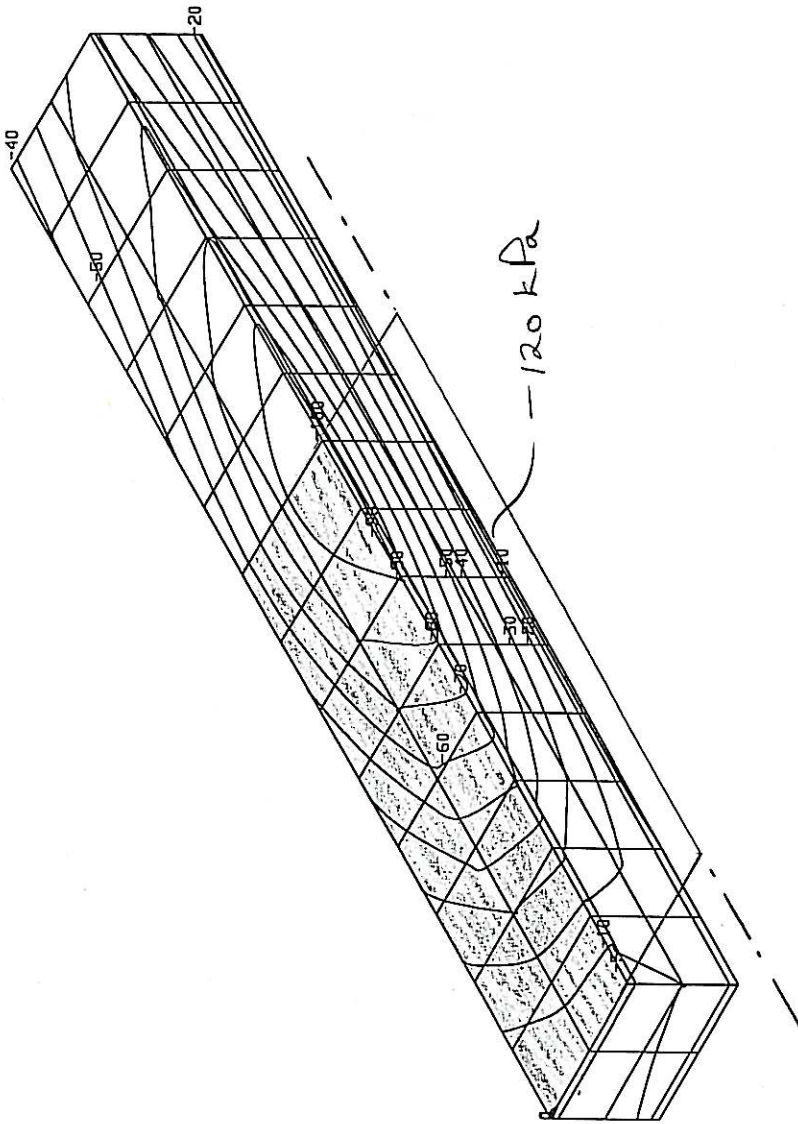
SCALE: 1:1

LENGTH
X #=1.8666cm
Y #=1.8666cm
Z #=1.8666cm

LOAD-STEP:
LS=40-1

PRESENTATION:
UNDEFORMED MESH
DETAIL

ARGUMENT:
STRESS
Z - COMPONENT
SIGN CONSIDERED
100% =
1386.841430kN/m²



DESIGN BY SGG/901-Lopez 8:23:29
1998-8-13 HU 20.00-08

STRUCTURE 1, MAX. DEFLECTION=0.34mm

Dyn 1 20

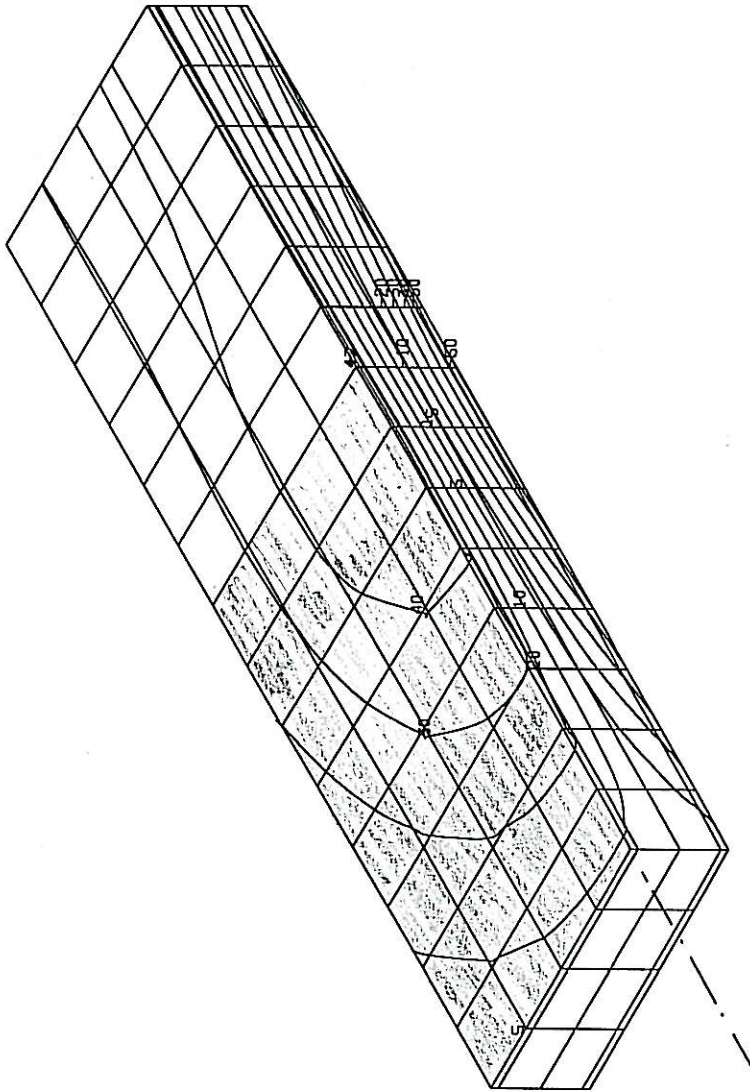
SCALE: 1:1

LENGTH
 X #=2.0999cm
 Y #=2.0999cm
 Z #=2.0999cm

LOAD-STEP:
 LS=40-1

PRESENTATION:
 UNDEFORMED MESH
 DETAIL

ARGUMENT:
 STRAIN
 Y -COMPONENT
 SIGN CONSIDERED
 100% =
 0.000328



DESIGN BY SGG/901-Lopez geofe modal HV 20.00-08
 1998-8-13 9:21:40

STRUCTURE 1, MAX. DEFLECTION=0.34mm

Dyn I 20

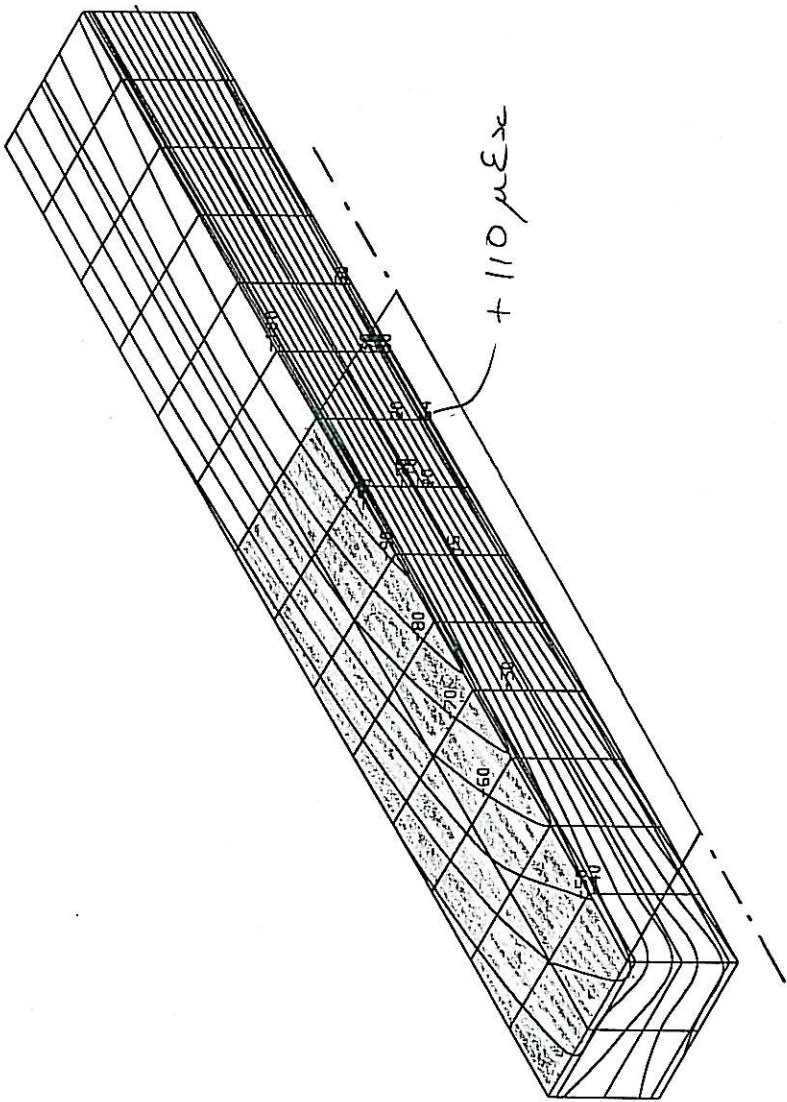
SCALE: 1# = 1cm

LENGTH
 X # = 1.8666cm
 Y # = 1.8666cm
 Z # = 1.8666cm

LOAD-STEP:
 LS=40-1

PRESENTATION:
 UNDEFORMED MESH
 DETAIL

ARGUMENT:
 STRAIN
 X -COMPONENT
 SIGN CONSIDERED
 100% =
 0.000169



DESIGN BY SGG/901-Lopez geofe model HV 20.00-08
 1998-8-13 8:28:54

STRUCTURE 1, MAX. DEFLECTION=0.34mm

Dyn I 20

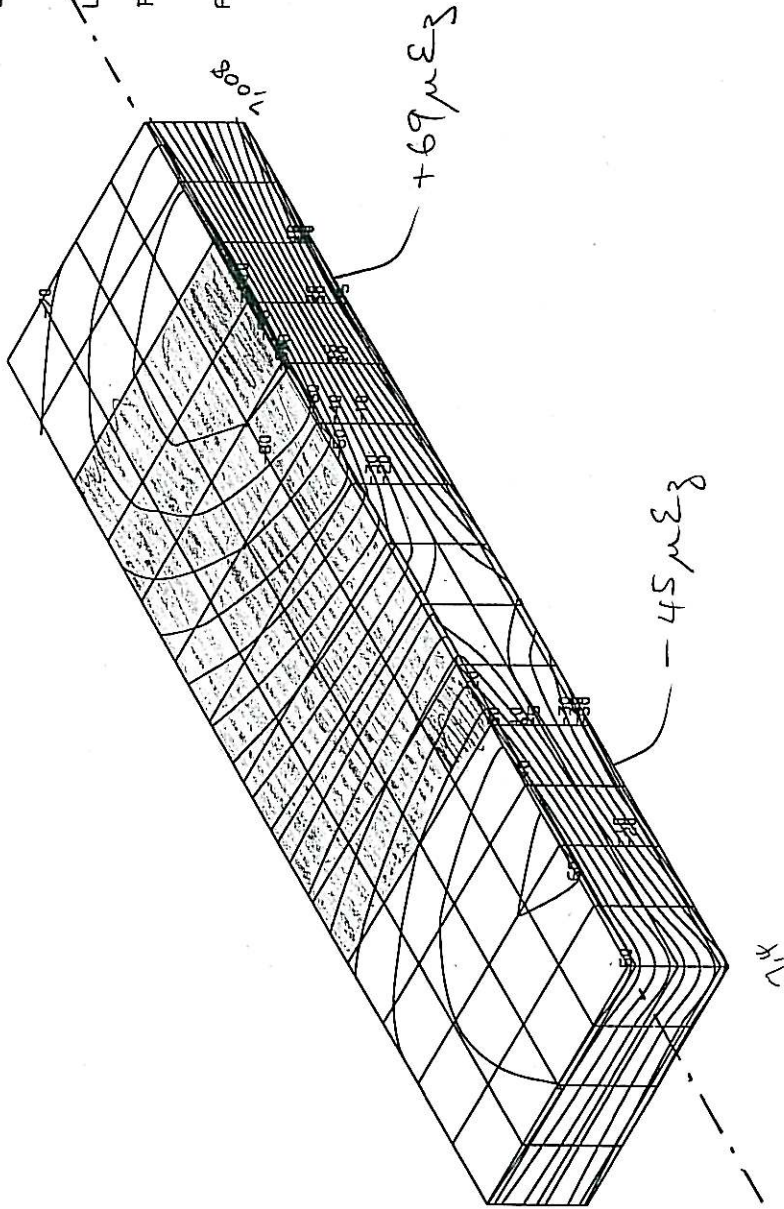
SCALE: 1# = 1

LENGTH
 X #=2.0999cm
 Y #=2.0999cm
 Z #=2.0999cm

LOAD-STEP,
 LS=40-1

PRESENTATION:
 UNDEFORMED MESH
 DETAIL

ARGUMENT:
 STRAIN
 Z - COMPONENT
 SIGN CONSIDERED
 100% =
 0.000090



DESIGN BY SGG/901-Lpaz geofe model NU 20.00-08
 1998-8-13 8:54:33

STRUCTURE 1, MAX. DEFLECTION=0.34mm

Dyn I 20

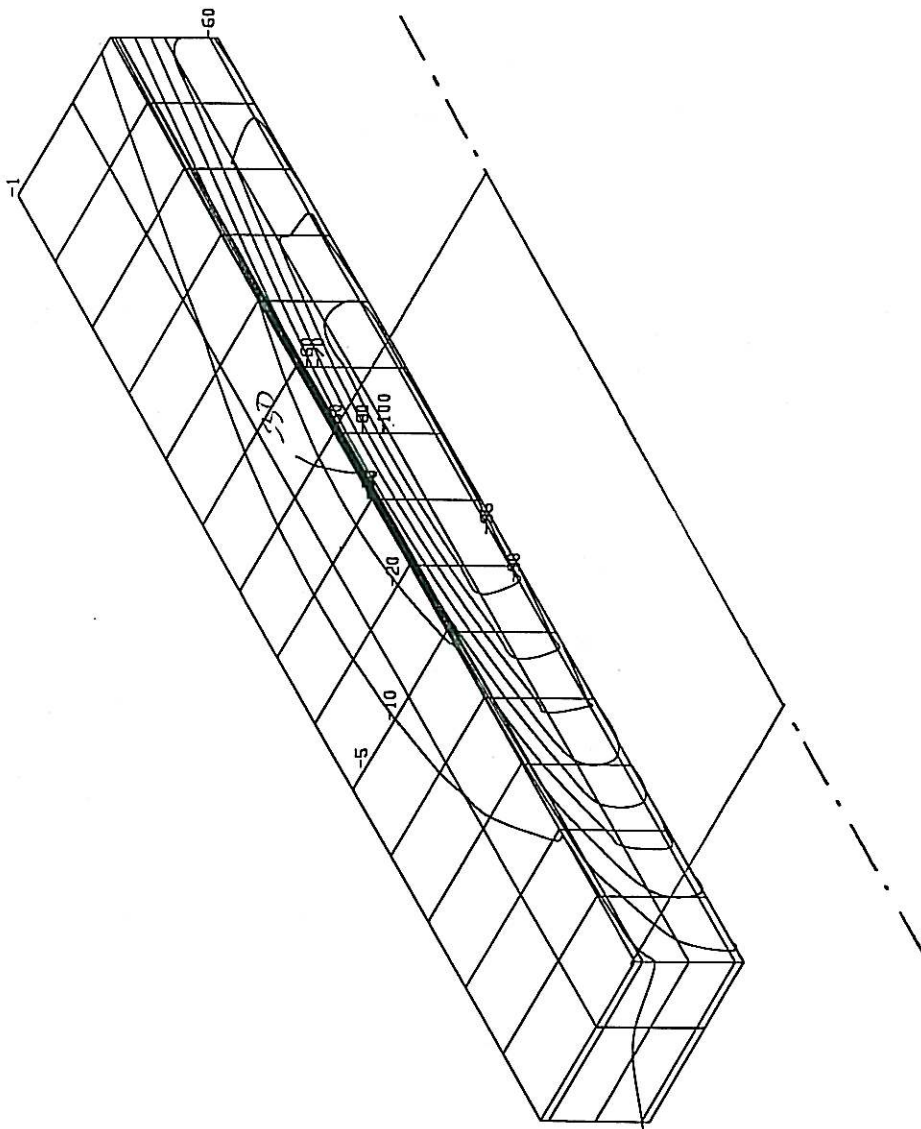
SCALE: 1# = 1

LENGTH
X # = 1.9166cm
Y # = 1.9166cm
Z # = 1.9166cm

LOAD-STEP:
LS=40-1

PRESENTATION:
UNDEFORMED MESH
DETAIL

ARGUMENT:
STRESS
Tau-XY
SIGN CONSIDERED
100% =
286.467163kN/m2



DESIGN BY SGG/901-topaz geofe model HU 20.00-08
1998-8-13 9114

STRUCTURE 1, MAX. DEFLECTION=0.34mm

Dyn I 20

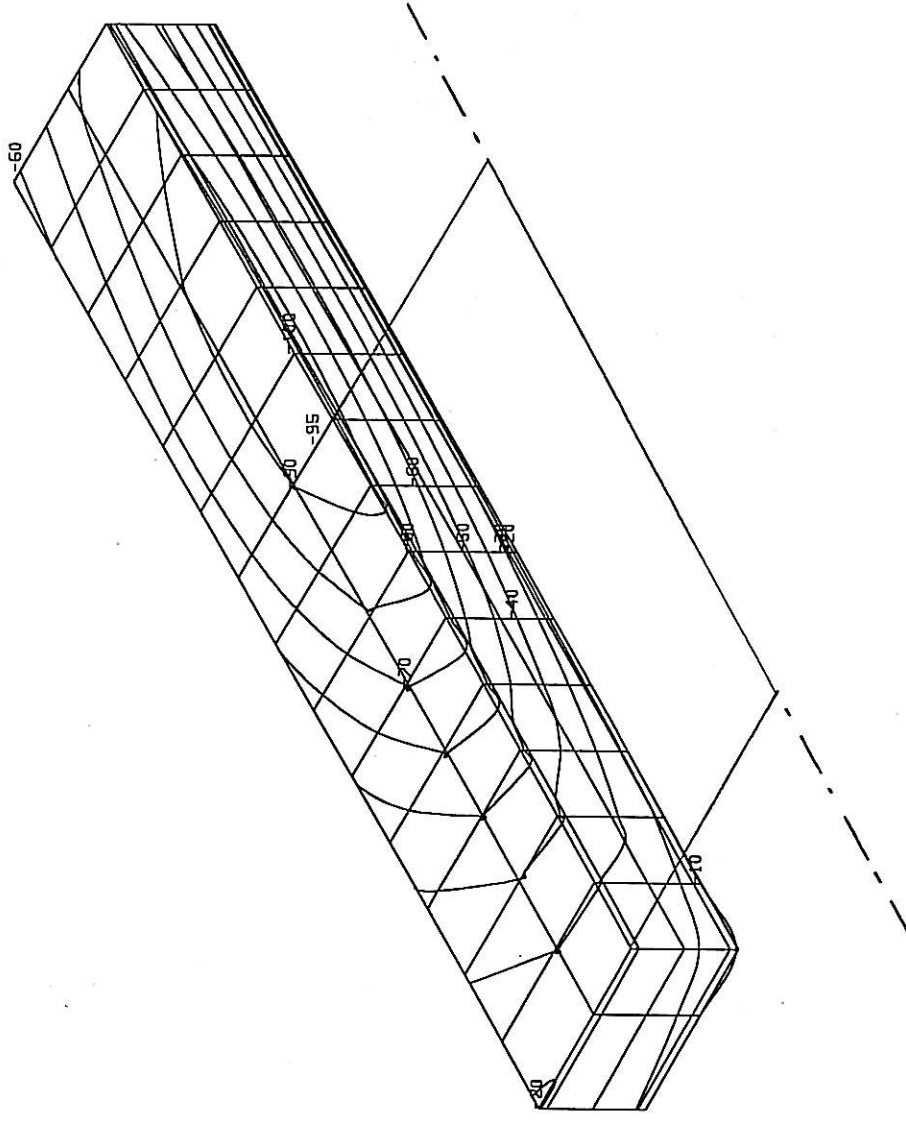
SCALE: 1/1

LENGTH
 X #=1.9166cm
 Y #=1.9166cm
 Z #=1.9166cm

LOAD-STEP:
 LS=40-1

PRESENTATION:
 UNDEFORMED MESH
 DETAIL

ARGUMENT:
 STRAIN
 Gamma-XY
 SIGN CONSIDERED
 100% =
 0.000593



DESIGN BY SGG/901-Lopez geofe model HU 20.00-08
 1998-8-13 9:21:46

STRUCTURE 1, MAX. DEFLECTION=0.34mm

Dyn 1 20

FINITE ELEMENT RESULTS
STRUCTURE 1: 80 KM/H

SCALE: 1/10

LENGTH

X = 20.343cm

Y = 20.343cm

Z = 20.343cm

DISPLACEMENT

X = 0.015893cm

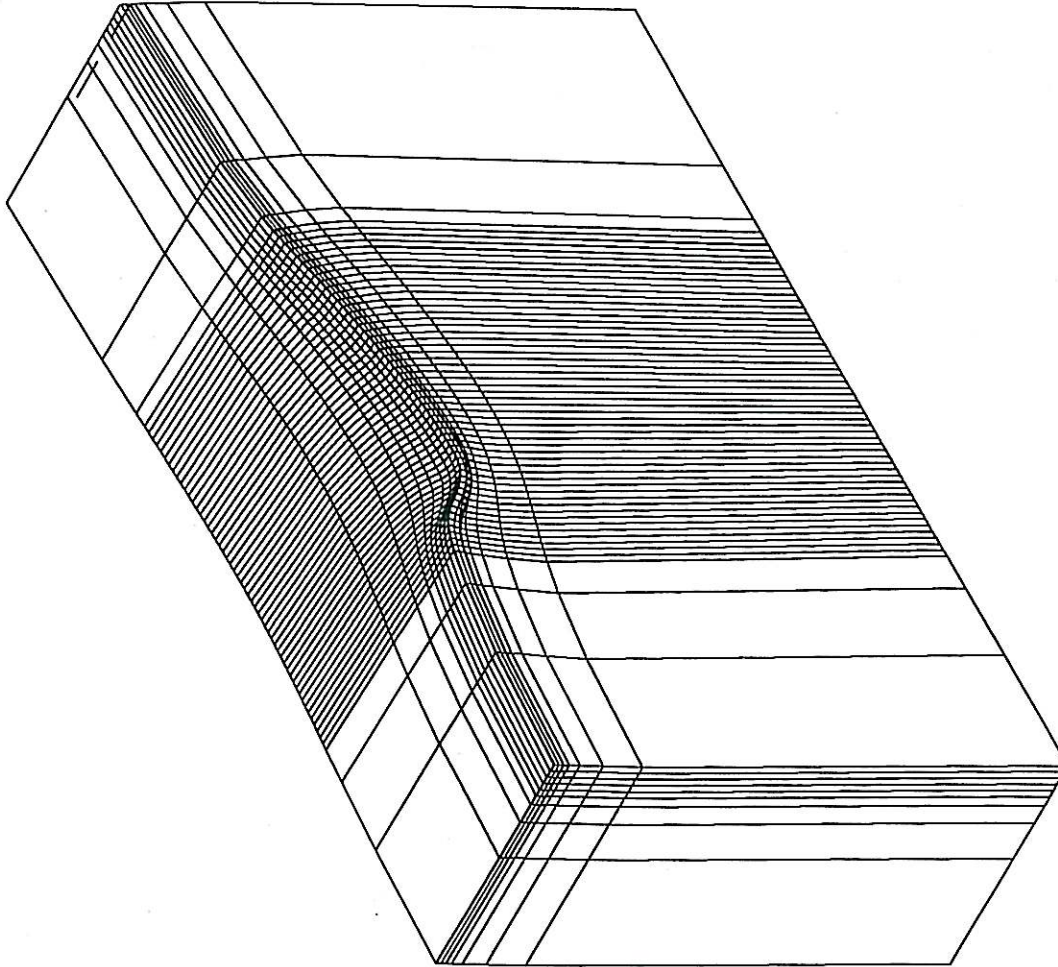
Y = 0.015893cm

Z = 0.015893cm

LOAD-STEP:

LS=40

PRESENTATION:
DEFORMED MESH
DETAIL



DESIGN BY SGG/901-Lopez 9/23/51
1998-8-13 20:00-08

STRUCTURE 1, MAX. DEFLECTION=0.24mm

DYN I
DISZ
REFA

TFA5/A/1
BKS (Pty) Ltd.
Dr JP Lourens
BOX 3173 PRETORIA
FAX 012 4213501

HMA PROJECT
TYRE @ 80km/hour; 40kN, 800kPa
FIG. 1: Deflection Bowl

Dyn I 80

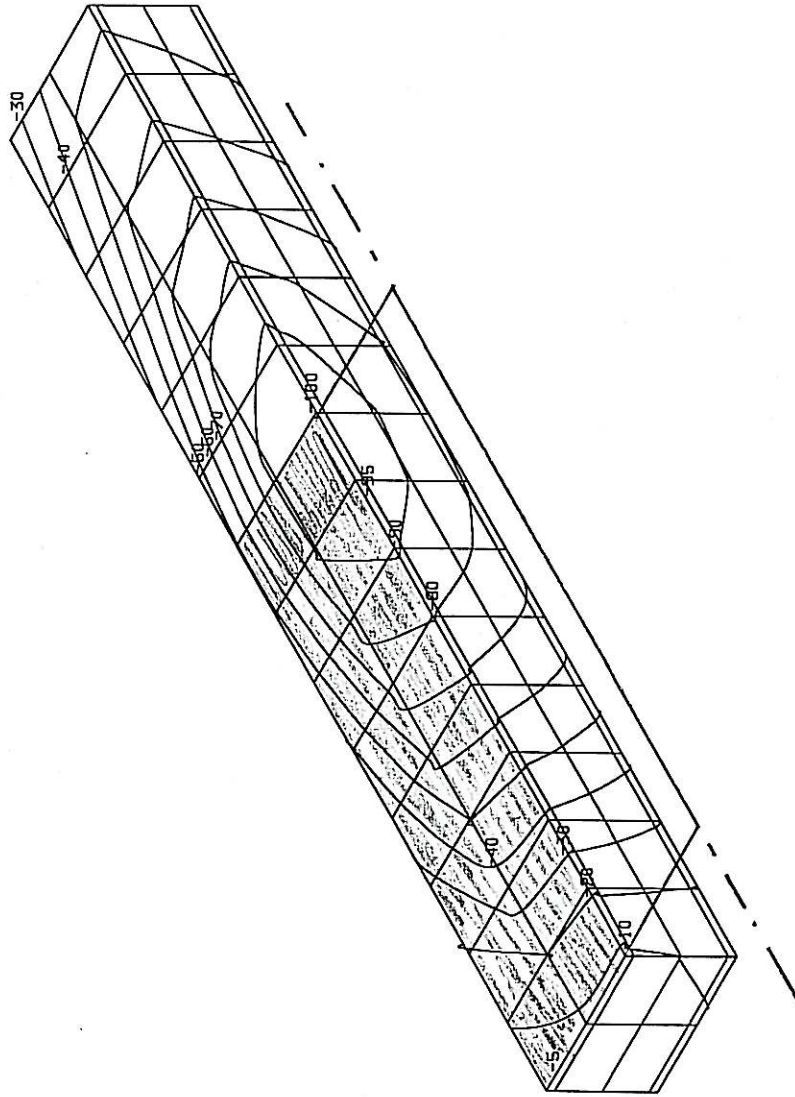
SCALE: 1/10

LENGTH
X #=1.8666cm
Y #=1.8666cm
Z #=1.8666cm

LOAD-STEP:
LS=40-1

PRESENTATION:
UNDEFORMED MESH
DETAIL

ARGUMENT:
STRESS
Y-COMPONENT
SIGN CONSIDERED
100% =
1025.248045kN/m²



DESIGN BY SGG/901-Lopez geofe model HU 20.00-08
1998-8-13 9:27:21

STRUCTURE 1, MAX. DEFLECTION=0.24mm

Dyn I 80

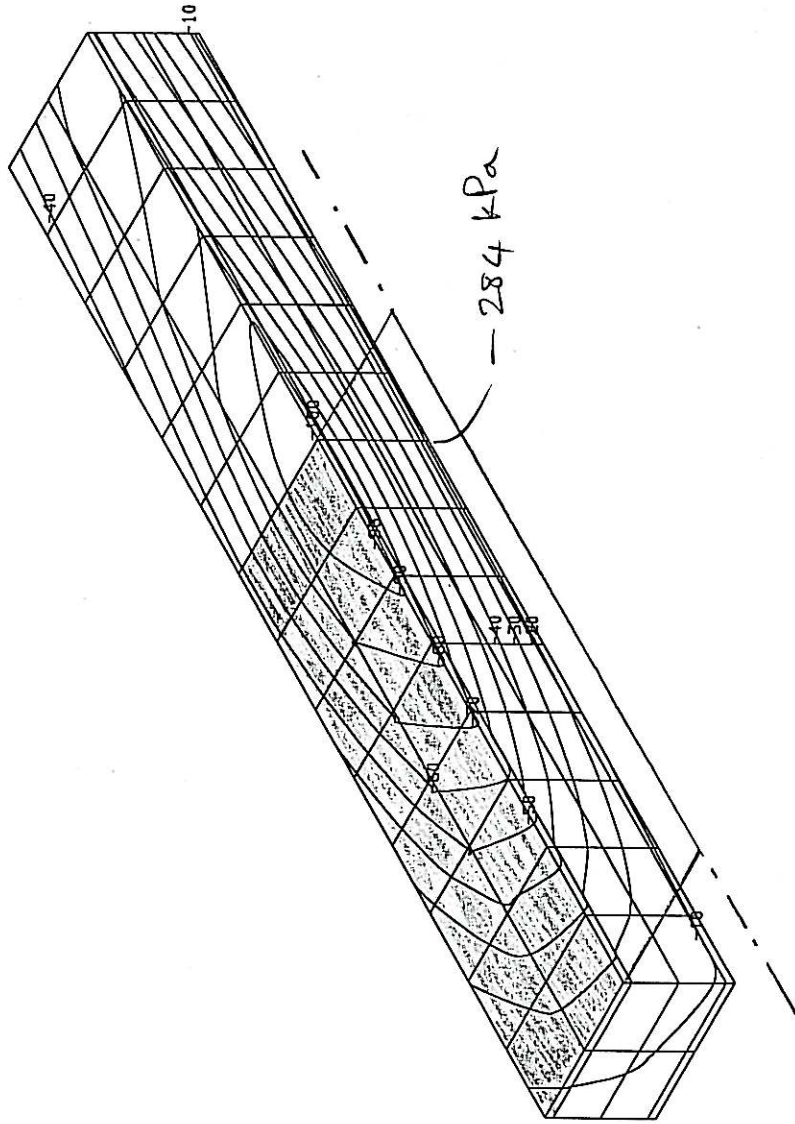
SCALE: 1# = 1

LENGTH
X # = 1.8666cm
Y # = 1.8666cm
Z # = 1.8666cm

LOAD-STEP:
LS=40-1

PRESENTATION:
UNDEFORMED MESH
DETAIL

ARGUMENT:
STRESS
X - COMPONENT
SIGN CONSIDERED
100% =
1420.798339kN/m²



DESIGN BY SGG/201-Lopez geofe model MU 20.00-08
1988-8-13 9:29:15

STRUCTURE 1, MAX. DEFLECTION=0.24mm

Dyn I 80

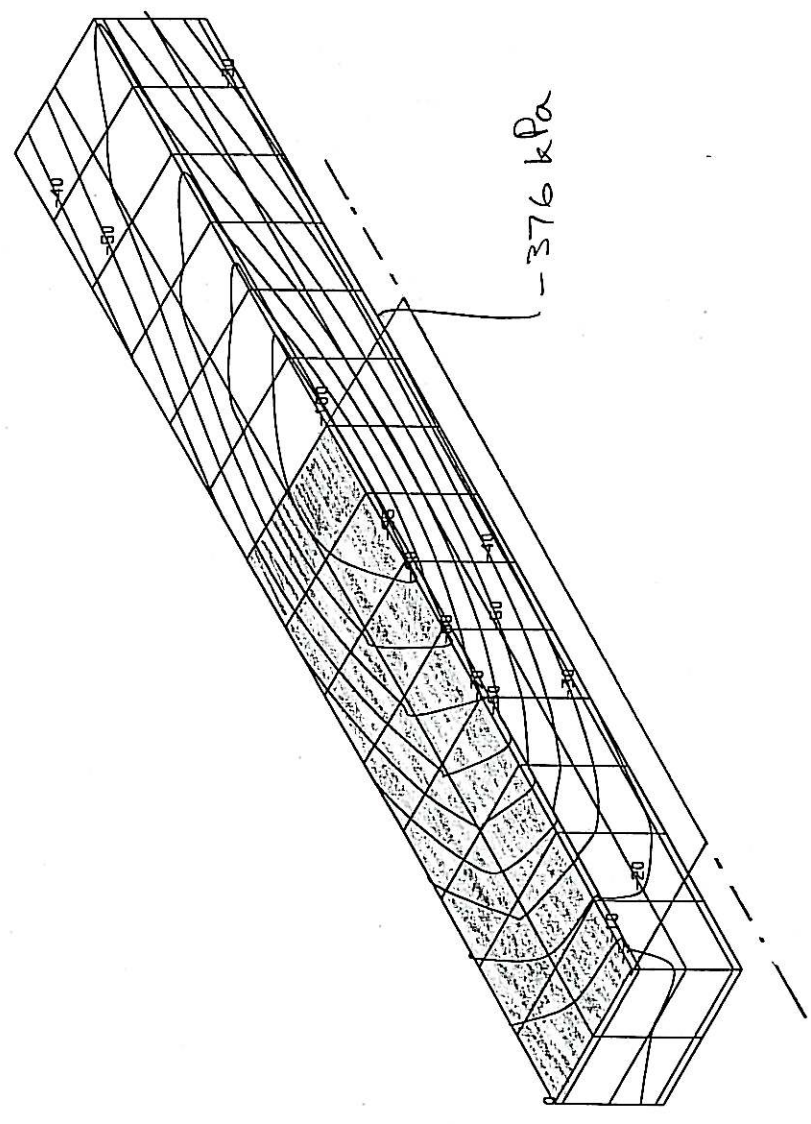
SCALE: 1:1

LENGTH
 X #=1.8666cm
 Y #=1.8666cm
 Z #=1.8666cm

LOAD-STEP:
 LS=40-1

PRESENTATION:
 UNDEFORMED MESH
 DETAIL

ARGUMENT:
 STRESS
 Z - COMPONENT
 SIGN CONSIDERED
 100% =
 1253.937744kN/m2



DESIGN BY SGG/901-Lopez geofe model HU 20.00-08
 1998-8-13 9:32:41

STRUCTURE 1, MAX. DEFLECTION=0.24mm

Dyn I 80

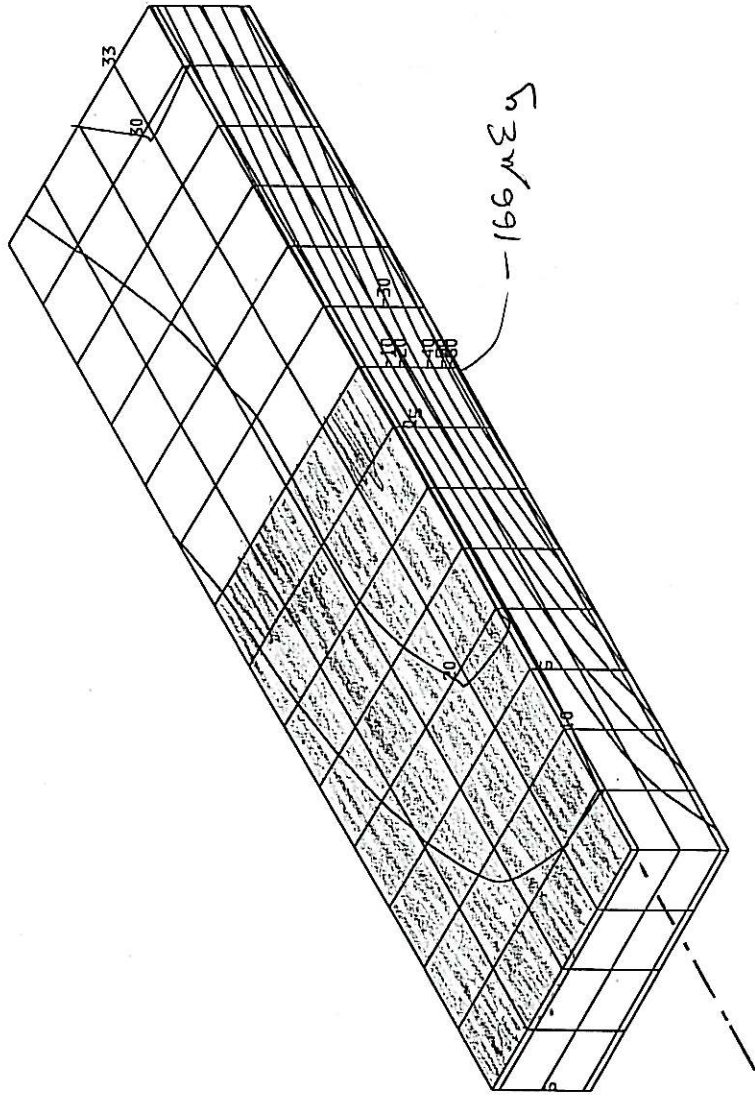
SCALE: 1# = 1

LENGTH
 X # = 2.0999cm
 Y # = 2.0999cm
 Z # = 2.0999cm

LOAD-STEP:
 LS=40-1

PRESENTATION:
 UNDEFORMED MESH
 DETAIL

ARGUMENT:
 STRAIN
 Y -COMPONENT
 SIGN CONSIDERED
 100% =
 0.000277



DESIGN BY SGG/901-Lopez geofe model HU 20.00-08
 1998-8-13 9:47:45

STRUCTURE 1, MAX. DEFLECTION=0.24mm

Dyn I 80

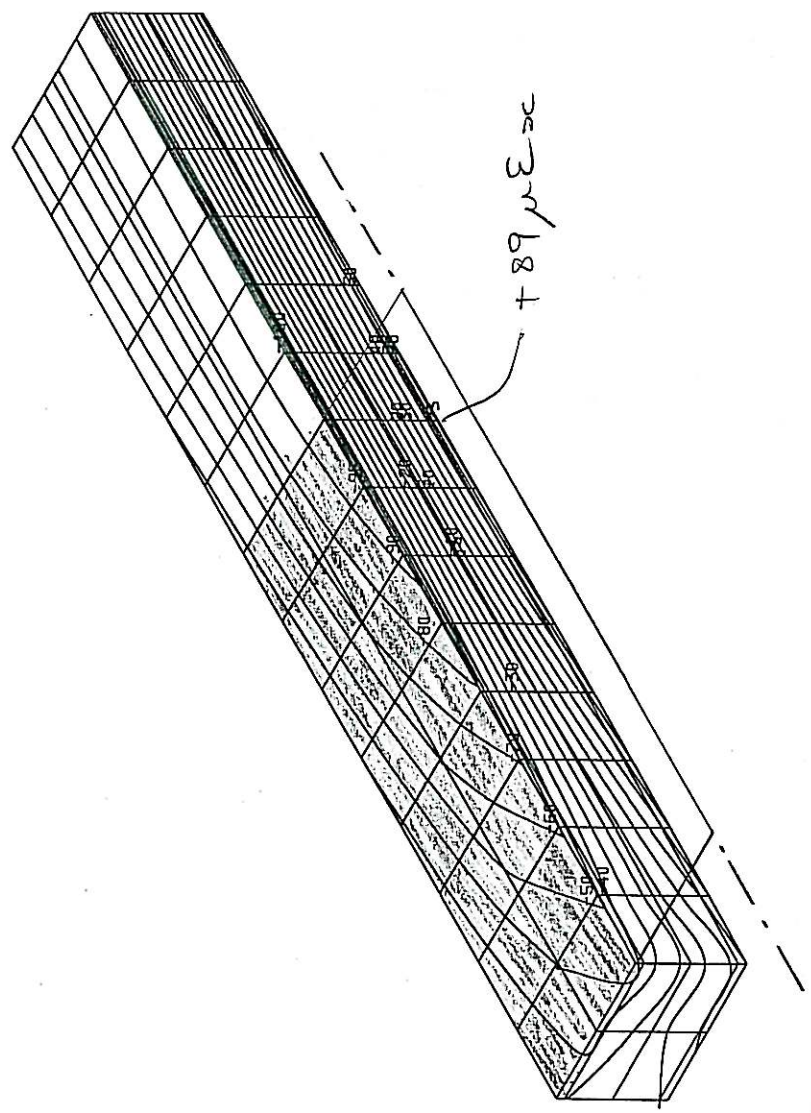
SCALE: 1/100

LENGTH
 X #=1.8666cm
 Y #=1.8666cm
 Z #=1.8666cm

LOAD-STEP:
 LS=40-1

PRESENTATION:
 UNDEFORMED MESH
 DETAIL

ARGUMENT:
 STRAIN
 X -COMPONENT
 SIGN CONSIDERED
 100% =
 0.000120



STRUCTURE 1, MAX. DEFLECTION=0.24mm

•DESIGN BY SGG/901-Lopez 9:35:52
 1998-8-13
 HU 20.00-08

Dym 1 80

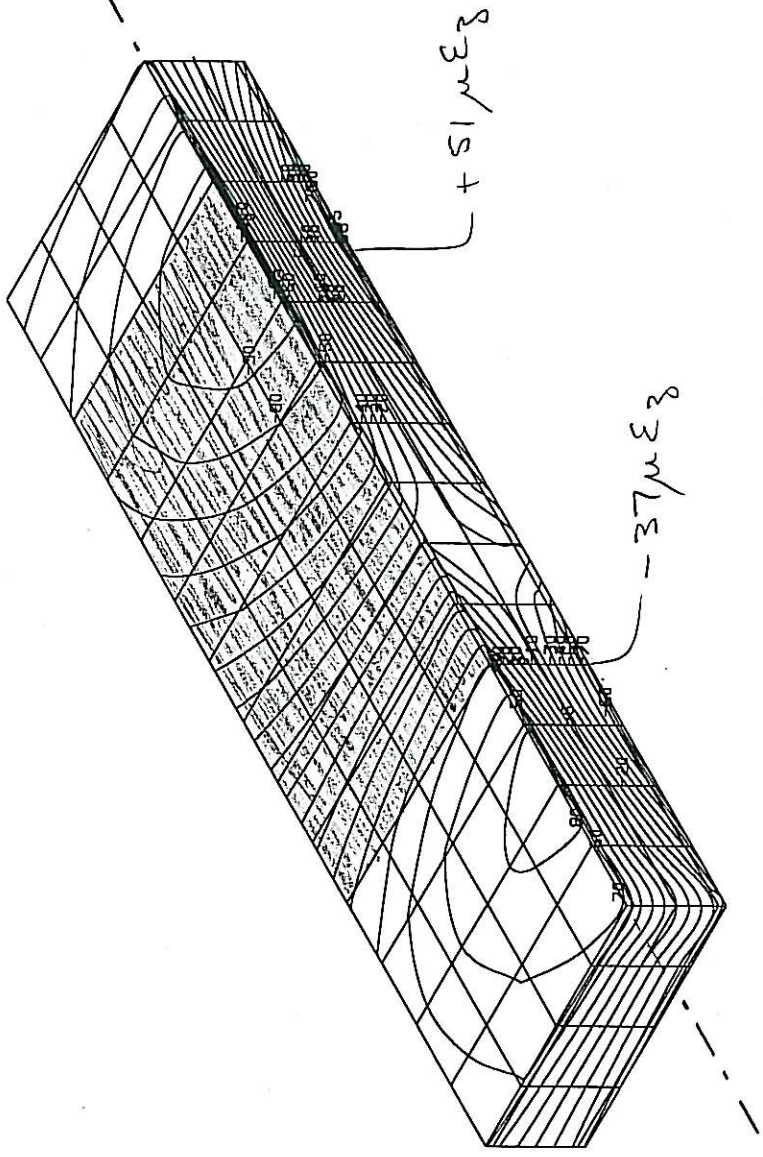
SCALE: 1:1

LENGTH
 X #=2.0999cm
 Y #=2.0999cm
 Z #=2.0999cm

LOAD-STEP:
 LS=40-1

PRESENTATION:
 UNDEFORMED MESH
 DETAIL

ARGUMENT:
 STRAIN
 Z -COMPONENT
 SIGN CONSIDERED
 100% =
 0.000053



DESIGN BY SGG/901-Lopez geofe model HU 20.00-08
 1998-8-13 9:41:2

STRUCTURE 1, MAX. DEFLECTION=0.24mm

Dyn 1 80

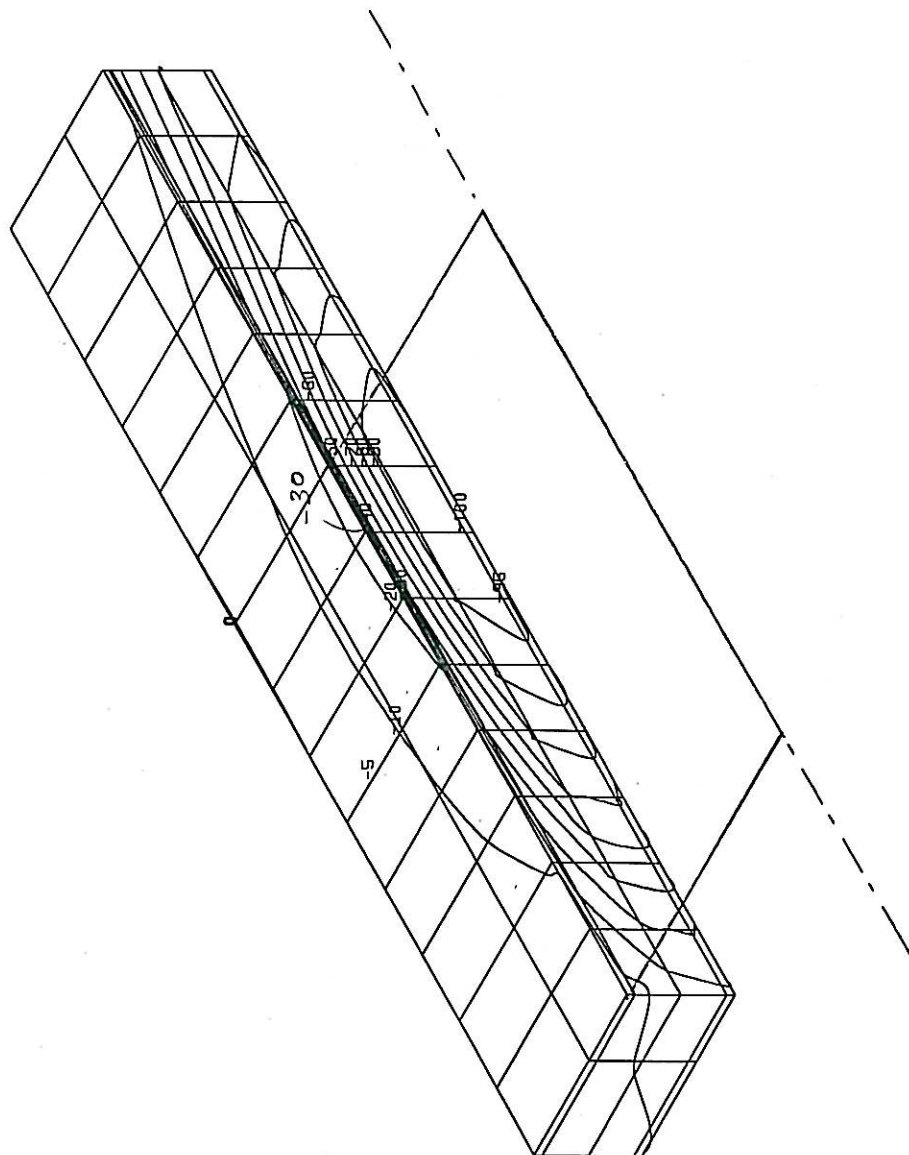
SCALE: 1:1

LENGTH
X #=1.9166cm
Y #=1.9166cm
Z #=1.9166cm

LOAD-STEP:
LS=40-1

PRESENTATION:
UNDEFORMED MESH
DETAIL

ARGUMENT:
STRESS
Tau-XY
SIGN CONSIDERED
100% =
297.882141kN/m²



DESIGN BY SGG/901-topaz geofe model1 HV 20.00-08
1998-8-13 9:53:29

STRUCTURE 1, MAX. DEFLECTION=0.24mm

Dyn I 80

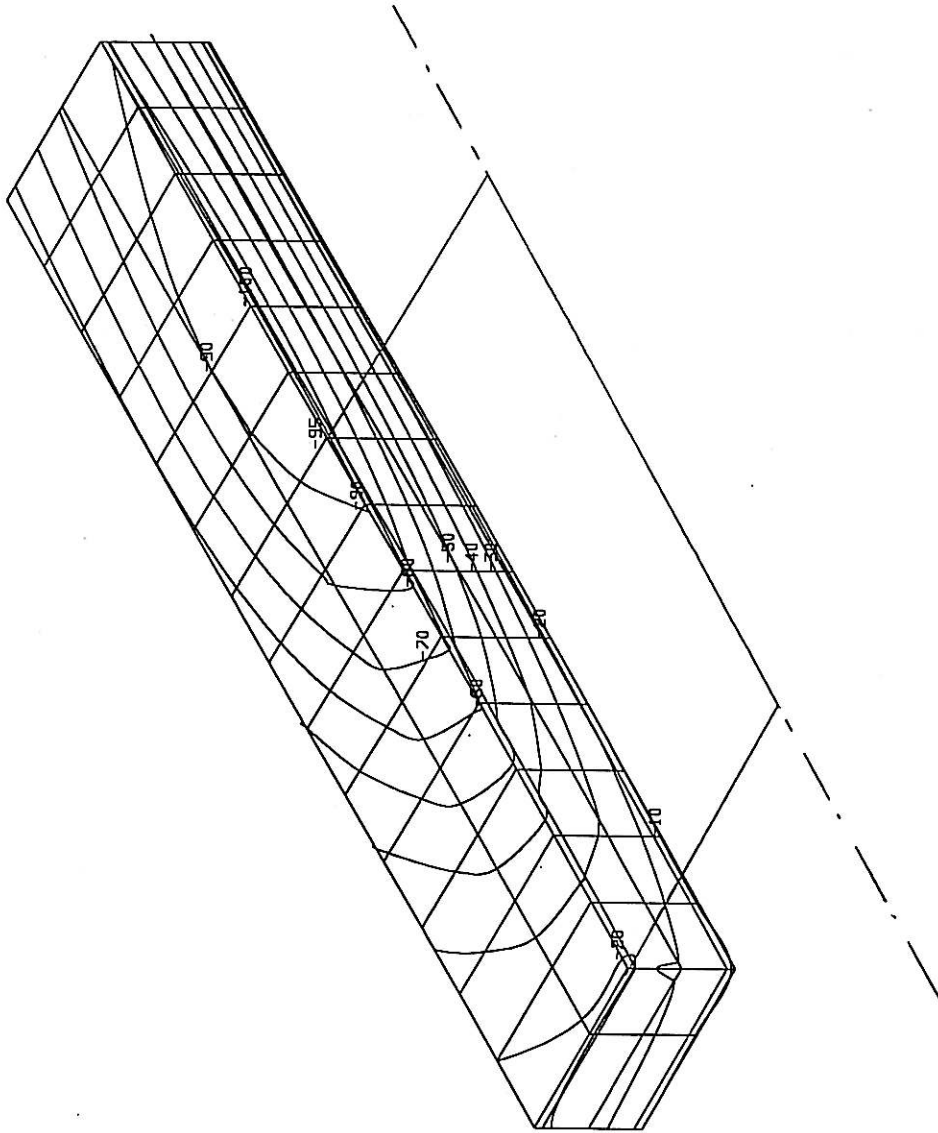
SCALE: 1/10

LENGTH
 X #=1.9166cm
 Y #=1.9166cm
 Z #=1.9166cm

LOAD-STEP:
 LS=40-1

PRESENTATION:
 UNDEFORMED MESH
 DETAIL

ARGUMENT:
 STRAIN
 Gamma-XY
 SIGN CONSIDERED
 100% =
 0.000442



STRUCTURE 1, MAX. DEFLECTION=0.24mm

•DESIGN BY SGG/901-Lopez geofE model1 HV 20.00-08
 1998-8-13 9.55.26

Dyn 1 80

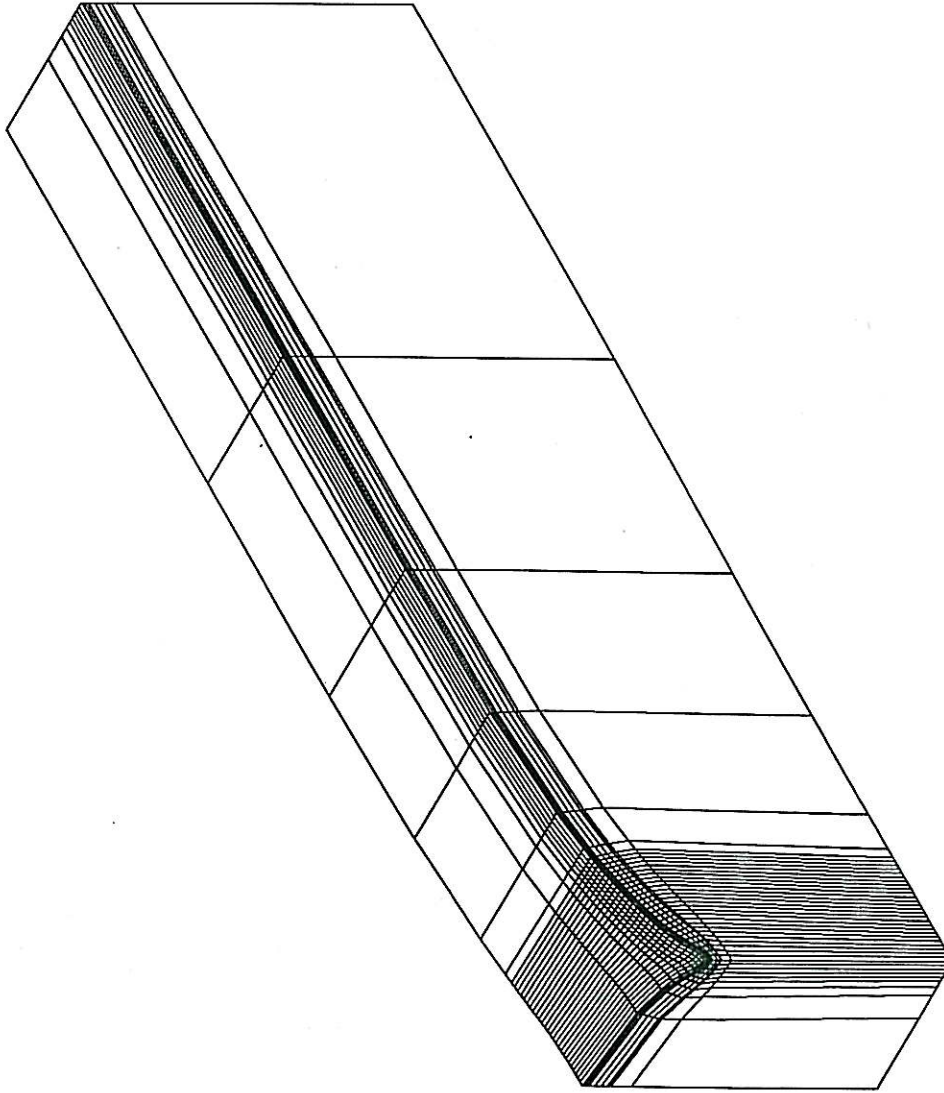
**FINITE ELEMENT RESULTS
STRUCTURE 2: STATIC ANALYSIS**

SCALE: 1# = 1

LENGTH
X # = 31.783cm
Y # = 31.783cm
Z # = 31.783cm
DISPLACEMENT
X # = 0.024269cm
Y # = 0.024269cm
Z # = 0.024269cm

LOAD-STEP:
LS=2

PRESENTATION:
DEFORMED MESH



DESIGN BY SGG/901-Lopez geofE model HV 20.00-08
1998-8-5 9:50:44

STRUCTURE 2, MAX. DEFLECTION=0.36mm

HMA PROJECT
STATIC TYRE, 40kN, 800kPa
FIG. 1: Deflection Bowl

TFA5/A/1

BKS (Pty) Ltd.
Jr. JP Laurens
BOX 3173 PRETORIA
FAX 012 4213501

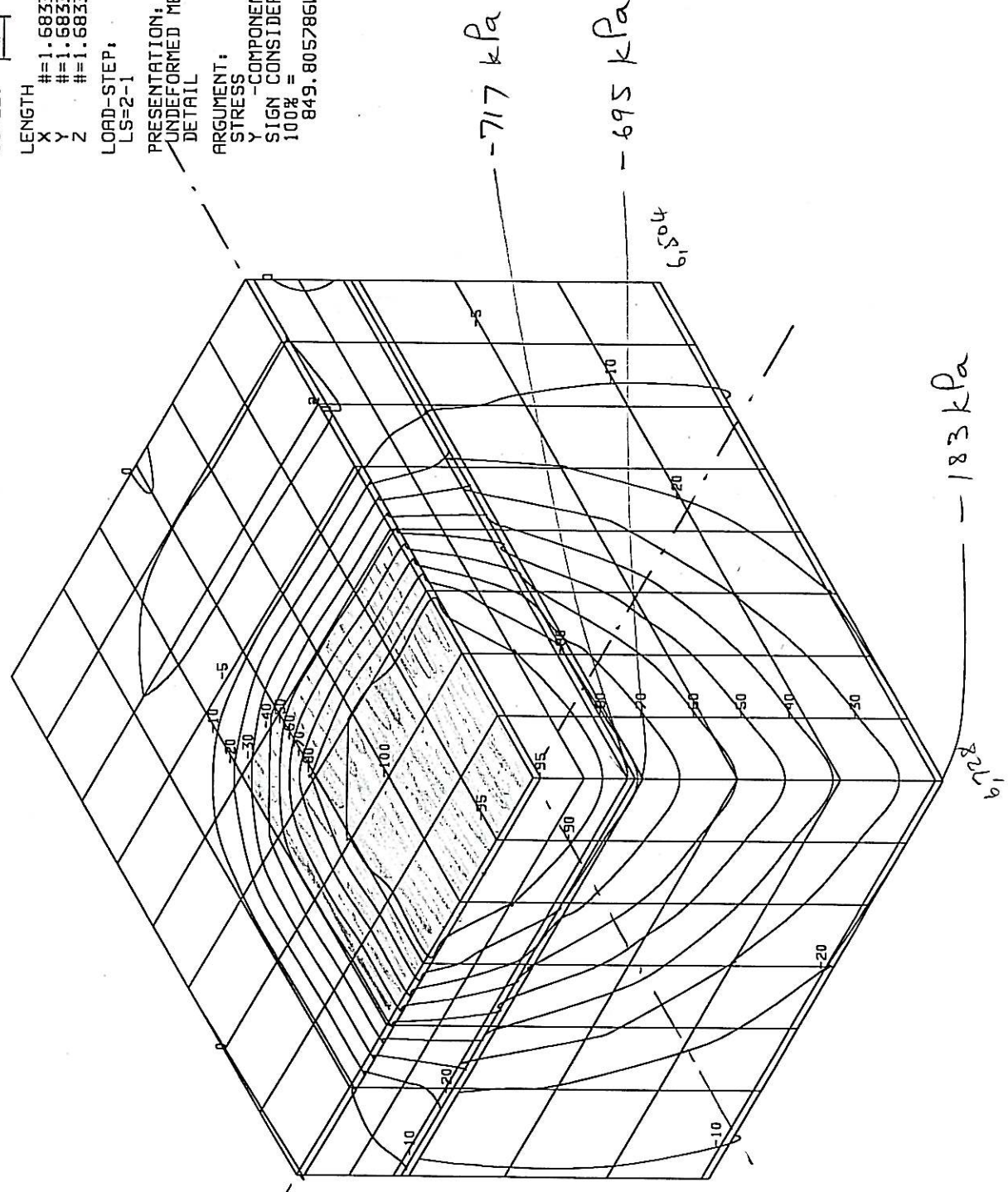
ROLS PROS
DISS

Dyn 2 Stat

Dyn 2
Stat
Ord

DESIGN BY SGG/901-lopaz geofe model NU 20.00-08
1998-8-5 9:57:32

SCALE: 1:1
LENGTH
X #=1.6833cm
Y #=1.6833cm
Z #=1.6833cm
LOAD-STEP:
LS=2-1
PRESENTATION:
UNDEFORMED MESH
DETAIL
ARGUMENT:
STRESS
Y -COMPONENT
SIGN CONSIDERED
100% =
849.805786kN/m2



STRUCTURE 2, MAX. DEFLECTION=0.36mm

SCALE: 1:1

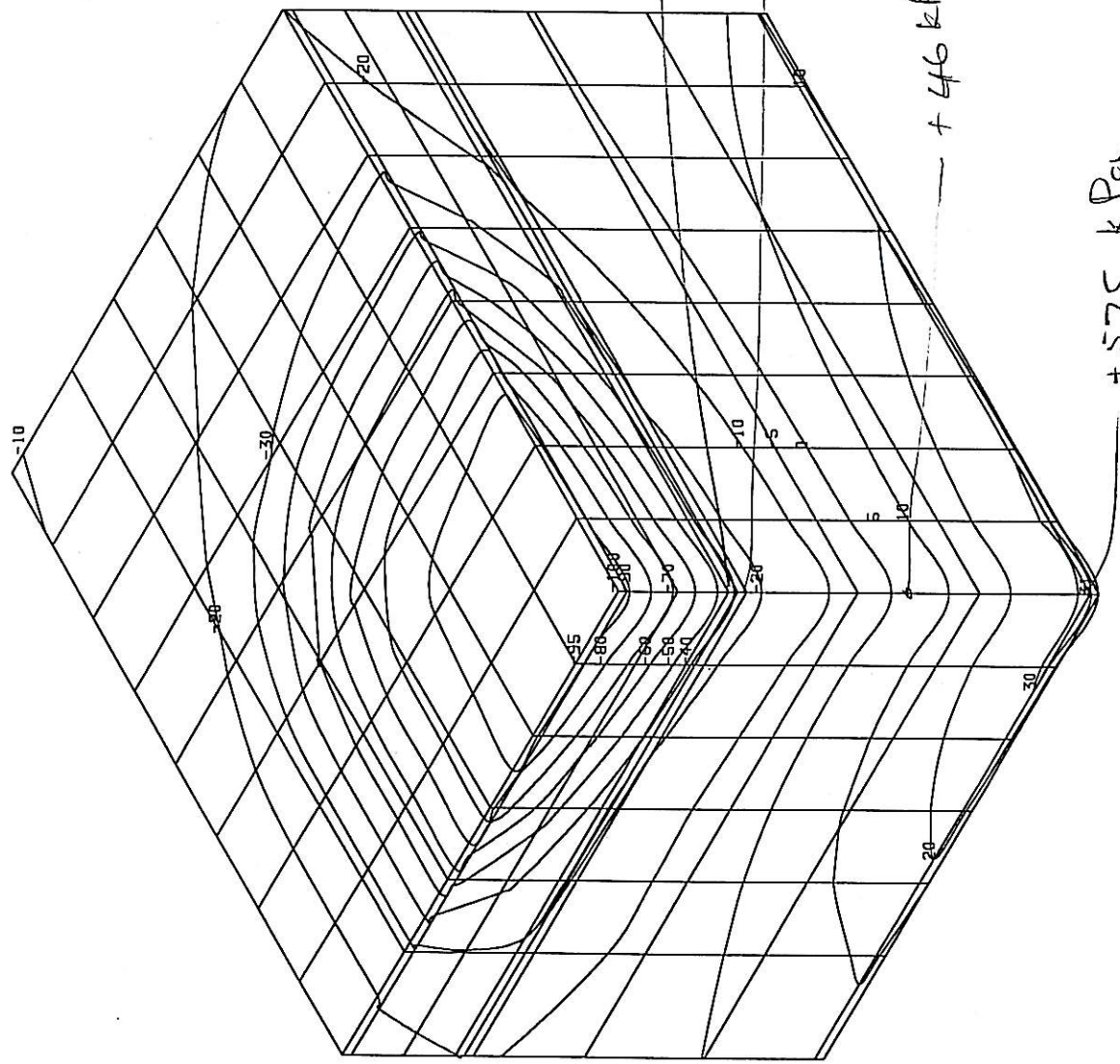
LENGTH
 X #=1.6833cm
 Y #=1.6833cm
 Z #=1.6833cm

LOAD-STEP:
 LS=2-1

PRESENTATION:
 UNDEFORMED MESH
 DETAIL

ARGUMENT:
 STRESS
 X -COMPONENT
 SIGN CONSIDERED
 100% =
 1527.678100kN/m²

z-komponent



DESIGN BY SGG/901-Lopez goFE model HU 20.00-08
 1998-8-5 9:59:41

Dyn 2 Stat

STRUCTURE 2, MAX. DEFLECTION=0.36mm

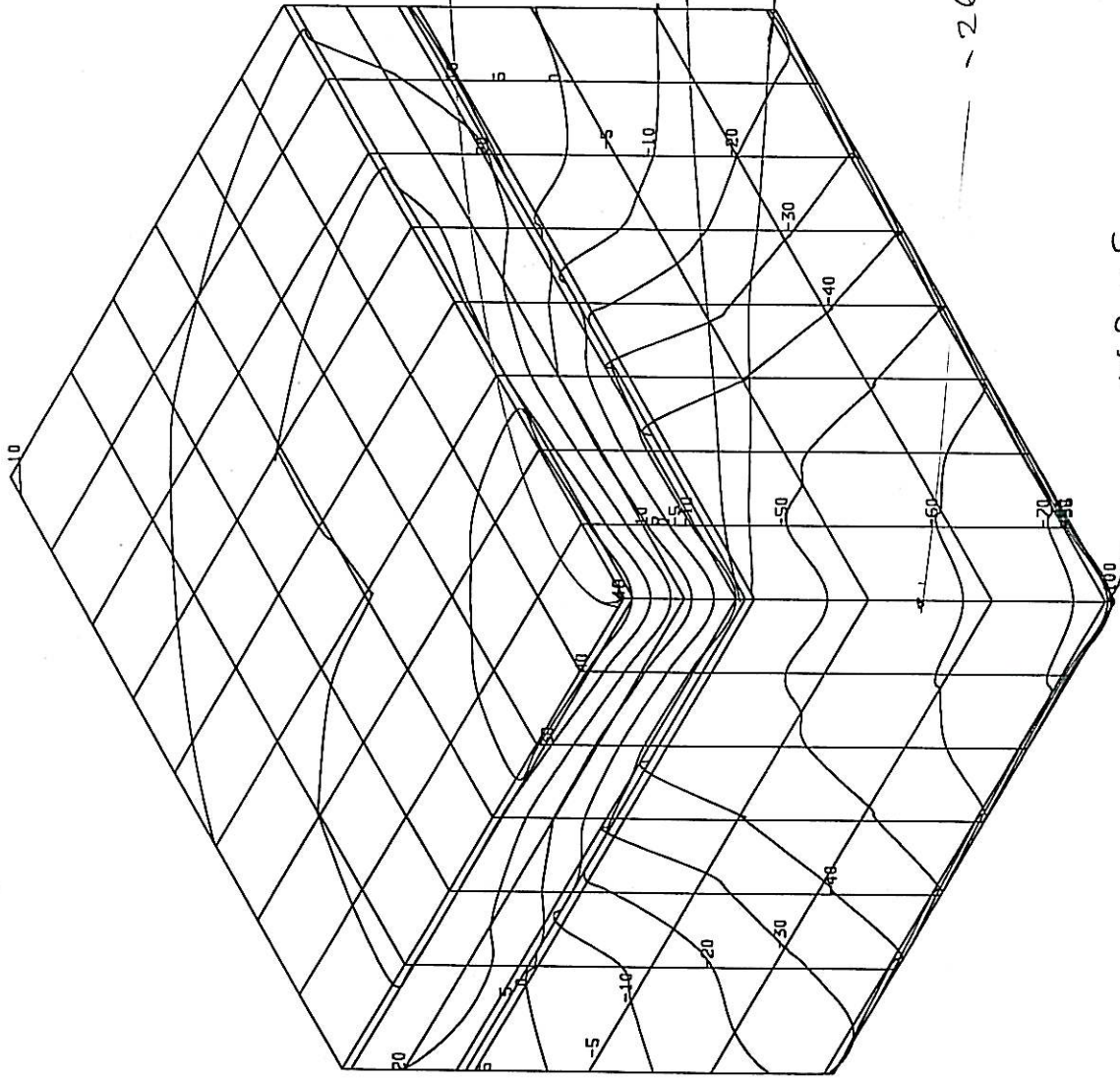
SCALE: 1:1

LENGTH
 X #=1.6833cm
 Y #=1.6833cm
 Z #=1.6833cm

LOAD-STEP:
 LS=2-1

PRESENTATION:
 UNDEFORMED MESH
 DETAIL

ARGUMENT:
 STRAIN
 Y -COMPONENT
 SIGN CONSIDERED
 100% =
 0.000462



DESIGN BY SGG/901-Lopez geofE model HU 20.00-08
 1998-8-5 10:51:23

Dyn 2 Stat

STRUCTURE 2, MAX. DEFLECTION=0.36mm

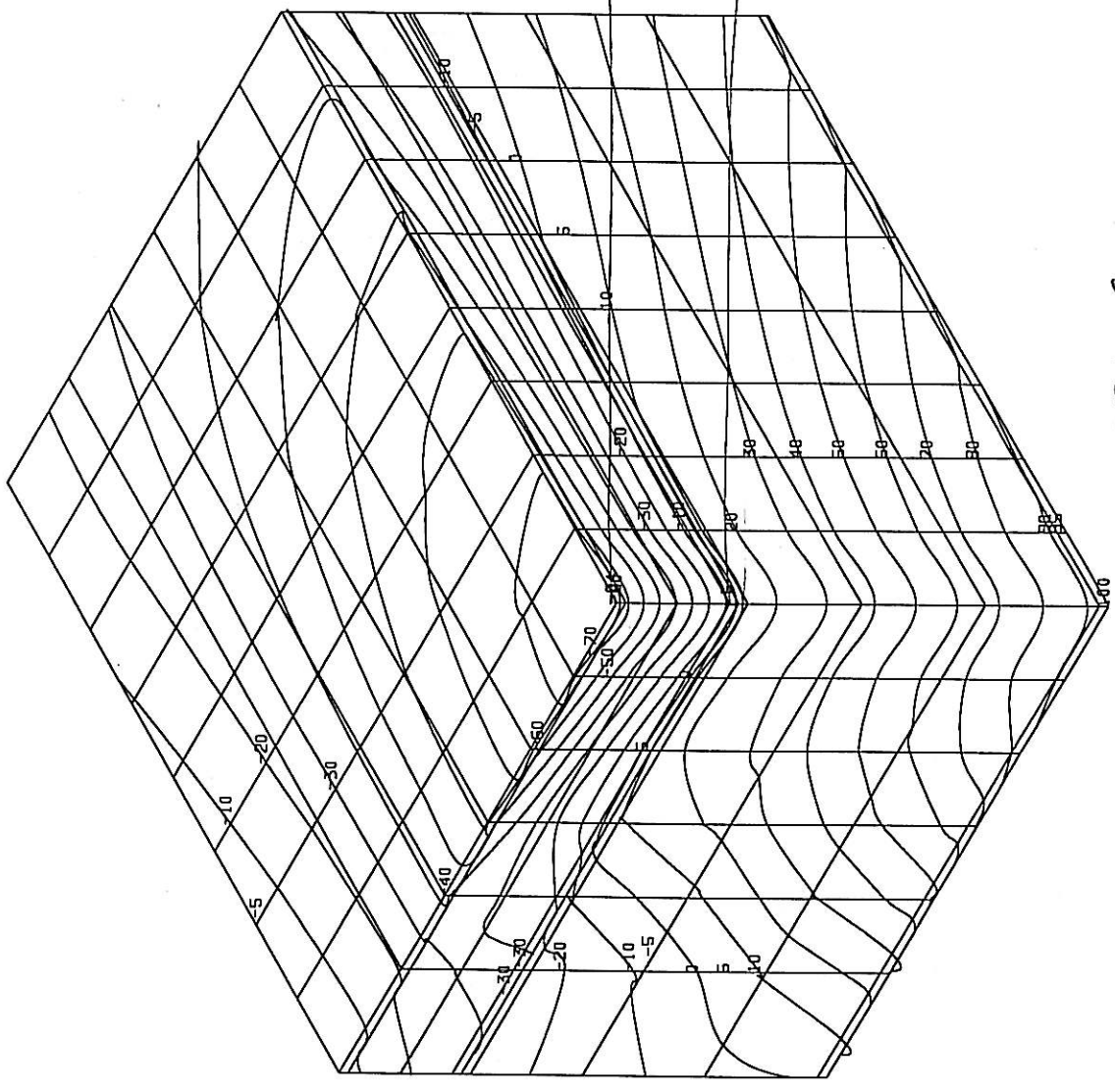
SCALE: 1# = 1cm

LENGTH
 X # = 1.6833cm
 Y # = 1.6833cm
 Z # = 1.6833cm

LOAD-STEP:
 LS=2-1

PRESENTATION:
 UNDEFORMED MESH
 DETAIL

ARGUMENT:
 STRAIN
 X -COMPONENT
 SIGN CONSIDERED
 100% =
 0.000221



DESIGN BY SGG/901-Lopez geofe model HV 20.00-08
 1998-8-5 10:8:39

Dyn 2 Stat

STRUCTURE 2, MAX. DEFLECTION=0.36mm

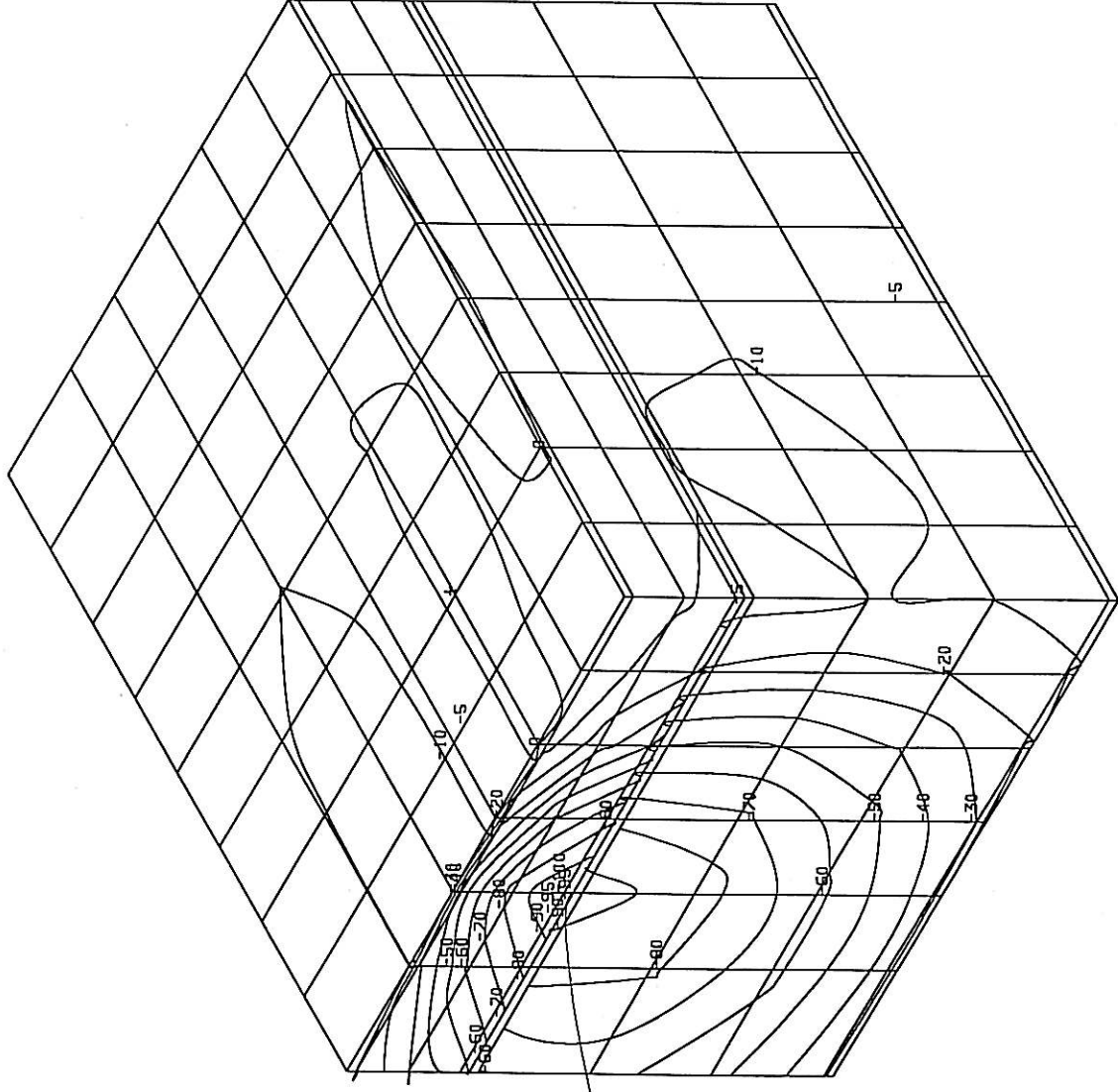
SCALE: 1# = 1cm

LENGTH
 X #=1.6833cm
 Y #=1.6833cm
 Z #=1.6833cm

LOAD-STEP:
 LS=2-1

PRESENTATION:
 UNDEFORMED MESH
 DETAIL

ARGUMENT:
 STRESS
 Tau-XY
 SIGN CONSIDERED
 100% =
 299.062225kN/m2



-299 kPa

STRUCTURE 2, MAX. DEFLECTION=0.36mm

DESIGN BY S66/901-Lopez geofe model HV 20.00-08
 1998-8-5 10:17:45

Dyn 2 Stat

0

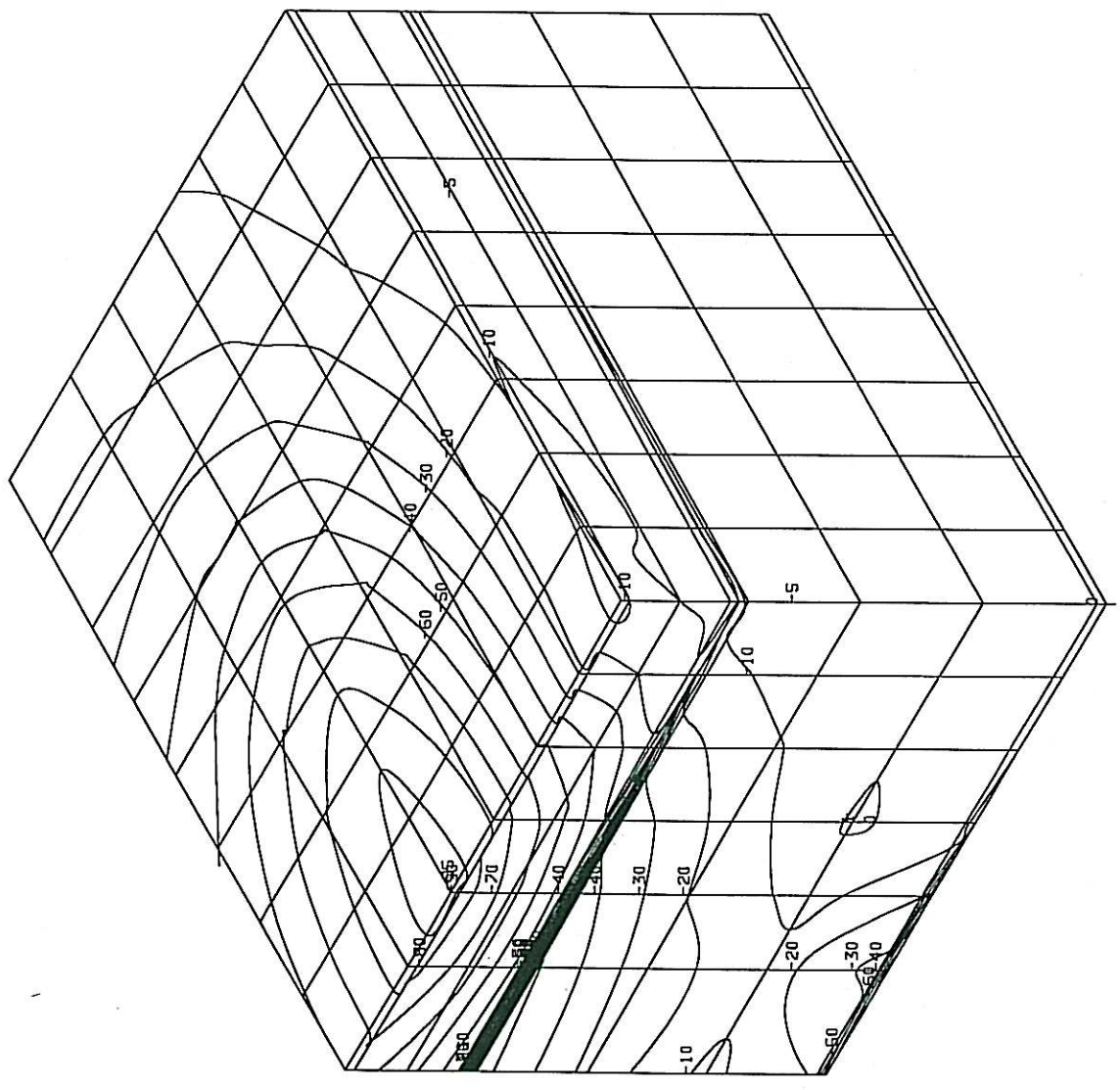
SCALE: |#|=

LENGTH
 X #=1.6833cm
 Y #=1.6833cm
 Z #=1.6833cm

LOAD-STEP:
 LS=2-1

PRESENTATION:
 UNDEFORMED MESH
 DETAIL

ARGUMENT:
 STRAIN
 Gamma-XY
 SIGN CONSIDERED
 100% =
 0.000459



DESIGN BY SGG/901-tpaz geofe model HV 20.00-08
 16.10.9
 1998-8-14

Dyn 2 Stat

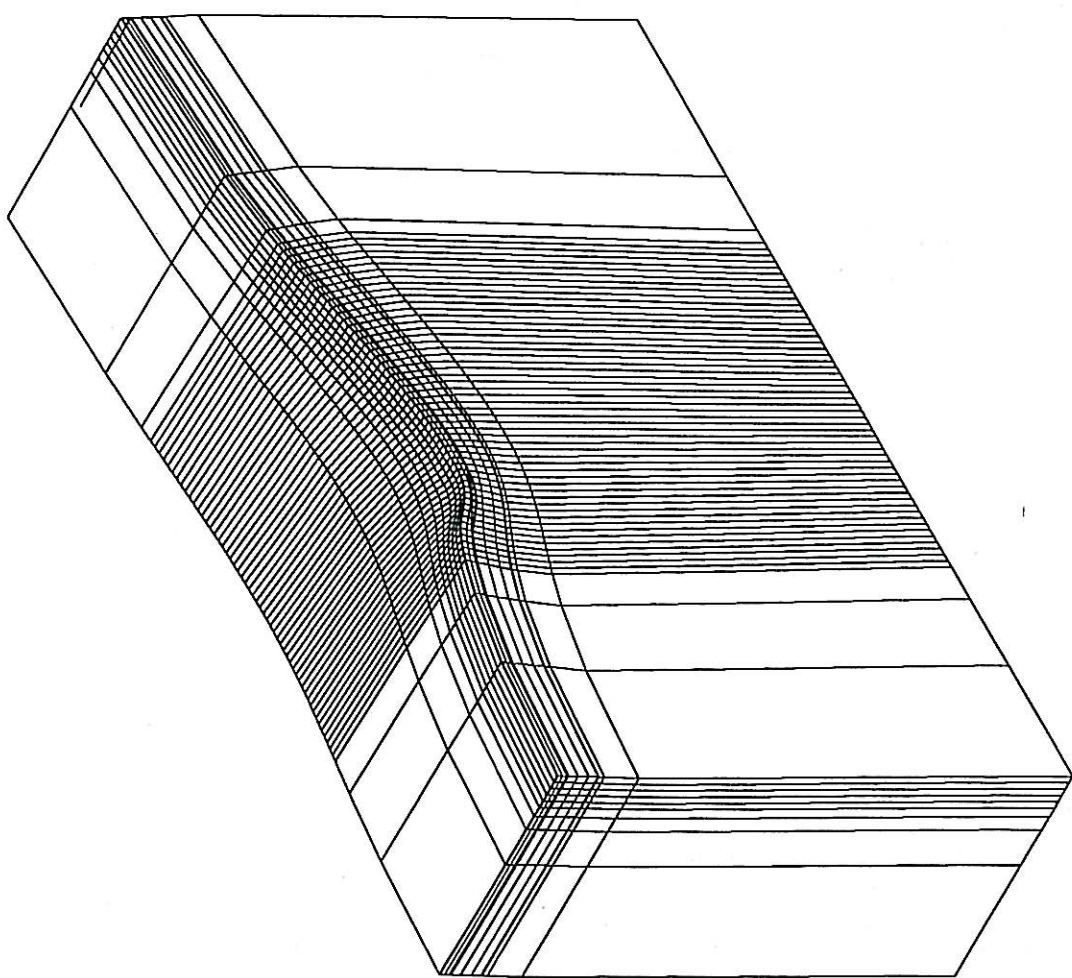
FINITE ELEMENT RESULTS
STRUCTURE 2: 20 KM/H

SCALE: 1# = 1

LENGTH
X # = 20.343cm
Y # = 20.343cm
Z # = 20.343cm
DISPLACEMENT
X # = 0.016360cm
Y # = 0.016360cm
Z # = 0.016360cm

LOAD-STEP:
LS=40

PRESENTATION:
DEFORMED MESH
DETAIL



STRUCTURE 2, MAX. DEFLECTION=0.25mm

DESIGN BY SGG/901-topaz geofe model MV 20.00-08
1998-8-17 B.S1.4

HMA PROJECT		TFA5/A/1
TYRE @ 20km/hour; 40kN, 800kPa		BKS (Pty) Ltd. Dr JP Lourens BOX 3173 PRETORIA FAX 012 4213501
FIG. 1: Deflection Bowl		

ROCWL2
DISR2
RROR2
Dyn 2 20

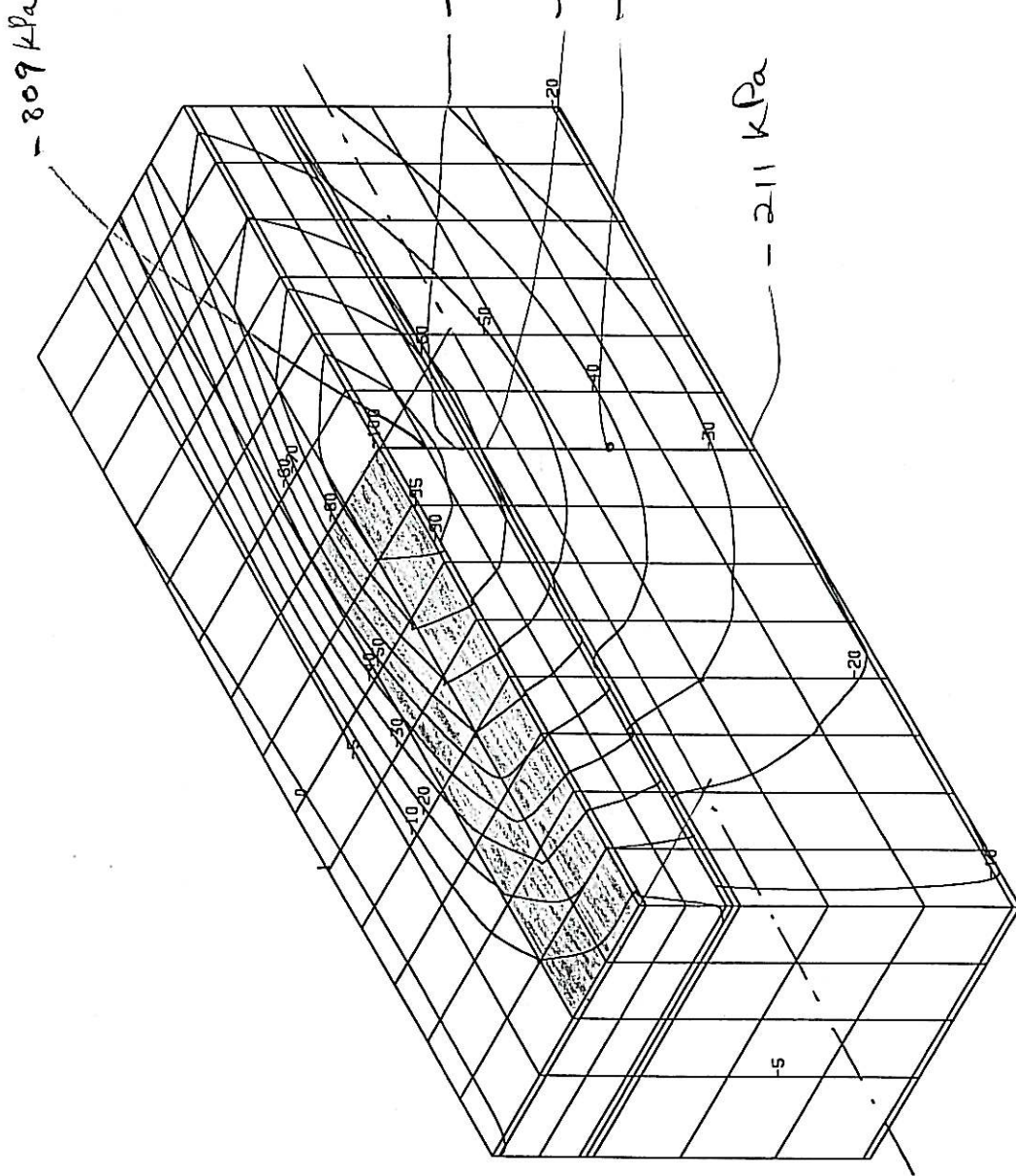
SCALE: 1:1

LENGTH
X #=2.1499cm
Y #=2.1499cm
Z #=2.1499cm

LOAD-STEP:
LS=40-1

PRESENTATION:
UNDEFORMED MESH
DETAIL

ARGUMENT:
STRESS
Y - COMPONENT
SIGN CONSIDERED
100% =
878.763488kN/m²



DESIGN BY SGG/901-Lopez geofe model NU 20.00-08
1998-8-17 8:33:51

STRUCTURE 2, MAX. DEFLECTION=0.25mm

Dyn 2 20

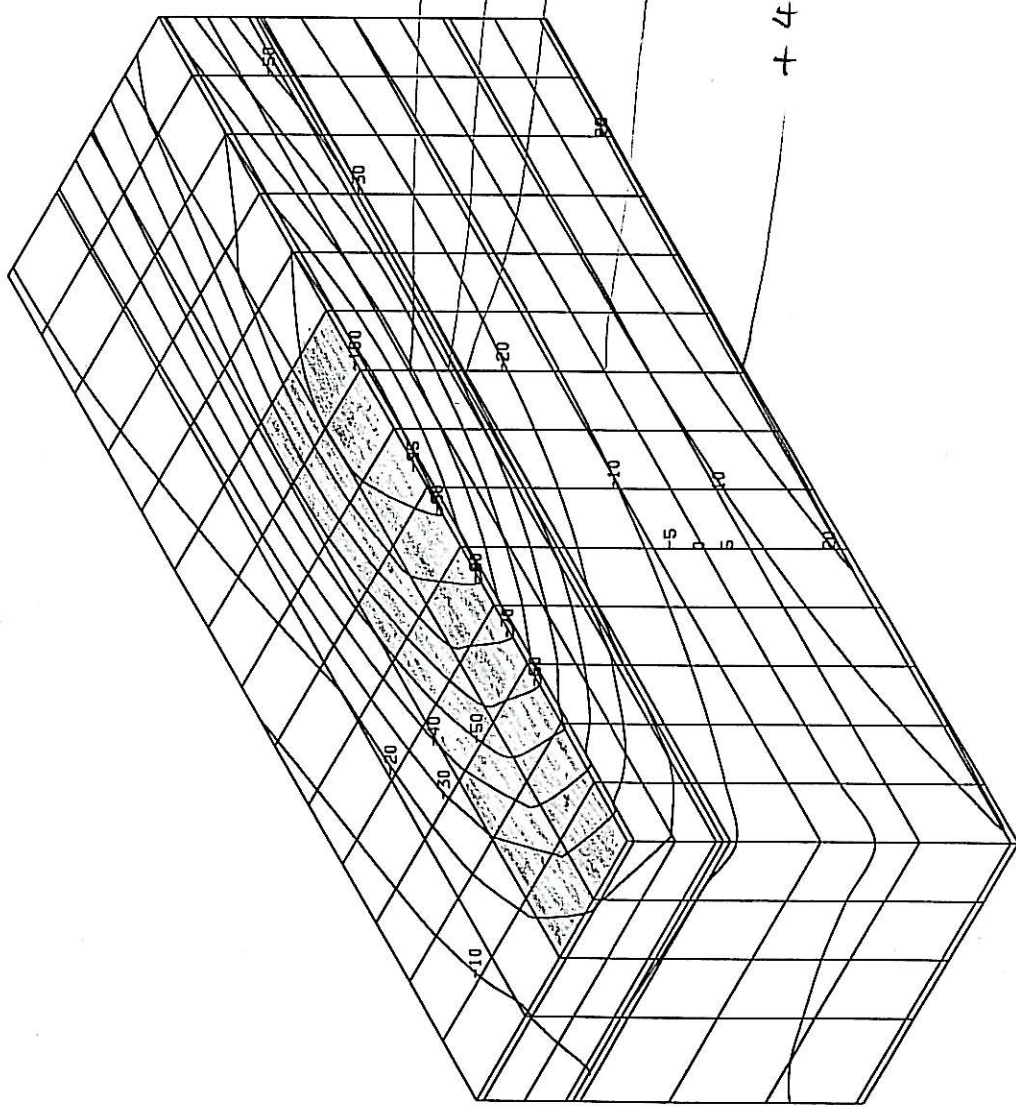
SCALE: 1#=1

LENGTH
 X #=2.1499cm
 Y #=2.1499cm
 Z #=2.1499cm

LOAD-STEP:
 LS=40-1

PRESENTATION:
 UNDEFORMED MESH
 DETAIL

ARGUMENT:
 STRESS
 X-COMPONENT
 SIGN CONSIDERED
 100% =
 1330.900390kN/m²



•DESIGN BY SGG/901-Lopez gsofe model NU 20.00-08
 1998-B-17 8.36.52

STRUCTURE 2, MAX. DEFLECTION=0.25mm

Dyn 2 20

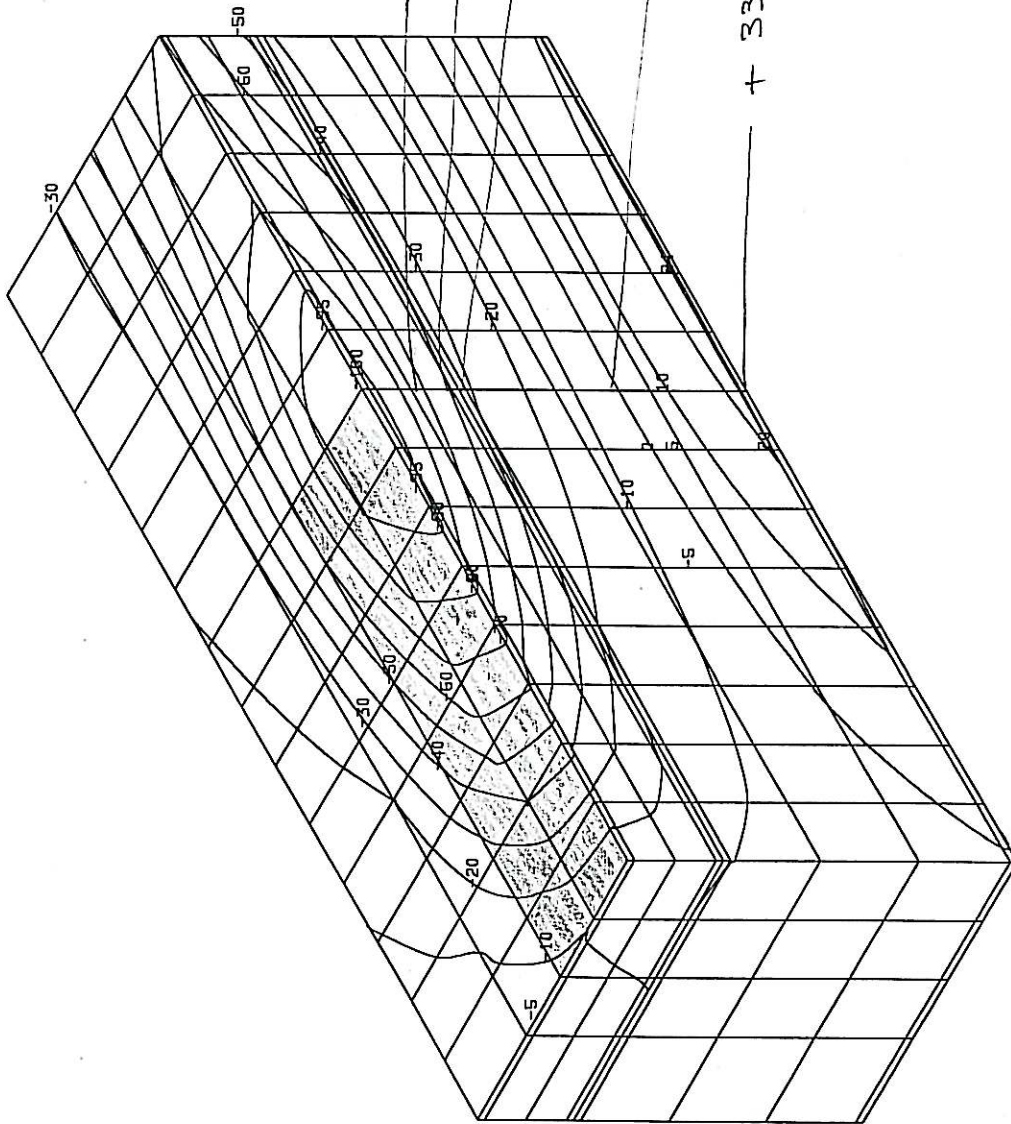
SCALE: $\frac{1}{10}$

LENGTH
 X #=2.1499cm
 Y #=2.1499cm
 Z #=2.1499cm

LOAD-STEP:
 LS=40-1

PRESENTATION:
 UNDEFORMED MESH
 DETAIL

ARGUMENT:
 STRESS
 - COMPONENT
 SIGN CONSIDERED
 100% =
 1208.216674kN/m²



- 918 kPa
 - 625 kPa
 - 440 kPa

0

+ 332 kPa

DESIGN BY SGG/901-Lopez gaeFE model MU 20.00-08
 1998-8-17 8:38:53

STRUCTURE 2, MAX. DEFLECTION=0.25mm

Dyn 2 20

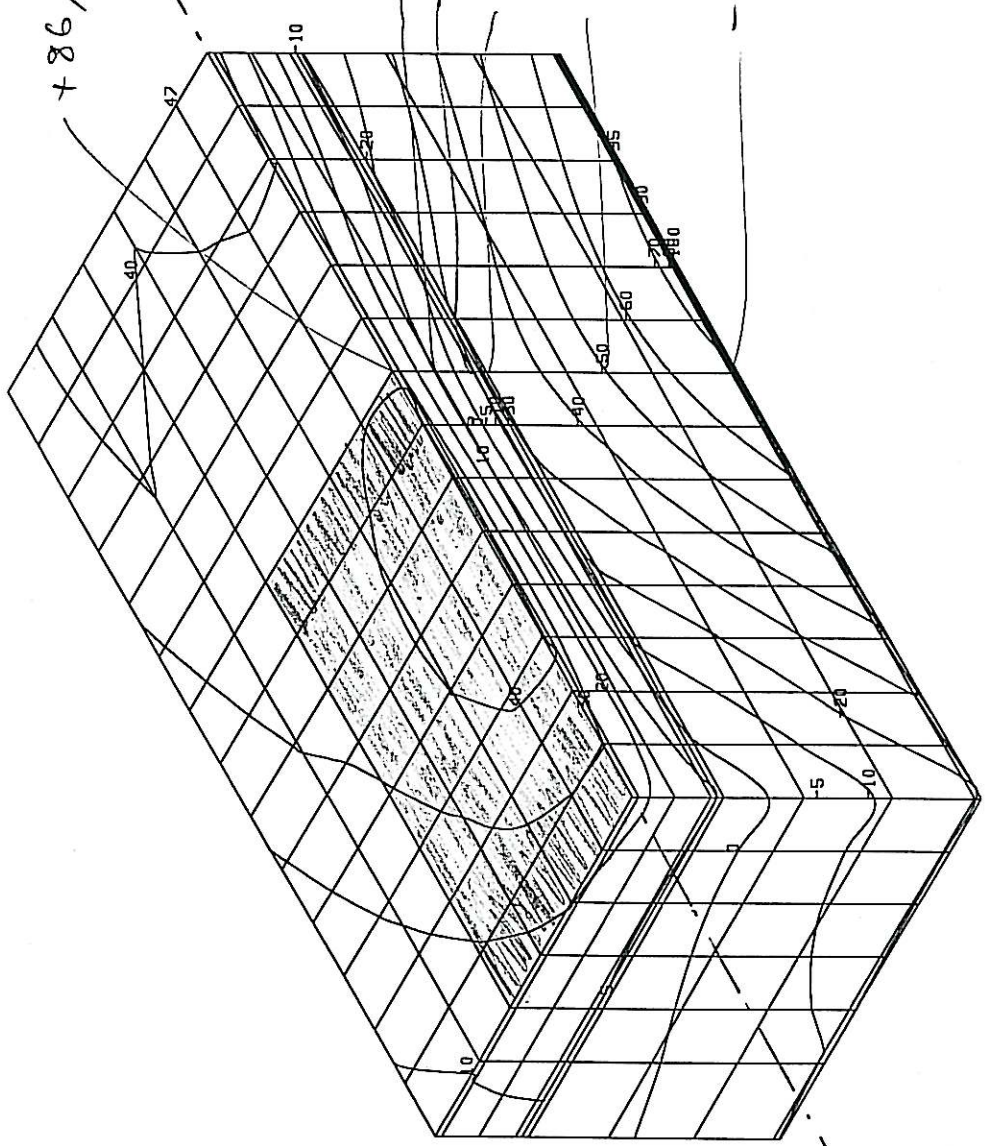
SCALE: 1:100

LENGTH
 X #=2.3832cm
 Y #=2.3832cm
 Z #=2.3832cm

LOAD-STEP:
 LS=40-1

PRESENTATION:
 UNDEFORMED MESH
 DETAIL

ARGUMENT:
 STRAIN
 Y-COMPONENT
 SIGN CONSIDERED
 100% =
 0.000215



STRUCTURE 2, MAX. DEFLECTION=0.25mm

DESIGN BY SGG/901-Lopez geofe model HU 20.00-08
 1998-8-17 9:20:26

Dyn 2 20

Dyn 2 20

DESIGN BY SGG/901-Lopez gaeE model HU 20.00-08
1998-8-17 8:41:16

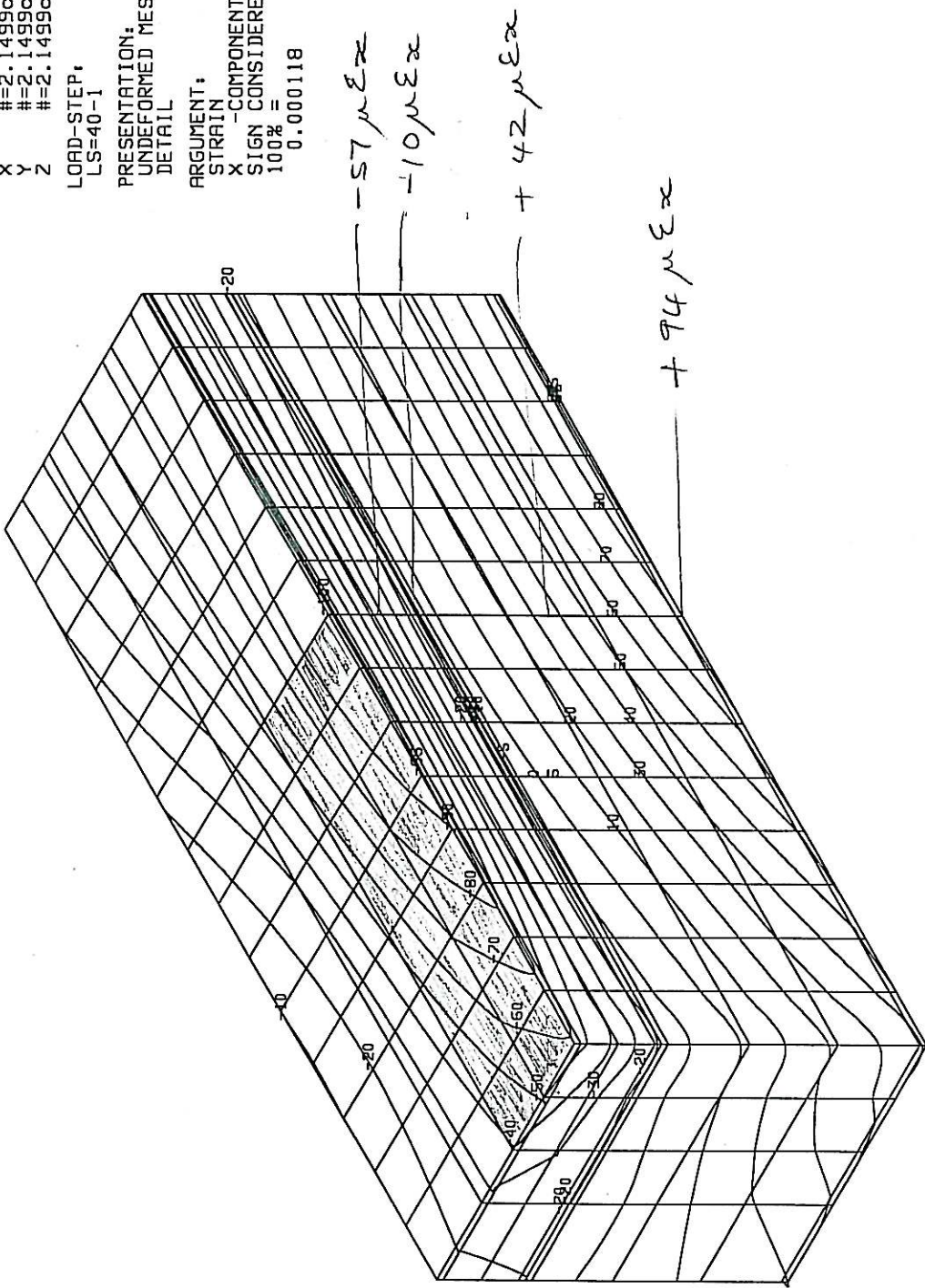
SCALE: 1# = 1

LENGTH
 X #=2.1499cm
 Y #=2.1499cm
 Z #=2.1499cm

LOAD-STEP:
 LS=40-1

PRESENTATION:
 UNDEFORMED MESH
 DETAIL

ARGUMENT:
 STRAIN
 X -COMPONENT
 SIGN CONSIDERED
 100% =
 0.000118



STRUCTURE 2, MAX. DEFLECTION=0.25mm

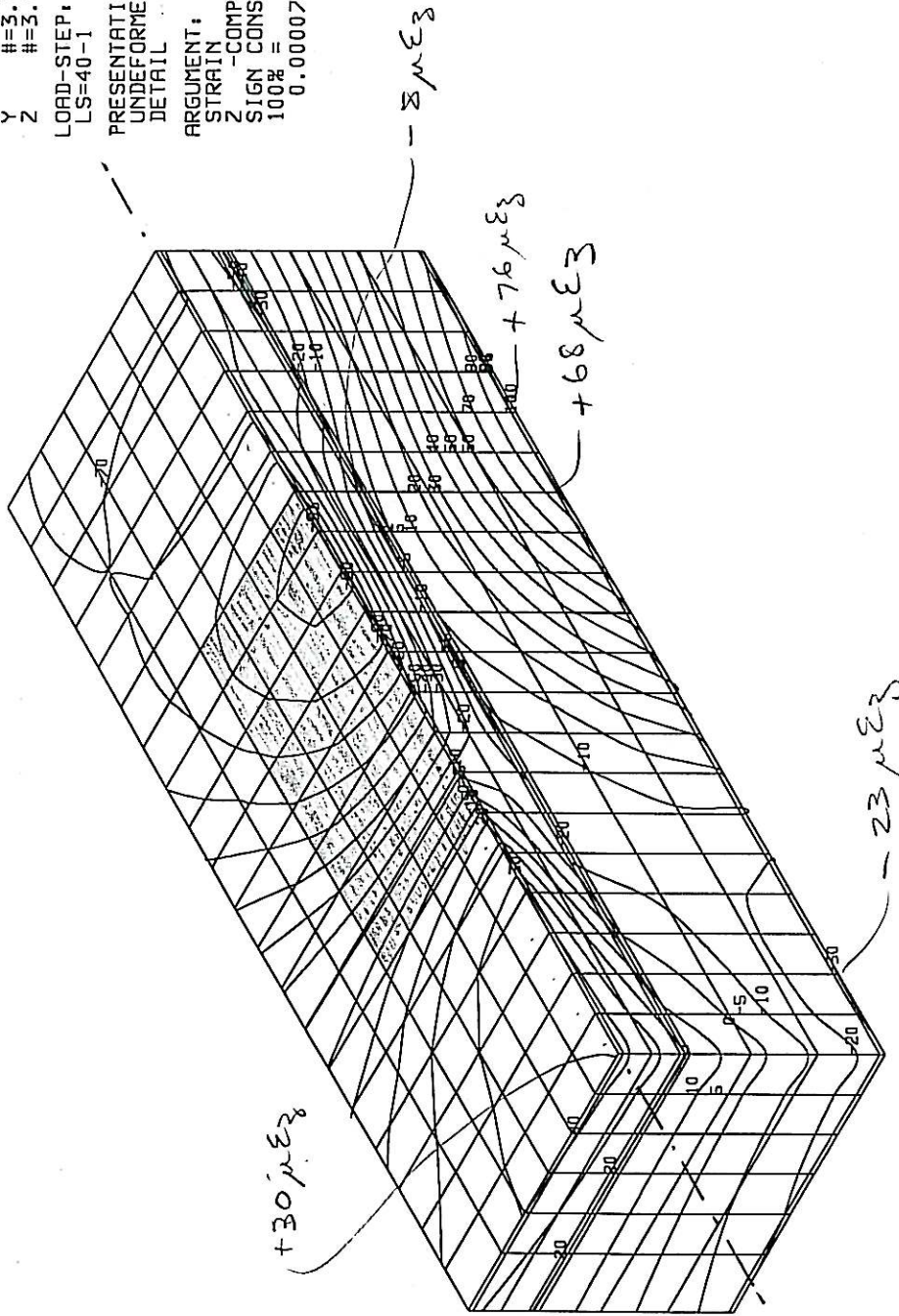
SCALE: 1# = 1

LENGTH
X # = 3.0832cm
Y # = 3.0832cm
Z # = 3.0832cm

LOAD-STEP:
LS=40-1

PRESENTATION:
UNDEFORMED MESH
DETAIL

ARGUMENT:
STRAIN
Z - COMPONENT
SIGN CONSIDERED
100% =
0.000076



DESIGN BY SGG/901-Lopez geofe model MU 20.00-08
1998-8-17 8:55:27

STRUCTURE 2, MAX. DEFLECTION=0.25mm

Dyn 2 20

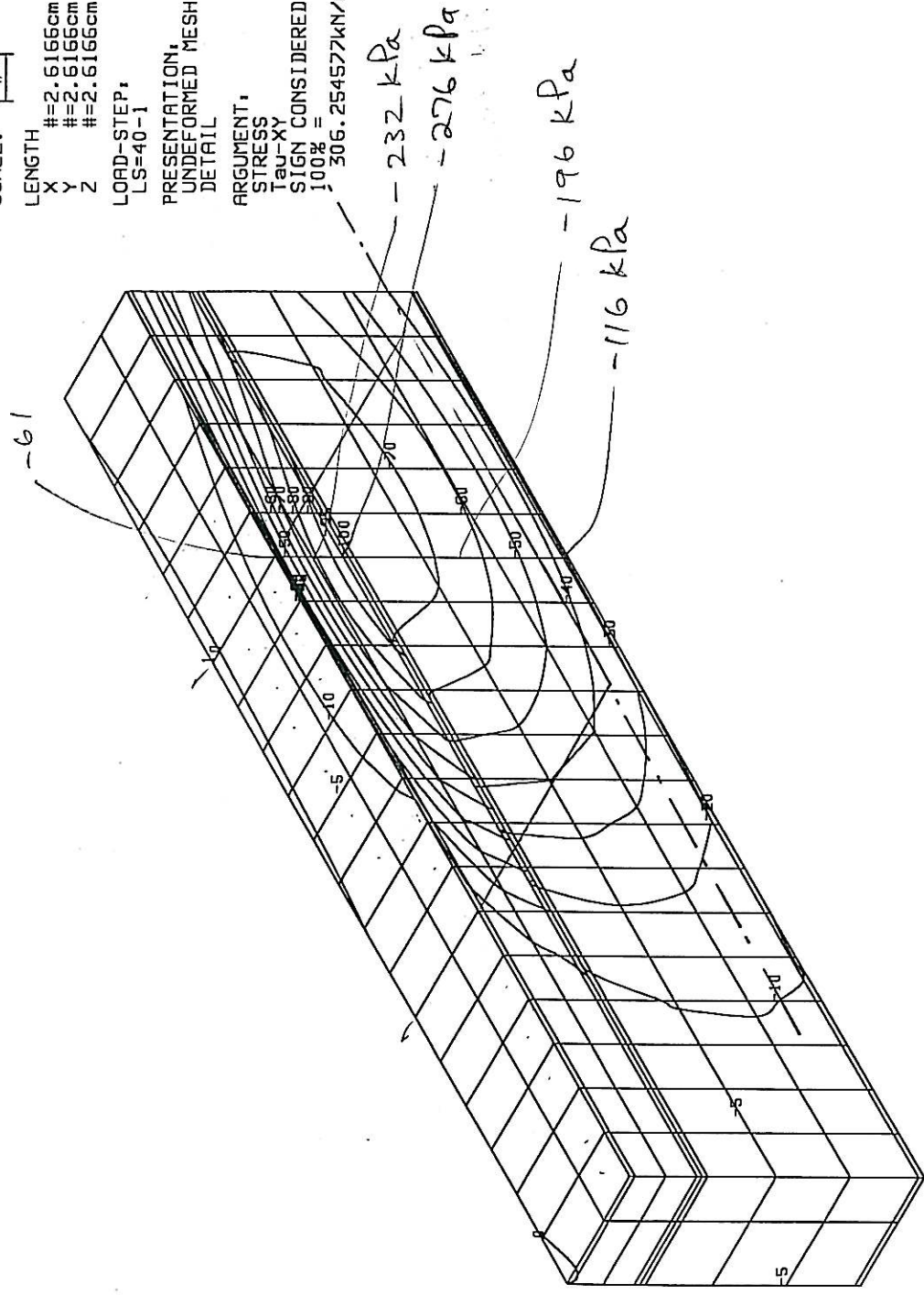
SCALE: 1# = 1

LENGTH
 X # = 2.6166cm
 Y # = 2.6166cm
 Z # = 2.6166cm

LOAD-STEP:
 LS=40-1

PRESENTATION:
 UNDEFORMED MESH
 DETAIL

ARGUMENT:
 STRESS
 Tau-XY
 SIGN CONSIDERED
 100% =
 306.254577kN/m2



DESIGN BY SGG/901-lopaz geofE model HV 20.00-08
 1998-8-17 9:11:39

STRUCTURE 2, MAX. DEFLECTION=0.25mm

Dyn 2 20

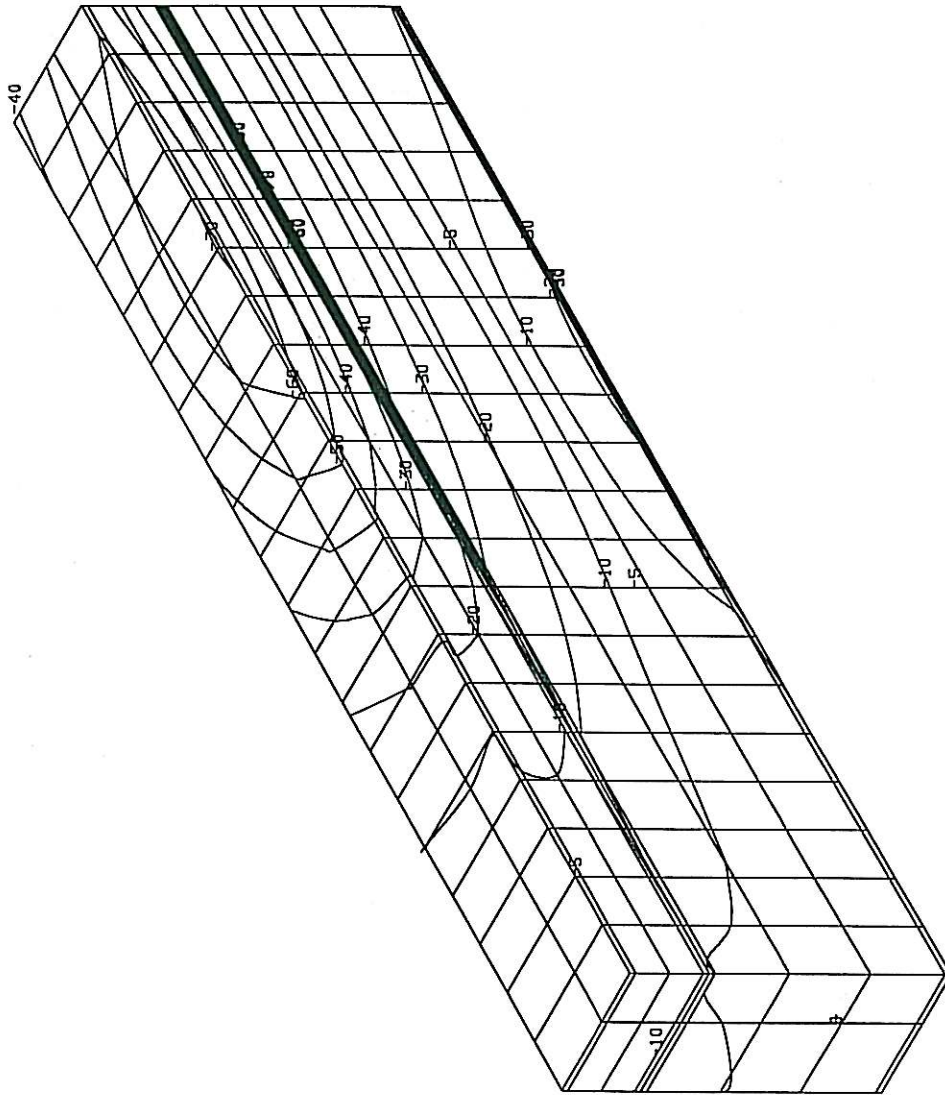
SCALE: 1#=#

LENGTH
 X #=2.6166cm
 Y #=2.6166cm
 Z #=2.6166cm

LOAD-STEP:
 LS=40-1

PRESENTATION:
 UNDEFORMED MESH
 DETAIL

ARGUMENT:
 STRAIN
 Gamma-XY
 SIGN CONSIDERED
 100% =
 0.000267



DESIGN BY 566/901-Lopez geofE model MV 20.00-08
 1998-8-17 9.31.45

STRUCTURE 2, MAX. DEFLECTION=0.25mm

Dyn 2 20

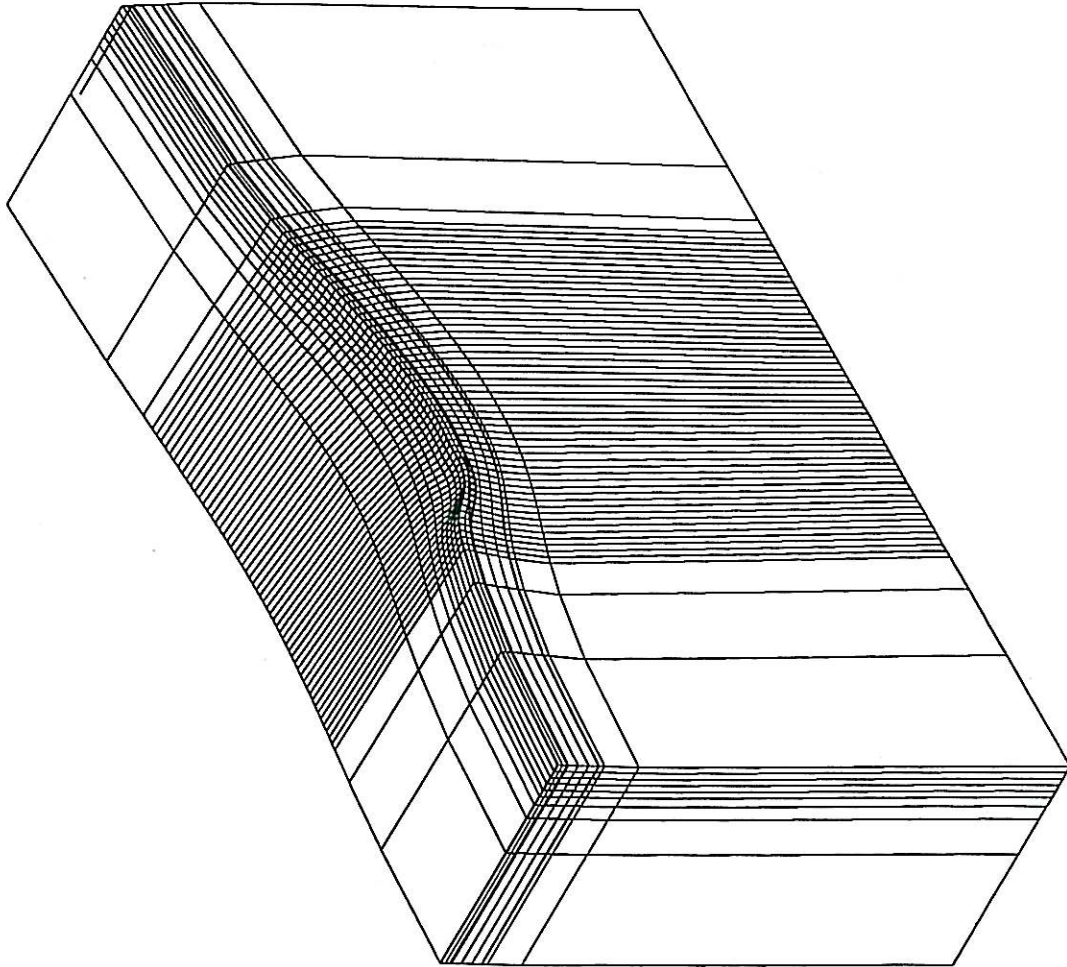
FINITE ELEMENT RESULTS
STRUCTURE 2:80 KM/H

SCALE: 1:1

LENGTH
X #=20.343cm
Y #=20.343cm
Z #=20.343cm
DISPLACEMENT
X #=0.011793cm
Y #=0.011793cm
Z #=0.011793cm

LOAD-STEP:
LS=40

PRESENTATION:
DEFORMED MESH
DETAIL



DESIGN BY SGG/901-Lopez geofe model HU 20.00-08
1998-B-14 8:29:32

STRUCTURE 2, MAX. DEFLECTION=0.18mm

	HMA PROJECT	TFAS/A/1
	TYRE @ 80km/hour; 40kN, 800kPa FIG. 1: Deflection Bowl	BKS (PTY) Ltd. Dr JP Lourens BOX 3173 PRETORIA FAX 012 4213501

ROLW/L2
DISRS
PRORB
Dyn 2 80

SCALE: 1:1

LENGTH
X #=2.1499cm
Y #=2.1499cm
Z #=2.1499cm

LOAD-STEP:
LS=40-1

PRESENTATION:
UNDEFORMED MESH
DETAIL

ARGUMENT:
STRESS
Y -COMPONENT
SIGN CONSIDERED
100% =
1015.575134KN/m2

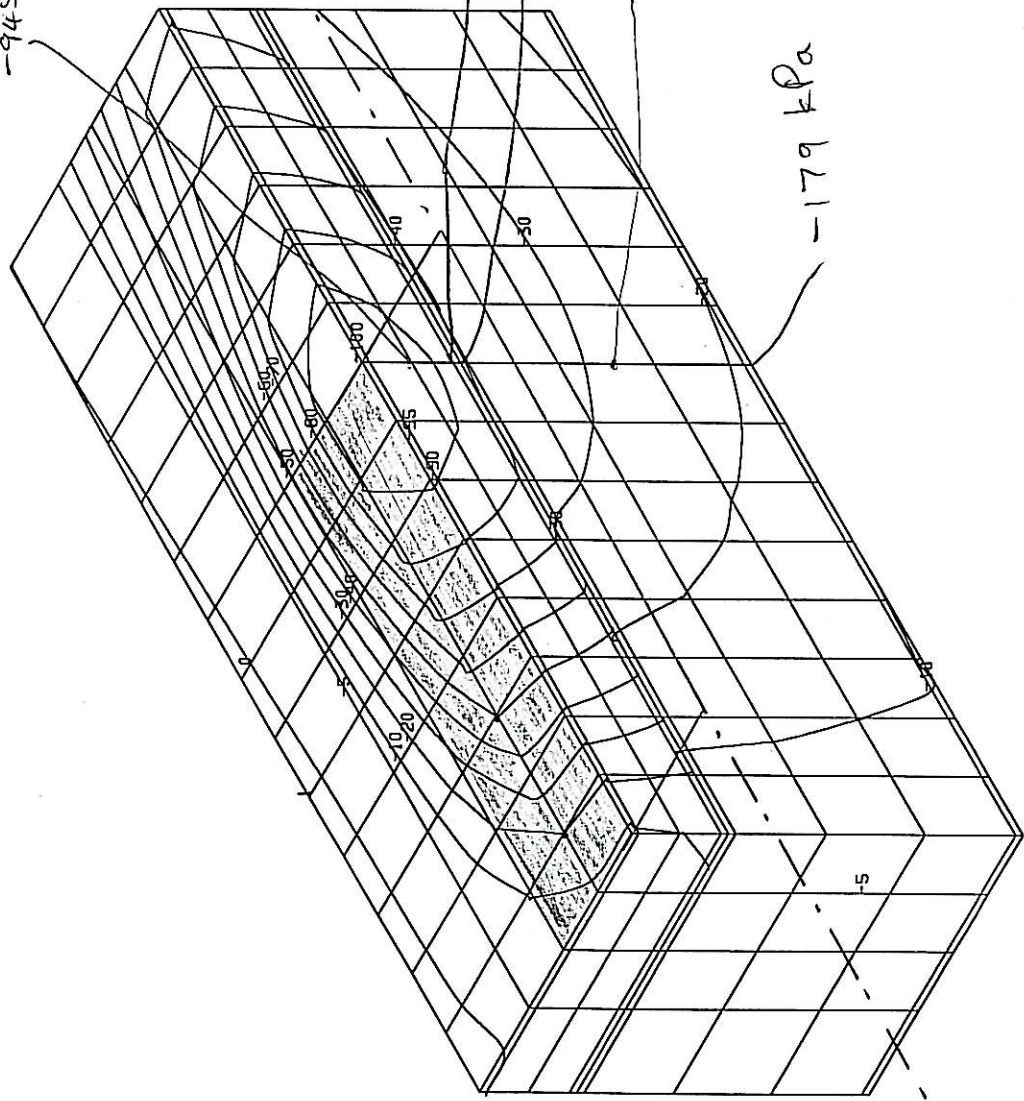
-945 kPa

-804 kPa

-406 kPa

-284 kPa

-179 kPa



DESIGN BY SGG/901-topaz geofe model1 MU 20.00-08
1998-B-14 B.33.1

STRUCTURE 2, MAX. DEFLECTION=0.18mm

Dyn 2 8

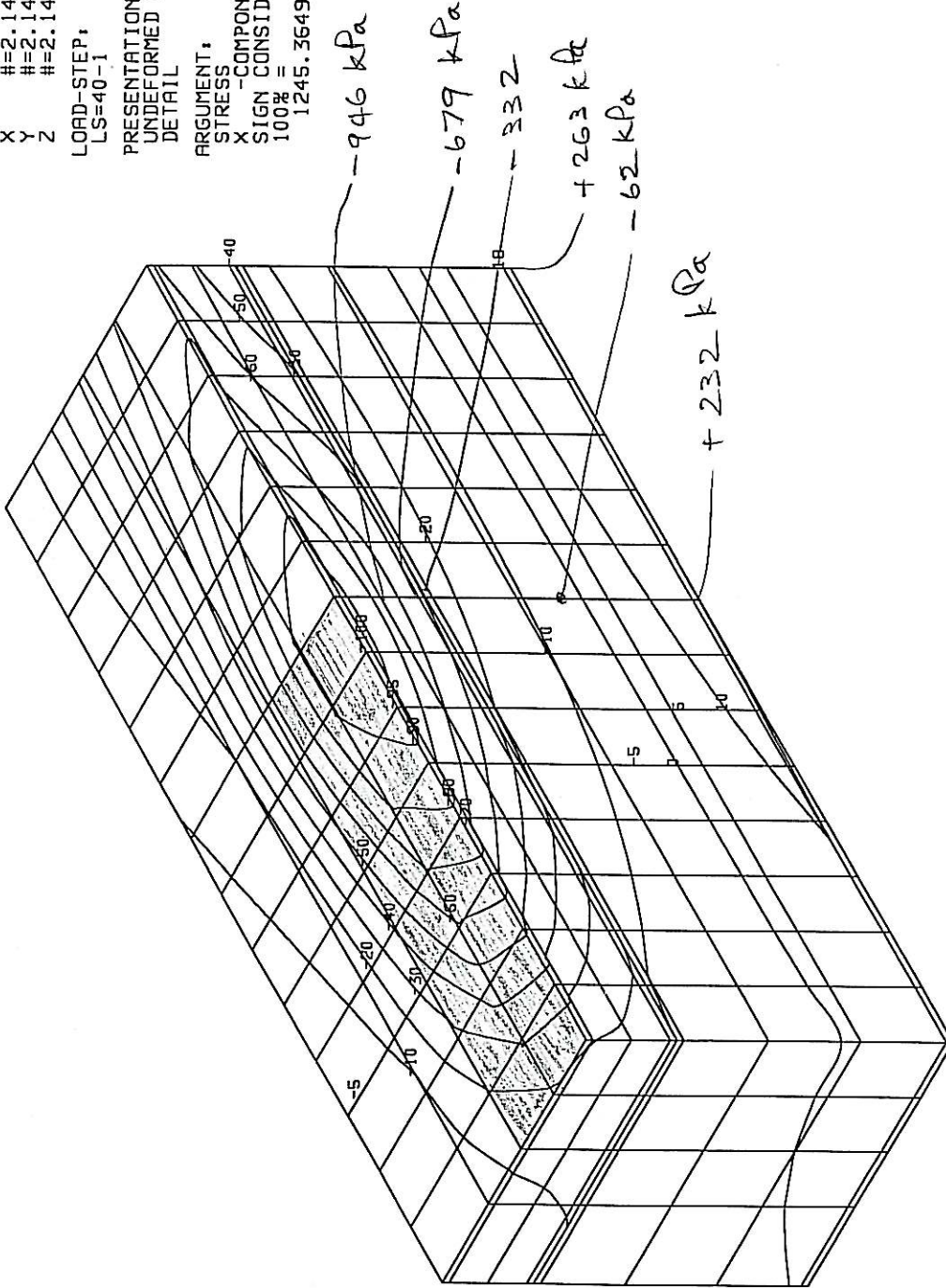
SCALE: 1/100

LENGTH
 X #=2.1499cm
 Y #=2.1499cm
 Z #=2.1499cm

LOAD-STEP:
 LS=40-1

PRESENTATION:
 UNDEFORMED MESH
 DETAIL

ARGUMENT:
 STRESS
 X -COMPONENT
 SIGN CONSIDERED
 100% =
 1245.364990kN/m2



DESIGN BY SGG/901-Lopez geofe model MU 20.00-08
 1998-8-14 8:35.9

STRUCTURE 2, MAX. DEFLECTION=0.18mm

Dyn 280

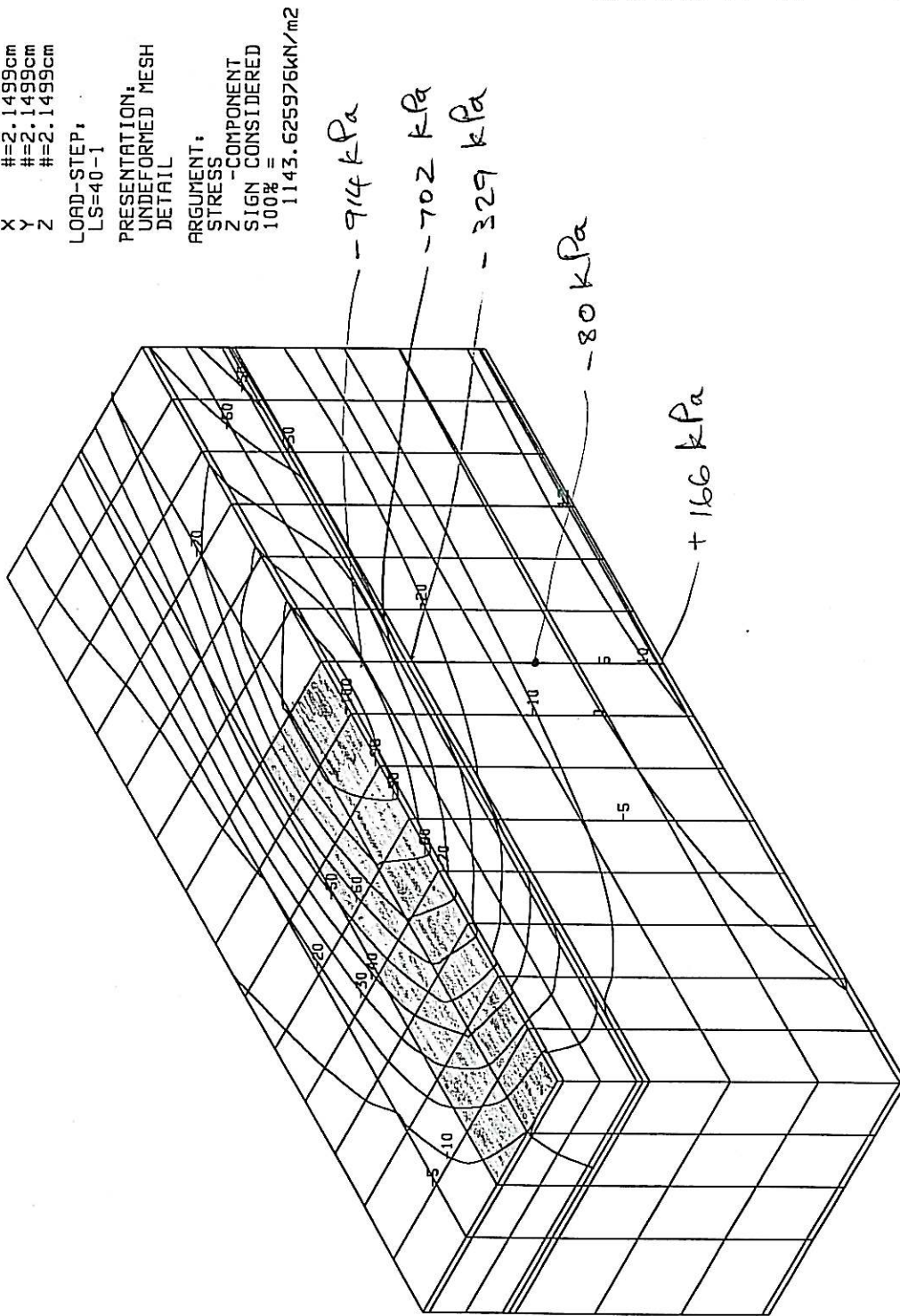
SCALE: 1# = 1

LENGTH
X # = 2.1499cm
Y # = 2.1499cm
Z # = 2.1499cm

LOAD-STEP:
LS=40-1

PRESENTATION:
UNDEFORMED MESH
DETAIL

ARGUMENT:
STRESS
Z -COMPONENT
SIGN CONSIDERED
100% =
1143.625976kN/m²



DESIGN BY SGG/901-Lopez geofe model HU 20.00-08
1998-8-14 B.38151

STRUCTURE 2, MAX. DEFLECTION=0.18mm

Dyn 2 80

SCALE: 1# = 1cm
 LENGTH
 X # = 3.0832cm
 Y # = 3.0832cm
 Z # = 3.0832cm

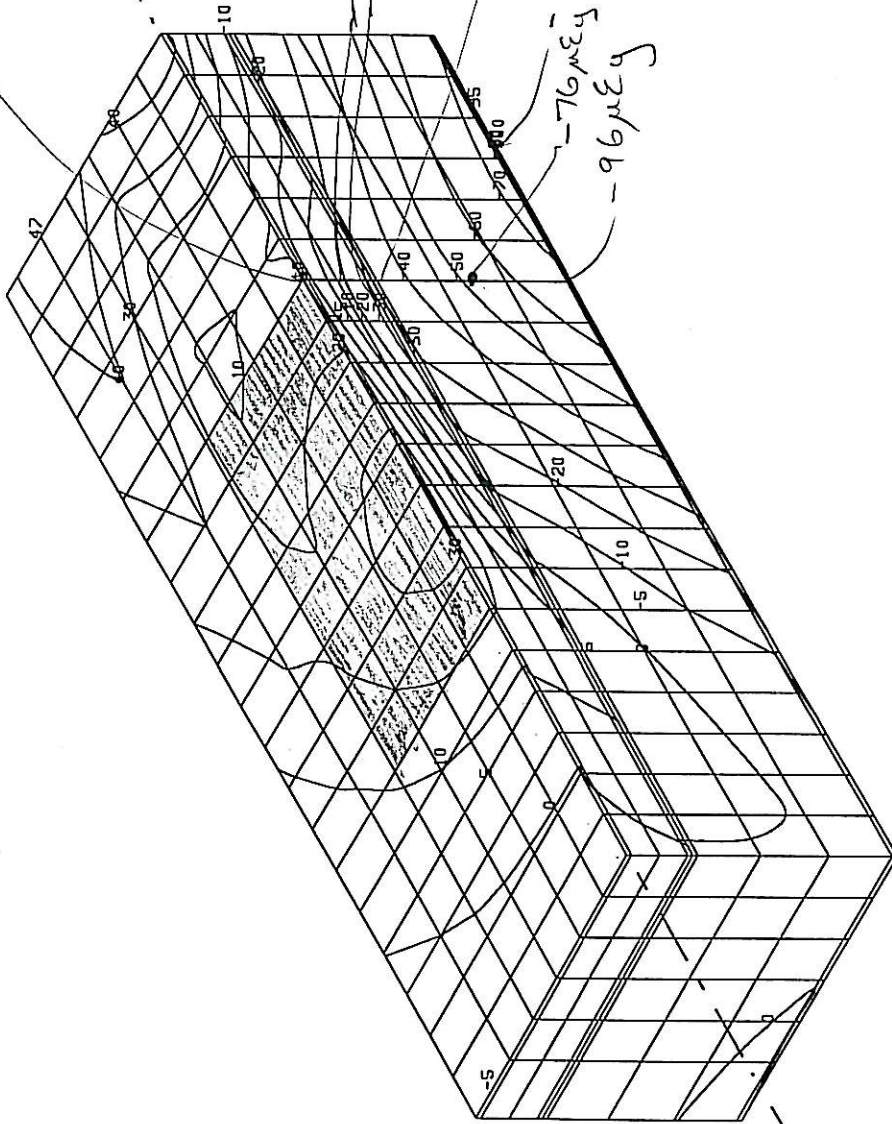
LOAD-STEP:
 LS=40-1
 PRESENTATION:
 UNDEFORMED MESH
 DETAIL

ARGUMENT:
 STRAIN
 Y -COMPONENT
 SIGN CONSIDERED
 100% =

0.000147
 -22 $\mu\epsilon_y$
 -59 $\mu\epsilon_y$

-44 $\mu\epsilon_y$

-76 $\mu\epsilon_y$ 147 $\mu\epsilon_y$
 -96 $\mu\epsilon_y$



DESIGN BY SGG/901-Lopez geofe model HU 20.00-08
 1998-8-14 8:59:26

STRUCTURE 2, MAX. DEFLECTION=0.18mm

Dyn 2 80

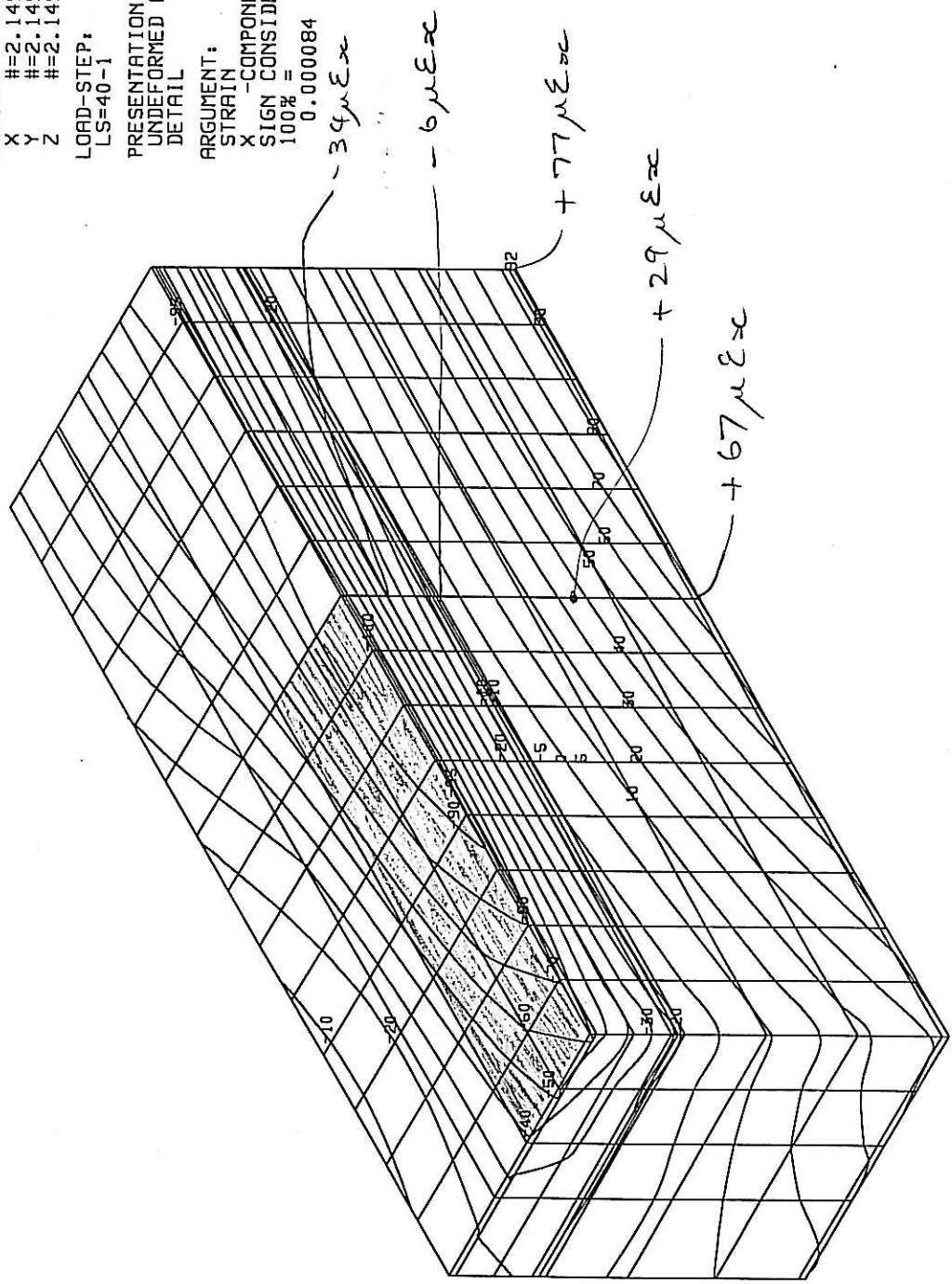
SCALE: 1# = 1

LENGTH
 X #=2.1499cm
 Y #=2.1499cm
 Z #=2.1499cm

LOAD-STEP:
 LS=40-1

PRESENTATION:
 UNDEFORMED MESH
 DETAIL

ARGUMENT:
 STRAIN
 X -COMPONENT
 SIGN CONSIDERED
 100% =
 0.000084



DESIGN BY SGG/901-Lopez geofe model HU 20.00-08
 1998-8-14 B142145

STRUCTURE 2, MAX. DEFLECTION=0.18mm

Dyn 2 80

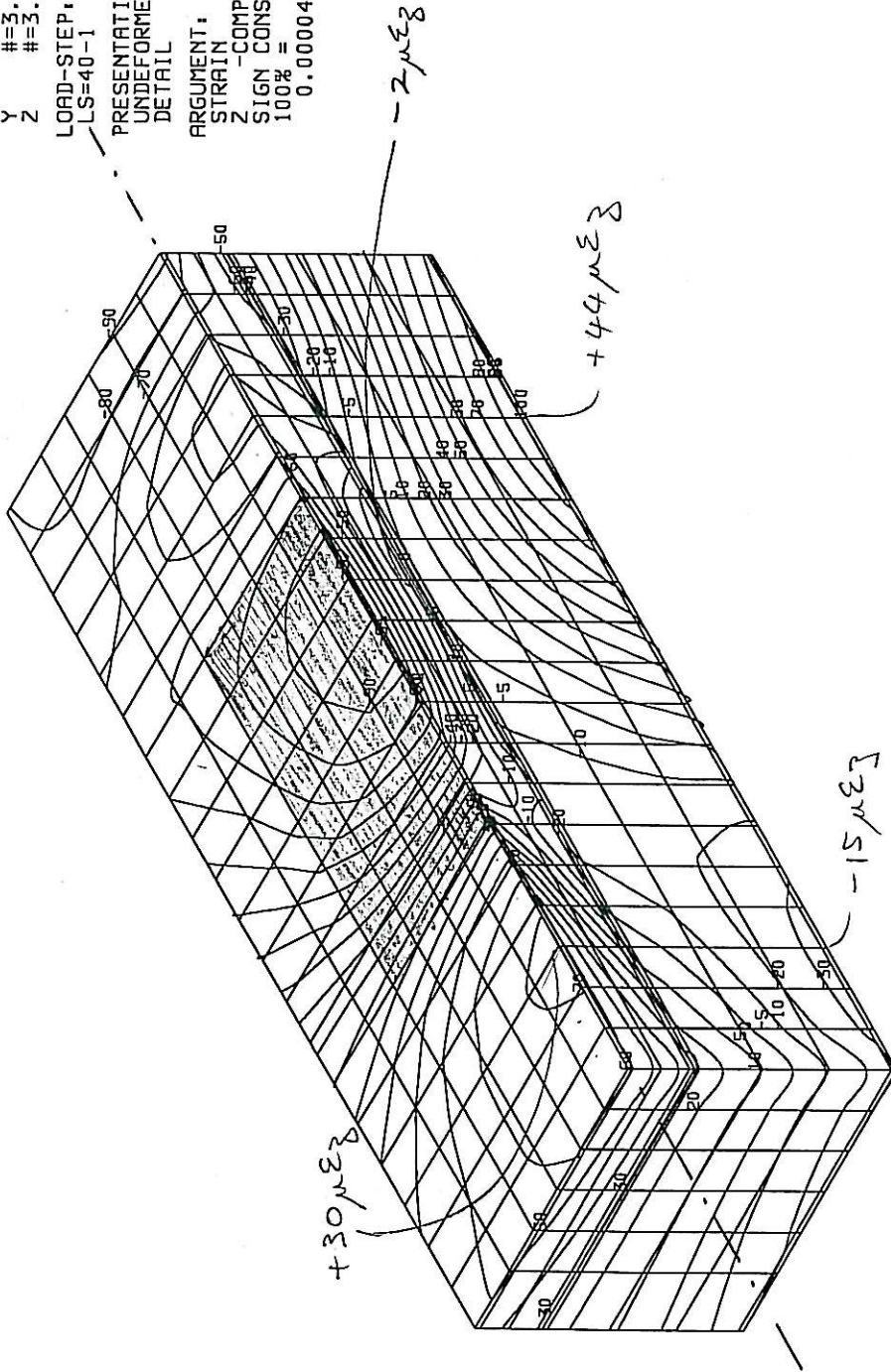
SCALE: $\frac{\#}{\#} =$

LENGTH
 X $\# = 3.0832 \text{ cm}$
 Y $\# = 3.0832 \text{ cm}$
 Z $\# = 3.0832 \text{ cm}$

LOAD-STEP:
 LS=40-1

PRESENTATION:
 UNDEFORMED MESH
 DETAIL

ARGUMENT:
 STRAIN
 Z -COMPONENT
 SIGN CONSIDERED
 100% =
 0.000044



DESIGN BY SGG/901-Lopez geofe model HU 20.00-08
 1998-8-14 8:55:50

Dyn 2 80

STRUCTURE 2, MAX. DEFLECTION=0.18mm

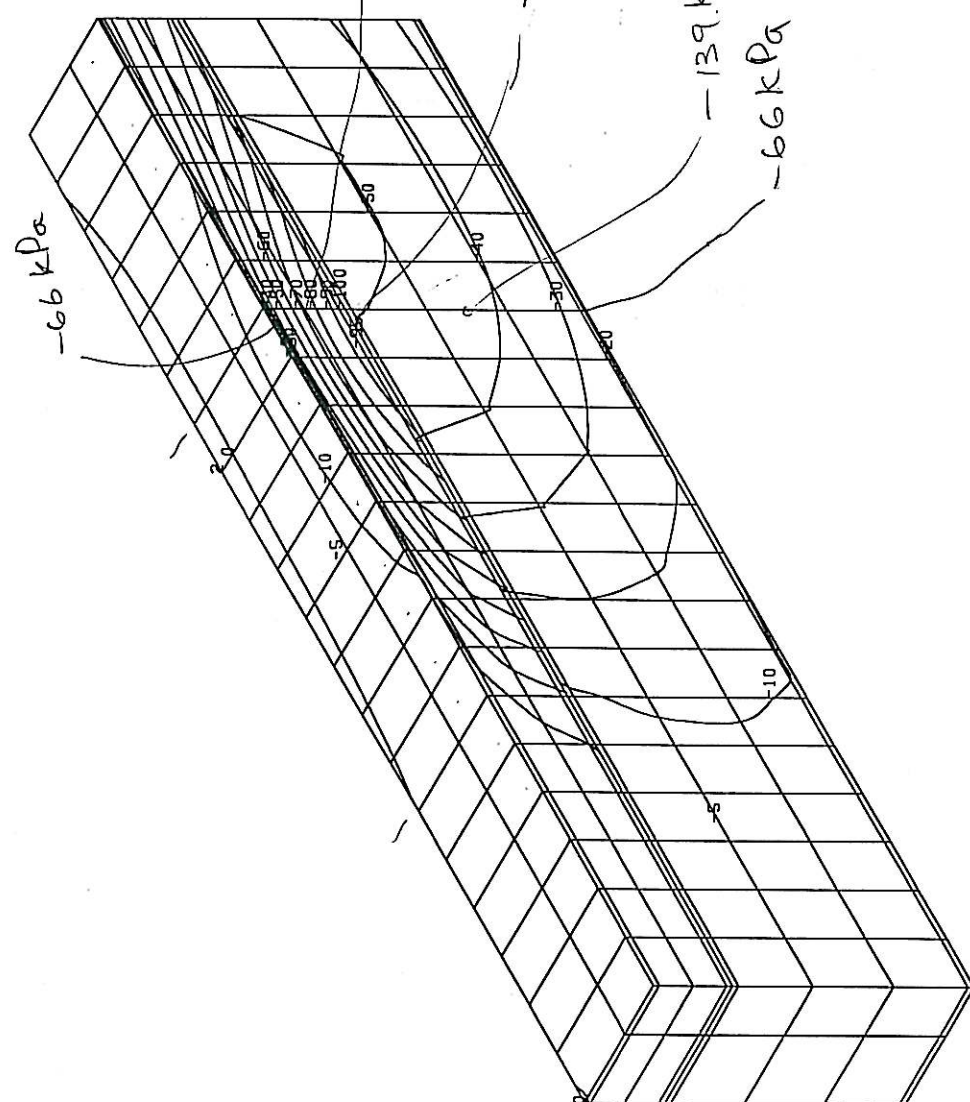
SCALE: 1:1

LENGTH
 X #=2.6166cm
 Y #=2.6166cm
 Z #=2.6166cm

LOAD-STEP:
 LS=40-1

PRESENTATION:
 UNDEFORMED MESH
 DETAIL

ARGUMENT:
 STRESS
 Tau-XY
 SIGN CONSIDERED
 100% =
 331.042785kN/m2



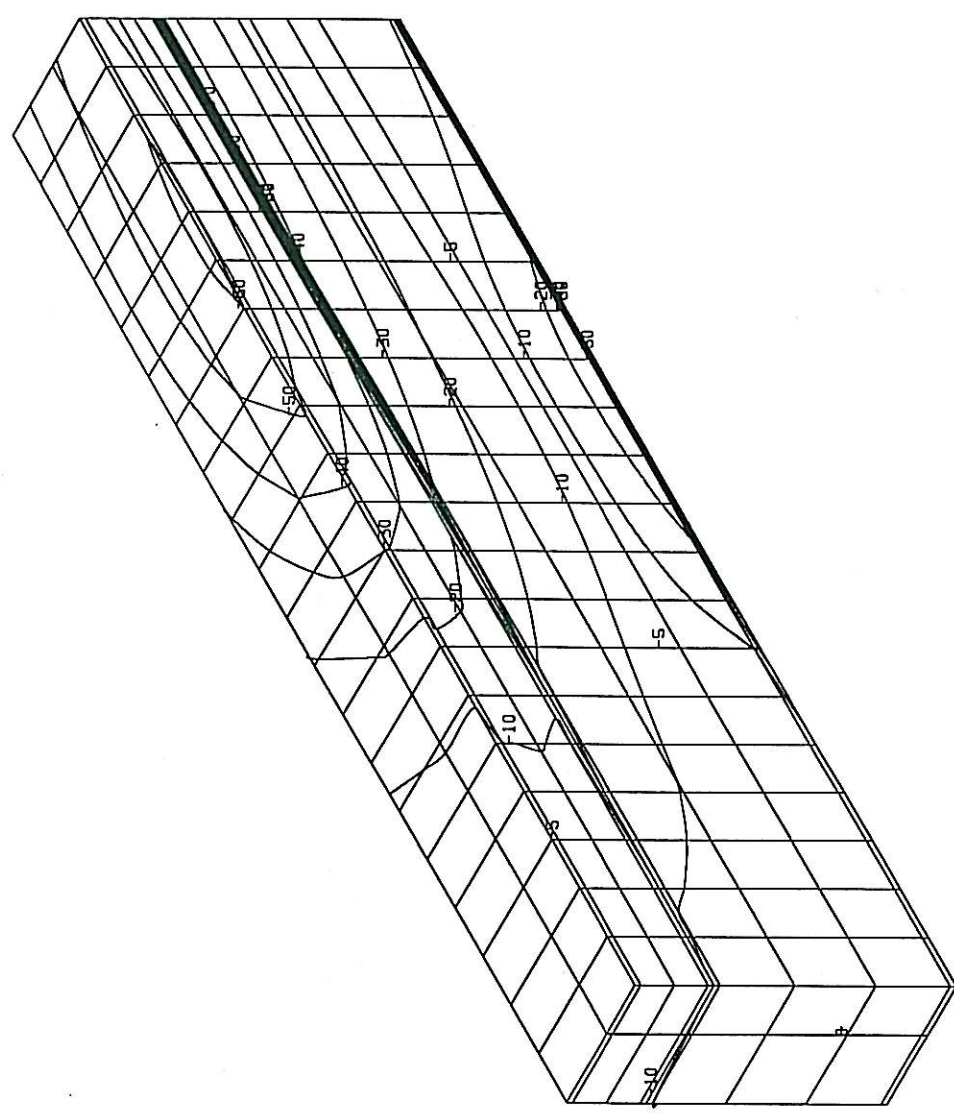
DESIGN BY SGG/901-Lopez geofe model NU 20.00-08
 1998-8-14 9:16

STRUCTURE 2, MAX. DEFLECTION=0.18mm

Dyn 2 80

Dyn 2 80

SCALE: 1:100
LENGTH
X #=2.6166cm
Y #=2.6166cm
Z #=2.6166cm
LOAD-STEP:
LS=40-1
PRESENTATION:
UNDEFORMED MESH
DETAIL
ARGUMENT:
STRAIN
Gamma-XY
SIGN CONSIDERED
100% =
0.000217



DESIGN BY SGG/901-Lcpaz geofe model HU 20.00-08
1998-8-14 9:10:53

STRUCTURE 2, MAX. DEFLECTION=0.18mm

APPENDIX B
ANALYSIS RESULTS: NONUNIFORM CONTACT STRESS
DISTRIBUTION

COMPARISON OF RESULTS FROM LET AND FE MODELS FOR ANALYSIS OF
NON-UNIFORM TYRE PRESSURE DISTRIBUTIONS

TABLE B1: STRESS RESULTS FOR STRUCTURE 1: ASPHALT SURFACING

OFFSET POSITION	DEPTH IN AC	MODEL	VERTIC SIG-YY	TRANSV SIG-XX	LONGI SIG-ZZ	SIG-XY	TAU-OCT
CENTRE OF WHEEL	TOP	LET	-700	-2280	-2280	0	745
		FE-UNIF	-923	-2875	-2321	375	877
		FE-NONU	-1609	-3250	-3180	787	993
	MIDDLE	LET	-697	-1170	-1170	0	223
		FE-UNIF	-902	-1150	-1251	51	152
		FE-NONU	-1062	-1006	-1096	0	37
	BOTTOM	LET	-674	-22	-22	0	307
		FE-UNIF	-831	575	24	-28	579
		FE-NONU	-788	390	223	-46	522
EDGE OF WHEEL	TOP	LET	-349	-1010	-1410	-264	488
		FE-UNIF	-381	-1293	-1465	-51	477
		FE-NONU	-2361	-4025	-3654	-92	717
	MIDDLE	LET	-328	-688	-705	-443	401
		FE-UNIF	-372	-948	-781	-493	470
		FE-NONU	-1251	-925	-1205	-665	562
	BOTTOM	LET	-303	-377	2	-268	273
		FE-UNIF	-343	-201	-171	-370	311
		FE-NONU	-708	1087	512	-370	807

TABLE B2: STRESS RESULTS FOR STRUCTURE 2: ASPHALT SURFACING

OFFSET POSITION	DEPTH IN AC	MODEL	VERTIC SIG-YY	TRANSV SIG-XX	LONGI SIG-ZZ	SIG-XY	TAU-OCT
CENTRE OF WHEEL	TOP	LET	-700	-2030	-2030	0	627
		FE-UNIF	-952	-2131	-2033	394	624
		FE-NONU	-1408	-2639	-2506	630	754
	MIDDLE	LET	-684	-1530	-1530	0	399
		FE-UNIF	-875	-1491	-1524	41	300
		FE-NONU	-1056	-1386	-1566	0	211
	BOTTOM	LET	-642	-1030	-1030	0	183
		FE-UNIF	-856	-1022	-1016	21	79
		FE-NONU	-797	-594	-783	0	93
EDGE OF WHEEL	TOP	LET	-342	-1110	-1310	-237	460
		FE-UNIF	-476	-1279	-1423	-62	420
		FE-NONU	-2346	-2969	-2819	-39	267
	MIDDLE	LET	-331	-884	-952	-332	388
		FE-UNIF	-466	-1022	-1077	-344	394
		FE-NONU	-1361	-1254	-1535	-551	465
	BOTTOM	LET	-305	-645	-622	-363	335
		FE-UNIF	-428	-639	-731	-414	361
		FE-NONU	-939	-726	-626	-472	407

TABLE B3: STRESS RESULTS FOR STRUCTURE 2: ASPHALT BASE

OFFSET POSITION	DEPTH IN AC	MODEL	VERTIC SIG-YY	TRANSV SIG-XX	LONGI SIG-ZZ	SIG-XY	TAU-OCT
CENTRE	TOP	LET	-636	-729	-729	0	44
		FE-UNIF	-799	-639	-1016	-20	155
		FE-NONU	-797	-594	-783	0	93
	MIDDLE	LET	-414	114	114	0	249
		FE-UNIF	-590	107	0	0	306
		FE-NONU	-540	165	157	0	330
	BOTTOM	LET	-229	987	987	0	573
		FE-UNIF	-286	788	691	-20	485
		FE-NONU	-235	759	752	0	467
EDGE OF WHEEL	TOP	LET	-302	-450	-427	-363	303
		FE-UNIF	-409	-532	-609	-414	348
		FE-NONU	-939	-726	-626	-472	407
	MIDDLE	LET	-206	4	104	-324	294
		FE-UNIF	-323	0	102	-332	326
		FE-NONU	-469	165	157	-315	393
	BOTTOM	LET	-134	447	656	-107	345
		FE-UNIF	-209	319	365	-103	274
		FE-NONU	-235	330	313	-79	270

Test No.: 6

Filename: SNSC77A

LOAD: 75 kN

INFLATION PRESSURE: 700 kPa

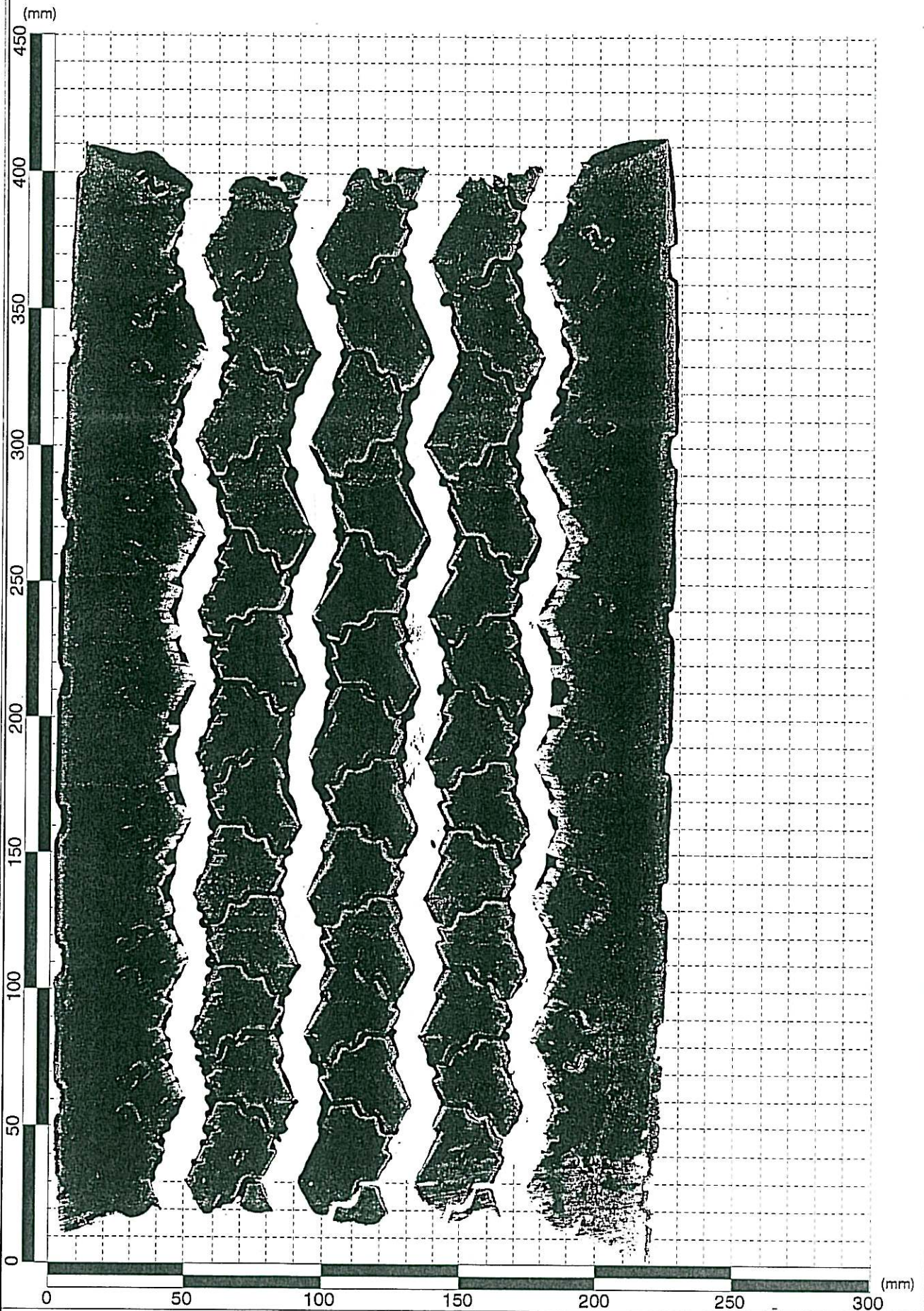


Figure B1

MICHELIN 315/80 R22.5

FINITE ELEMENT RESULTS
STRUCTURE 1: RECTANGULAR LOAD AREA WITH UNIFORM CONTACT
PRESSURE

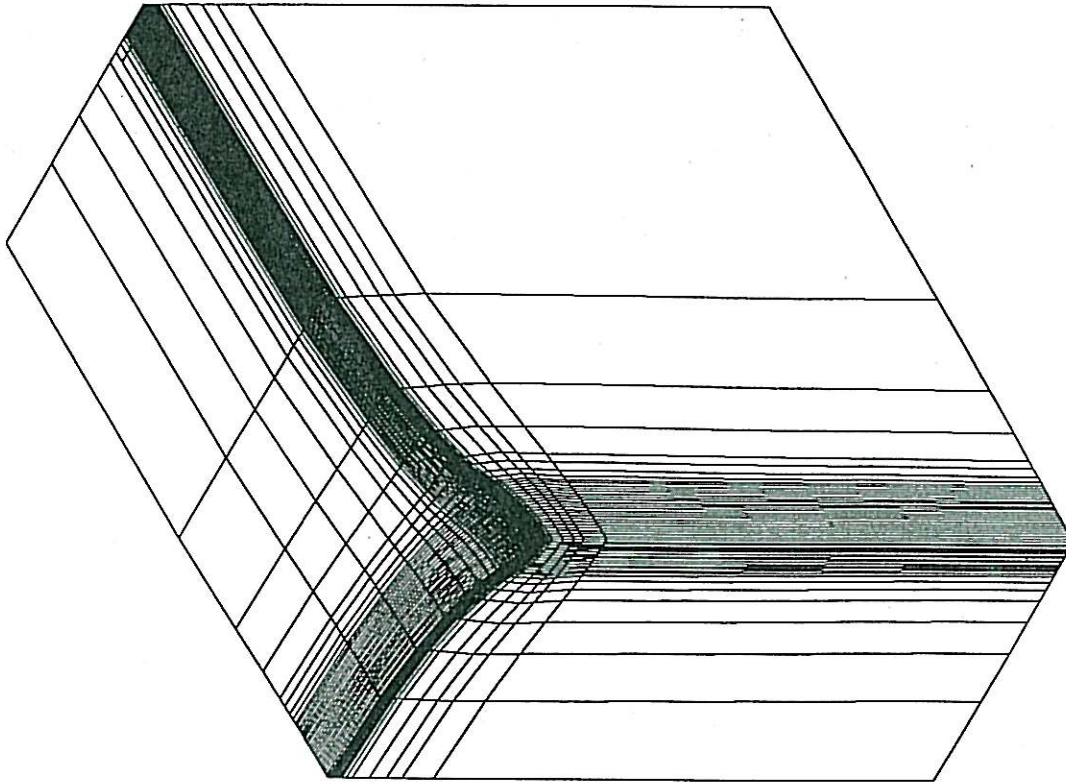
SCALE: 1# = 1

LENGTH
 X # = 16.911cm
 Y # = 16.911cm
 Z # = 16.911cm

DISPLACEMENT
 X # = 0.064006cm
 Y # = 0.064006cm
 Z # = 0.064006cm

LOAD-STEP:
 LS=2

PRESENTATION:
 DEFORMED MESH



DESIGN BY SGG/501-Lopez geofe model HU 20.00-08
 1998-8-3 10.51.35

STRUCTURE 1, LOAD=80kN, MAX. DEFLECTION=.96mm

NIEUW
 DISANA

51 ~~1~~ Univ

	HMA PROJECT UNIFORM PRESSURE DISTRIBUTION FIG. 1: Deflection Bowl	TFAS/A/1 BKS (Pty) Ltd. Dr. JP Laurens BOX 3173 PRETORIA FAX 012 4213501
--	---	--

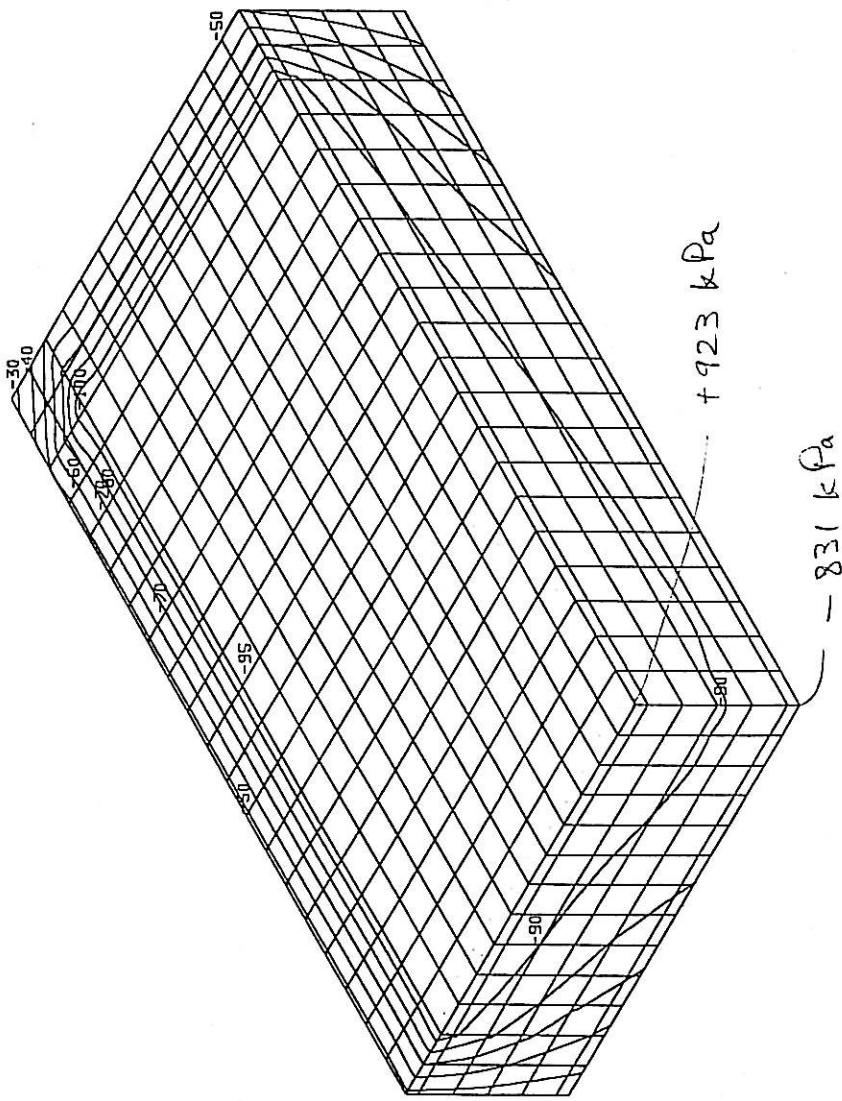
SCALE: 1:1

LENGTH
 X #=1.2770cm
 Y #=1.2770cm
 Z #=1.2770cm

LOAD-STEP:
 LS=2-1

PRESENTATION:
 UNDEFORMED MESH
 DETAIL

ARGUMENT:
 STRESS
 Y -COMPONENT
 SIGN CONSIDERED
 100% =
 992.812622kN/m²



DESIGN BY SGG/901-Lopez geofe model HU 20.00-08
 1998-8-3 10,18,38

STRUCTURE 1, LOAD=80kN, MAX. DEFLECTION=.96mm

51 amb

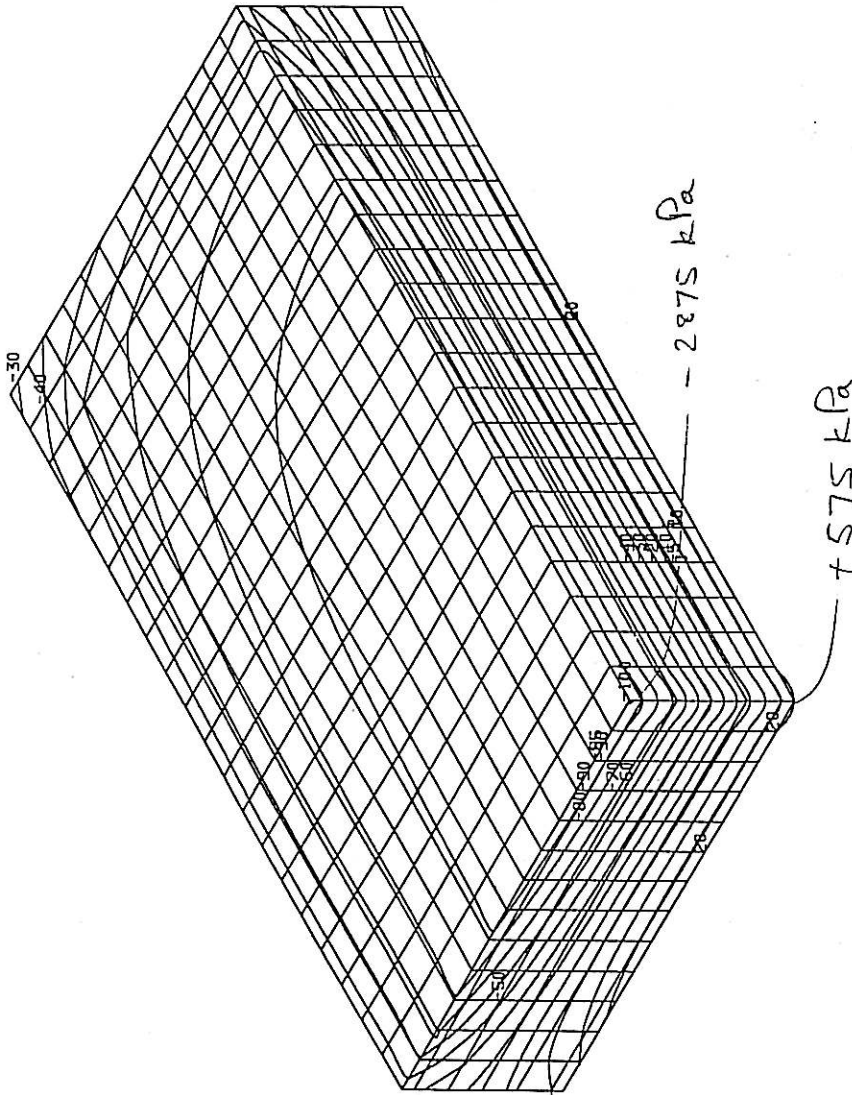
SCALE: 1# = 1

LENGTH
 X # = 1.2770cm
 Y # = 1.2770cm
 Z # = 1.2770cm

LOAD-STEP:
 LS=2-1

PRESENTATION:
 UNDEFORMED MESH
 DETAIL

ARGUMENT:
 STRESS
 X - COMPONENT
 SIGN CONSIDERED
 100% =
 2875.358886kN/m2



DESIGN BY SGG/901-Lopez gaoFE model MU 20.00-08
 1998-8-3 10:21:14

STRUCTURE 1, LOAD=80kN, MAX. DEFLECTION=.96mm

SI unuf

SCALE: 1# = 1

LENGTH

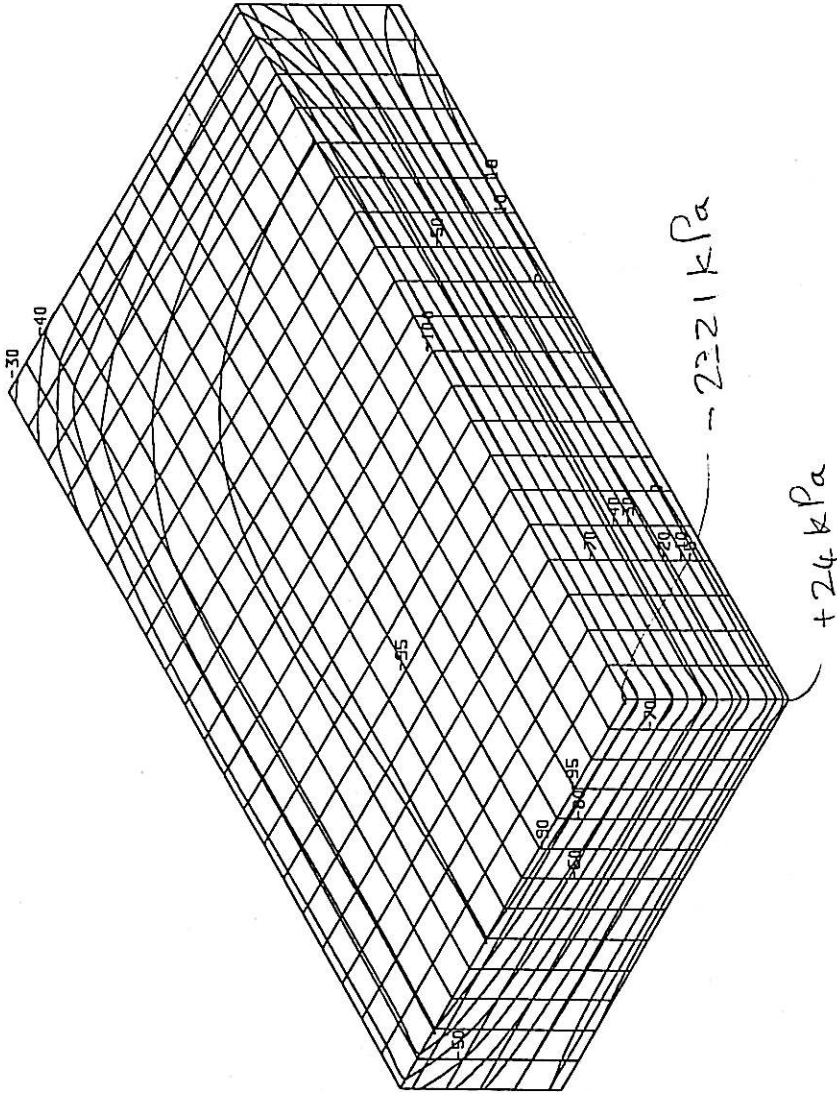
X # = 1.2770 cm
Y # = 1.2770 cm
Z # = 1.2770 cm

LOAD-STEP:
LS = 2-1

PRESENTATION:
UNDEFORMED MESH
DETAIL

ARGUMENT:

STRESS
Z - COMPONENT
SIGN CONSIDERED
100% =
2502.035156 kN/m²



• DESIGN BY SGG/901-Lopez geofe model NU 20.00-08
1998-B-3 10/23/95

STRUCTURE 1, LOAD=80kN, MAX. DEFLECTION=.96mm

SI Umf

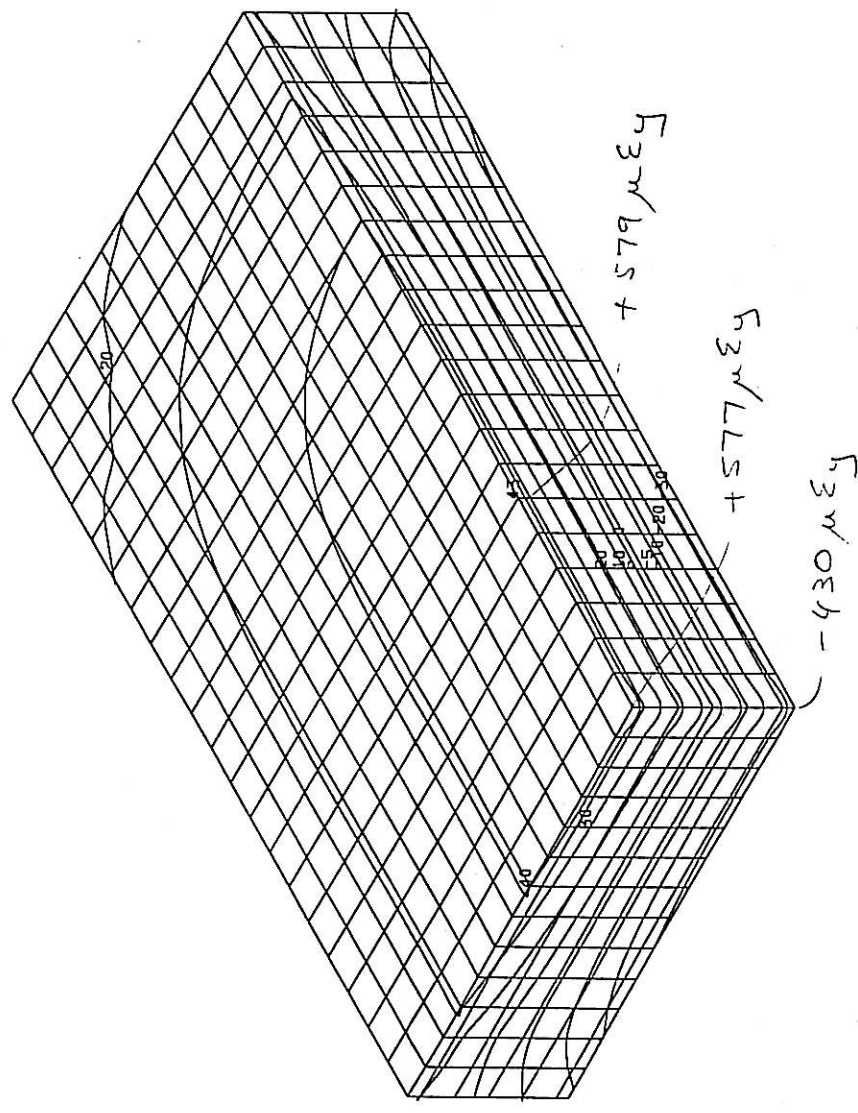
SCALE: 1# = 1

LENGTH
 X # = 1.2770 cm
 Y # = 1.2770 cm
 Z # = 1.2770 cm

LOAD-STEP:
 LS=2-1

PRESENTATION:
 UNDEFORMED MESH
 DETAIL

ARGUMENT:
 STRAIN
 Y - COMPONENT
 SIGN CONSIDERED
 100% =
 0.001346



DESIGN BY SGG/901-Lopez geofe model MV 20.00-08
 1998-8-3 10:31:11

STRUCTURE 1, LOAD=80kN, MAX. DEFLECTION=.96mm

Si Unif

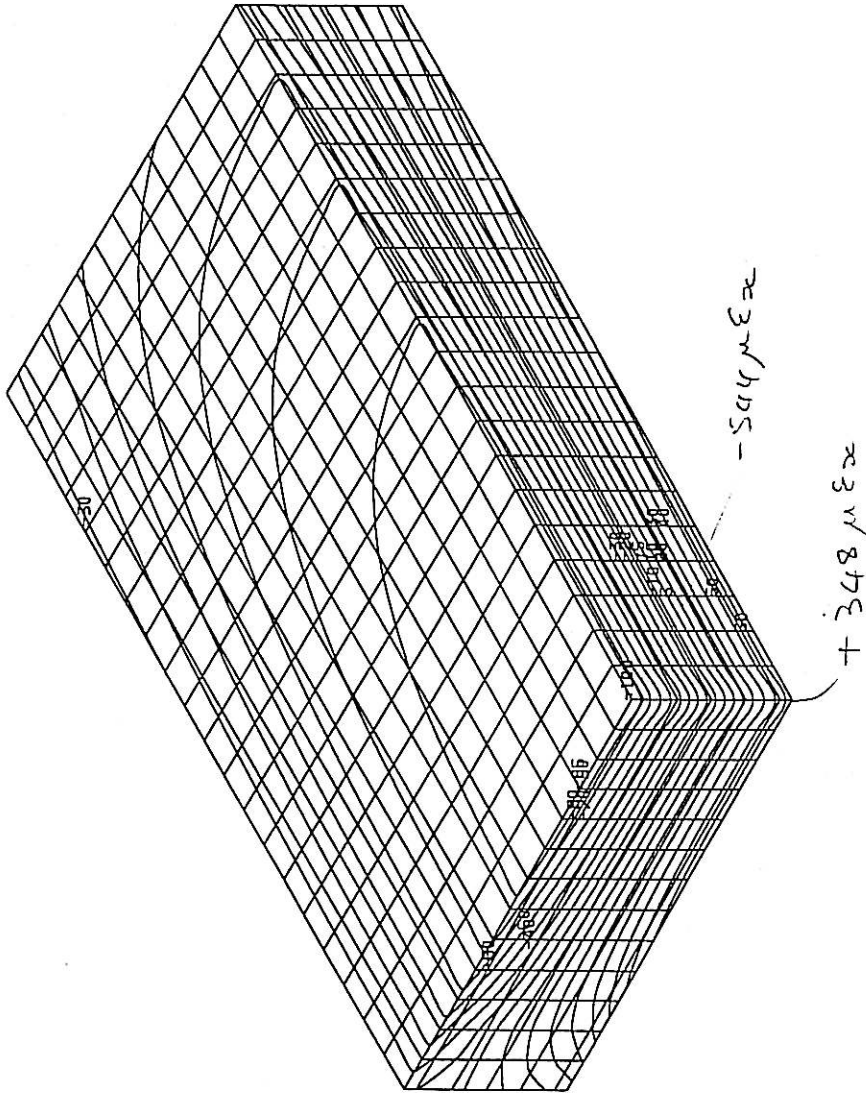
SCALE: 1# = 1

LENGTH
 X # = 1.2770 cm
 Y # = 1.2770 cm
 Z # = 1.2770 cm

LOAD-STEP:
 LS = 2-1

PRESENTATION:
 UNDEFORMED MESH
 DETAIL

ARGUMENT:
 STRAIN
 X -COMPONENT
 SIGN CONSIDERED
 100% =
 0.000544



DESIGN BY SGG/901-Lopez GEOFE model NU 20.00-08
 1998-8-3 10:35:48

STRUCTURE 1, LOAD=80kN, MAX. DEFLECTION=.96mm

SA Umf

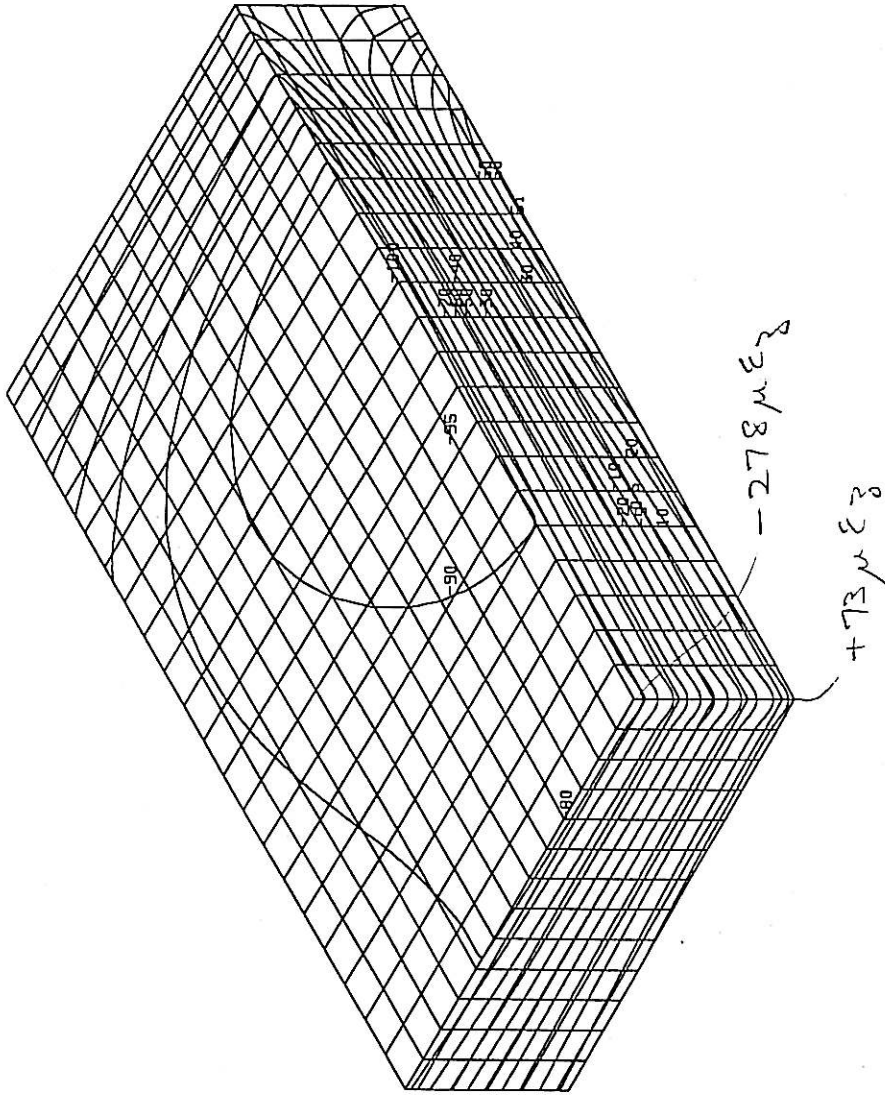
SCALE: 1:1

LENGTH #=1.2720cm
 X #=1.2720cm
 Y #=1.2720cm
 Z #=1.2720cm

LOAD-STEP:
 LS=2-1

PRESENTATION:
 UNDEFORMED MESH
 DETAIL

ARGUMENT:
 STRAIN
 Z -COMPONENT
 SIGN CONSIDERED
 100% =
 0.000338



DESIGN BY SGG/901-Lopez gaeFE model HU 20.00-08
 1998-8-3 10:36:20

STRUCTURE 1, LOAD=80kN, MAX. DEFLECTION=.96mm

SI Unif

SCALE: 1# = 1

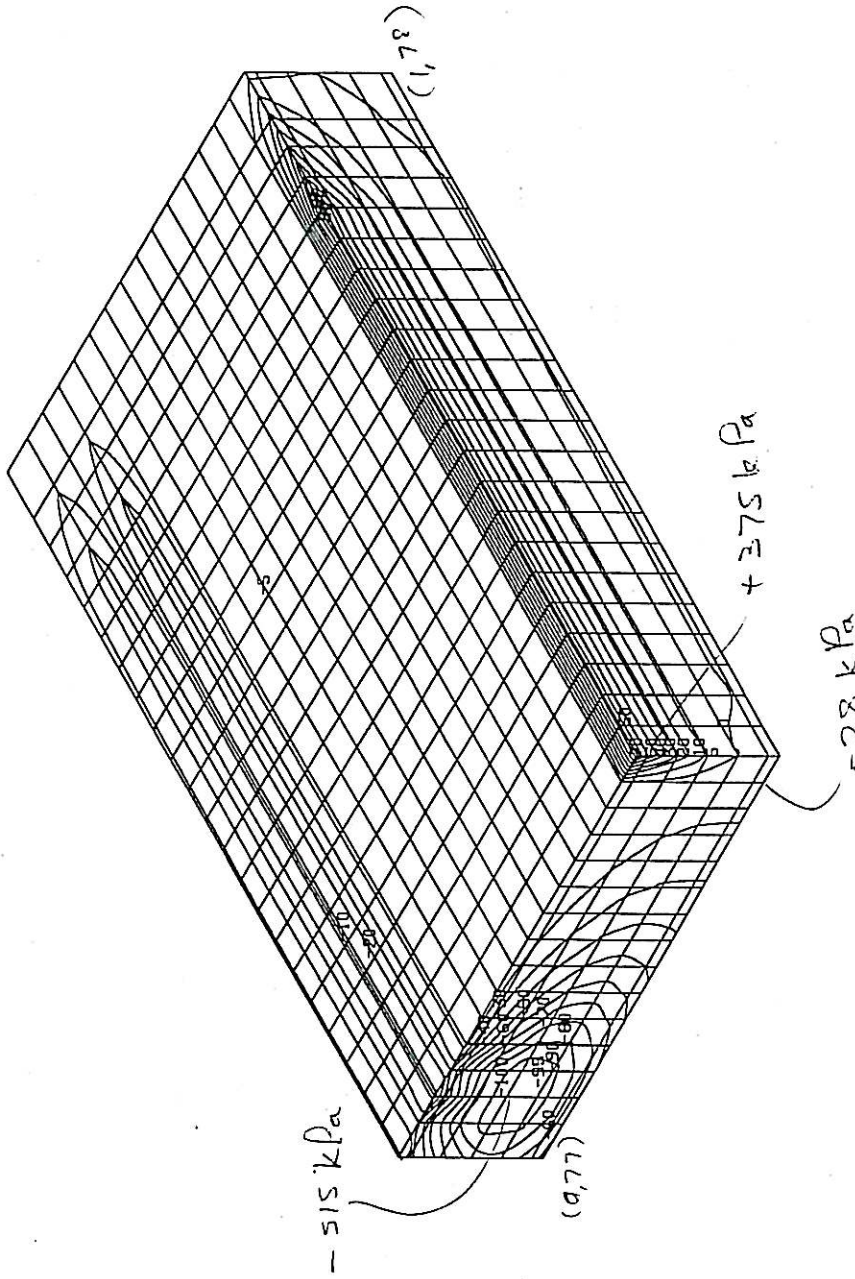
LENGTH
X # = 1.4583cm
Y # = 1.4583cm
Z # = 1.4583cm

LOAD-STEP:
LS=2-1

PRESENTATION:
UNDEFORMED MESH
DETAIL

ARGUMENT:
STRESS

Tau-XY
SIGN CONSIDERED
100% = 514.821472kN/m²



DESIGN BY SGG/901-Lopez geofe model HU 20.00-08
1998-8-3 10.57.12

STRUCTURE 1, LOAD=80kN, MAX. DEFLECTION=.96mm

SI unit

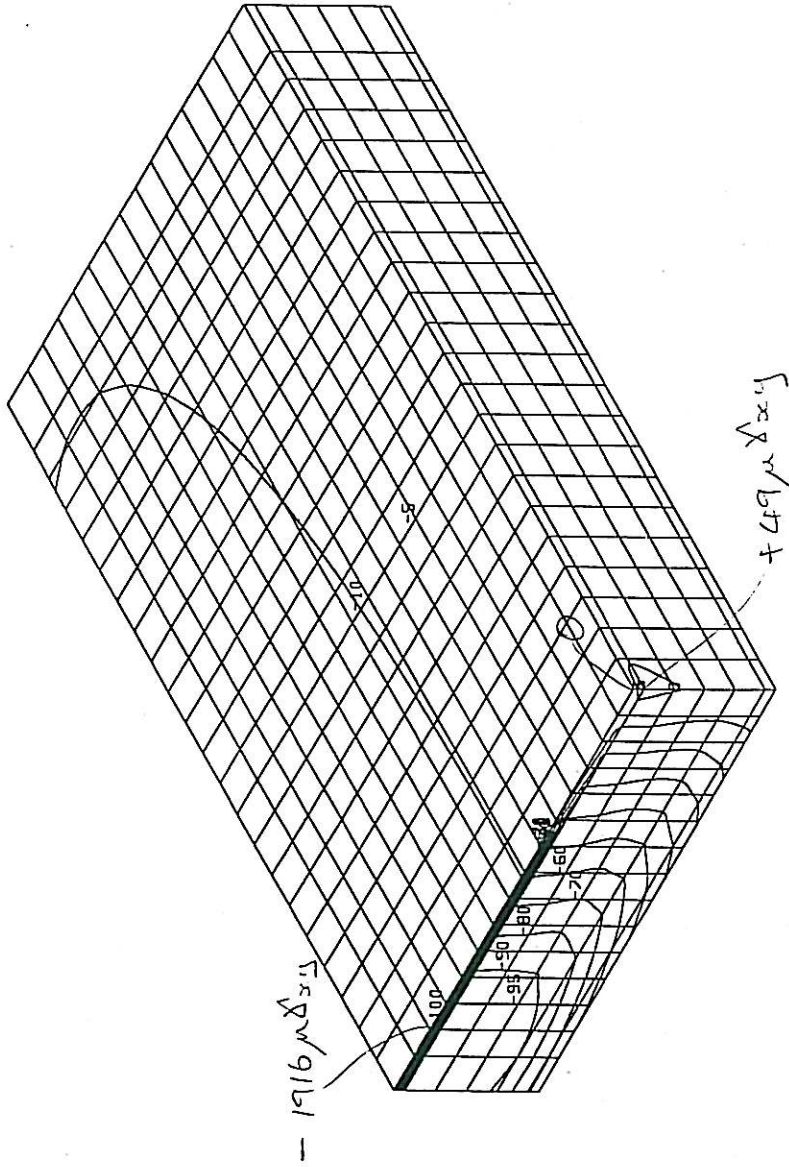
SCALE: 1# = 1

LENGTH
 X # = 1.4583cm
 Y # = 1.4583cm
 Z # = 1.4583cm

LOAD-STEP:
 LS=2-1

PRESENTATION:
 UNDEFORMED MESH
 DETAIL

ARGUMENT:
 STRAIN
 Gamma-XY
 SIGN CONSIDERED
 100% =
 0.001916



DESIGN BY SGG/901-Lopaz GeofE model HU 20.00-08
 1998-8-3 10:59:53

STRUCTURE 1, LOAD=80kN, MAX. DEFLECTION=.96mm

SI Unif

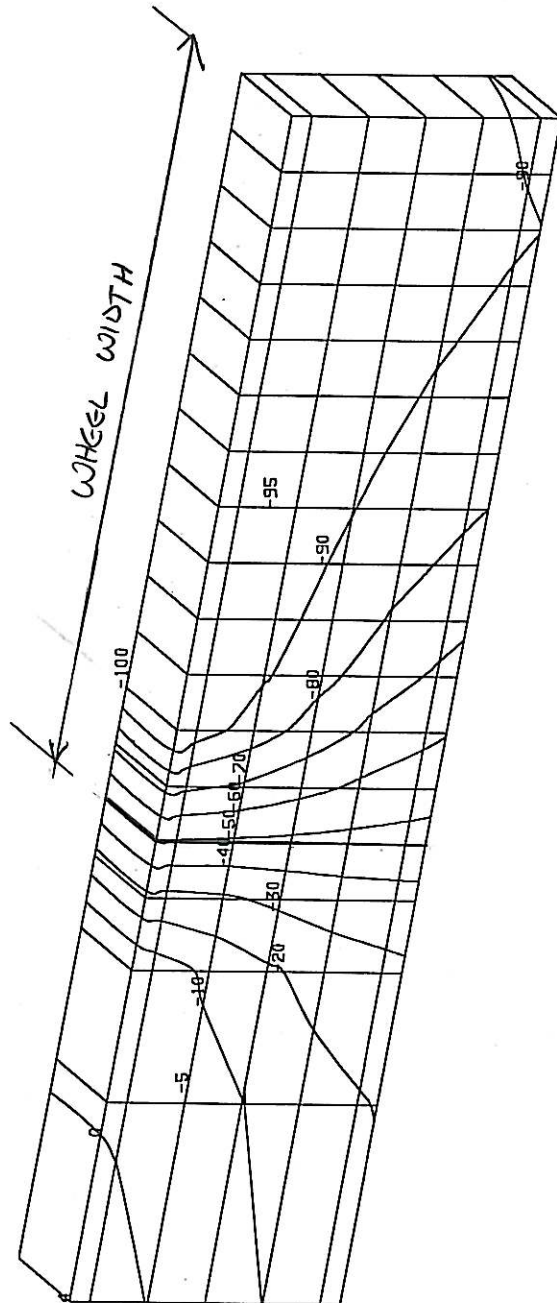
SCALE: 1# = 1

LENGTH
X #=0.276651cm
Y #=0.276651cm
Z #=0.276651cm

LOAD-STEP:
LS=2-1

PRESENTATION:
UNDEFORMED MESH
DETAIL

ARGUMENT:
STRESS
Y -COMPONENT
SIGN CONSIDERED
100% =
954.439025kN/m2



SI Unif

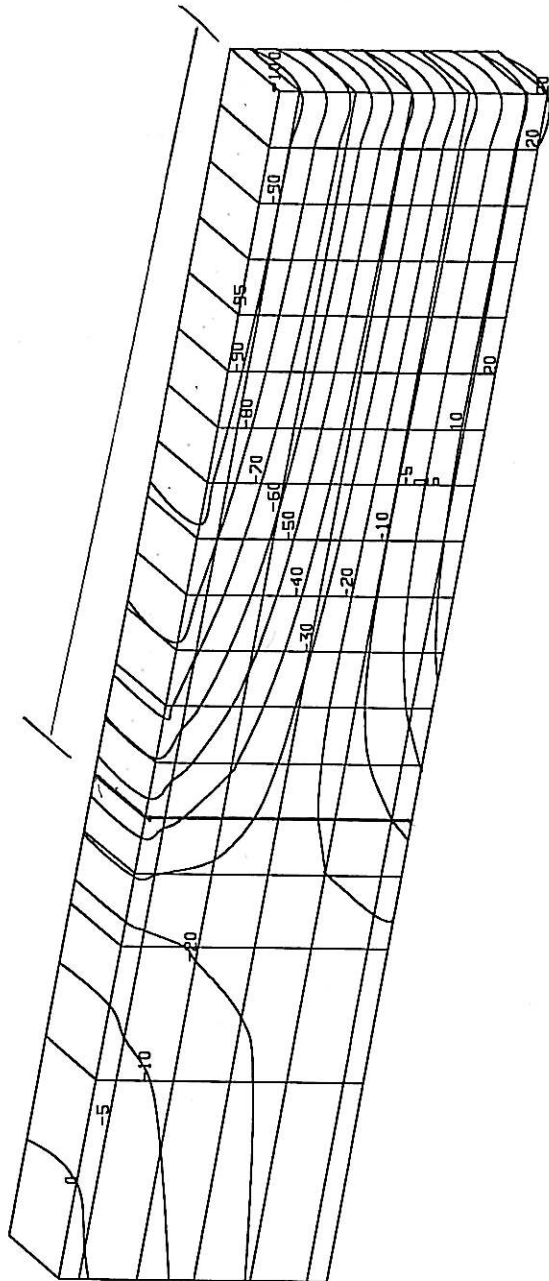
SCALE: 1# = 1

LENGTH
X #=0.776651cm
Y #=0.776651cm
Z #=0.776651cm

LOAD-STEP:
LS=2-1

PRESENTATION:
UNDEFORMED MESH
DETAIL

ARGUMENT:
STRESS
X -COMPONENT
SIGN CONSIDERED
100% =
2875.35886kN/m2



DESIGN BY SGG/901-Lopez geofe model HU 20.00-08
198-8-17 16.29.21

SI Unif

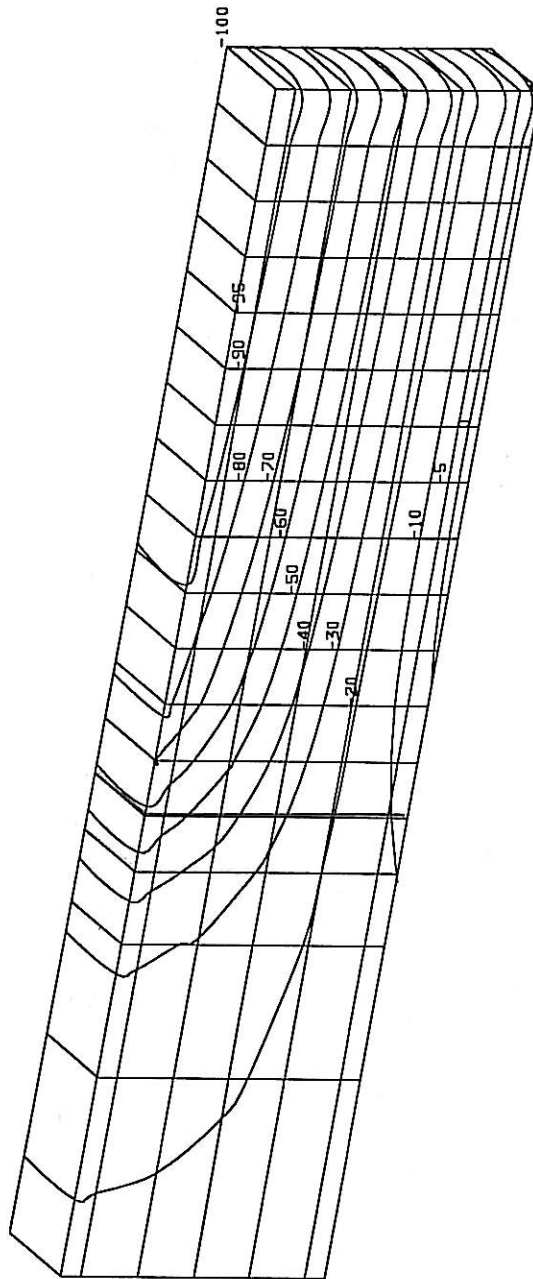
SCALE: 1# = 1

LENGTH
X #=0.776651cm
Y #=0.776651cm
Z #=0.776651cm

LOAD-STEP:
LS=2-1

PRESENTATION:
UNDEFORMED MESH
DETAIL

ARGUMENT:
STRESS
Z - COMPONENT
SIGN CONSIDERED
100% =
2443.054199kN/m2



•DESIGN BY SGG/901-Lgpaz geofe model HU 20.00-08
1998-8-17 16:31:35

SI unit

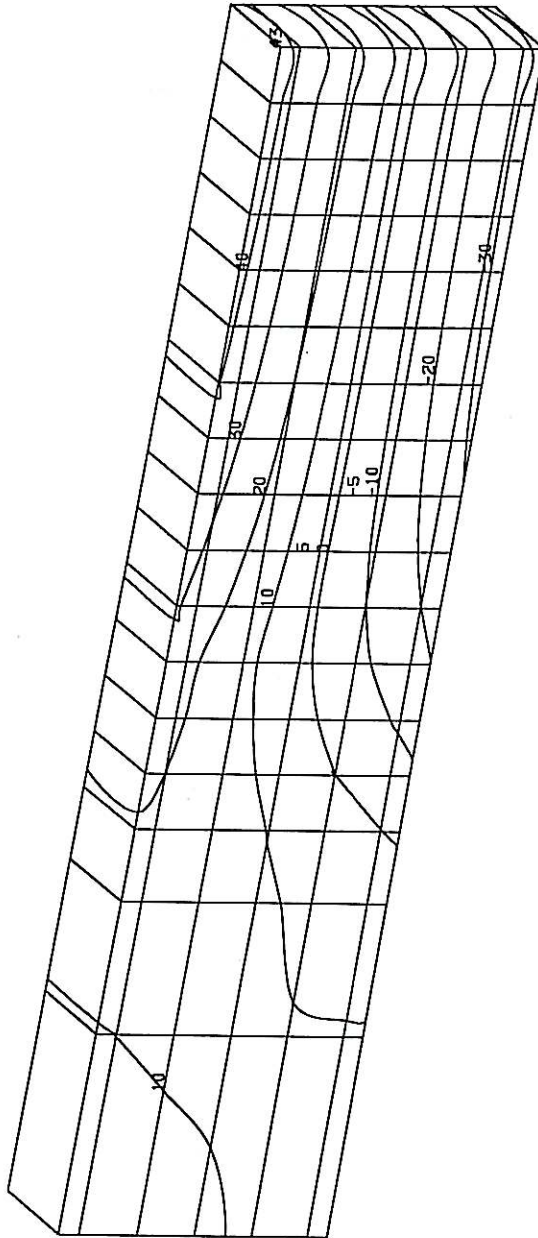
SCALE: 1# = 1

LENGTH #=0.776651cm
X #=0.776651cm
Y #=0.776651cm
Z #=0.776651cm

LOAD-STEP:
LS=2-1

PRESENTATION:
UNDEFORMED MESH
DETAIL

ARGUMENT:
STRAIN
Y -COMPONENT
SIGN CONSIDERED
100% =
0.001346



DESIGN BY SGG/901-lopaz gaeFE model HU 20.00-08
1998-8-17 16:33:19

SI Unit

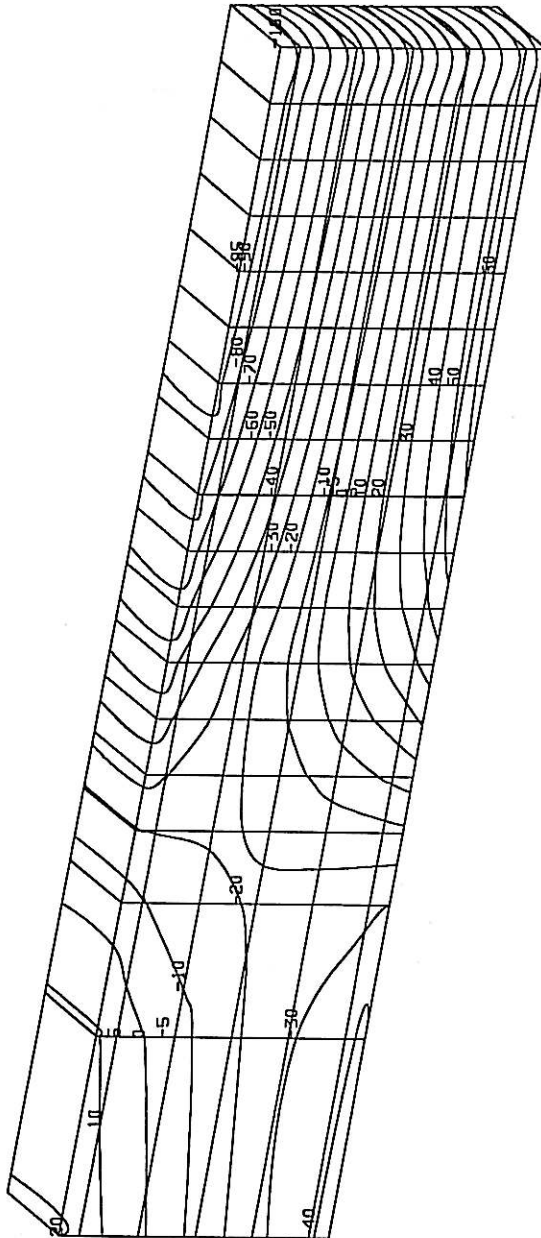
SCALE: 1/10

LENGTH
X #=0.726651cm
Y #=0.726651cm
Z #=0.726651cm

LOAD-STEP:
LS=2-1

PRESENTATION:
UNDEFORMED MESH
DETAIL

ARGUMENT:
STRAIN
X -COMPONENT
SIGN CONSIDERED
100% =
0.000544



• DESIGN BY SGG/901-topaz geofe model HV 20.00-08
1998-8-17 16:34:58

Si Vunf

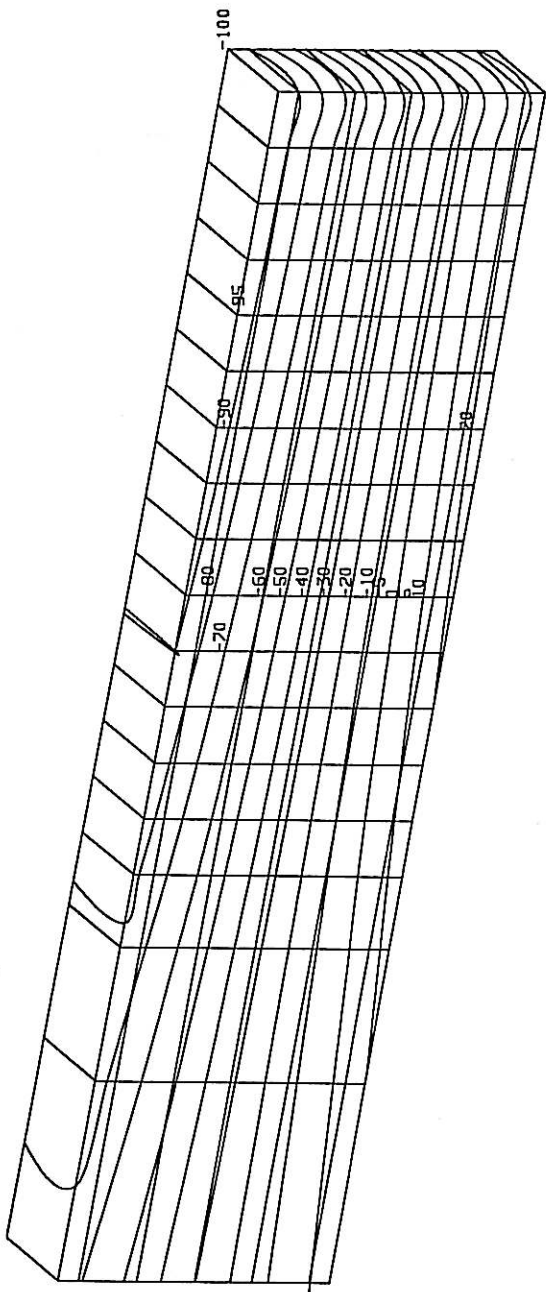
SCALE: 1/1

LENGTH
X #=0.726651cm
Y #=0.726651cm
Z #=0.726651cm

LOAD-STEP:
LS=2-1

PRESENTATION:
UNDEFORMED MESH
DETAIL

ARGUMENT:
STRAIN
Z -COMPONENT
SIGN CONSIDERED
100% =
0.000293



Si Unif

SCALE: 1-#-1

LENGTH

X #=0.776651cm
Y #=0.776651cm
Z #=0.776651cm

LOAD-STEP:

LS=2-1

PRESENTATION:

UNDEFORMED MESH
DETAIL

ARGUMENT:

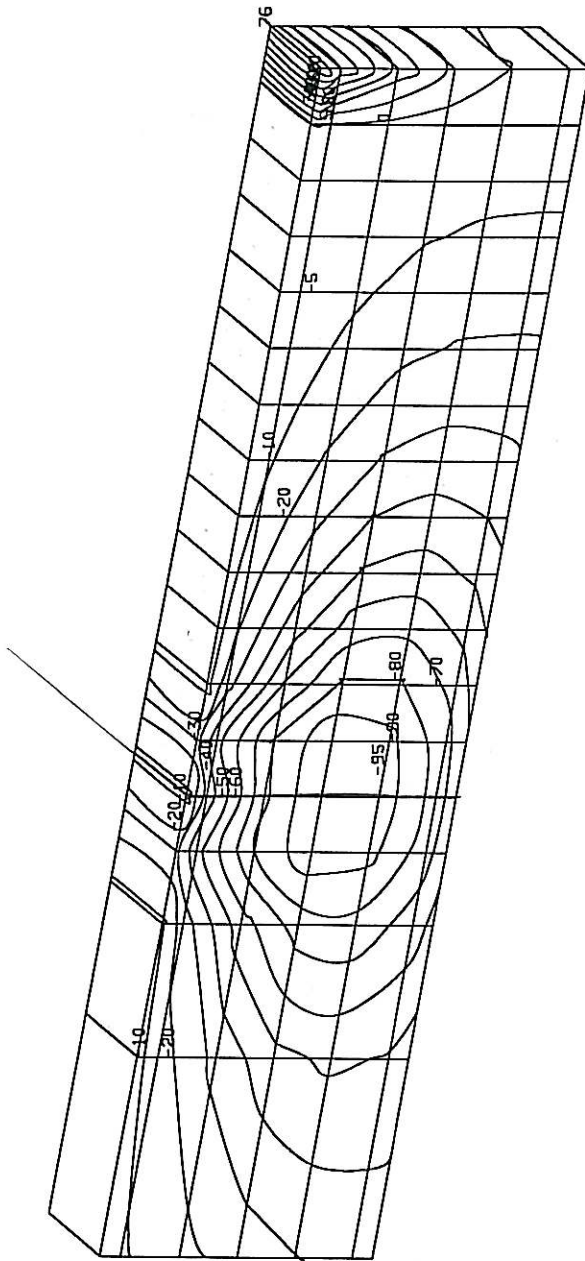
STRESS

Tau-XY

SIGN CONSIDERED

100% =

514.888549kN/m2



SI Unif

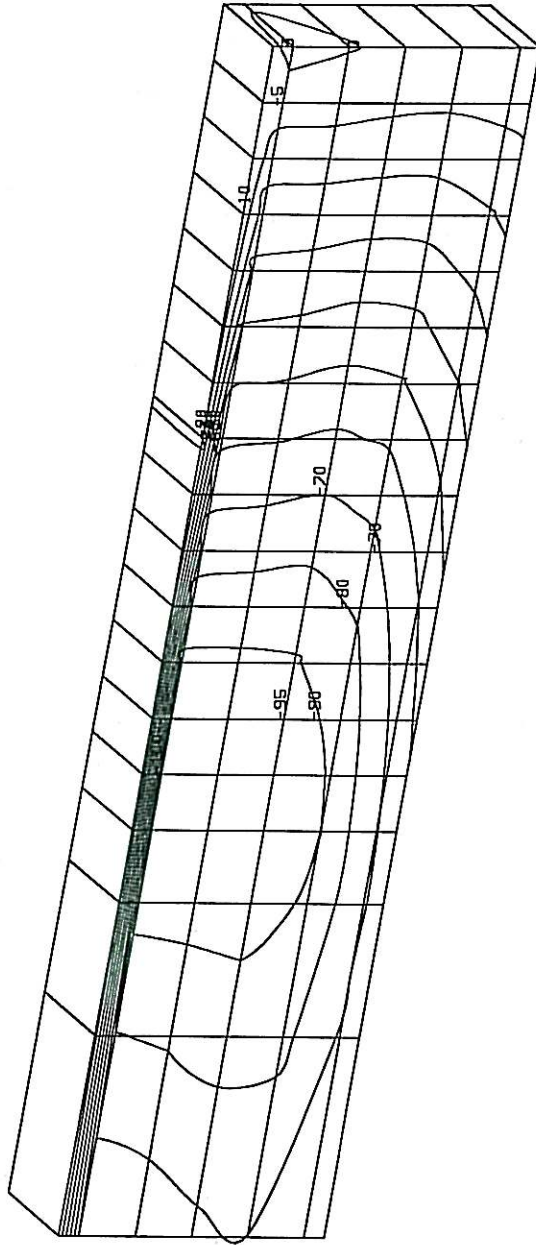
SCALE: 1:1

LENGTH
X #=0.726651cm
Y #=0.726651cm
Z #=0.726651cm

LOAD-STEP:
LS=2-1

PRESENTATION:
UNDEFORMED MESH
DETAIL

ARGUMENT:
STRAIN
Gamma-XY
SIGN CONSIDERED
100% =
0.001916



DESIGN BY SGG/901-Lopez geofe model HU 20.00-08
1998-8-17 16.38.55

SI thing

FINITE ELEMENT RESULTS
STRUCTURE 1: RECTANGULAR LOAD AREA WITH NON-UNIFORM CONTACT
PRESSURE

SCALE: 1:1

LENGTH

X #=16.911cm
Y #=16.911cm
Z #=16.911cm

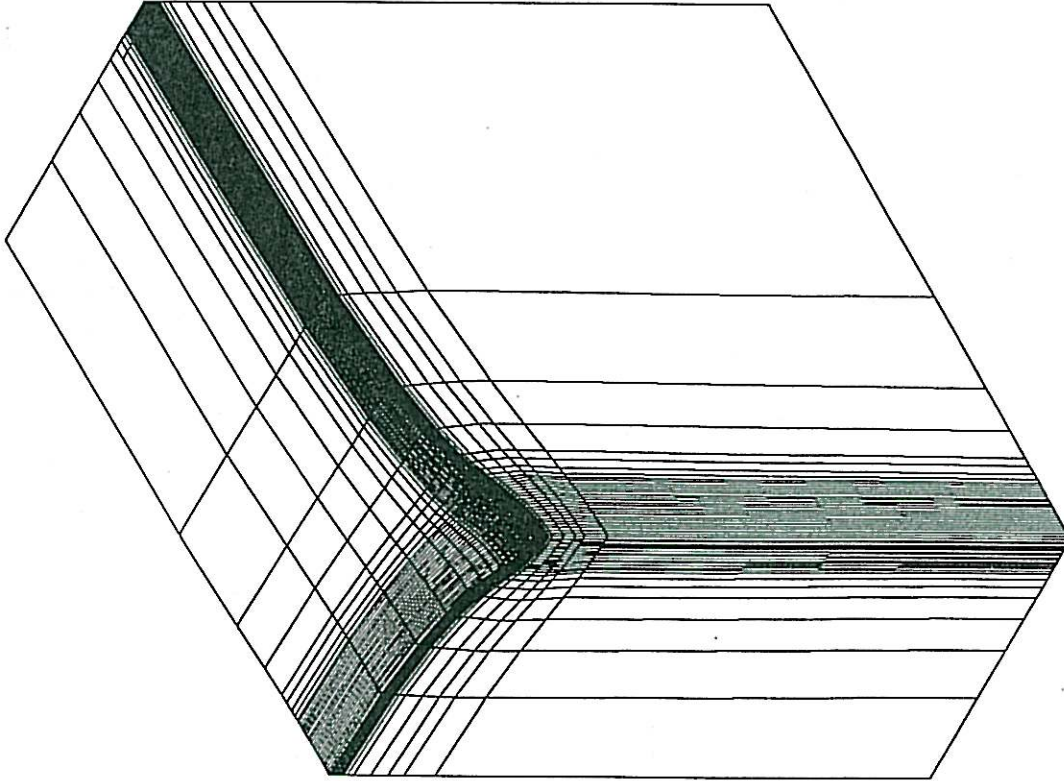
DISPLACEMENT

X #=0.065114cm
Y #=0.065114cm
Z #=0.065114cm

LOAD-STEP:

LS=2

PRESENTATION:
DEFORMED MESH



DESIGN BY SGG/901-Lopez geofe model MU 20.00-08
1998-0-3 12.45.38

STRUCTURE 1, LOAD=80kN, MAX. DEFLECTION=0.98mm

HMA PROJECT		TFAS/A/1
NON-UNIFORM TYRE PRESSURE		BKS (Pty) Ltd. Dr JP Laurens BOX 3173 PRETORIA FAX 012 4213501
FIG. 1: Deflection Bowl		

NIEUW
DISAHI

S1 N-U

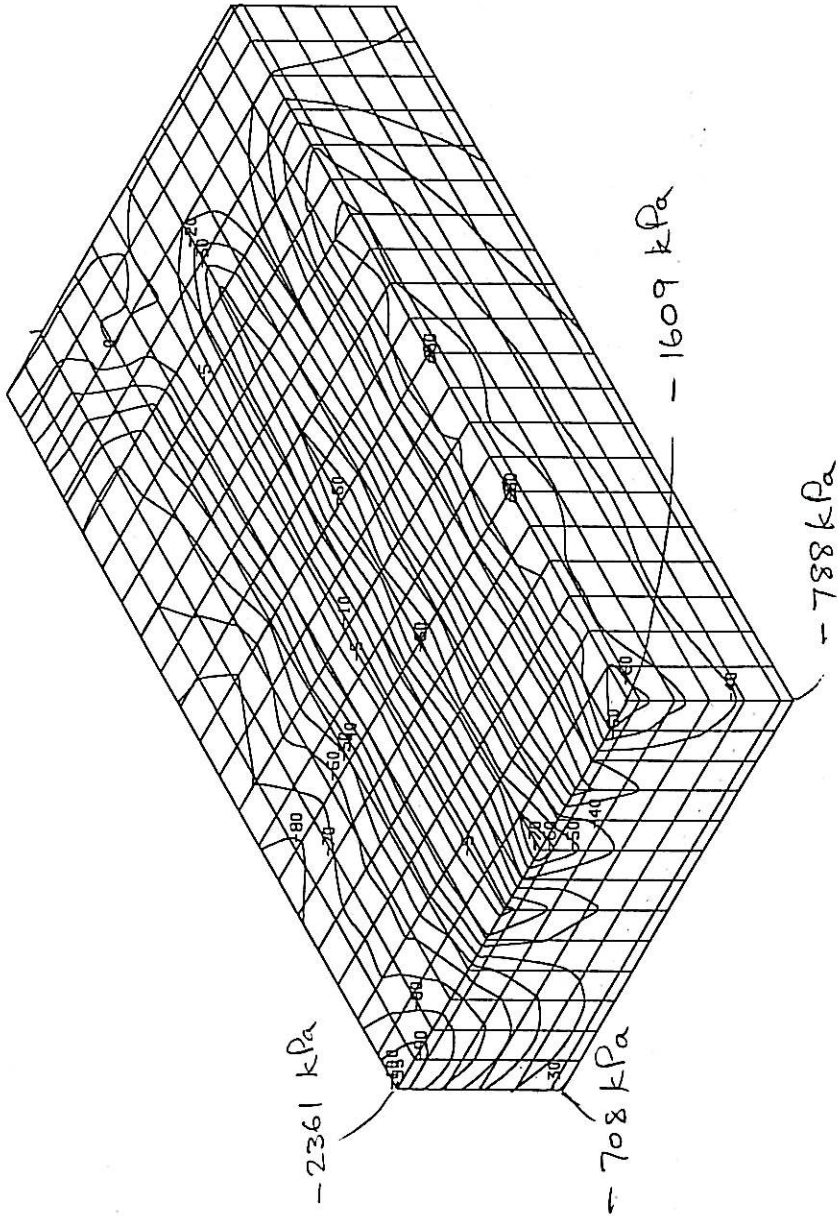
SCALE: 1:1

LENGTH
X #=1.2720cm
Y #=1.2720cm
Z #=1.2720cm

LOAD-STEP:
LS=2-1

PRESENTATION:
UNDEFORMED MESH
DETAIL

ARGUMENT:
STRESS
Y -COMPONENT
SIGN CONSIDERED
100% =
2361.238769kN/m2



DESIGN BY SGG/901-lopaz geofc model NU 20.00-08
1998-8-3 12:47:58

STRUCTURE 1, LOAD=80kN, MAX. DEFLECTION=0.98mm

SI - NU

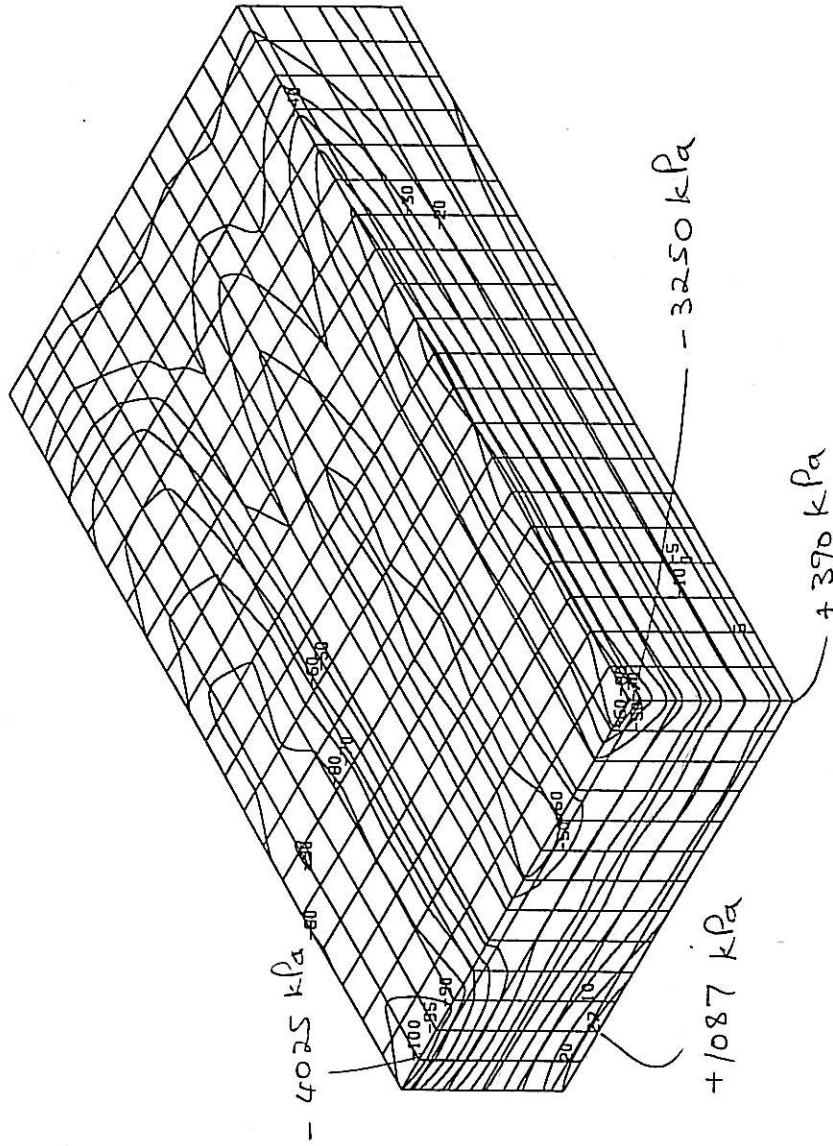
SCALE: 1# = 1

LENGTH
X # = 1.2770 cm
Y # = 1.2770 cm
Z # = 1.2770 cm

LOAD-STEP:
LS = 2-1

PRESENTATION:
UNDEFORMED MESH
DETAIL

ARGUMENT:
STRESS
X - COMPONENT
SIGN CONSIDERED
100% =
4025.957031 kN/m²



DESIGN BY SGG/901-Lopez geofe model HU 20.00-08
1998-8-3 13.11.5

STRUCTURE 1, LOAD=80kN, MAX. DEFLECTION=0.98mm

SI N-U

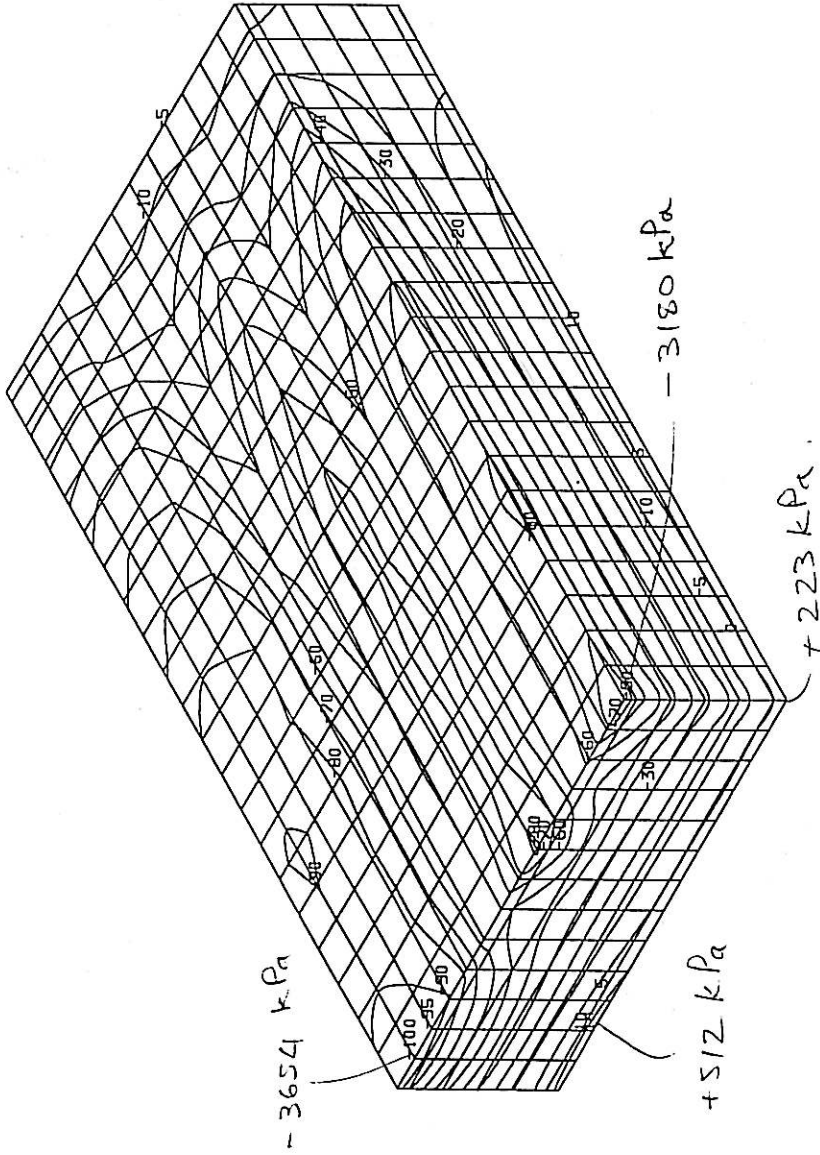
SCALE: 1:1

LENGTH
X #=1.2720cm
Y #=1.2720cm
Z #=1.2720cm

LOAD-STEP:
LS=2-1

PRESENTATION:
UNDEFORMED MESH
DETAIL

ARGUMENT:
STRESS
Z - COMPONENT
SIGN CONSIDERED
100% =
3654.208496kN/m²



DESIGN BY 566/901-Lopez Geofe model HU 20.00-08
1998-8-3 13:41:32

STRUCTURE 1, LOAD=80kN, MAX. DEFLECTION=0.98mm

SI N-U

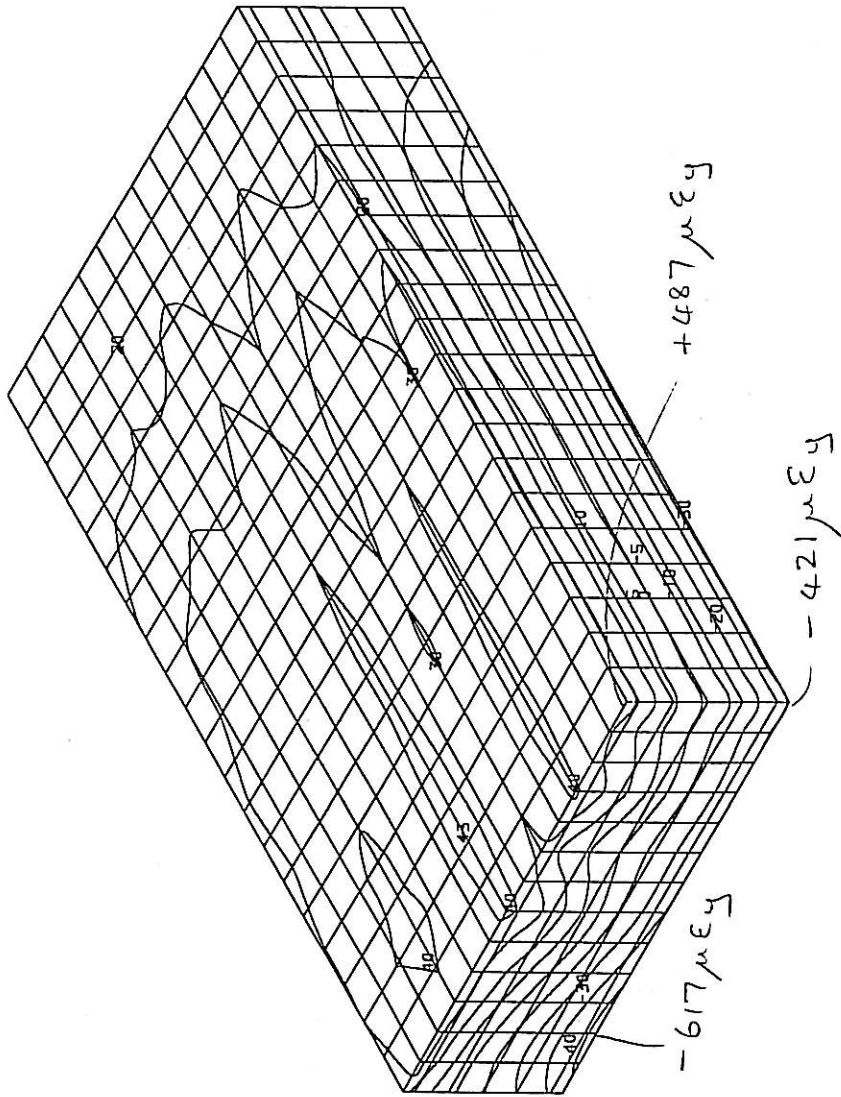
SCALE: $\frac{1}{1}$

LENGTH
 X $\# = 1.2770 \text{ cm}$
 Y $\# = 1.2770 \text{ cm}$
 Z $\# = 1.2770 \text{ cm}$

LOAD-STEP,
 LS=2-1

PRESENTATION:
 UNDEFORMED MESH
 DETAIL

ARGUMENT:
 STRAIN
 Y - COMPONENT
 SIGN CONSIDERED
 100% =
 0.001402



DESIGN BY 566/901-Lopez geofe model NU 20.00-08
 1998-8-3 13.7.24

STRUCTURE 1, LOAD=80kN, MAX. DEFLECTION=0.98mm

SI N-U

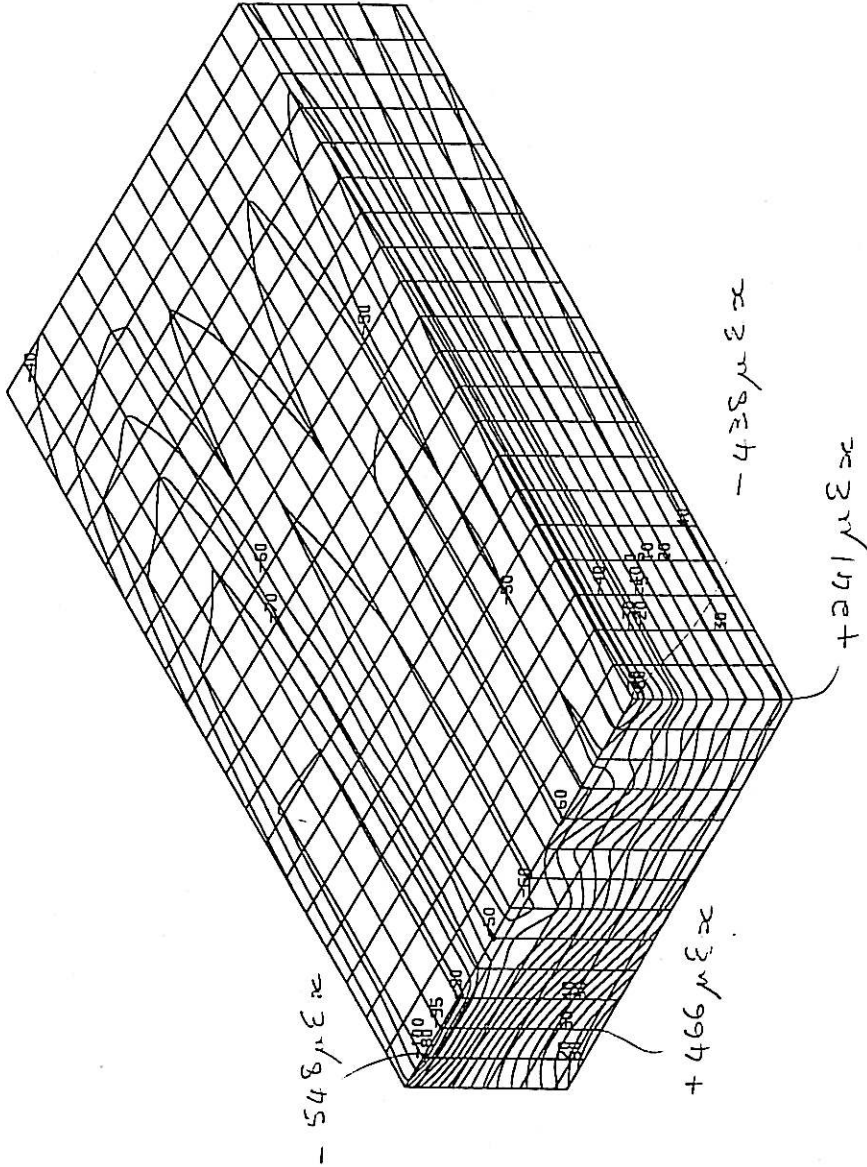
SCALE: $1 \text{ cm} = 1 \text{ m}$

LENGTH
 X $\# = 1.2770 \text{ cm}$
 Y $\# = 1.2770 \text{ cm}$
 Z $\# = 1.2770 \text{ cm}$

LOAD-STEP:
 LS=2-1

PRESENTATION:
 UNDEFORMED MESH
 DETAIL

ARGUMENT:
 STRAIN
 X - COMPONENT
 SIGN CONSIDERED
 100% =
 0.000548



DESIGN BY SGG/901-Lopez GeofE model RV 20.00-08
 1998-8-3 16:18:22

STRUCTURE 1, LOAD=80kN, MAX. DEFLECTION=0.98mm

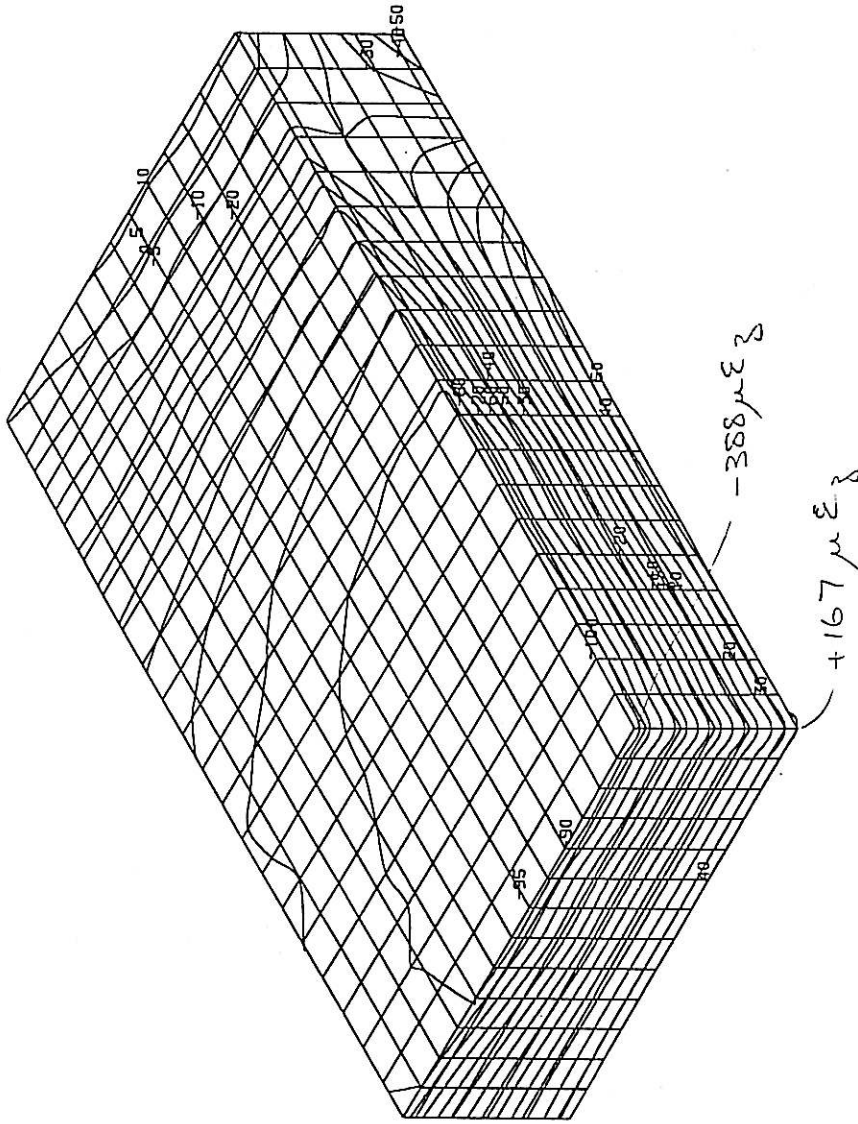
SCALE: $\frac{1}{\#}$

LENGTH
 X $\# = 1.2770 \text{ cm}$
 Y $\# = 1.2770 \text{ cm}$
 Z $\# = 1.2770 \text{ cm}$

LOAD-STEP:
 LS=2-1

PRESENTATION:
 UNDEFORMED MESH
 DETAIL

ARGUMENT:
 STRAIN
 Z -COMPONENT
 SIGN CONSIDERED
 100% =
 0.000417



DESIGN BY SGG/901-topaz geofe model1 MV 20.00-08
 1998-8-3 16:21:11

SRUCTURE 1, LOAD=80kN, MAX. DEFLECTION=0.98mm

SI N-U

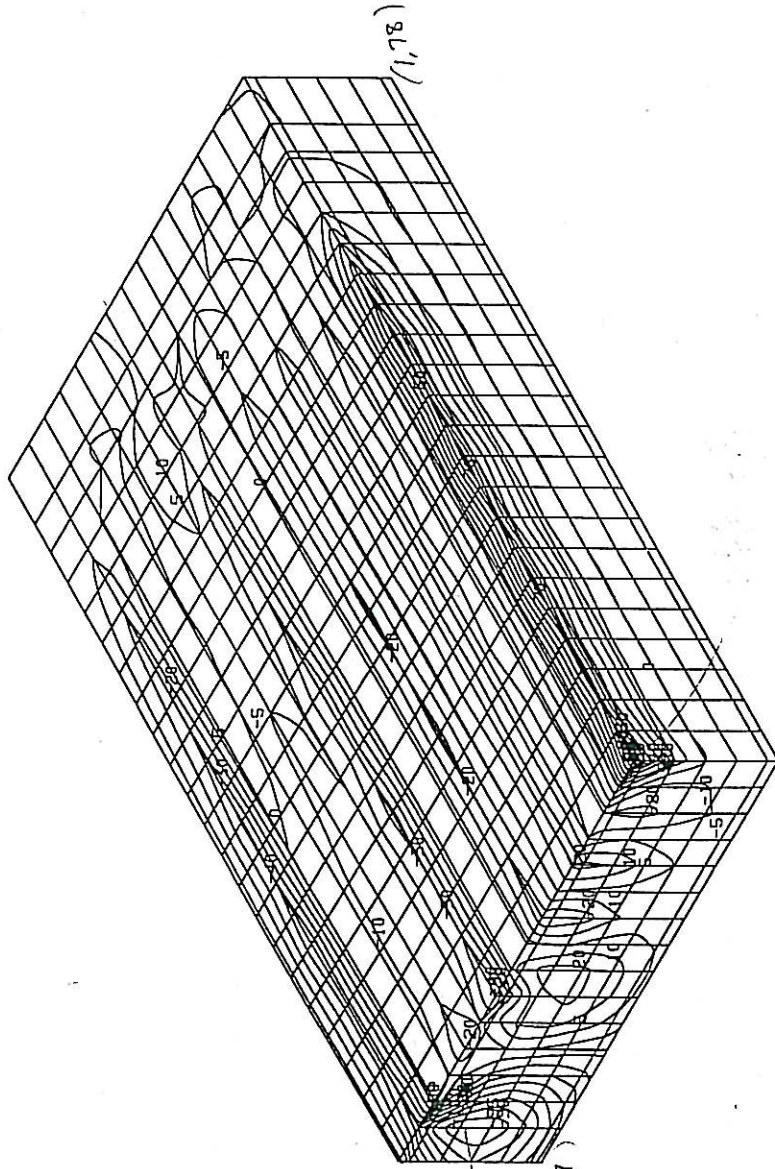
SCALE: 1:1

LENGTH
X #=1.4583cm
Y #=1.4583cm
Z #=1.4583cm

LOAD-STEP:
LS=2-1

PRESENTATION:
UNDEFORMED MESH
DETAIL

ARGUMENT:
STRESS
TAU-XY
SIGN CONSIDERED
100% =
924.744750kN/m²



- 925 kPa

(0,77)

(1,78)

0

DESIGN BY SGG/901-Lopez geofe model HU 20.00-08
1998-8-3 16:39:25

SRUCTURE 1, LOAD=80kN, MAX. DEFLECTION=0.98mm

SIN-U

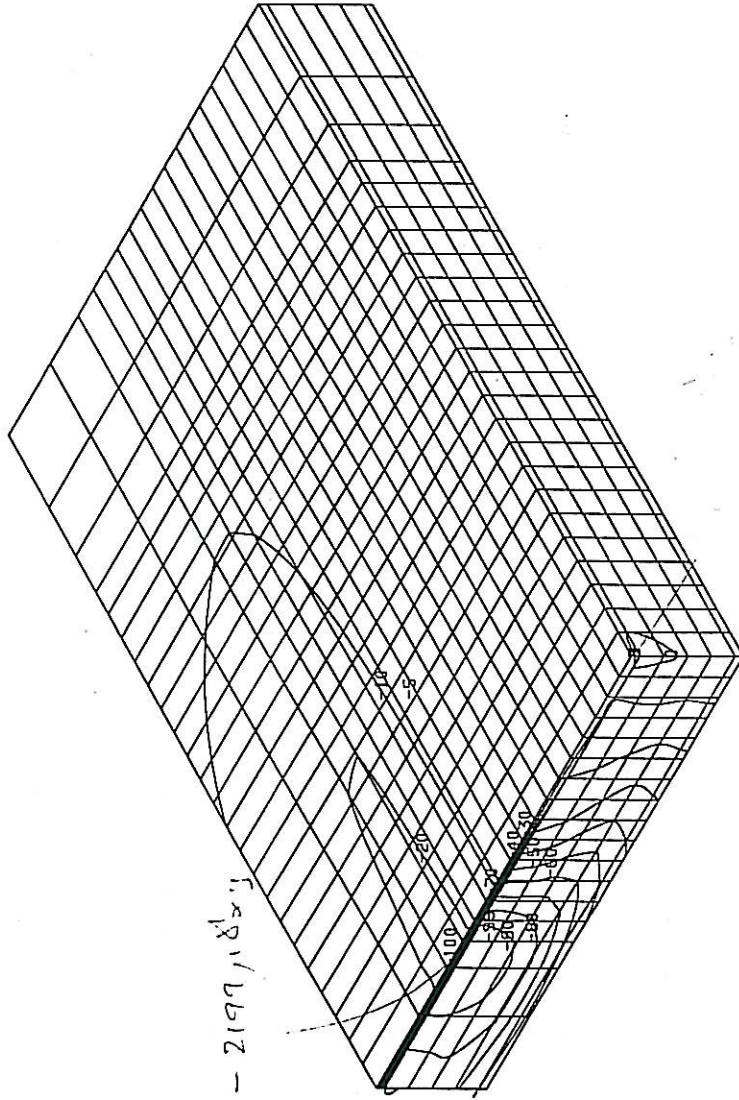
SCALE: $\frac{1}{100}$

LENGTH
 X #=1.8749cm
 Y #=1.8749cm
 Z #=1.8749cm

LOAD-STEP:
 LS=2-1

PRESENTATION:
 UNDEFORMED MESH
 DETAIL

ARGUMENT:
 STRAIN
 Gamma-XY
 SIGN CONSIDERED
 100% =
 0.002199



DESIGN BY SGG/901-Lopez geofc model HU 20.00-08
 1998-8-3 16:49:53

SRUCTURE 1, LOAD=80kN, MAX. DEFLECTION=0.98mm

SI N-W

SCALE: 1# = 1

LENGTH

X #=0.776651cm

Y #=0.776651cm

Z #=0.776651cm

LOAD-STEP:

LS=2-1

PRESENTATION:

UNDEFORMED MESH

DETAIL

ARGUMENT:

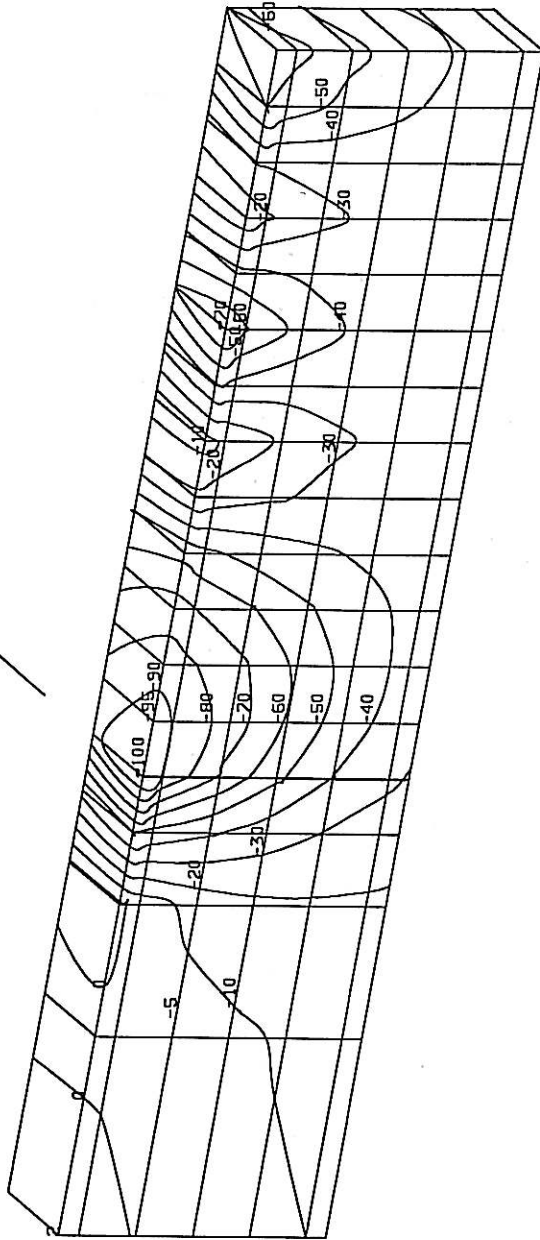
STRESS

Y -COMPONENT

SIGN CONSIDERED

100% =

2361.238769kN/m²



DESIGN BY SGG/901-Lopez geofe model HV 20.00-08
1998-B-17 16.3.10

STRUCTURE 1, LOAD=80kN, MAX. DEFLECTION=0.98mm

SI N-U

SCALE: 1# = 1

LENGTH

X #=0.776651cm

Y #=0.776651cm

Z #=0.776651cm

LOAD-STEP:

LS=2-1

PRESENTATION:

UNDEFORMED MESH

DETAIL

ARGUMENT:

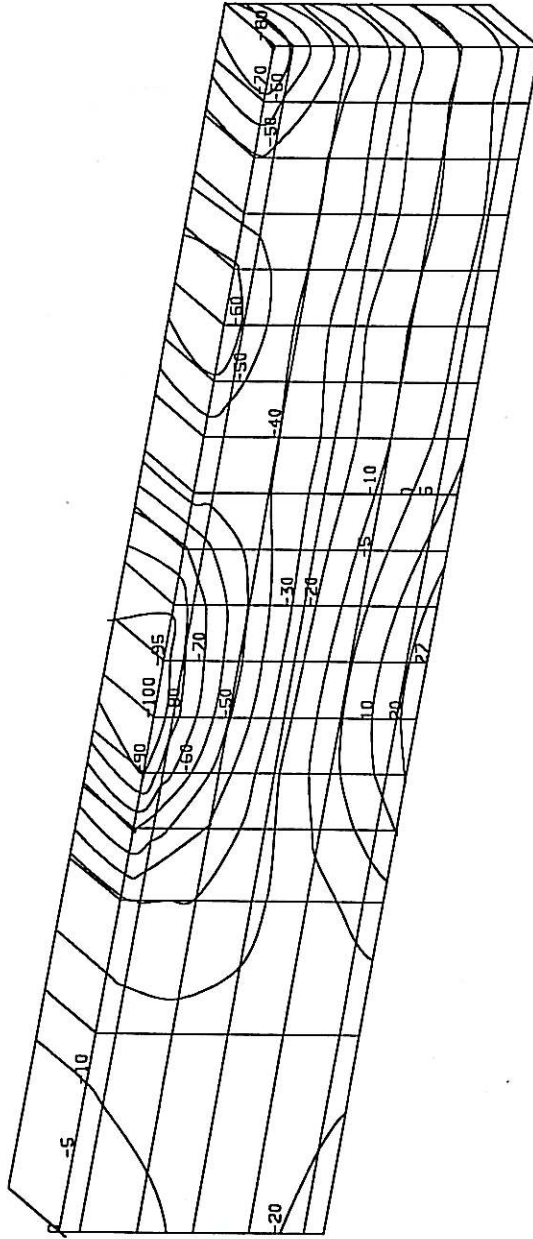
STRESS

X -COMPONENT

SIGN CONSIDERED

100% =

4025.957031kN/m²



DESIGN BY SGG/901-Lopez geofe model HV 20.00-08
1998-8-17 16:4:53

STRUCTURE 1, LOAD=80kN, MAX. DEFLECTION=0.98mm

SI N-W

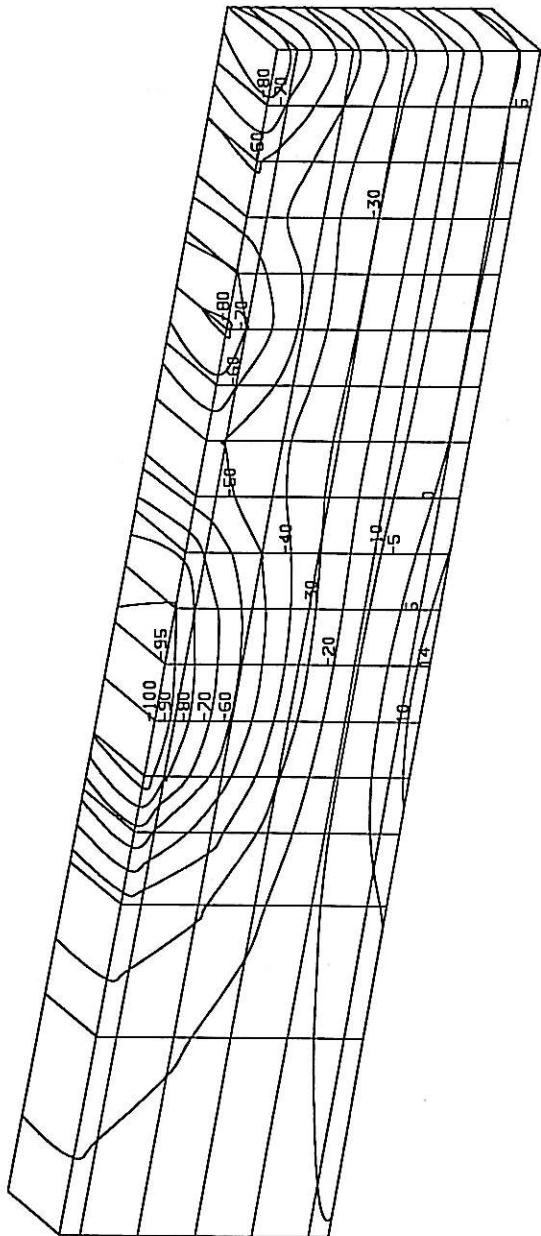
SCALE: 1# = 1

LENGTH
X #=0.776651cm
Y #=0.776651cm
Z #=0.776651cm

LOAD-STEP:
LS=2-1

PRESENTATION:
UNDEFORMED MESH
DETAIL

ARGUMENT:
STRESS
Z -COMPONENT
SIGN CONSIDERED
100% =
3654.208496kN/m2



DESIGN BY SGG/901-Lopez geofe model NU 20.00-08
1998-8-17 16:8:5

STRUCTURE 1, LOAD=80kN, MAX. DEFLECTION=0.98mm

SI N-U

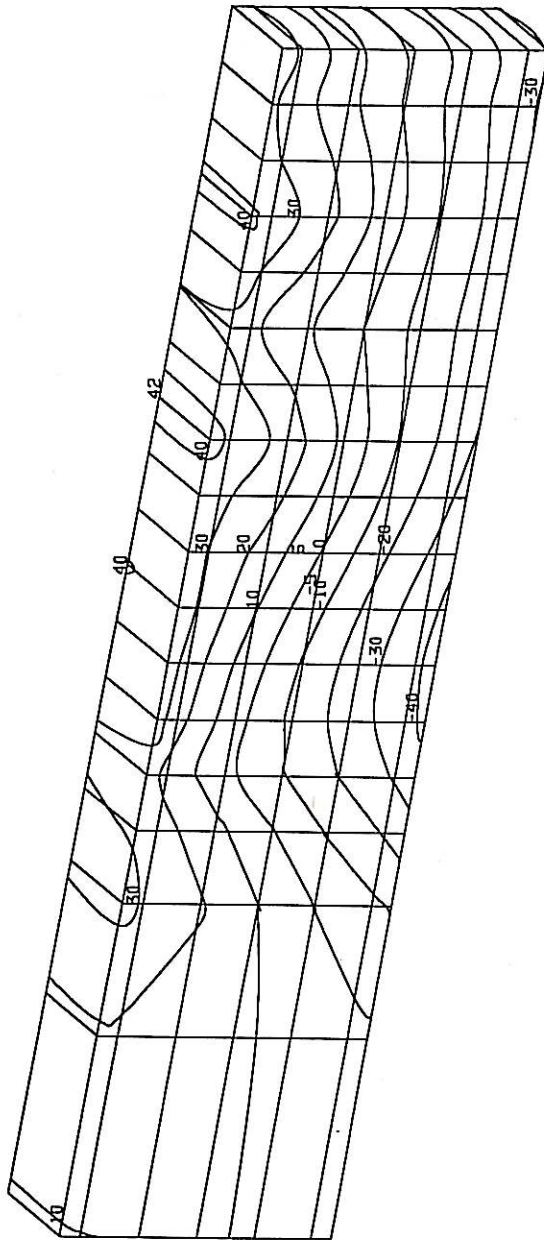
SCALE: 1/10

LENGTH #=0.776651cm
X #=0.776651cm
Y #=0.776651cm
Z #=0.776651cm

LOAD-STEP:
LS=2-1

PRESENTATION:
UNDEFORMED MESH
DETAIL

ARGUMENT:
STRAIN
Y -COMPONENT
SIGN CONSIDERED
100% =
0.001402



•DESIGN BY SGG/901-Lopez geofe model MV 20.00-08
1998-8-12 16.10.11

STRUCTURE 1, LOAD=80kN, MAX. DEFLECTION=0.98mm

81 N-W

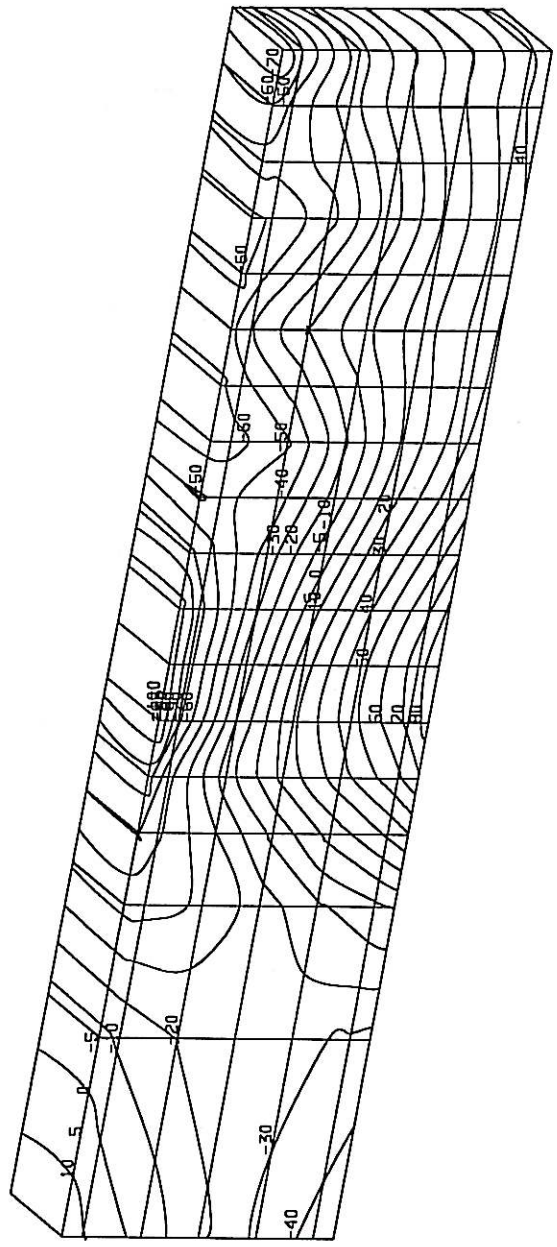
SCALE: 1:1

LENGTH
 X #=0.776651cm
 Y #=0.776651cm
 Z #=0.776651cm

LOAD-STEP:
 LS=2-1

PRESENTATION:
 UNDEFORMED MESH
 DETAIL

ARGUMENT:
 STRAIN
 X -COMPONENT
 SIGN CONSIDERED
 100% =
 0.000548



•DESIGN BY SGG/901-Lopez geofc model HU 20.00-08
 1998-8-17 16:14:41

STRUCTURE 1, LOAD=80kN, MAX. DEFLECTION=0.98mm

SI N-U

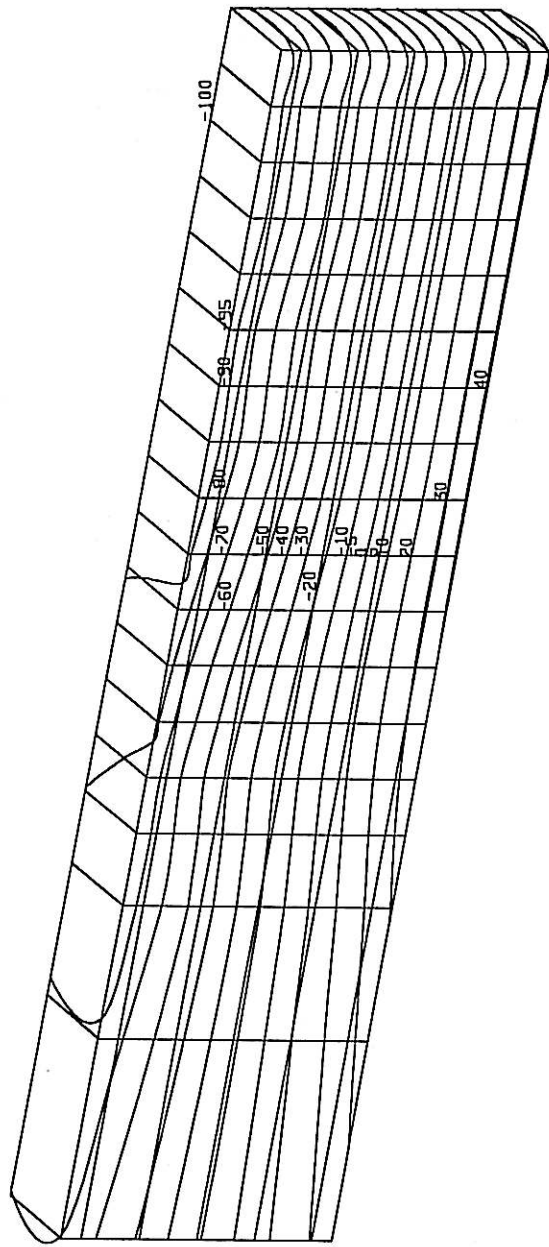
SCALE: 1# = 1

LENGTH #=0.776651cm
 X #=0.776651cm
 Y #=0.776651cm
 Z #=0.776651cm

LOAD-STEP:
 LS=2-1

PRESENTATION:
 UNDEFORMED MESH
 DETAIL

ARGUMENT:
 STRAIN
 Z - COMPONENT
 SIGN CONSIDERED
 100% =
 0.000411



STRUCTURE 1, LOAD=80kN, MAX. DEFLECTION=0.98mm

DESIGN BY SGG/901-Logaz BOCFE Model HV 20.00-08
 1998-8-17 16:16:22

SI NW

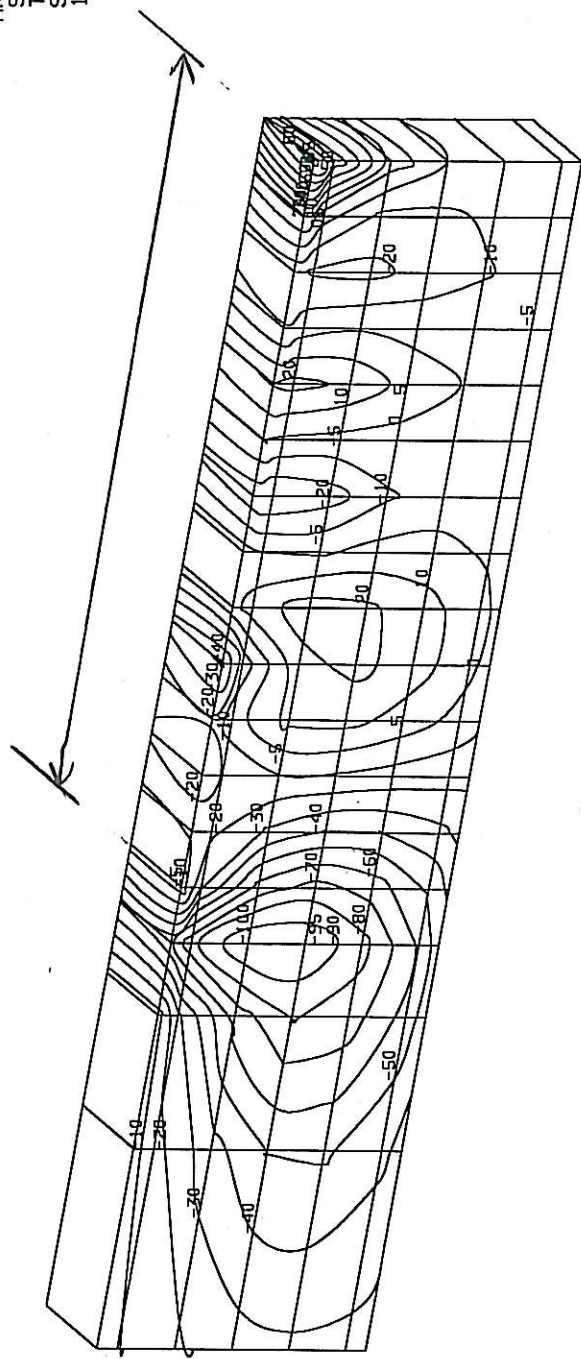
SCALE: 1# = 1

LENGTH
X #=0.776651cm
Y #=0.776651cm
Z #=0.776651cm

LOAD-STEP:
LS=2-1

PRESENTATION:
UNDEFORMED MESH
DETAIL

ARGUMENT:
STRESS
Tau-XY
SIGN CONSIDERED
100% = 924.744750kN/m2



DESIGN BY SGG/901-Lopez GeoFE model MU 20.00.08
1998-8-17 16:18:15

STRUCTURE 1, LOAD=80kN, MAX. DEFLECTION=0.98mm

SI N-U

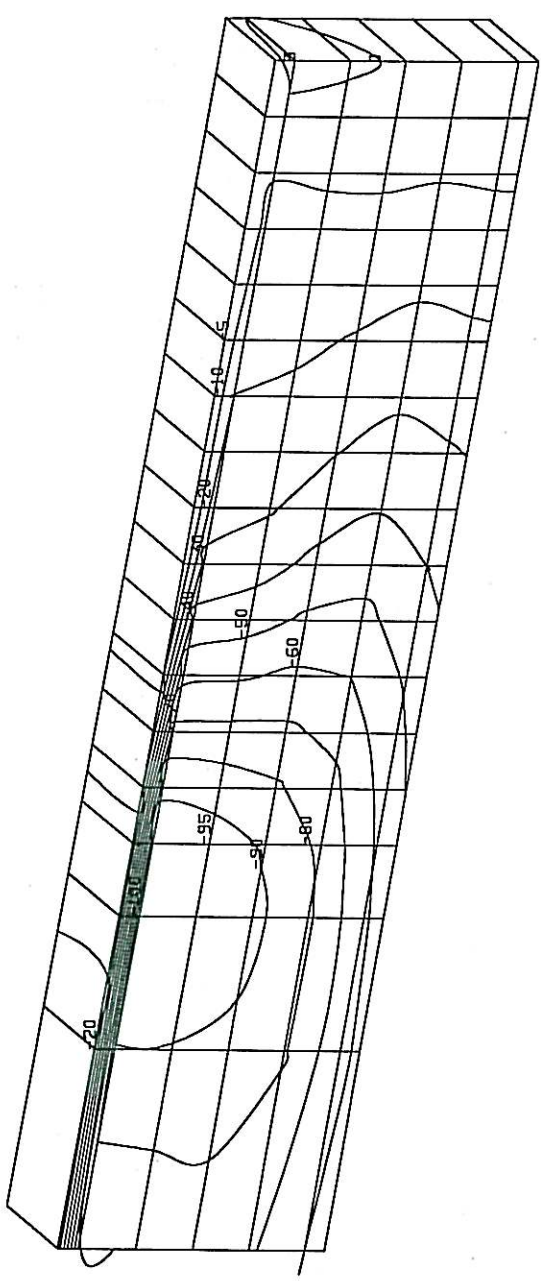
SCALE: 1# = 1

LENGTH #=0.776651cm
 X #=0.776651cm
 Y #=0.776651cm
 Z #=0.776651cm

LOAD-STEP:
 LS=2-1

PRESENTATION:
 UNDEFORMED MESH
 DETAIL

ARGUMENT:
 STRAIN
 Gamma-XY
 SIGN CONSIDERED
 100% =
 0.002199



DESIGN BY SGG/901-lppaz gafe model HV 20.00-08
 1998-8-17 16:20:3

STRUCTURE 1, LOAD=80kN, MAX. DEFLECTION=0.98mm

SIN-N

FINITE ELEMENT RESULTS
STRUCTURE 2: RECTANGULAR LOAD AREA WITH UNIFORM CONTACT
PRESSURE

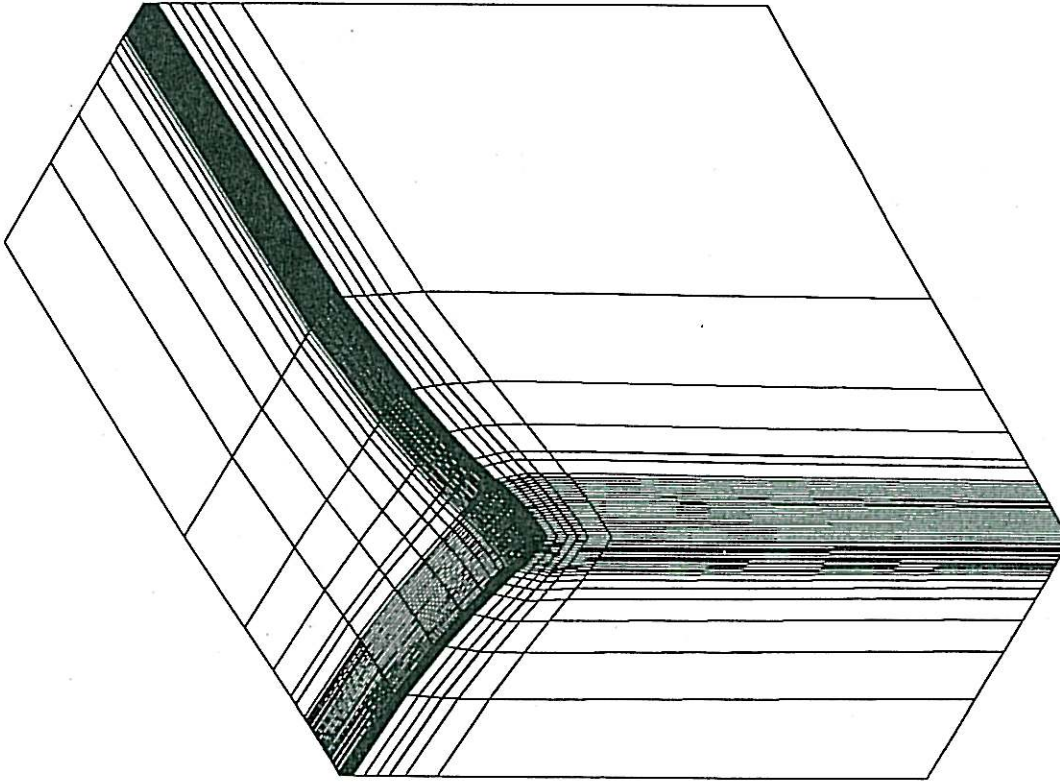
SCALE: 1:1

LENGTH
 X #=16.911cm
 Y #=16.911cm
 Z #=16.911cm

DISPLACEMENT
 X #=0.042546cm
 Y #=0.042546cm
 Z #=0.042546cm

LOAD-STEP:
 LS=2

PRESENTATION:
 DEFORMED MESH



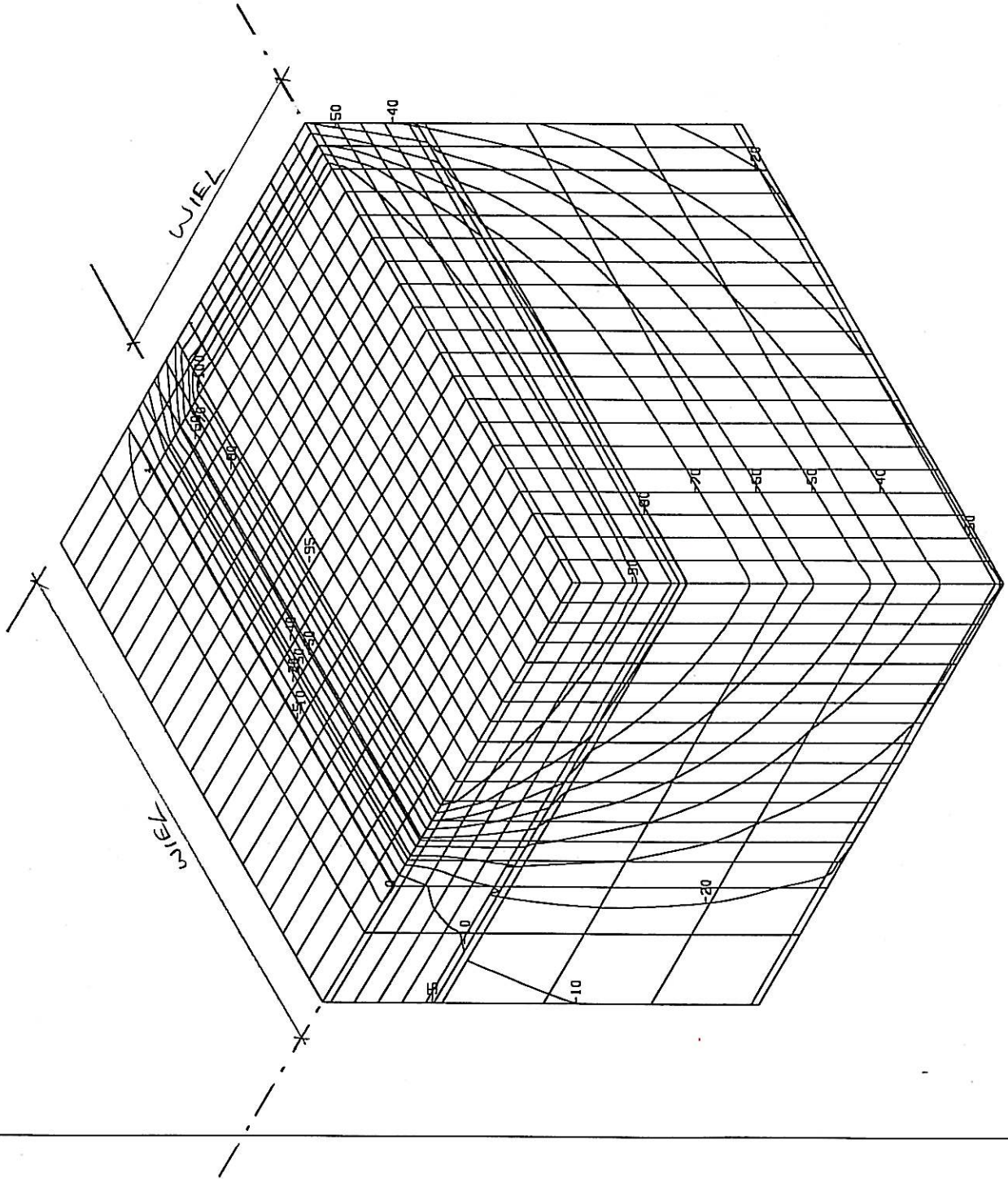
STRUCTURE 2, LOAD=80kN, MAX. DEFLECTION=0.64mm

• DESIGN BY SGG/901-topaz geofe model HU 20.00-08
 1998-B-4 13.51.40

S2 Un
 NIEU2
 DISB2 PA03

HMA PROJECT	TFAS/A/1
UNIFORM TYRE PRESSURE	BKS (Pty) Ltd. Dr JP Laurens BOX 3173 PRETORIA FAX 012 4213501
FIG. 1: Deflection Bowl	

SCALE: 1#=
LENGTH
X #=1.5666cm
Y #=1.5666cm
Z #=1.5666cm
LOAD-STEP:
LS=2-1
PRESENTATION:
UNDEFORMED MESH
DETAIL
ARGUMENT:
STRESS
Y
-COMPONENT
SIGN CONSIDERED
100% =
989.687866kN/m2



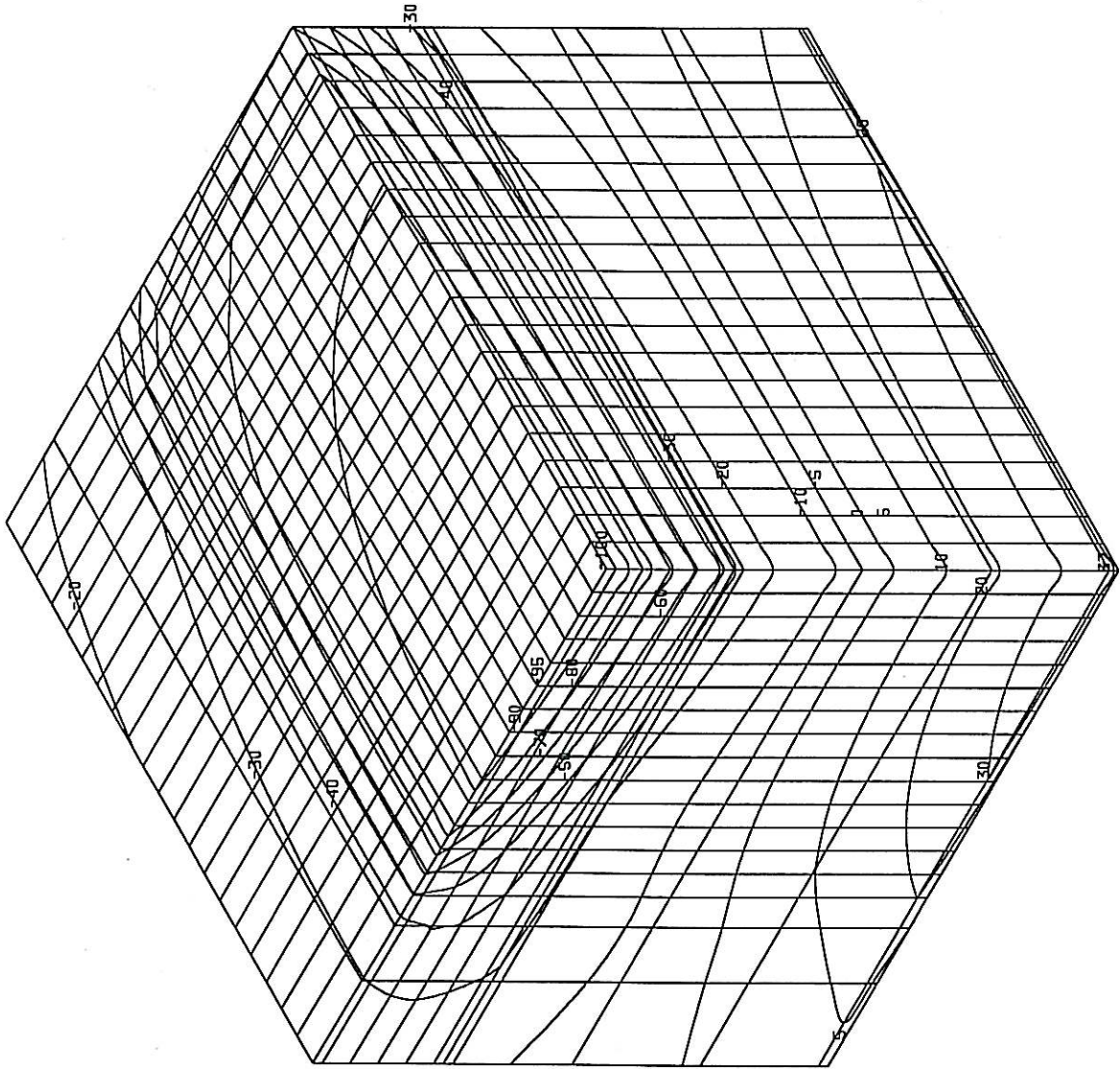
S2 m

SCALE: 1/10
LENGTH
X #=1.5666cm
Y #=1.5666cm
Z #=1.5666cm

LOAD-STEP:
LS=2-1

PRESENTATION:
UNDEFORMED MESH
DETAIL

ARGUMENT:
STRESS
X -COMPONENT
SIGN CONSIDERED
100% =
2131.232910kN/m²



DESIGN BY SGG/901-Lopez geofE model HU 20.00-08
1998-8-18 10:15:15

Sz Uw

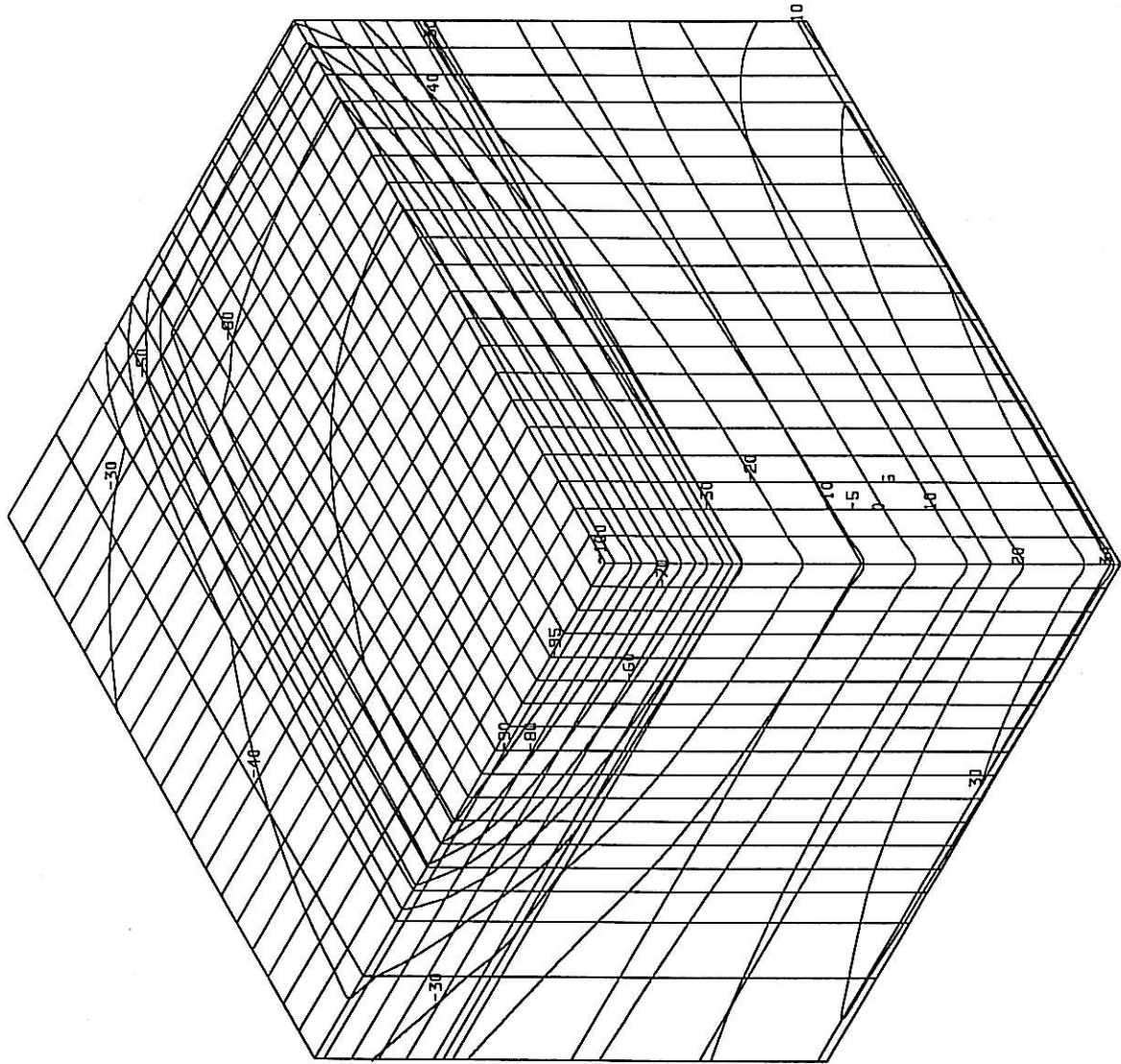
SCALE: 1# =

LENGTH
X # = 1.5666cm
Y # = 1.5666cm
Z # = 1.5666cm

LOAD-STEP:
LS=2-1

PRESENTATION:
UNDEFORMED MESH
DETAIL

ARGUMENT:
STRESS
Z - COMPONENT
SIGN CONSIDERED
100% =
2033.277709kN/m2



DESIGN BY SGG/901-Lopez 10:16:36
1998-8-18
2033.277709kN/m2
HU 20.00-08 gacfe model

S2 Un

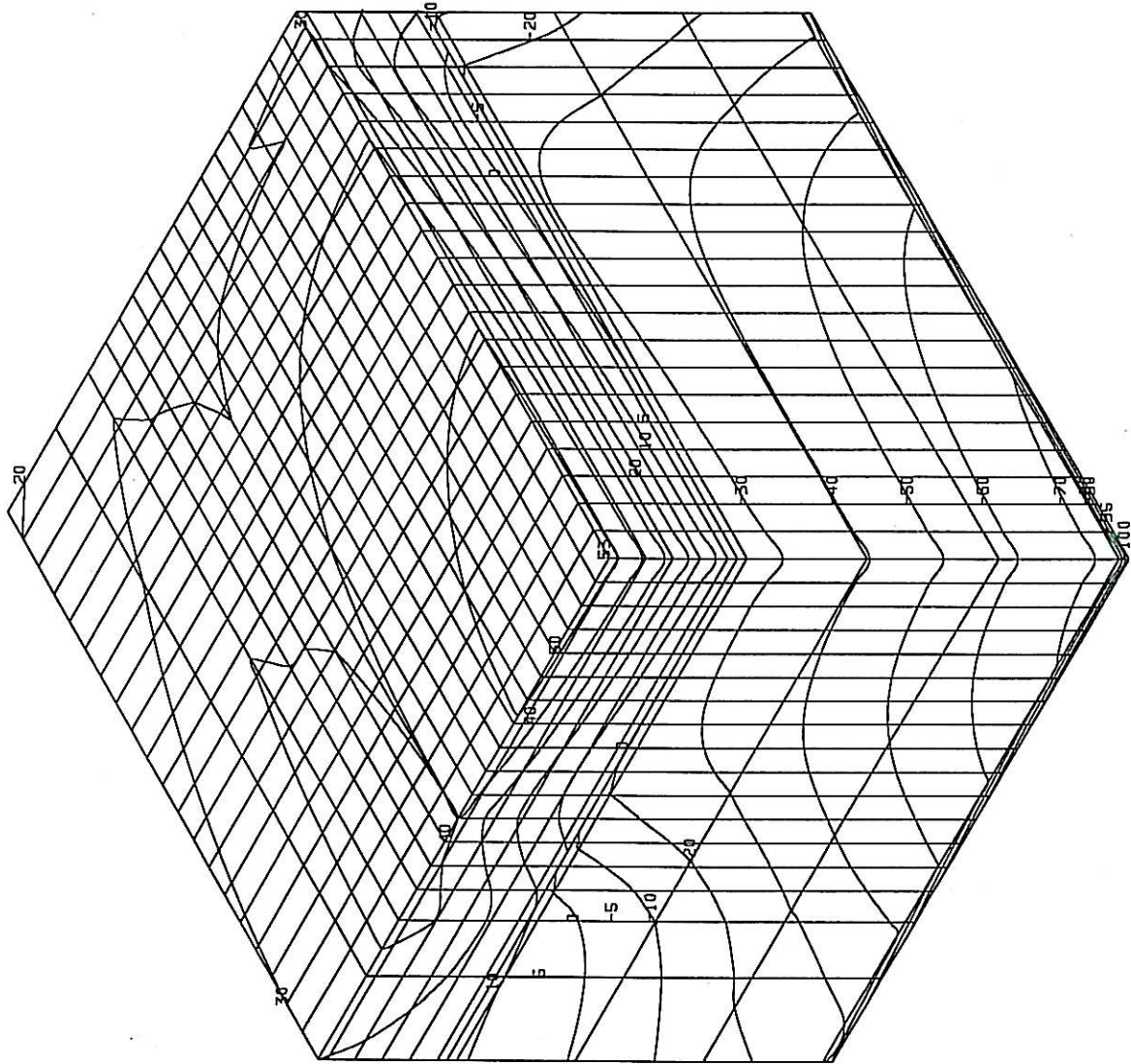
SCALE: 1# = 1

LENGTH # = 1.5666cm
 X # = 1.5666cm
 Y # = 1.5666cm
 Z # = 1.5666cm

LOAD-STEP:
 LS=2-1

PRESENTATION:
 UNDEFORMED MESH
 DETAIL

ARGUMENT:
 STRAIN
 Y - COMPONENT
 SIGN CONSIDERED
 100% = 0.000705



•DESIGN BY S66/901-Lopez geofe model HV 20.00-08
 1998-8-18 10:17:45

S2 Un

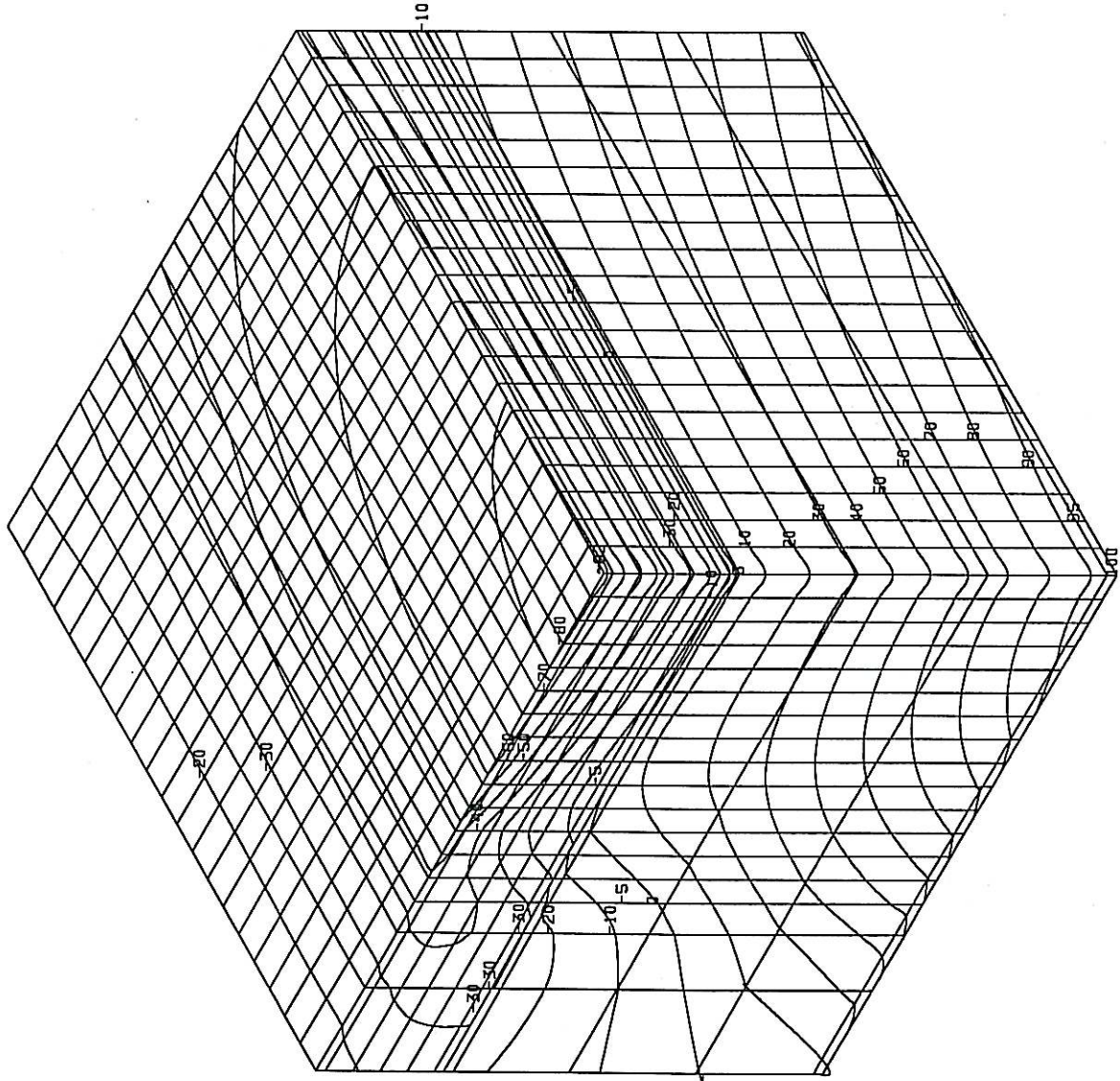
SCALE: 1:1

LENGTH
 X #=1.5666cm
 Y #=1.5666cm
 Z #=1.5666cm

LOAD-STEP:
 LS=2-1

PRESENTATION:
 UNDEFORMED MESH
 DETAIL

ARGUMENT:
 STRAIN
 X -COMPONENT
 SIGN CONSIDERED
 100% =
 0.000389



DESIGN BY SGG/901-10paz geofe model HU 20.00-08
 1998-8-18 10:19:15

Sz Uu

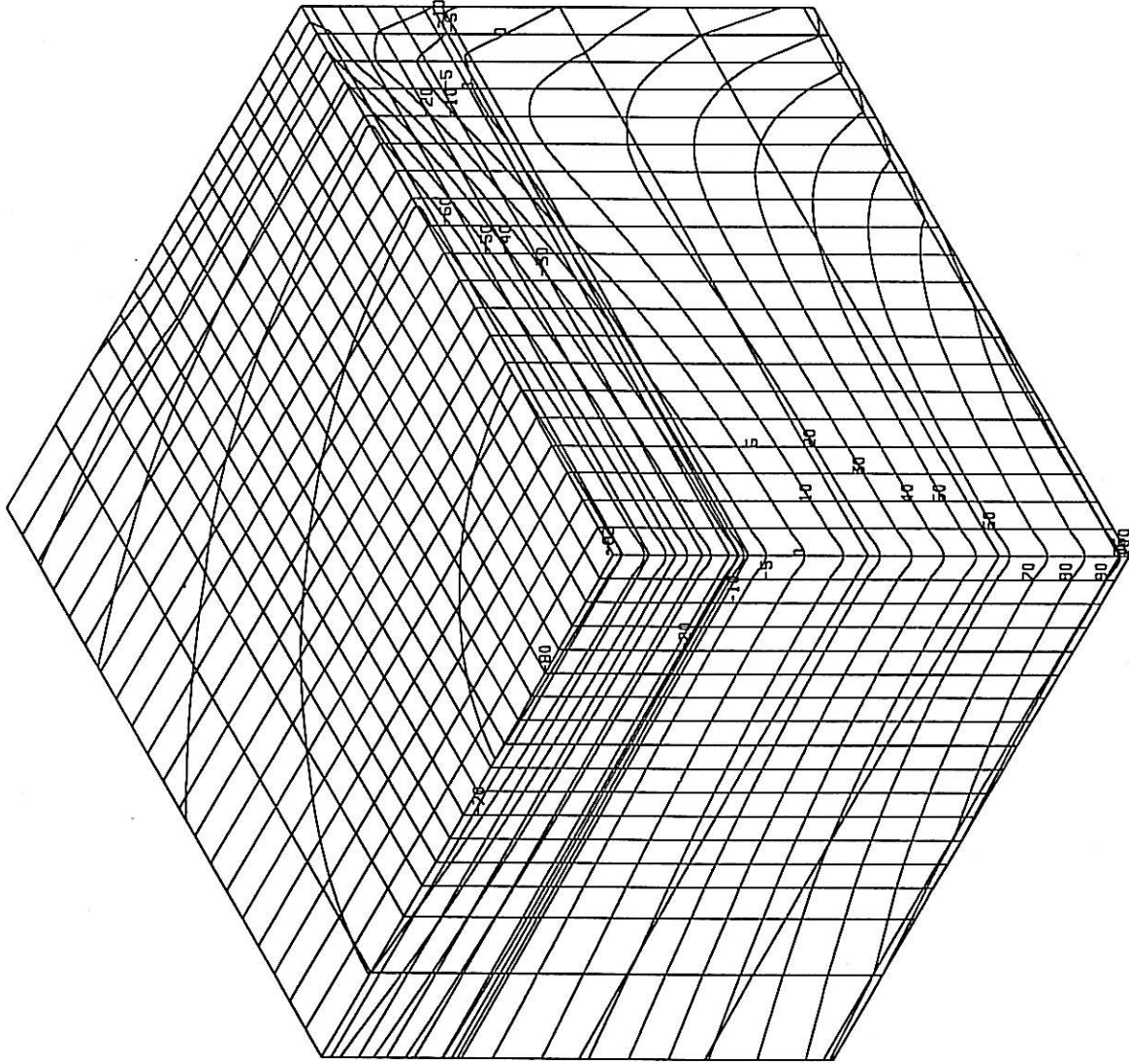
SCALE: 1#=1

LENGTH
 X #=1.5666cm
 Y #=1.5666cm
 Z #=1.5666cm

LOAD-STEP:
 LS=2-1

PRESENTATION:
 UNDEFORMED MESH
 DETAIL

ARGUMENT:
 STRAIN
 Z -COMPONENT
 SIGN CONSIDERED
 100% =
 0.000315



Sz Un

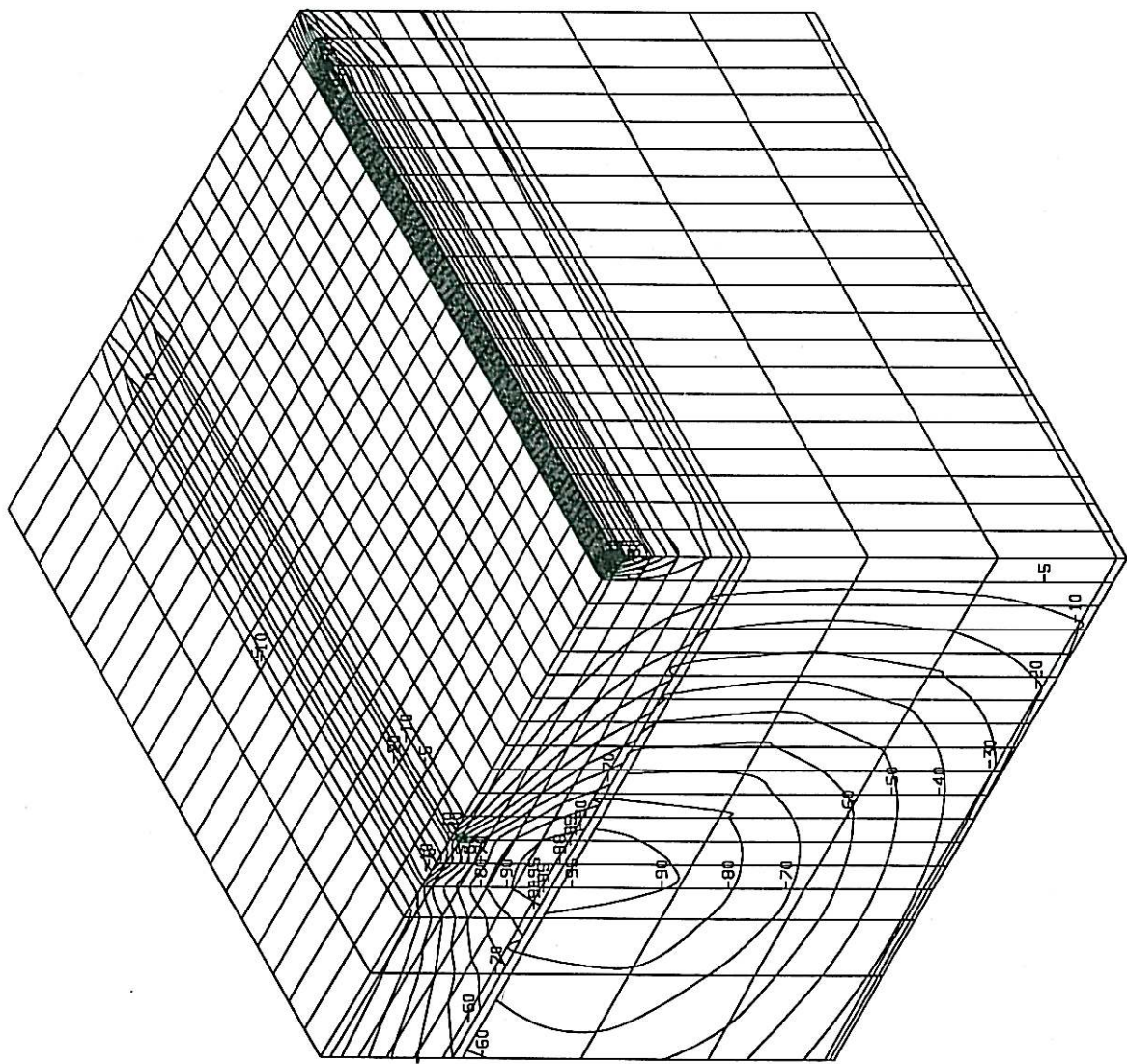
SCALE: 1# = 1

LENGTH
 X # = 1.5666cm
 Y # = 1.5666cm
 Z # = 1.5666cm

LOAD-STEP:
 LS=2-1

PRESENTATION:
 UNDEFORMED MESH
 DETAIL

ARGUMENT:
 STRESS
 Tau-XY
 SIGN CONSIDERED
 100% =
 423.457855kN/m2



DESIGN BY SGG/901-100az GeofE model HV 20.00-08
 1998-8-18 10:22:38

Sz Un

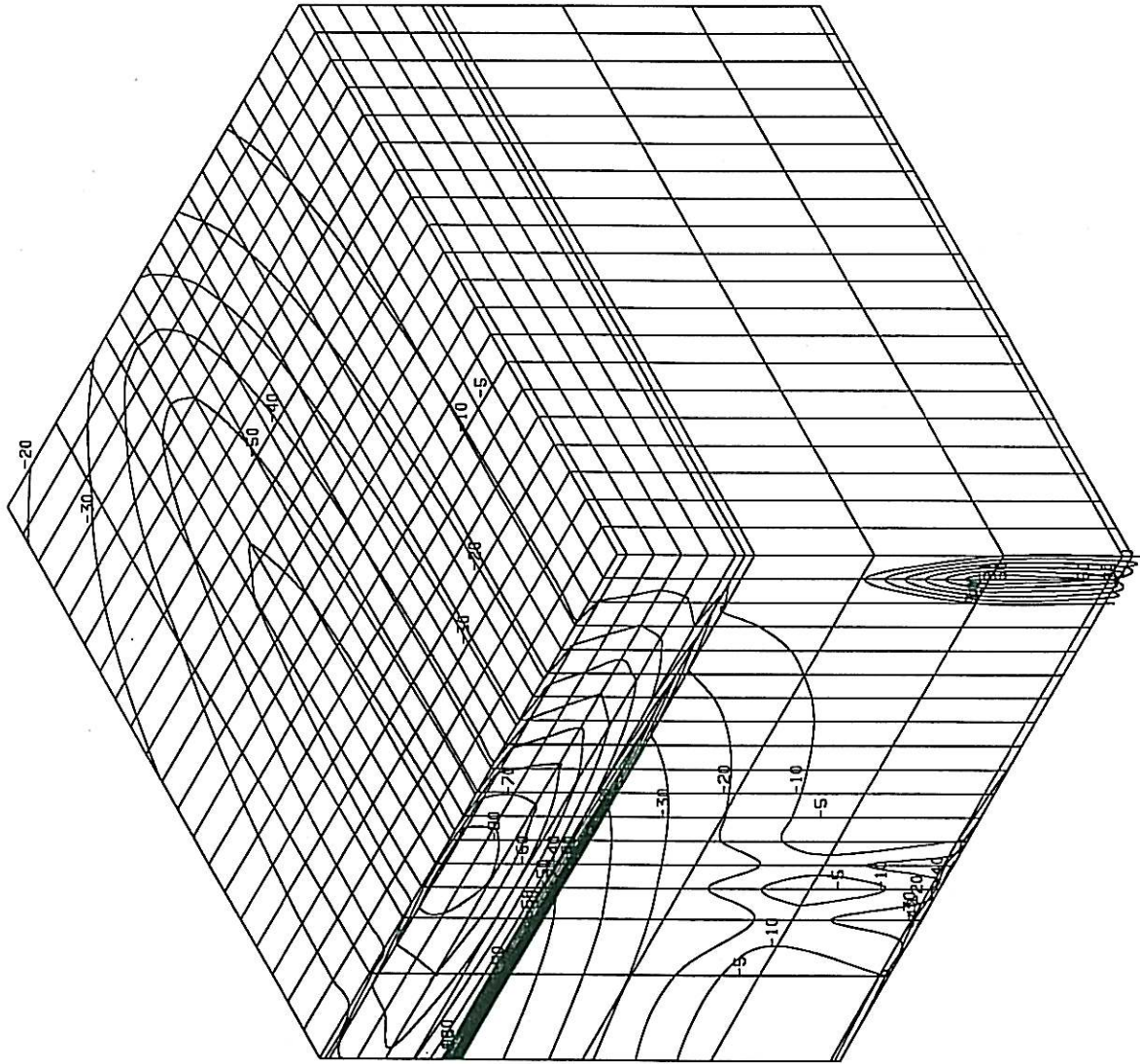
SCALE: 1:1

LENGTH
 X #=1.5666cm
 Y #=1.5666cm
 Z #=1.5666cm

LOAD-STEP:
 LS=2-1

PRESENTATION:
 UNDEFORMED MESH
 DETAIL

ARGUMENT:
 STRAIN
 Gamma-XY
 SIGN CONSIDERED
 100% =
 0.000741



Sz Un

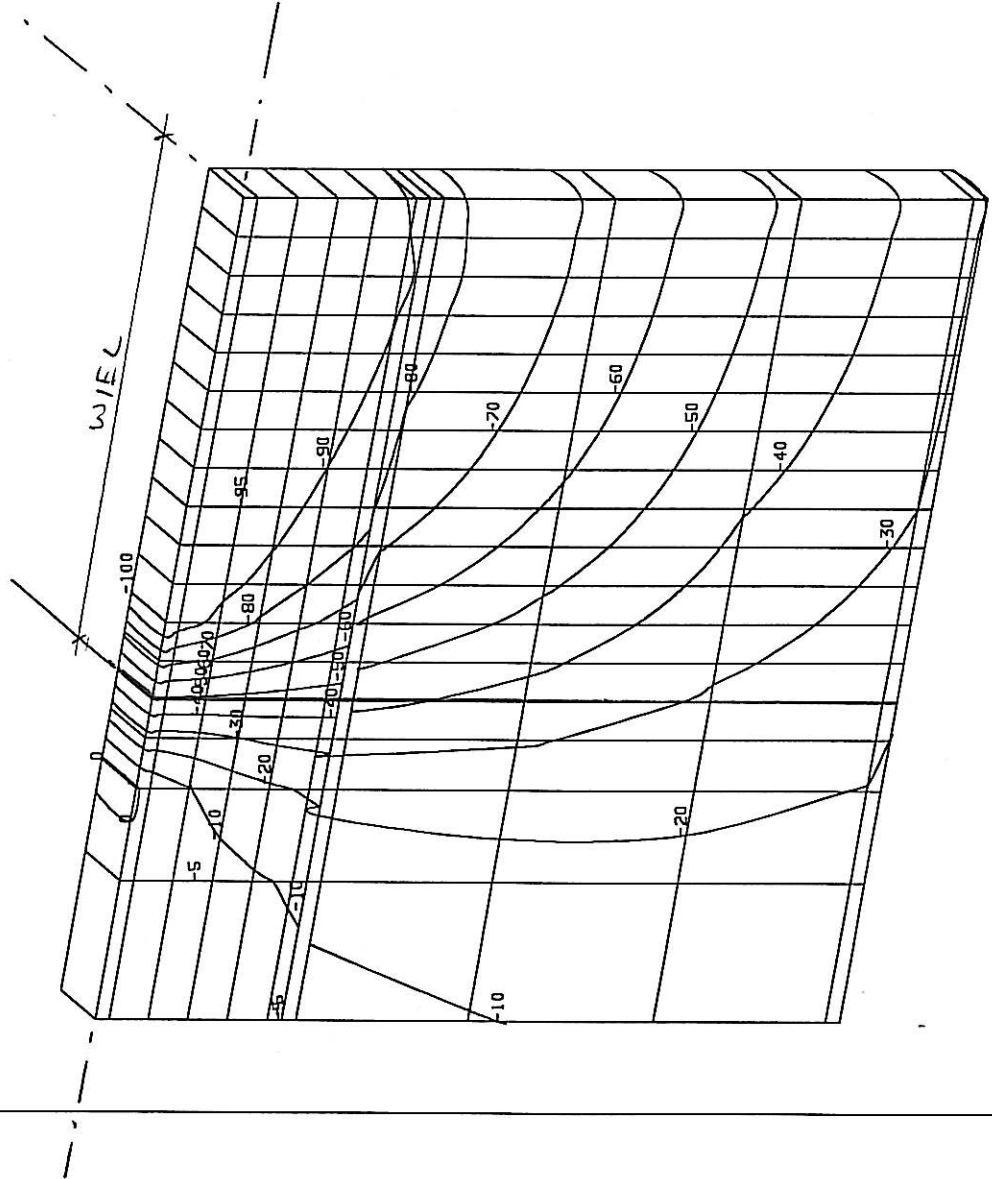
SCALE: 1:100

LENGTH
X #=1.1281cm
Y #=1.1281cm
Z #=1.1281cm

LOAD-STEP:
LS=2-1

PRESENTATION:
UNDEFORMED MESH
DETAIL

ARGUMENT:
STRESS
Y - COMPONENT
SIGN CONSIDERED
100% =
952.369079kN/m²



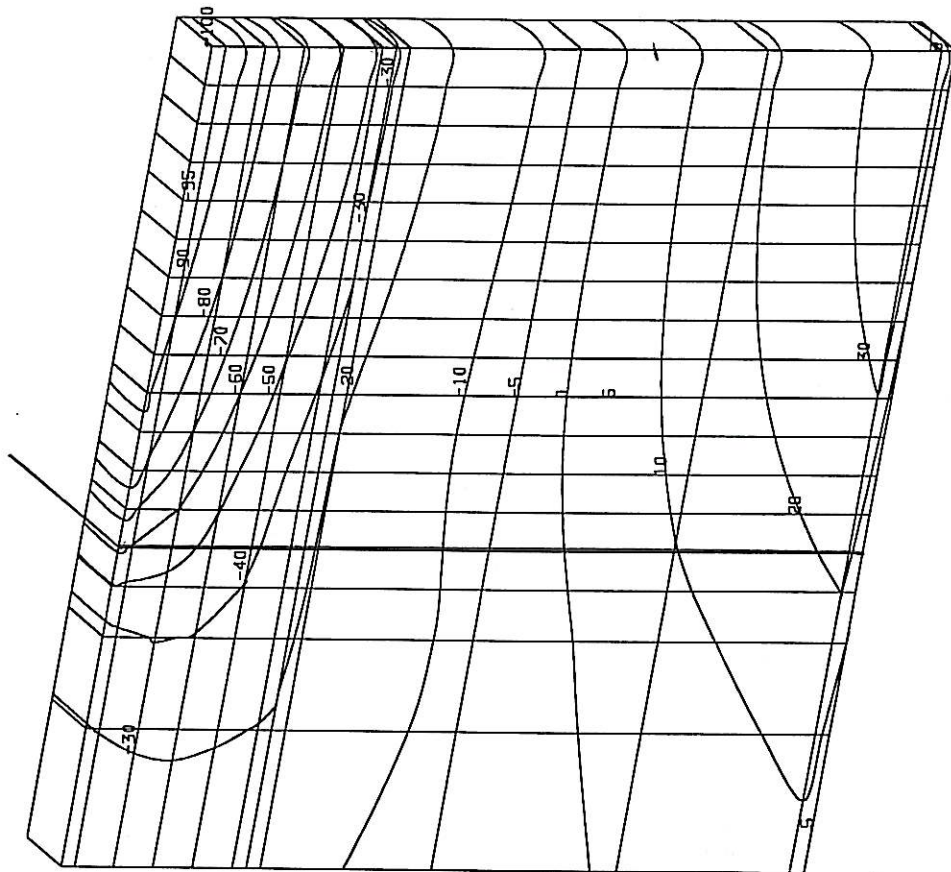
S2 Un

SCALE, $\frac{\#}{\#}$ = $\frac{1}{1}$
LENGTH
X $\# = 1.1281 \text{ cm}$
Y $\# = 1.1281 \text{ cm}$
Z $\# = 1.1281 \text{ cm}$

LOAD-STEP,
LS=2-1

PRESENTATION:
UNDEFORMED MESH
DETAIL

ARGUMENT,
STRESS
X -COMPONENT
SIGN CONSIDERED
100% =
2131.232910kN/m²



Sz Un

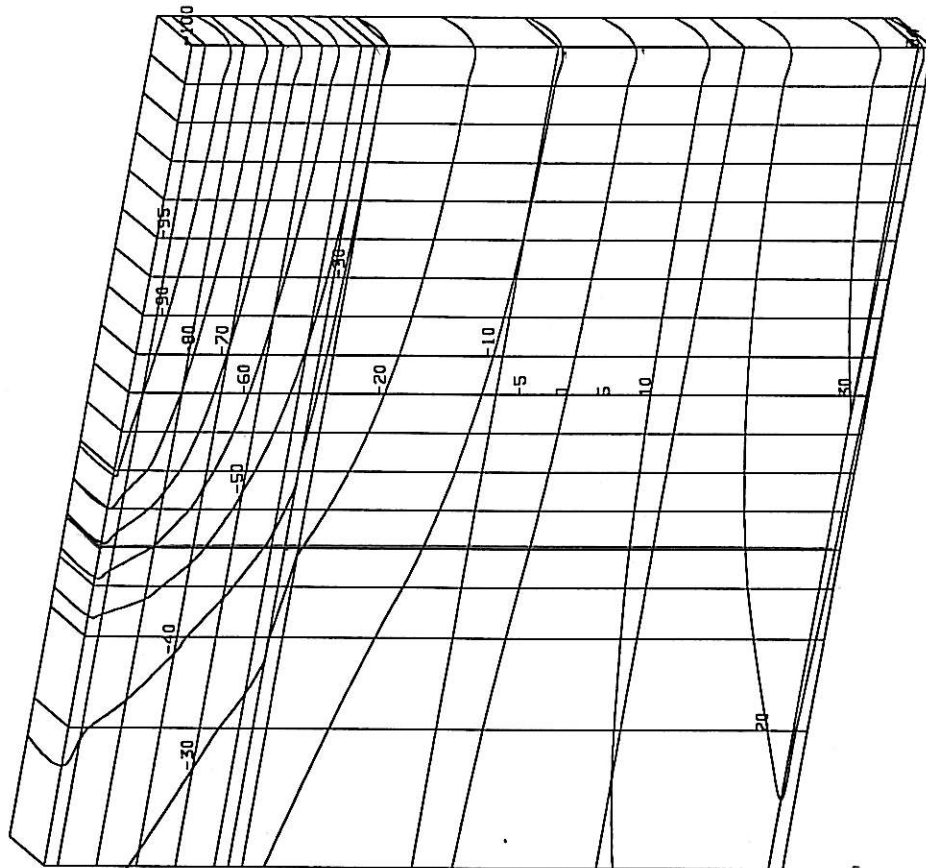
SCALE: 1# = 1

LENGTH
X #=1.1281cm
Y #=1.1281cm
Z #=1.1281cm

LOAD-STEP:
LS=2-1

PRESENTATION:
UNDEFORMED MESH
DETAIL

ARGUMENT:
STRESS
Z - COMPONENT
SIGN CONSIDERED
100% =
2033.277709kN/m²



•DESIGN BY SGG/901-Lopez geofe model MU 20.00-08
1998-8-18 10.28.27

S2 Un

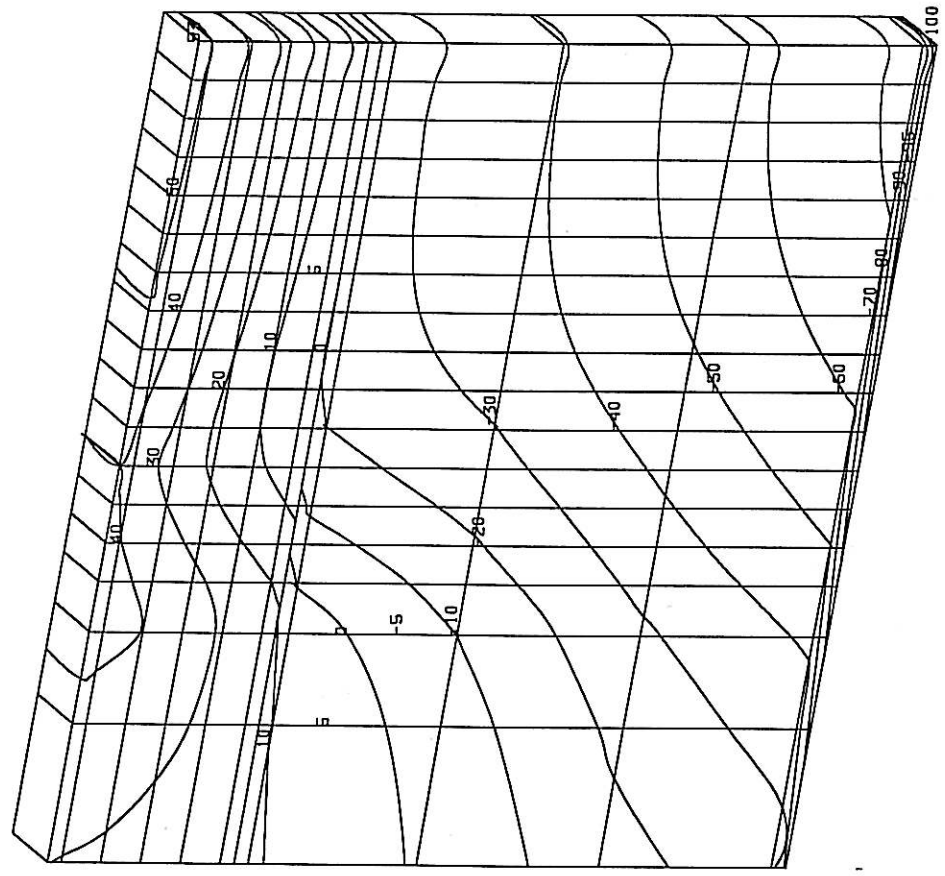
SCALE: $\frac{1}{100}$

LENGTH
 X #=1.1281cm
 Y #=1.1281cm
 Z #=1.1281cm

LOAD-STEP:
 LS=2-1

PRESENTATION:
 UNDEFORMED MESH
 DETAIL

ARGUMENT:
 STRAIN
 Y - COMPONENT
 SIGN CONSIDERED
 100% =
 0.000705



•DESIGN BY SGG/901-Lopez geofE model HU 20.00-08
 1998-8-18 10.29.18

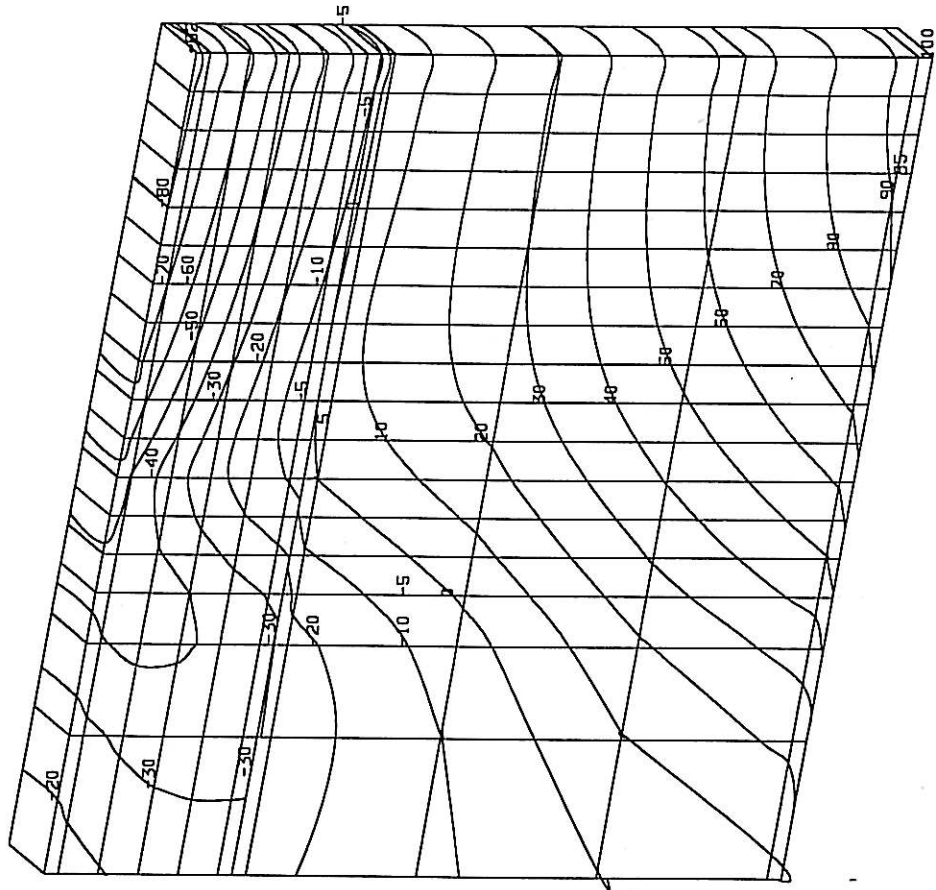
S2 Un

SCALE: $\frac{1}{10}$
LENGTH
X #=1.1281cm
Y #=1.1281cm
Z #=1.1281cm

LOAD-STEP:
LS=2-1

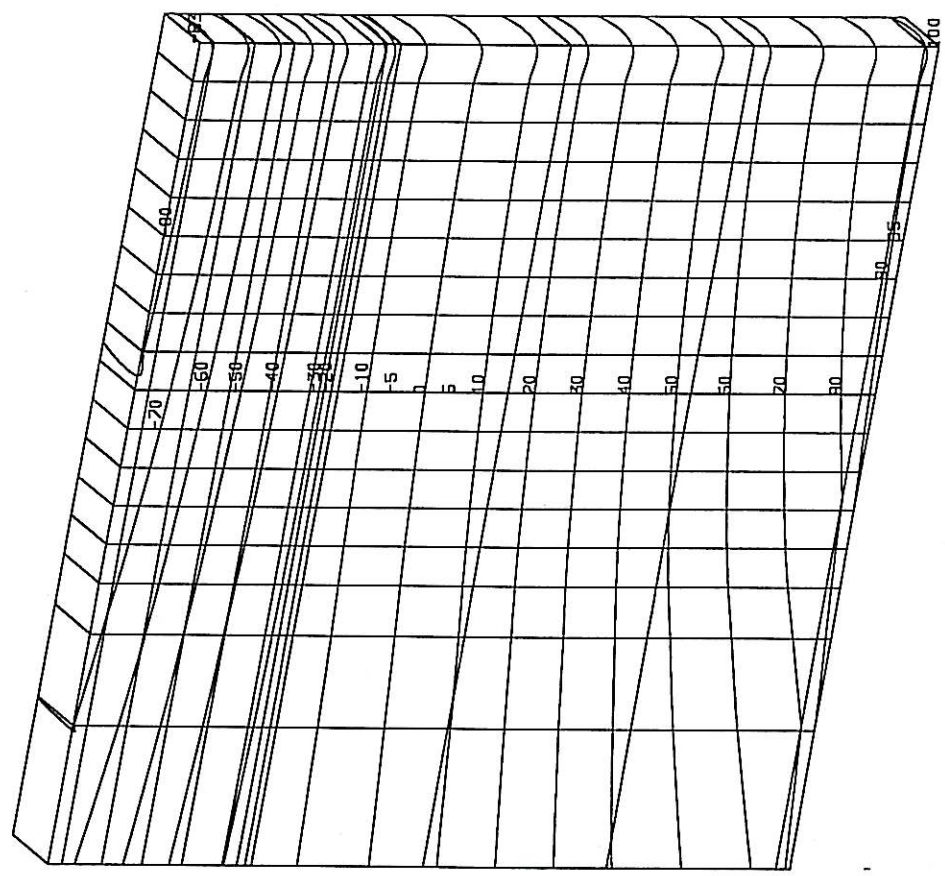
PRESENTATION:
UNDEFORMED MESH
DETAIL

ARGUMENT:
STRAIN
X -COMPONENT
SIGN CONSIDERED
100% =
0.000389



S2 Un

SCALE: 1#=
 LENGTH #=1.1281cm
 X #=1.1281cm
 Y #=1.1281cm
 Z #=1.1281cm
 LOAD-STEP:
 LS=2-1
 PRESENTATION:
 UNDEFORMED MESH
 DETAIL
 ARGUMENT:
 STRAIN
 Z -COMPONENT
 SIGN CONSIDERED
 100% =
 0.000315



Sz Un

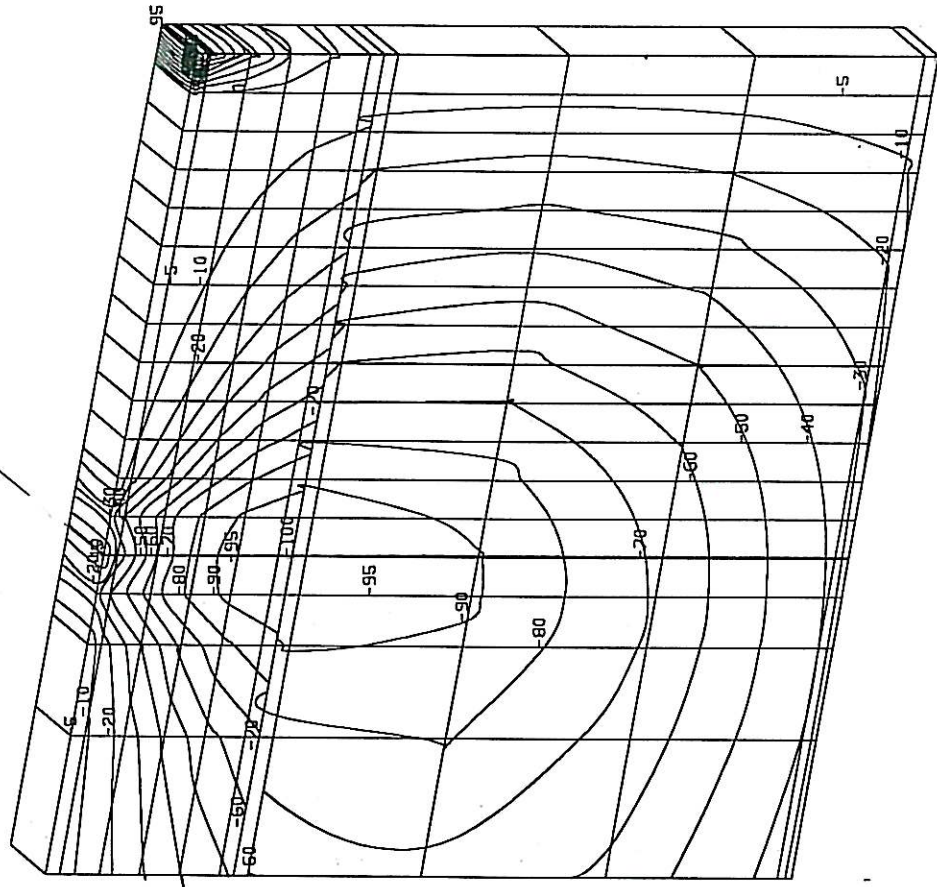
SCALE: 1# = 1cm

LENGTH
 X #=1.1281cm
 Y #=1.1281cm
 Z #=1.1281cm

LOAD-STEP:
 LS=2-1

PRESENTATION:
 UNDEFORMED MESH
 DETAIL

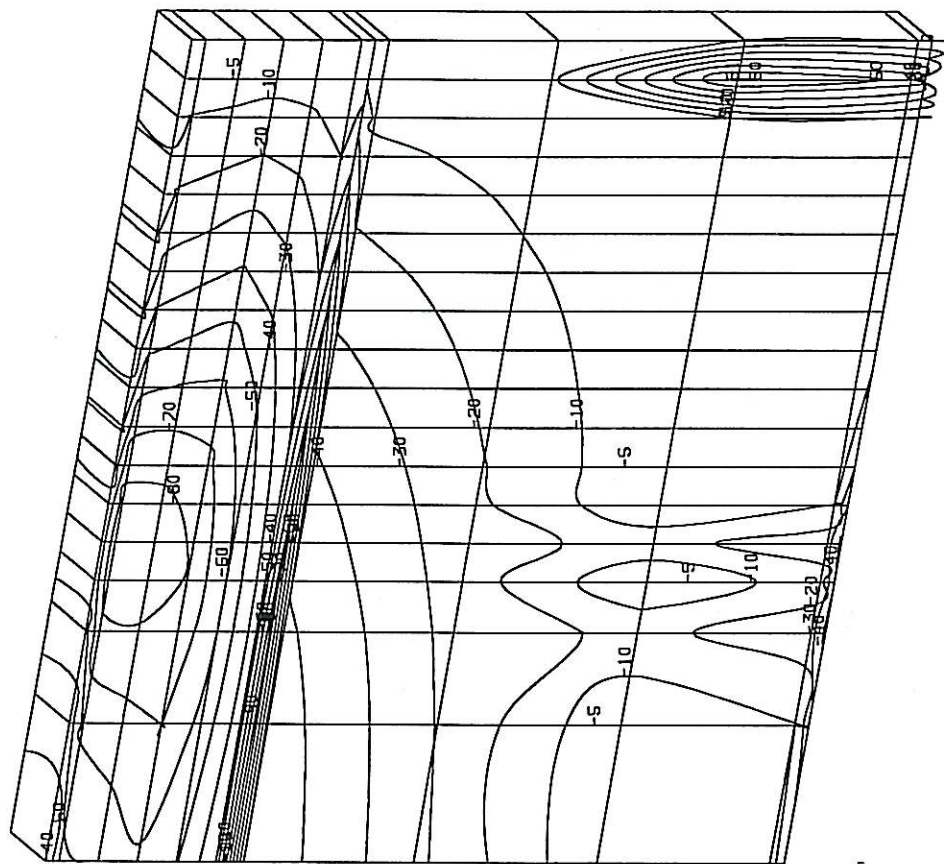
ARGUMENT:
 STRESS
 Tau-XY
 SIGN CONSIDERED
 100% = 414.671936kN/m2



DESIGN BY SGG/901-lopaz 10.31.55
 1998-8-18
 geofE model MU 20.00-08

S2 Un

SCALE: $\frac{1}{1}$
LENGTH
X #=1.1281cm
Y #=1.1281cm
Z #=1.1281cm
LOAD-STEP:
LS=2-1
PRESENTATION:
UNDEFORMED MESH
DETAIL
ARGUMENT:
STRAIN
Gamma-XY
SIGN CONSIDERED
100% =
0.000741



DESIGN BY SGG/901-Lopaz 10:32:56
1998-8-18
geofe model HU 20.00-08

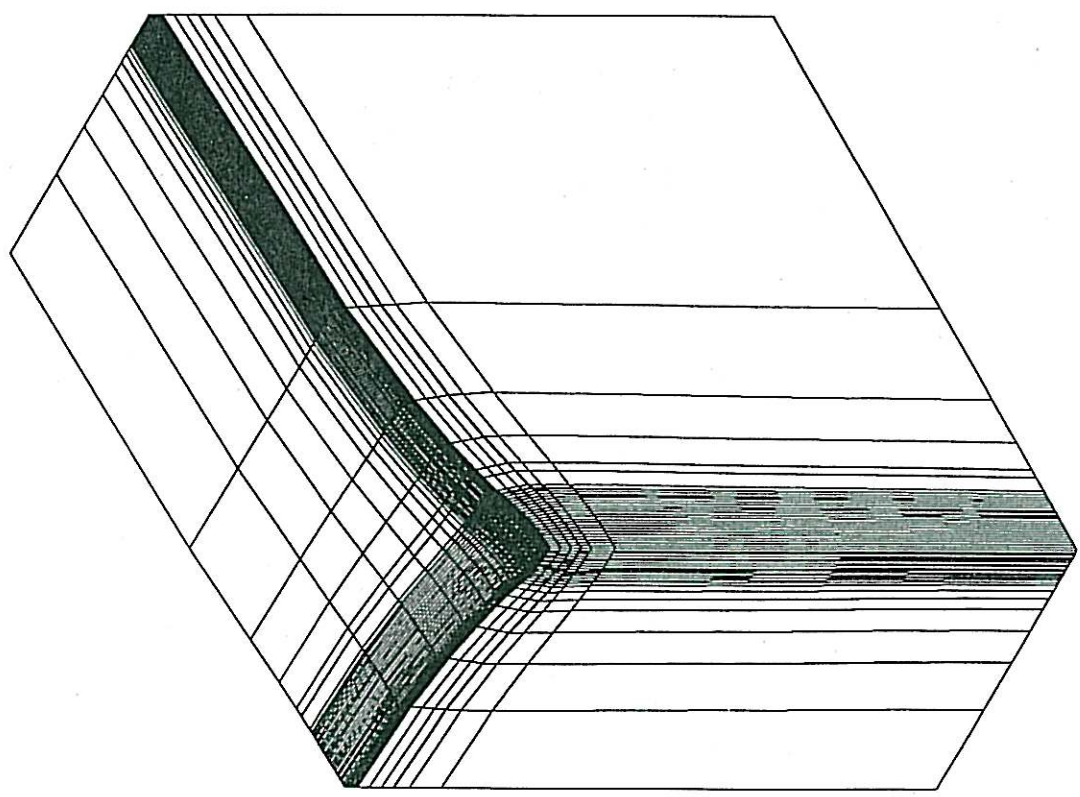
S2 Un

FINITE ELEMENT RESULTS
STRUCTURE 2: RECTANGULAR LOAD AREA WITH NON-UNIFORM CONTACT
PRESSURE

S2 N-U
 NIEUZ
 DISAZ

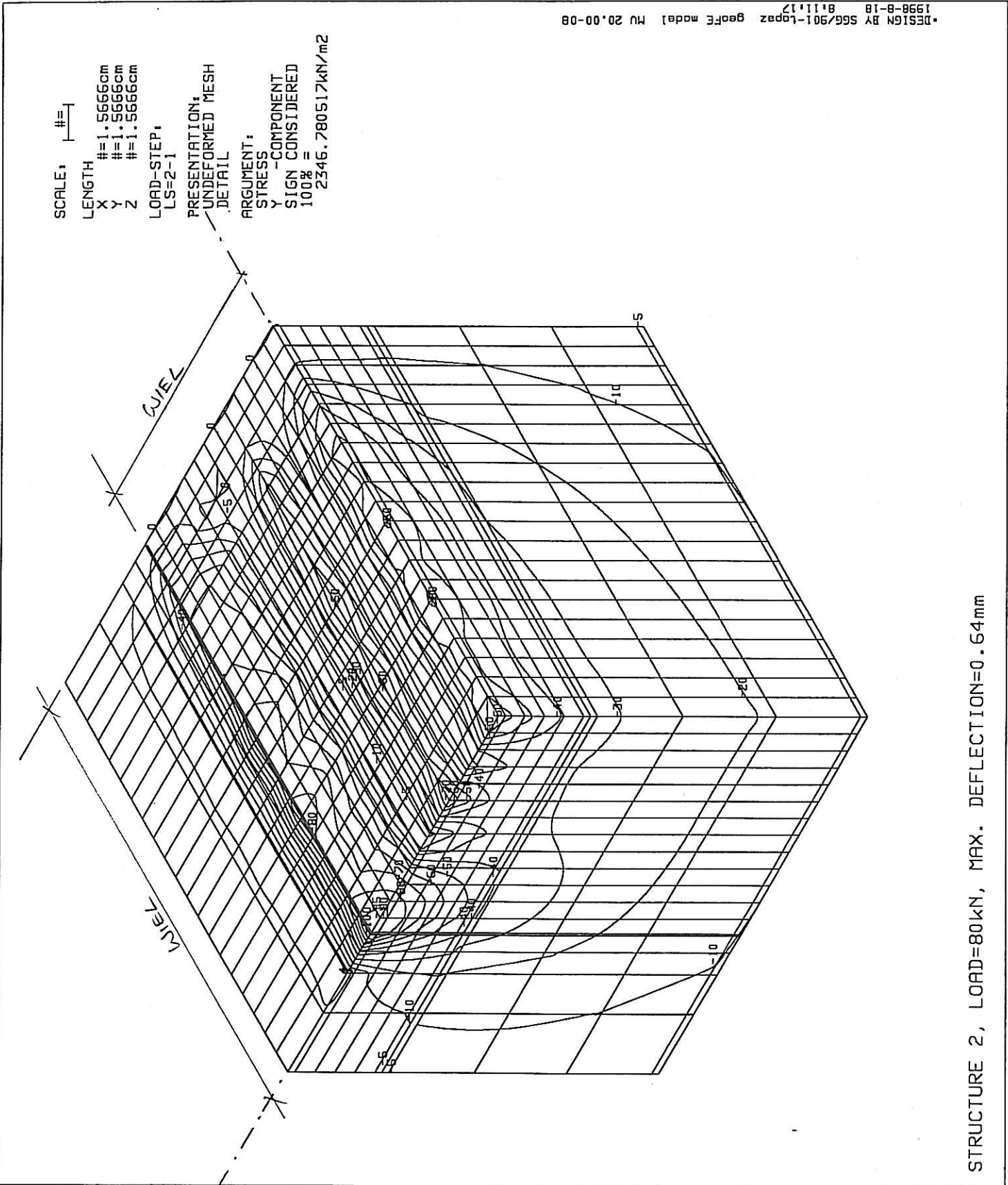
DESIGN BY SGG/901-topaz geofe model MU 20.00-08
 1998-8-4 10.11.54

SCALE: 1:100
 LENGTH
 X #=16.911cm
 Y #=16.911cm
 Z #=16.911cm
 DISPLACEMENT
 X #=0.043298cm
 Y #=0.043298cm
 Z #=0.043298cm
 LOAD-STEP:
 LS=2
 PRESENTATION:
 DEFORMED MESH



STRUCTURE 2, LOAD=80kN, MAX. DEFLECTION=0.64mm

TFA5/A/1	HMA PROJECT	
BKS (Pty) Ltd. Dr JP Laurens BOX 3173 PRETORIA FAX 012 4213501	NON-UNIFORM TYRE PRESSURE FIG. 1: Deflection Bowl	



STRUCTURE 2, LOAD=80kN, MAX. DEFLECTION=0.64mm

S2 N-U

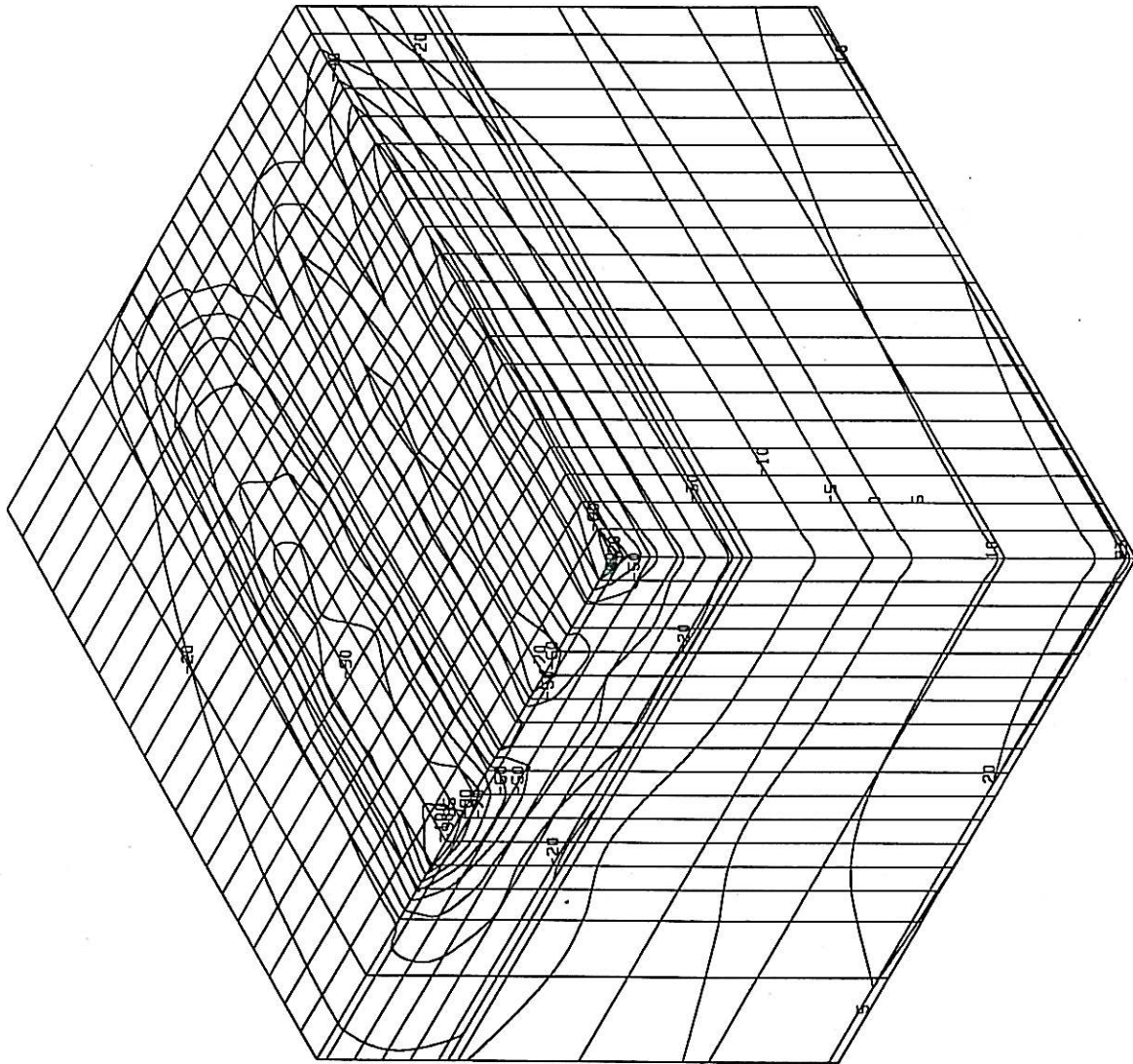
SCALE: 1/10

LENGTH #=1.5666cm
X #=1.5666cm
Y #=1.5666cm
Z #=1.5666cm

LOAD-STEP:
LS=2-1

PRESENTATION:
UNDEFORMED MESH
DETAIL

ARGUMENT:
STRESS
X -COMPONENT
SIGN CONSIDERED
100% =
3299.313720kN/m2



DESIGN BY SGG/901-Lopez geofe model HU 20.00-08
1998-8-18 8:13:52

STRUCTURE 2, LOAD=80kN, MAX. DEFLECTION=0.64mm

S2 N-U

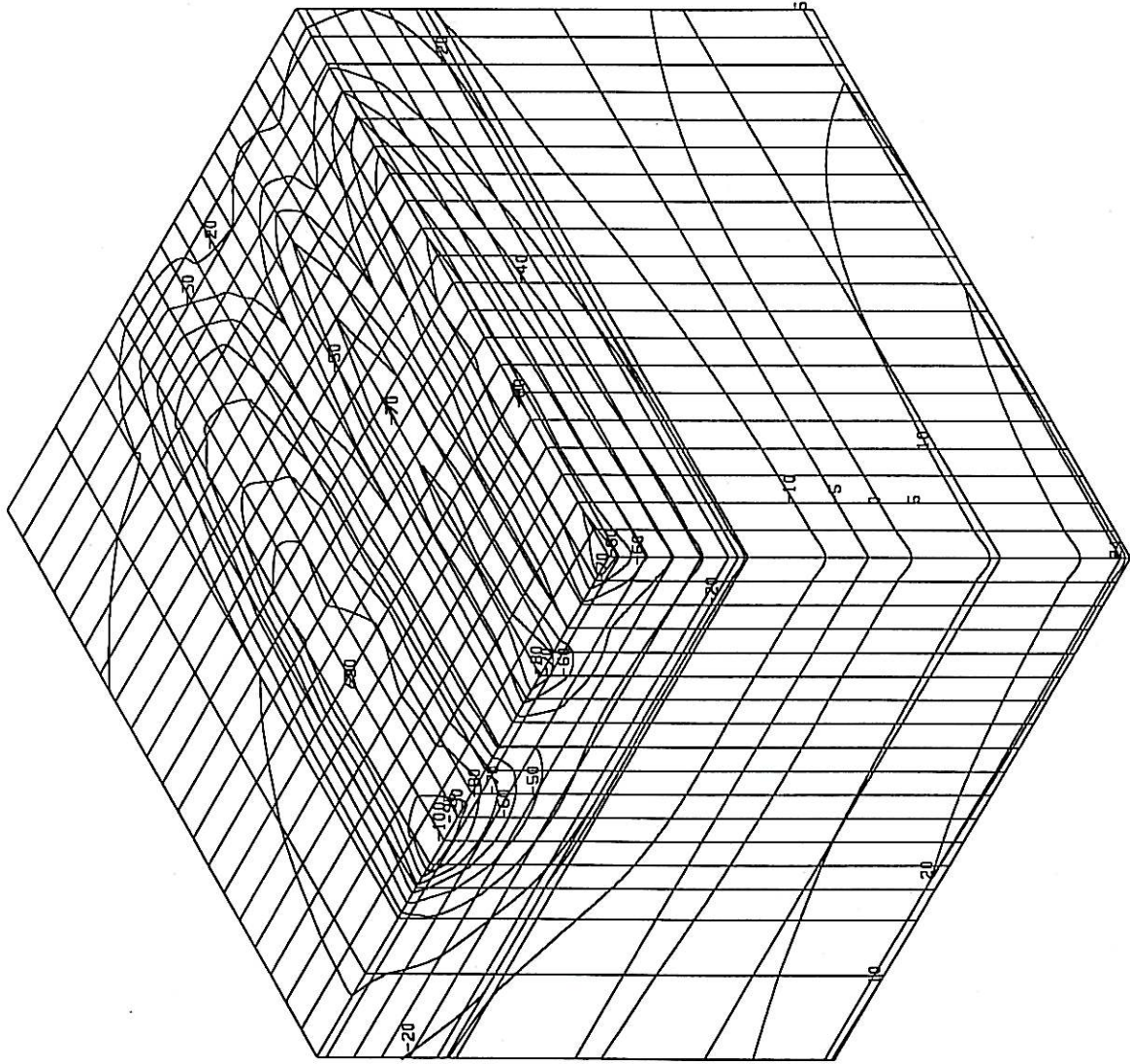
SCALE: 1/10

LENGTH
X #=1.5666cm
Y #=1.5666cm
Z #=1.5666cm

LOAD-STEP:
LS=2-1

PRESENTATION:
UNDEFORMED MESH
DETAIL

ARGUMENT:
STRESS
Z -COMPONENT
SIGN CONSIDERED
100% =
3131.81298kN/m²



DESIGN BY SGG/901-Lopez geofE model HV 20.00-08
1998-8-18 8.1912

STRUCTURE 2, LOAD=80kN, MAX. DEFLECTION=0.64mm

S2 N-U

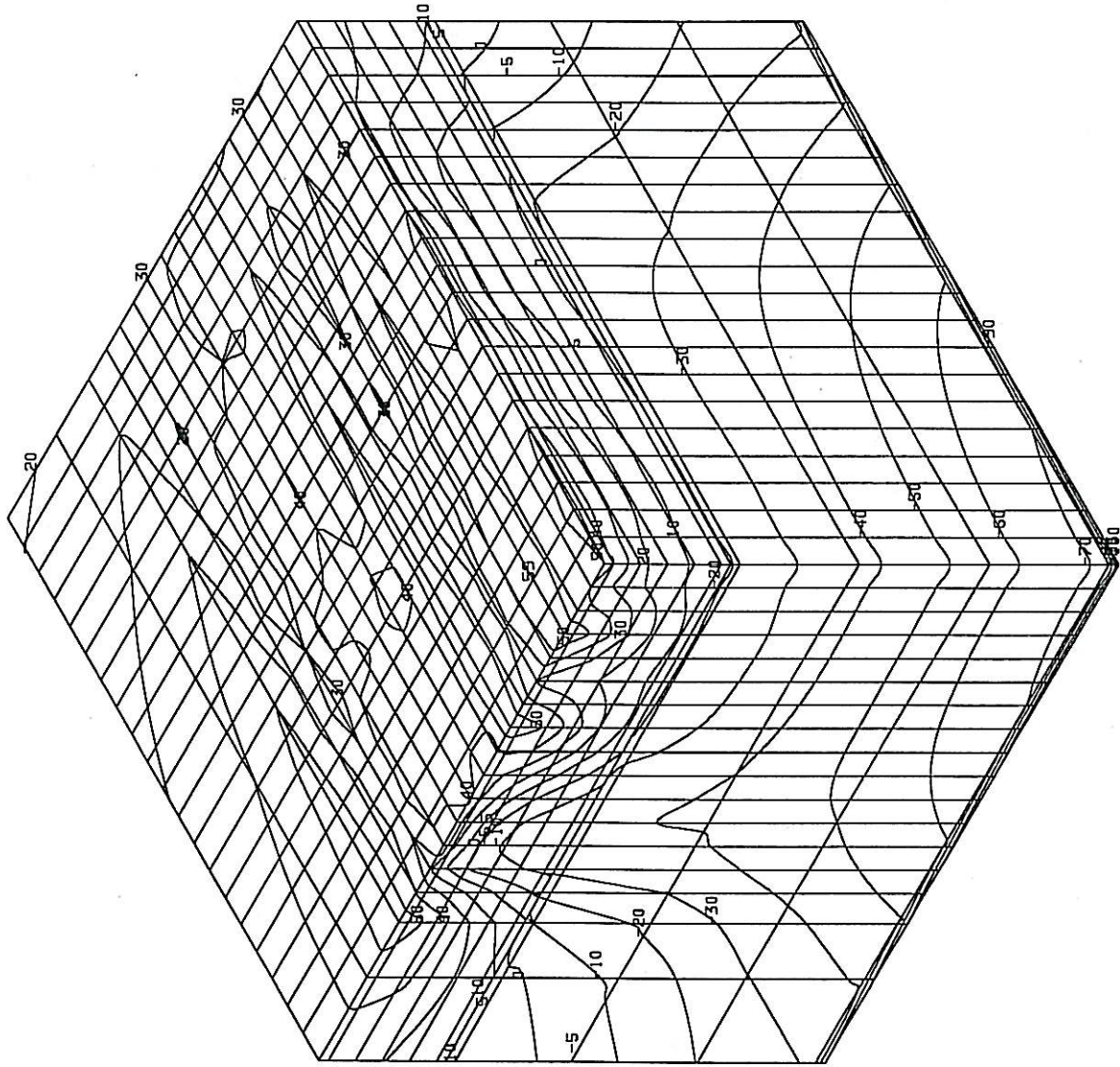
SCALE: 1# = 1

LENGTH
 X # = 1.5666cm
 Y # = 1.5666cm
 Z # = 1.5666cm

LOAD-STEP:
 LS=2-1

PRESENTATION:
 UNDEFORMED MESH
 DETAIL

ARGUMENT:
 STRAIN
 Y - COMPONENT
 SIGN CONSIDERED
 100% =
 0.000718



STRUCTURE 2, LOAD=80kN, MAX. DEFLECTION=0.64mm

DESIGN BY SGG/901-topaz geofE model HU 20.00-08
 1998-8-18 8:21:27

S2 N-U

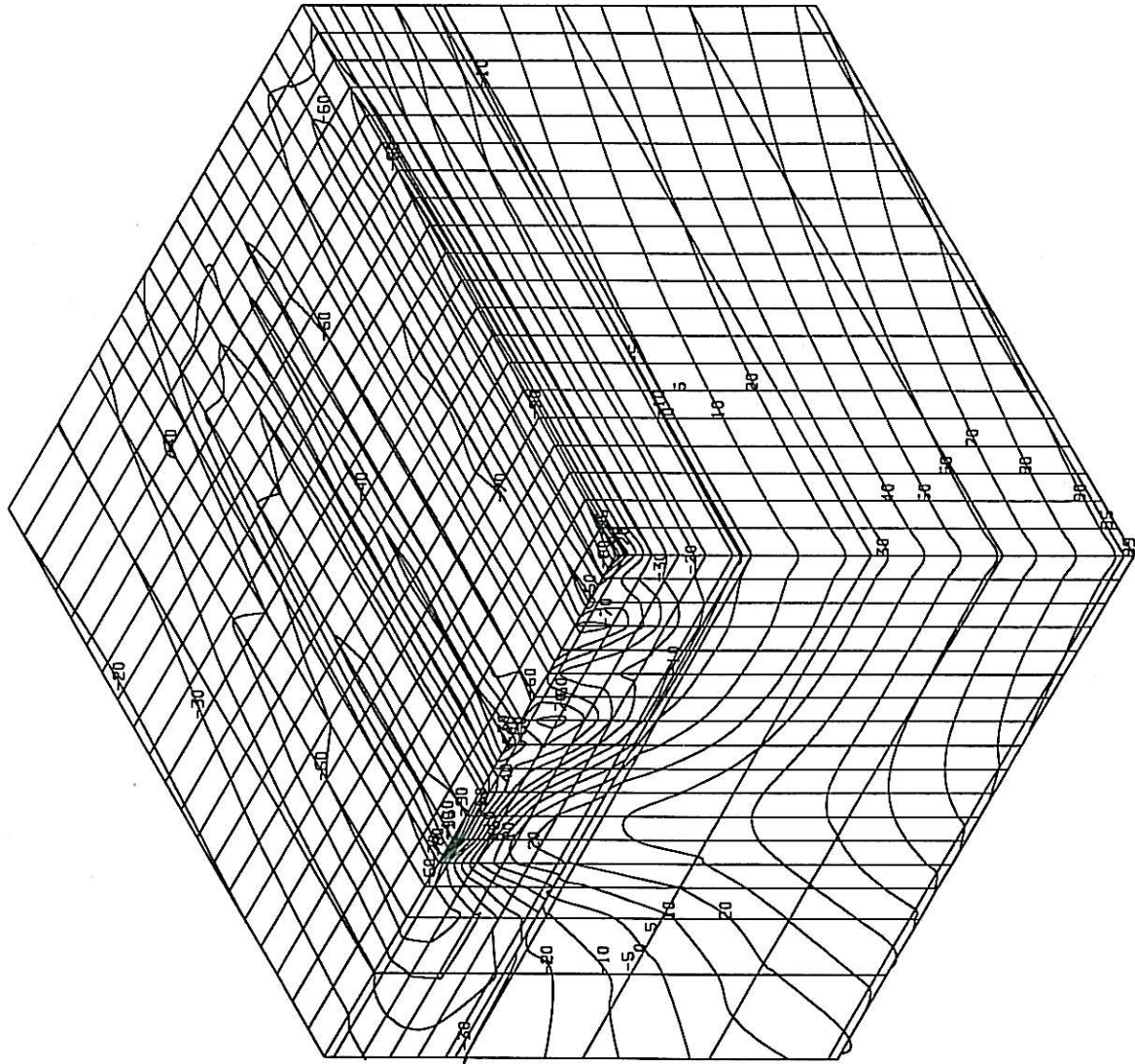
SCALE: 1:1

LENGTH
 X #=1.5666cm
 Y #=1.5666cm
 Z #=1.5666cm

LOAD-STEP:
 LS=2-1

PRESENTATION:
 UNDEFORMED MESH
 DETAIL

ARGUMENT:
 STRAIN
 X -COMPONENT
 SIGN CONSIDERED
 100% =
 0.000354



DESIGN BY SGG/901-topaz geofe model MU 20.00-08
 1998-8-18 8:31:18

STRUCTURE 2, LOAD=80kN, MAX. DEFLECTION=0.64mm

S2 N-U

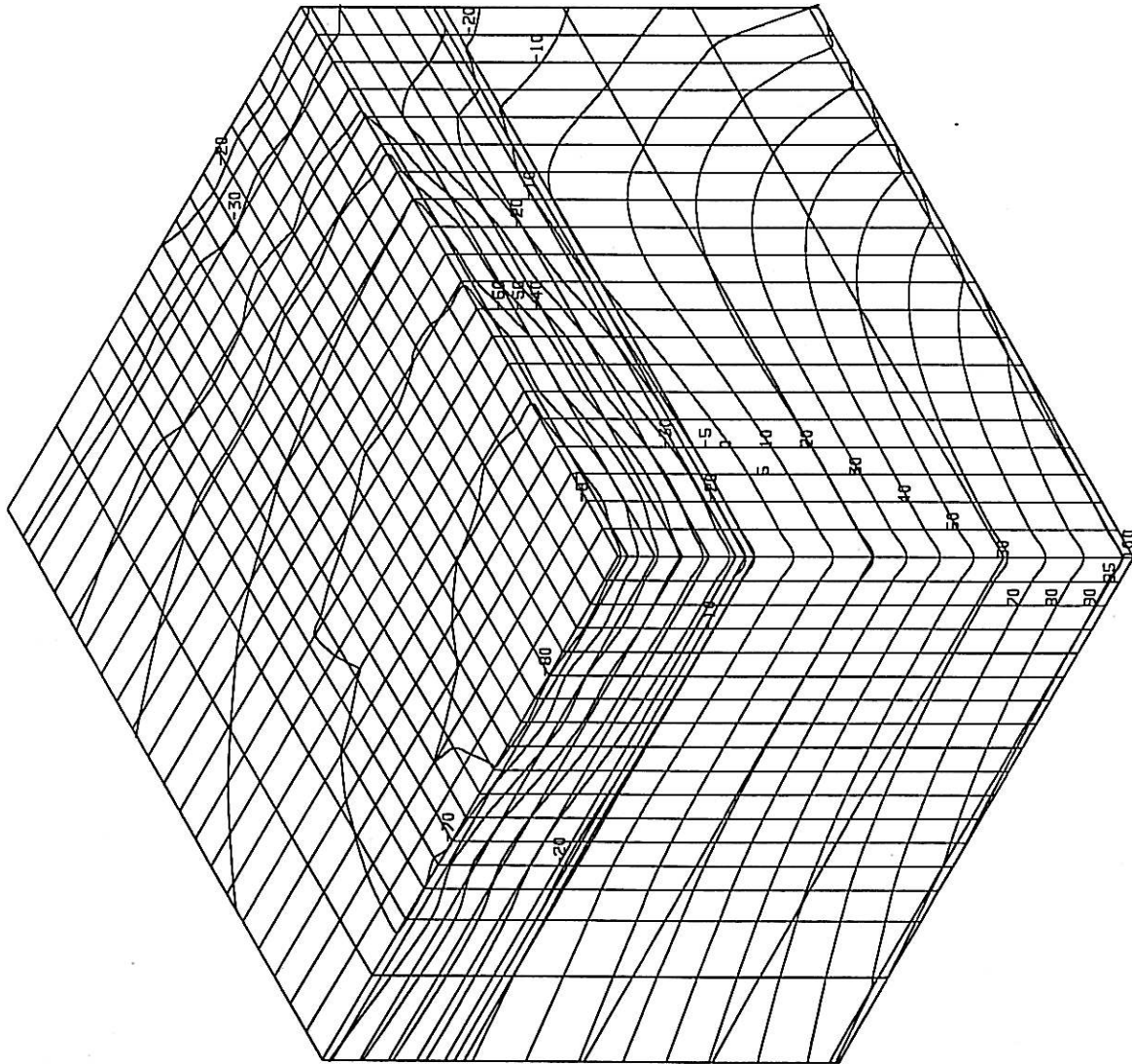
SCALE: 1# = 1

LENGTH
 X # = 1.56666cm
 Y # = 1.56666cm
 Z # = 1.56666cm

LOAD-STEP:
 Ls=2-1

PRESENTATION:
 UNDEFORMED MESH
 DETAIL

ARGUMENT:
 STRAIN
 Z -COMPONENT
 SIGN CONSIDERED
 100% =
 0.000363



DESIGN BY 566/901-Lopez GeofE model NU 20.00-08
 1998-8-18 8:34:11

STRUCTURE 2, LOAD=80kN, MAX. DEFLECTION=0.64mm

S2 N-U

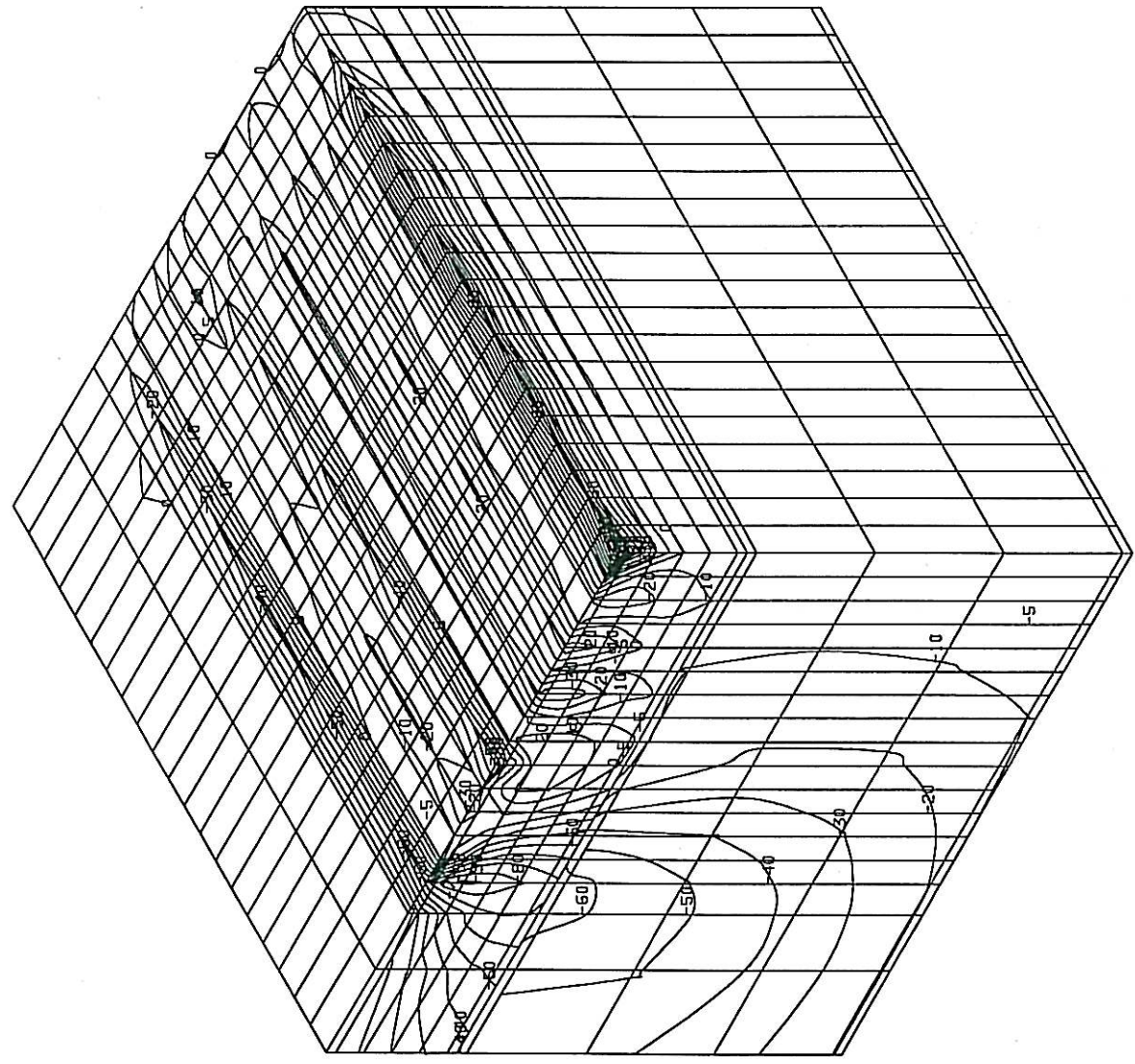
SCALE: 1:1

LENGTH #=1.5666cm
X #=1.5666cm
Y #=1.5666cm
Z #=1.5666cm

LOAD-STEP:
LS=2-1

PRESENTATION:
UNDEFORMED MESH
DETAIL

ARGUMENT:
STRESS
Tau-xy
SIGN CONSIDERED
100% =
787.155090kN/m2



DESIGN BY SGG/901-topaz geofe model HU 20.00-08
1998-8-18 8132114

STRUCTURE 2, LOAD=80kN, MAX. DEFLECTION=0.64mm

Sz N-u

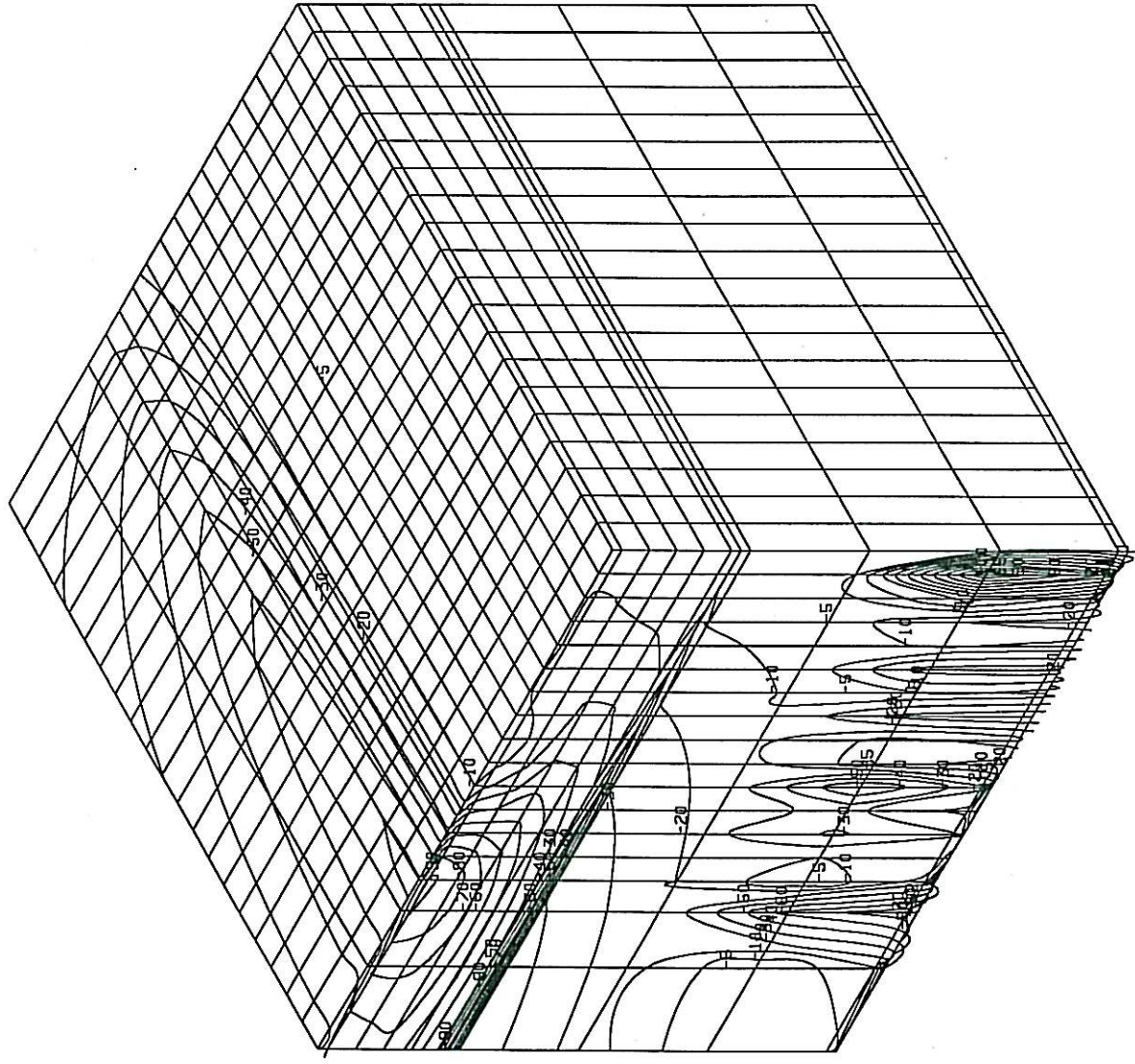
SCALE: 1# = 1m

LENGTH
 X # = 1.5666cm
 Y # = 1.5666cm
 Z # = 1.5666cm

LOAD-STEP:
 LS=2-1

PRESENTATION:
 UNDEFORMED MESH
 DETAIL

ARGUMENT:
 STRAIN
 Gamma-XY
 SIGN CONSIDERED
 100% =
 0.000913



•DESIGN BY 566/901-Lopez geofe model NU 20.00-08
 1998-8-18 8:49:11

STRUCTURE 2, LOAD=80kN, MAX. DEFLECTION=0.64mm

Sz Nu

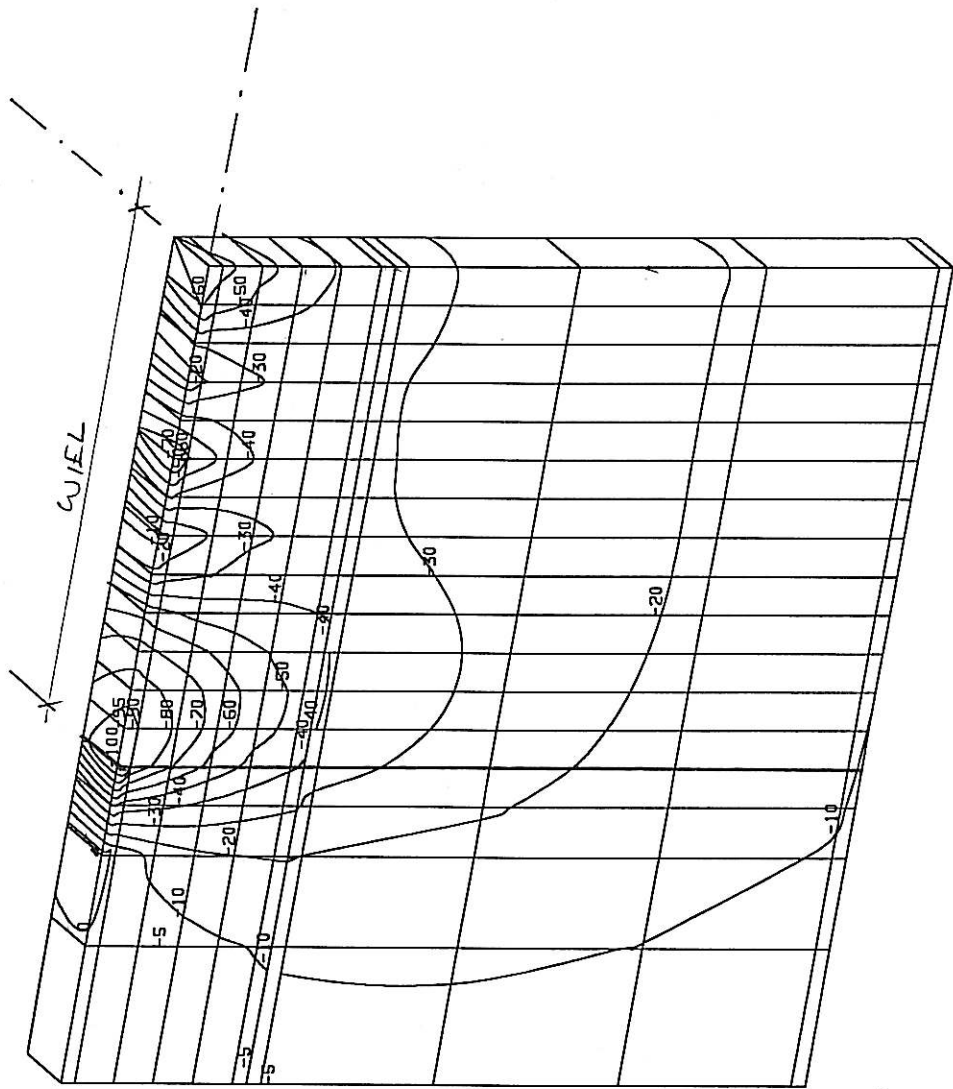
SCALE: 1/20

LENGTH
 X #=1.1281cm
 Y #=1.1281cm
 Z #=1.1281cm

LOAD-STEP:
 LS=2-1

PRESENTATION:
 UNDEFORMED MESH
 DETAIL

ARGUMENT:
 STRESS
 Y -COMPONENT
 SIGN CONSIDERED
 100% =
 2346.780517kN/m2



DESIGN BY SGG/901-topaz geofE model HU 20.00-08
 1998-8-18 8:52:11

STRUCTURE 2, LOAD=80kN, MAX. DEFLECTION=0.64mm

Sz Nu

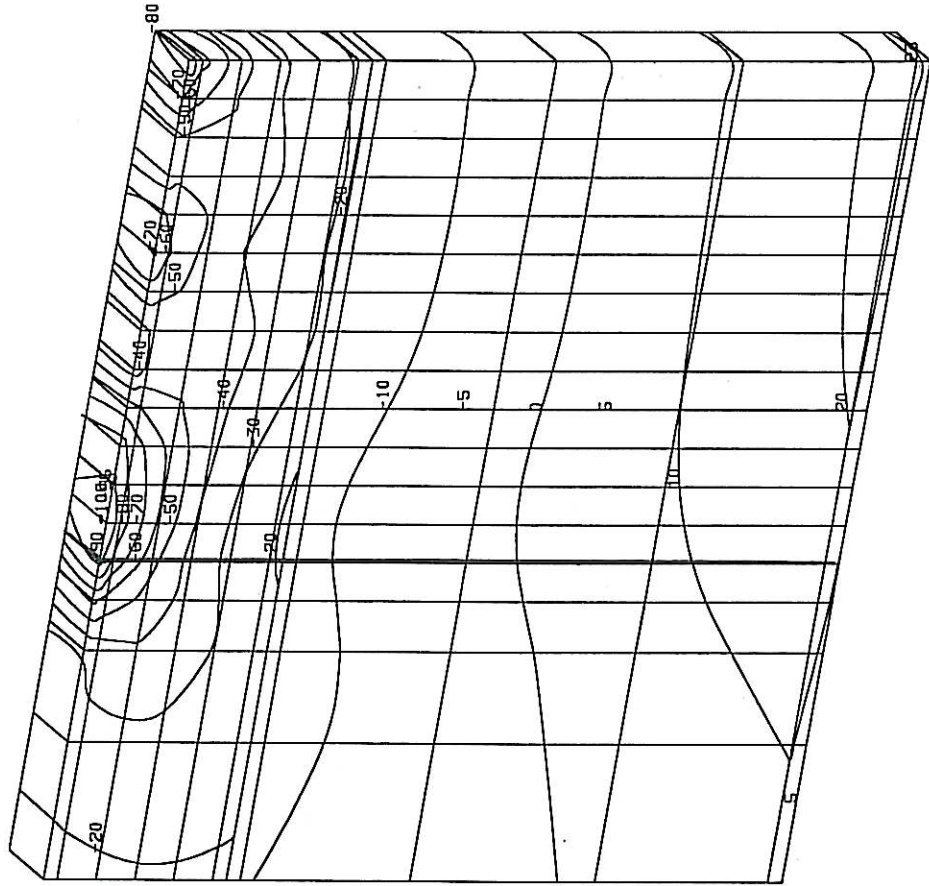
SCALE: 1:1

LENGTH
 X #=1.1281cm
 Y #=1.1281cm
 Z #=1.1281cm

LOAD-STEP:
 LS=2-1

PRESENTATION:
 UNDEFORMED MESH
 DETAIL

ARGUMENT:
 STRESS
 X - COMPONENT
 SIGN CONSIDERED
 100% =
 3299.313720kN/m2



DESIGN BY SGG/901-Lopez 8.54.12
 1998-8-18
 geofe model MV 20.00-08

STRUCTURE 2, LOAD=80kN, MAX. DEFLECTION=0.64mm

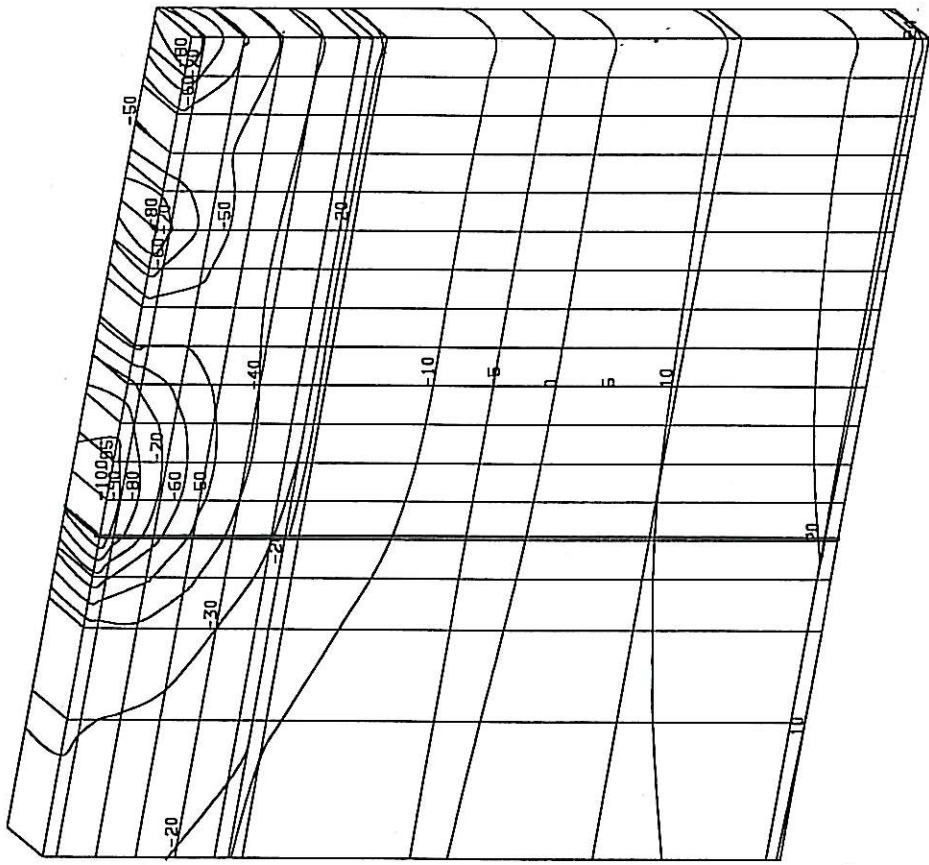
S2 N-U

SCALE: 1#=
 LENGTH
 X #=1.1281cm
 Y #=1.1281cm
 Z #=1.1281cm

LOAD-STEP:
 LS=2-1

PRESENTATION:
 UNDEFORMED MESH
 DETAIL

ARGUMENT:
 STRESS
 Z -COMPONENT
 SIGN CONSIDERED
 100% =
 3131.812988kN/m2



•DESIGN BY SGG/901-Lopez geofe model HU 20.00-08
 1998-8-18 8.55:47

STRUCTURE 2, LOAD=80kN, MAX. DEFLECTION=0.64mm

S2 N-U

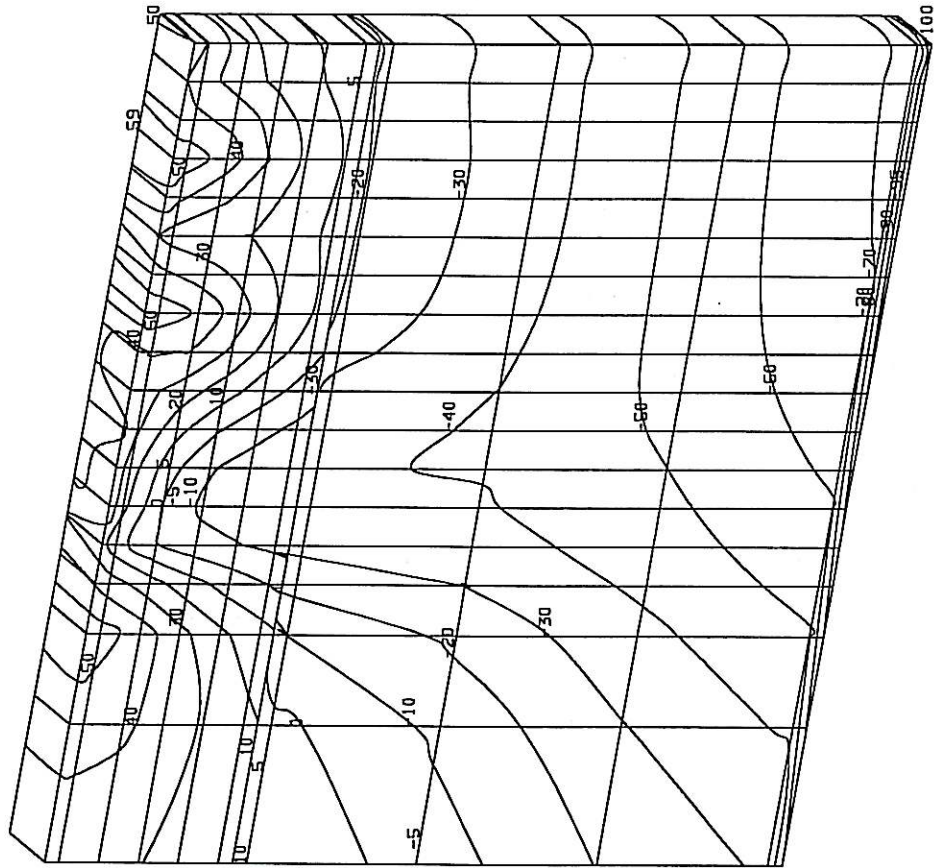
SCALE: 1:100

LENGTH
 X #=1.1281cm
 Y #=1.1281cm
 Z #=1.1281cm

LOAD-STEP:
 LS=2-1

PRESENTATION:
 UNDEFORMED MESH
 DETAIL

ARGUMENT:
 STRAIN
 Y -COMPONENT
 SIGN CONSIDERED
 100% =
 0.000718



DESIGN BY SGG/901-Lopez 8.58.29
 1998-8-18 HU 20.00-08

STRUCTURE 2, LOAD=80kN, MAX. DEFLECTION=0.64mm

S2 N-W

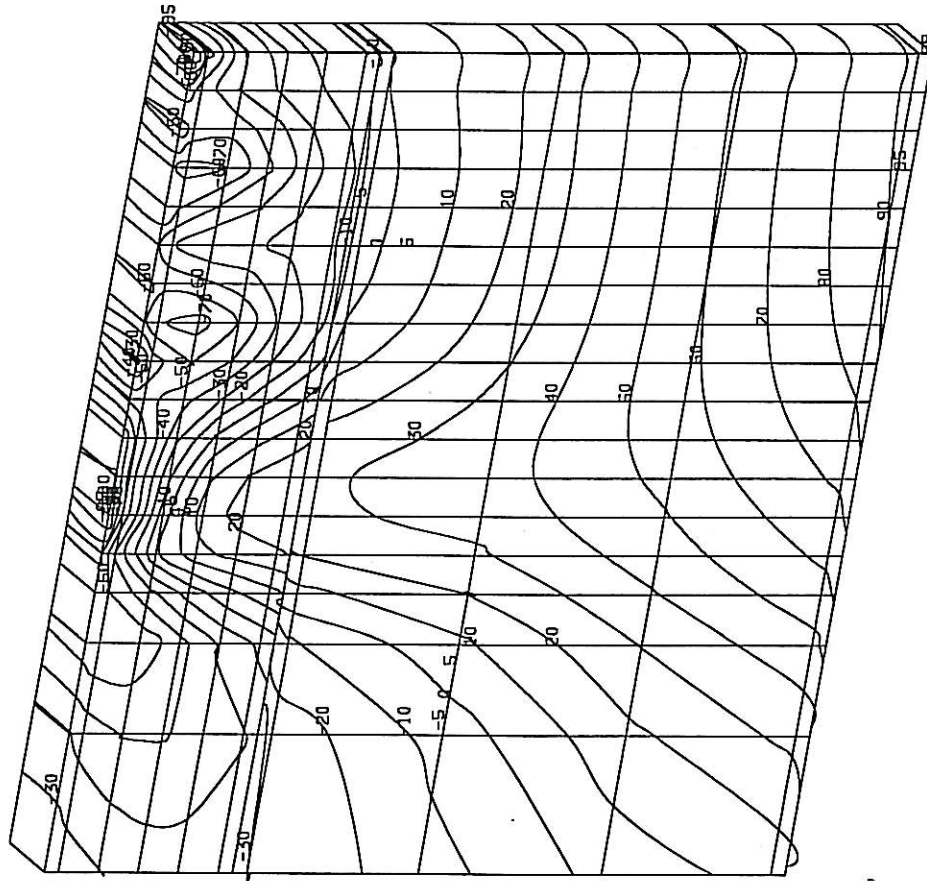
SCALE: $\frac{1}{100}$

LENGTH
 X #=1.1281cm
 Y #=1.1281cm
 Z #=1.1281cm

LOAD-STEP:
 LS=2-1

PRESENTATION:
 UNDEFORMED MESH
 DETAIL

ARGUMENT:
 STRAIN
 X -COMPONENT
 SIGN CONSIDERED
 100% =
 0.000354



STRUCTURE 2, LOAD=80kN, MAX. DEFLECTION=0.64mm

•DESIGN BY SGG/901-Lopez GEOFE model HU 20.00-08
 1998-8-18 9:4:18

S2 N-U

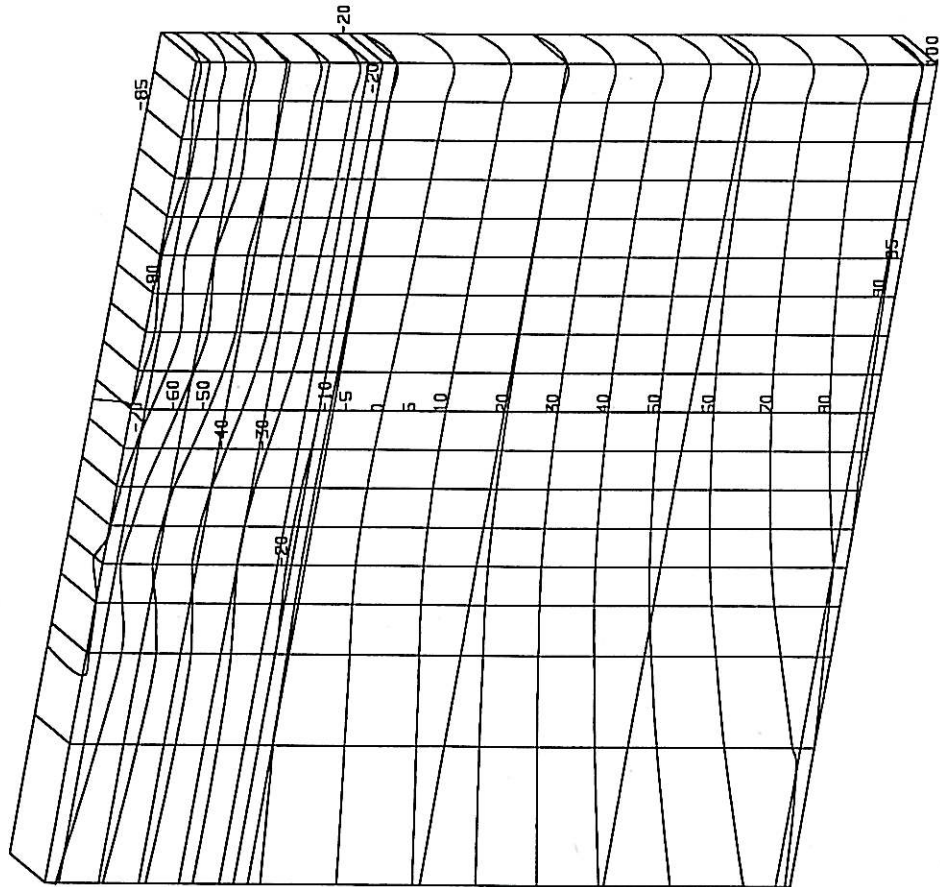
SCALE: 1/100

LENGTH
 X #=1.1281cm
 Y #=1.1281cm
 Z #=1.1281cm

LOAD-STEP:
 LS=2-1

PRESENTATION:
 UNDEFORMED MESH
 DETAIL

ARGUMENT:
 STRAIN
 Z -COMPONENT
 SIGN CONSIDERED
 100% =
 0.000363



•DESIGN BY SGG/901-Lopez geofE model MV 20.00-08
 1998-8-18 9.9.23

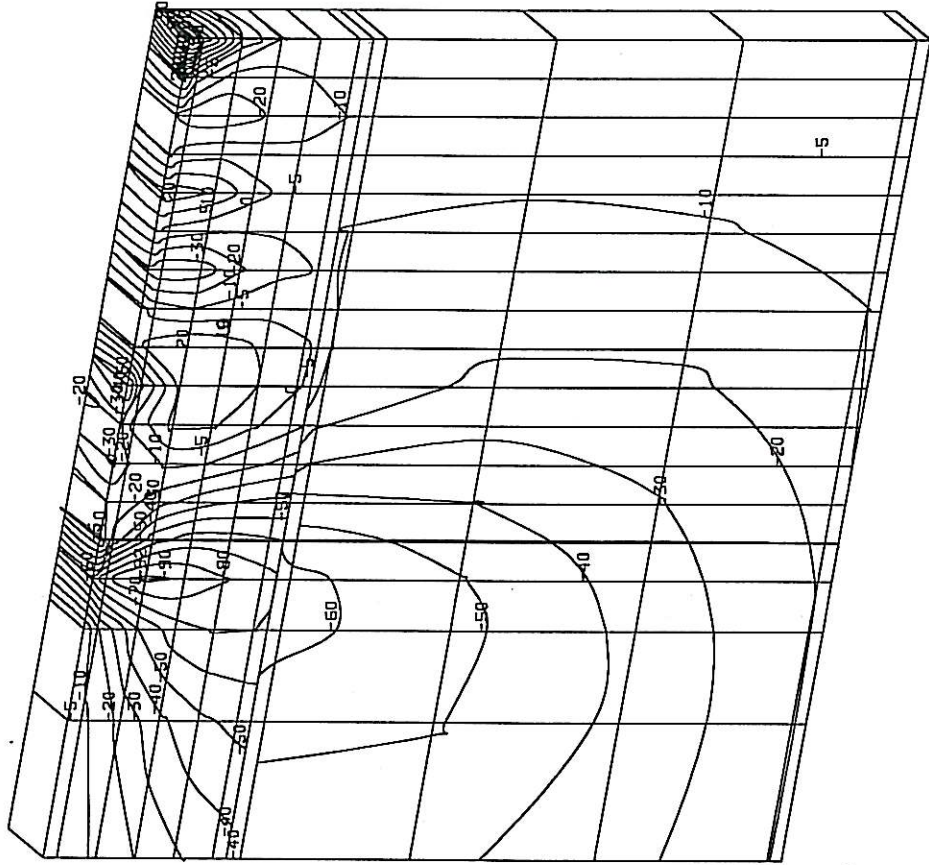
STRUCTURE 2, LOAD=80kN, MAX. DEFLECTION=0.64mm

S2 NU

SCALE: 1:100
LENGTH
X #=1.1281cm
Y #=1.1281cm
Z #=1.1281cm

LOAD-STEP:
LS=2-1
PRESENTATION:
UNDEFORMED MESH
DETAIL

ARGUMENT:
STRESS
Tau-XY
SIGN CONSIDERED
100% =
787.155090kN/m2

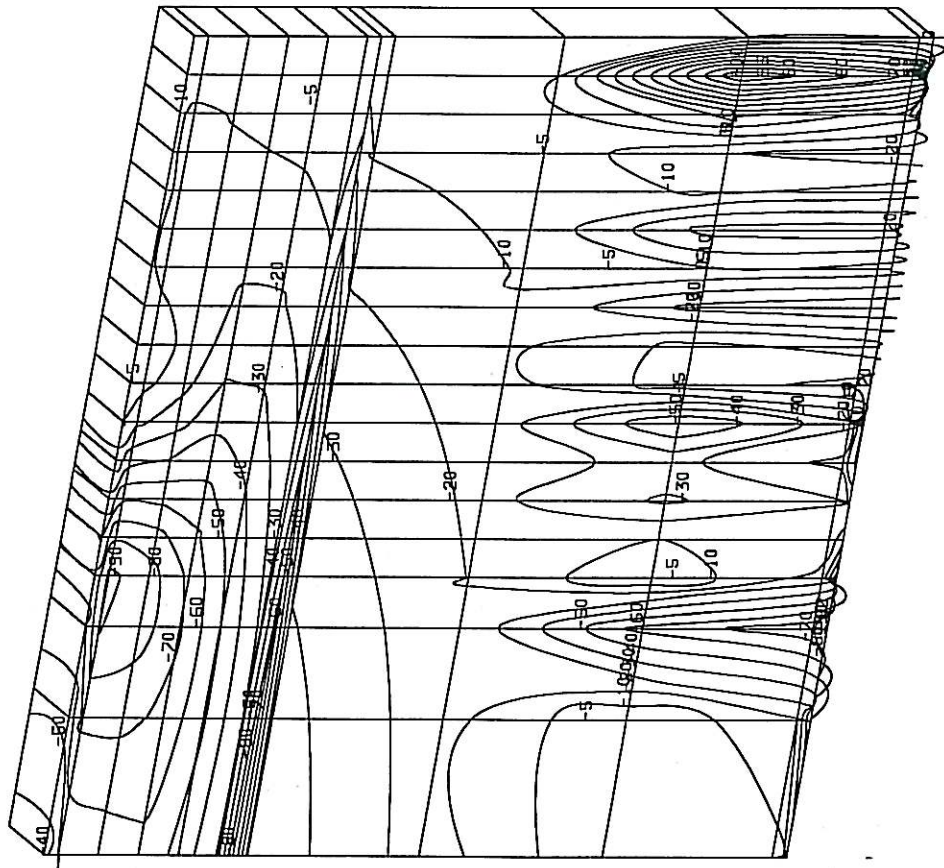


•DESIGN BY SGG/901-Lopez geofe model1 MV 20.00-08
1998-8-18 9.12.52

STRUCTURE 2, LOAD=80kN, MAX. DEFLECTION=0.64mm

S2 N-W

SCALE: 1# = 1
 LENGTH
 X # = 1.1281cm
 Y # = 1.1281cm
 Z # = 1.1281cm
 LOAD-STEP:
 LS=2-1
 PRESENTATION:
 UNDEFORMED MESH
 DETAIL
 ARGUMENT:
 STRAIN
 Gamma-XY
 SIGN CONSIDERED
 100% =
 0.000913



STRUCTURE 2, LOAD=80kN, MAX. DEFLECTION=0.64mm

DESIGN BY SGG/901-Lopez 9.16.24
 1998-8-18
 geofe model MV 20.00-08

S2 N-U

APPENDIX C
ANALYSIS RESULTS: HORIZONTAL SHEAR FORCE EFFECTS

RESULTS FROM LET AND FE MODELS FOR ANALYSIS OF HORIZONTAL SHEAR

TABLE C1: STRESS RESULTS FOR STRUCTURE 2: ASPHALT SURFACING

DEPTH IN AC	MODEL	VERTIC SIG-YY	TRANSV SIG-XX	LONGI SIG-ZZ	SIG-XY	TAU-OCT
TOP	LET	-800	-1730	-1730	0	438.4
	FE NO SHEAR	-850	-1528	-1528	0	319.6
	FE WITH SHEAR	-860	-1506	-1527	0	309.6
MIDDLE	LET	-783	-1190	-1190	0	191.9
	FE NO SHEAR	-791	-1077	-1077	0	134.8
	FE WITH SHEAR	-800	-1054	-1044	-8	117.6
BOTTOM	LET	-725	-711	-711	0	6.6
	FE NO SHEAR	-717	-615	-615	0	48.1
	FE WITH SHEAR	-730	-602	-643	-15	54.8

TABLE C2: STRESS RESULTS FOR STRUCTURE 2: ASPHALT BASE

DEPTH IN AC	MODEL	VERTIC SIG-YY	TRANSV SIG-XX	LONGI SIG-ZZ	SIG-XY	TAU-OCT
TOP	LET	-721	-548	-548	0	81.6
	FE NO SHEAR	-695	-427	-427	0	126.3
	FE WITH SHEAR	-730	-600	-640	-15	55.7
MIDDLE	LET	-410	99	99	0	239.9
	FE NO SHEAR	-425	46	46	0	222.0
	FE WITH SHEAR	-430	75	80	-30	240.5
BOTTOM	LET	-169	746	746	0	431.3
	FE NO SHEAR	-183	575	575	0	357.3
	FE WITH SHEAR	-172	452	482	-15	301.7

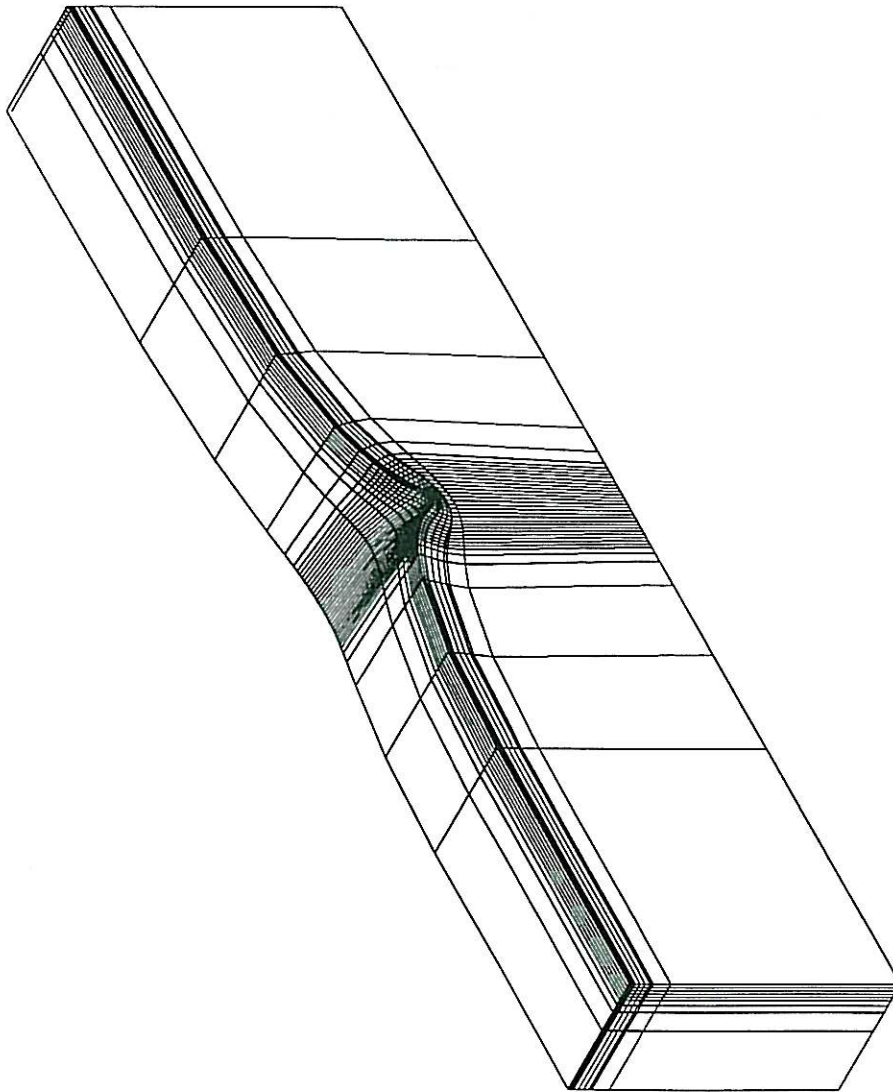
SCALE: 1# = 1

LENGTH
X # = 38.483cm
Y # = 38.483cm
Z # = 38.483cm

DISPLACEMENT
X # = 0.023749cm
Y # = 0.023749cm
Z # = 0.023749cm

LOAD-STEP:
LS=2

PRESENTATION:
DEFORMED MESH



DESIGN BY SGG/901-Lopez geofe model HU 20.00-08
1998-10-15 9.8.41

STRUCTURE 2, MAX. DEFLECTION=0.36mm

SKUF
DISSG

Shear F

HMA PROJECT	TFAS/A/1
STATIC 40kN 800kPa 6% INCLINE	BKS (Pty) Ltd. Dr. JP Laurens BOX 3173 PRETORIA FAX 012 4213501
FIG. 1: Deflection Bowl	

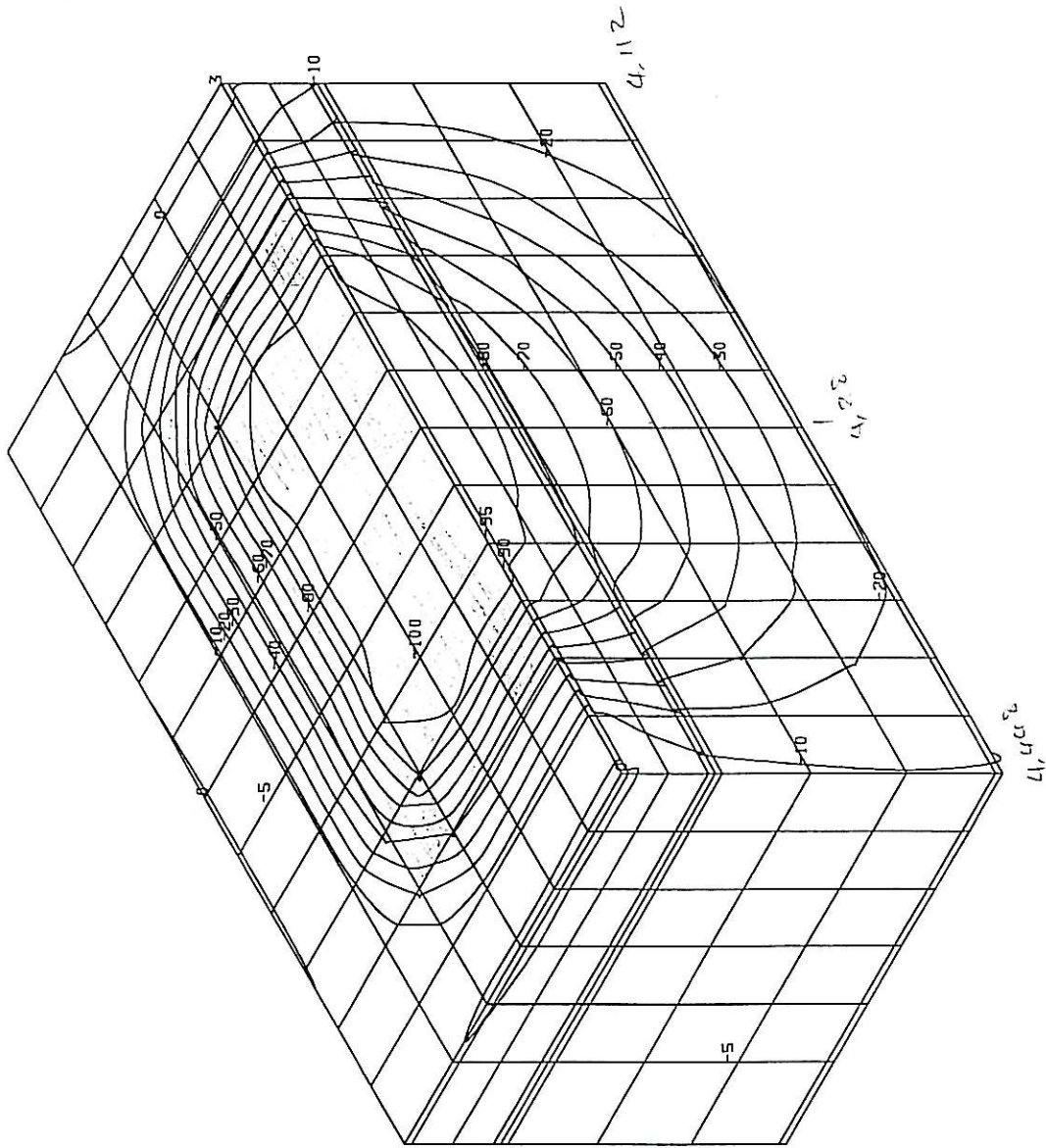
SCALE: $\frac{1}{10}$

LENGTH
 X H=2.1499cm
 Y H=2.1499cm
 Z H=2.1499cm

LOAD-STEP:
 LS=2-1

PRESENTATION:
 UNDEFORMED MESH
 DETAIL

ARGUMENT:
 STRESS
 Y - COMPONENT
 SIGN CONSIDERED
 100% =
 860.983886kN/m²



DESIGN BY SGG/901-Lopez geofE model RV 20.00-08
 1998-10-15 9:40:40

Shaw f

STRUCTURE 2, MAX. DEFLECTION=0.36mm

SCALE: 1/100

LENGTH

X #=2.1499cm

Y #=2.1499cm

Z #=2.1499cm

LOAD-STEP:

LS=2-1

PRESENTATION:

UNDEFORMED MESH

DETAIL

ARGUMENT:

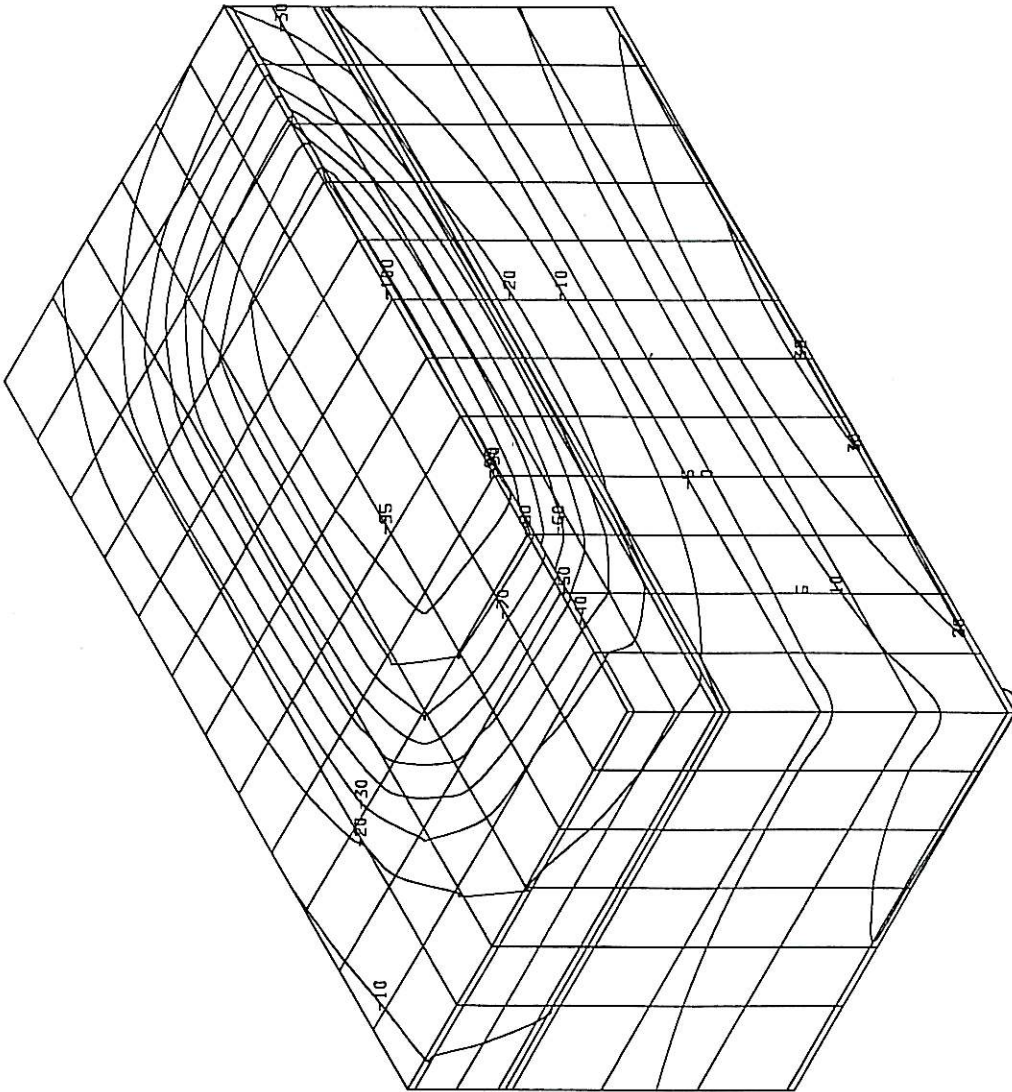
STRESS

X -COMPONENT

SIGN CONSIDERED

100% =

1506.044921kN/m²



DESIGN BY 566/901-10002 gaoFE model HU 20.00-08
1998-10-15 9142132

STRUCTURE 2, MAX. DEFLECTION=0.36mm

Shear F

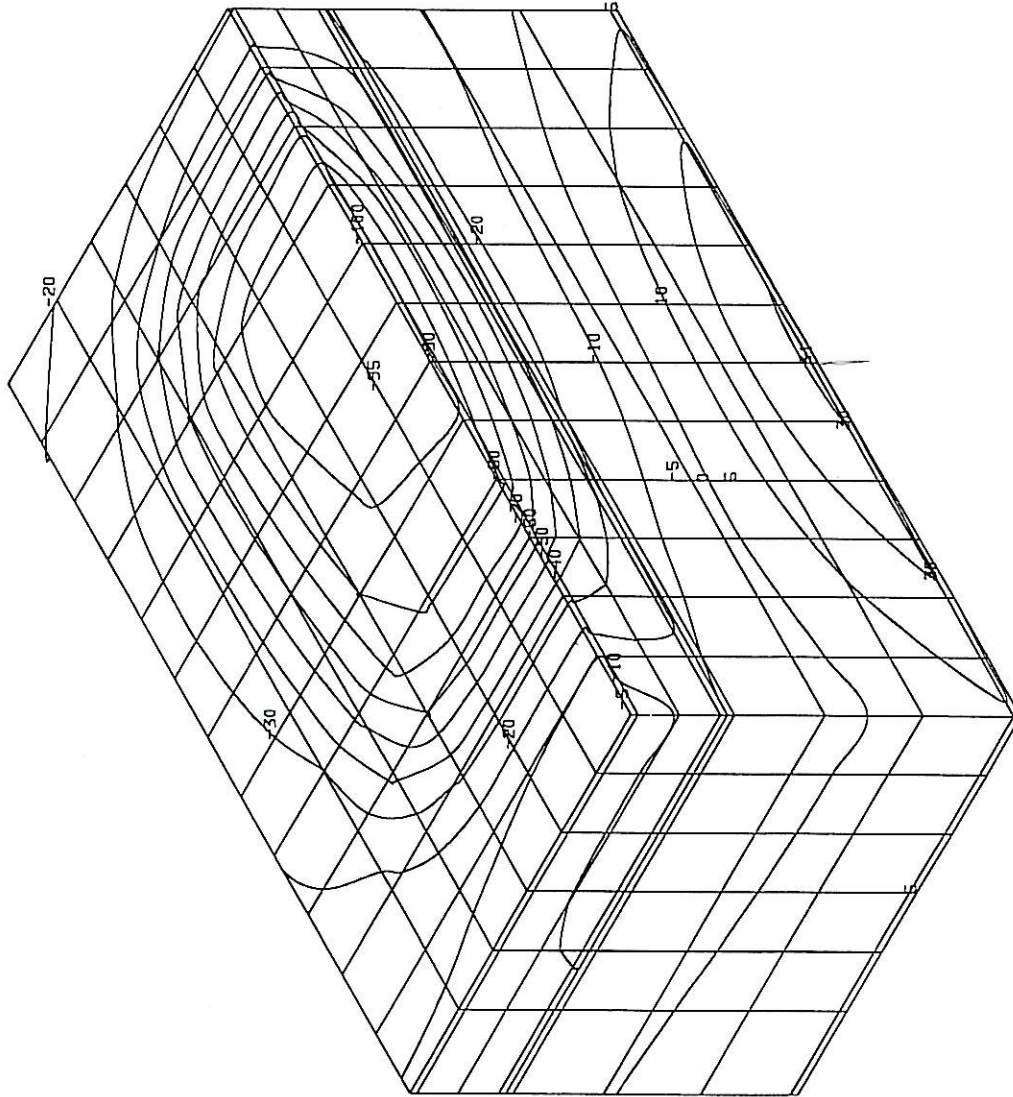
SCALE: 1# = 1

LENGTH
X #=2.1499cm
Y #=2.1499cm
Z #=2.1499cm

LOAD-STEP:
LS=2-1

PRESENTATION:
UNDEFORMED MESH
DETAIL

ARGUMENT:
STRESS
Z -COMPONENT
SIGN CONSIDERED
100% =
1607.171386kN/m²



DESIGN BY SGG/901-topaz geofe model HV 20.00-08
1998-10-15 9:42:11

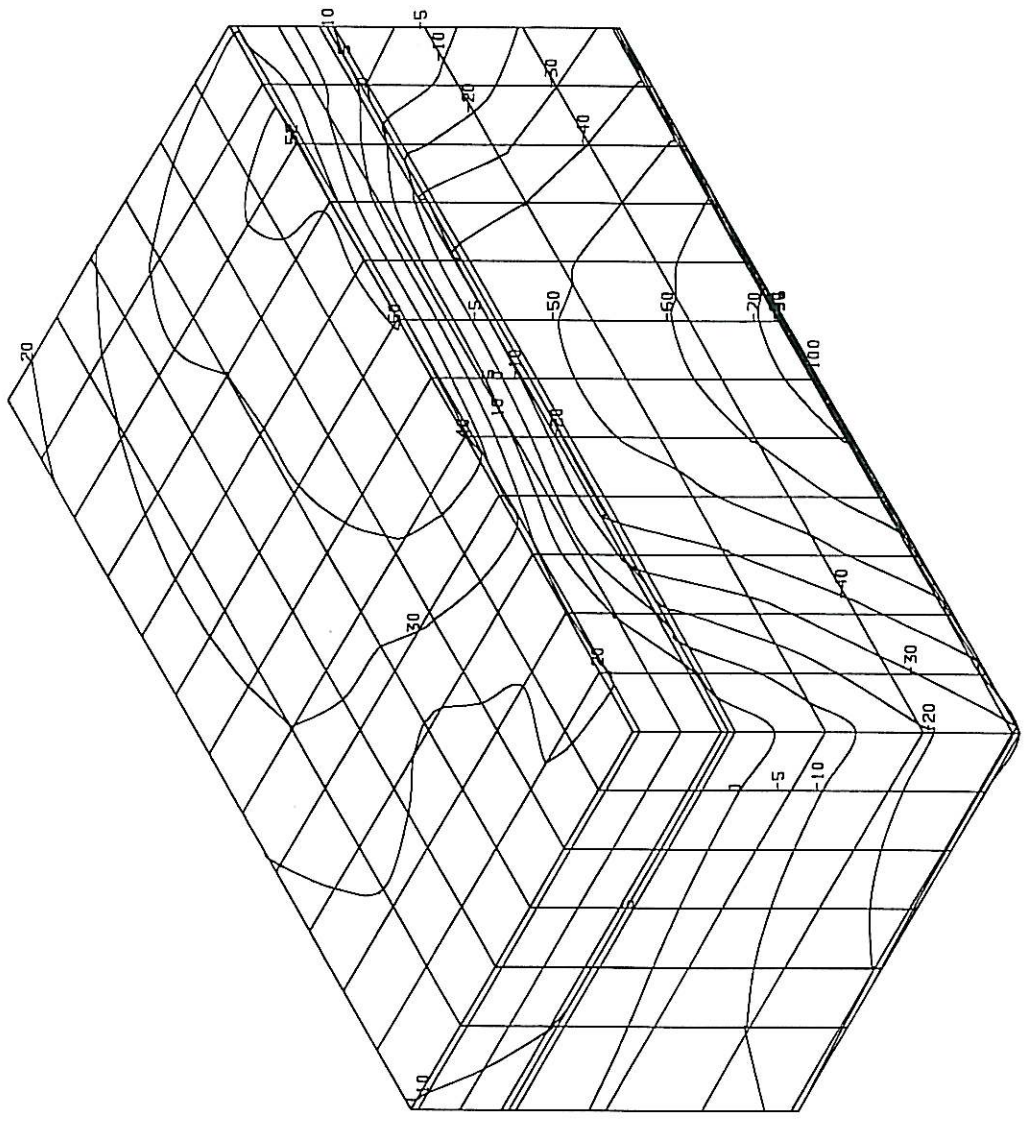
STRUCTURE 2, MAX. DEFLECTION=0.36mm

Shear f

Shear f

DESIGN BY SGG/901-Lopez 9149131
1998-10-15 MU 20.00-08

SCALE: 1#=
LENGTH #=2.1499cm
X #=2.1499cm
Y #=2.1499cm
Z #=2.1499cm
LOAD-STEP,
LS=2-1
PRESENTATION:
UNDEFORMED MESH
DETAIL
ARGUMENT:
STRAIN
Y -COMPONENT
SIGN CONSIDERED
100% =
0.000461



STRUCTURE 2, MAX. DEFLECTION=0.36mm

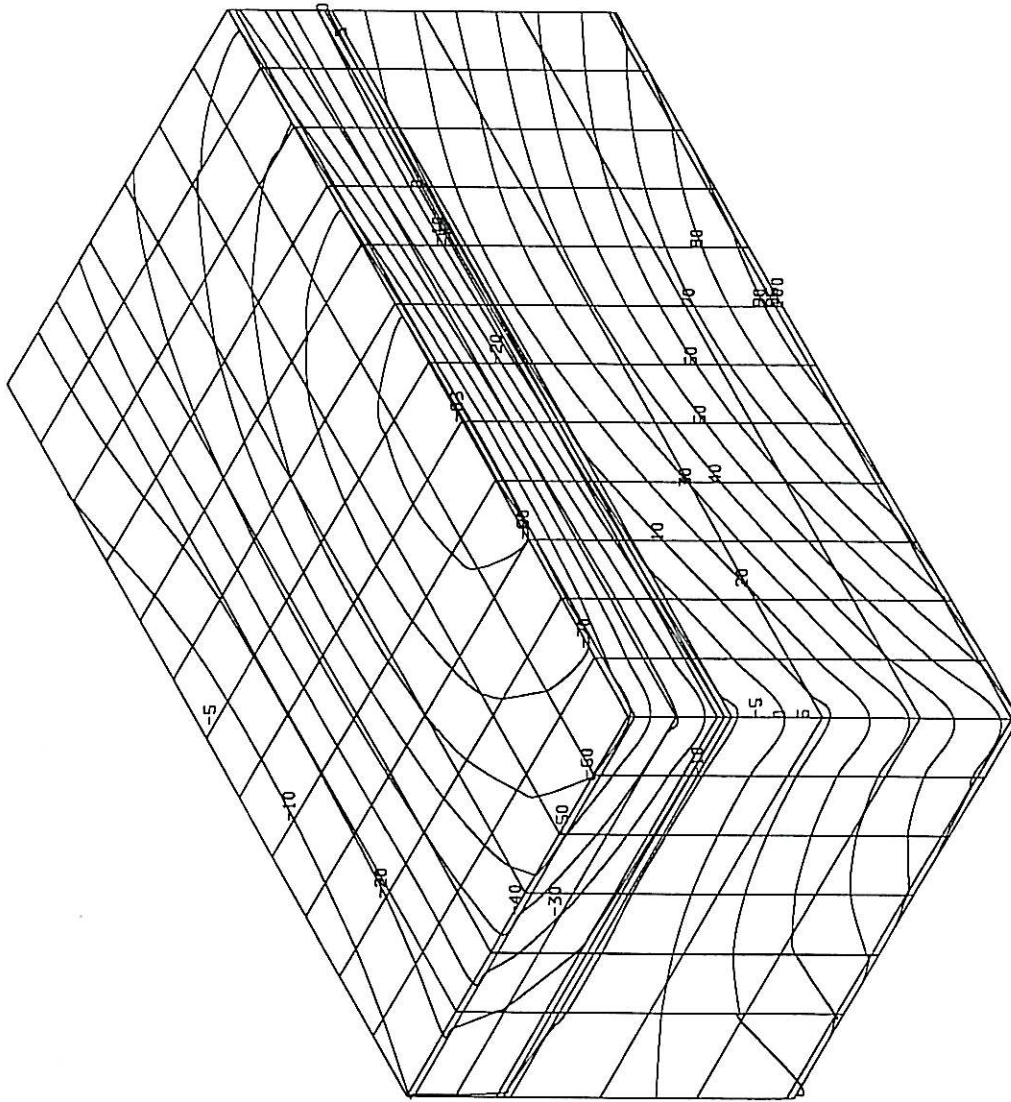
SCALE: 1# = 1

LENGTH # = 2.1499cm
 X # = 2.1499cm
 Y # = 2.1499cm
 Z # = 2.1499cm

LOAD-STEP:
 LS=2-1

PRESENTATION:
 UNDEFORMED MESH
 DETAIL

ARGUMENT:
 STRAIN
 X - COMPONENT
 SIGN CONSIDERED
 100% = 0.000221



STRUCTURE 2, MAX. DEFLECTION=0.36mm

DESIGN BY SGG/901-Lopez 9,51,21
 1998-10-15
 geofe model MV 20.00-08

Shear f

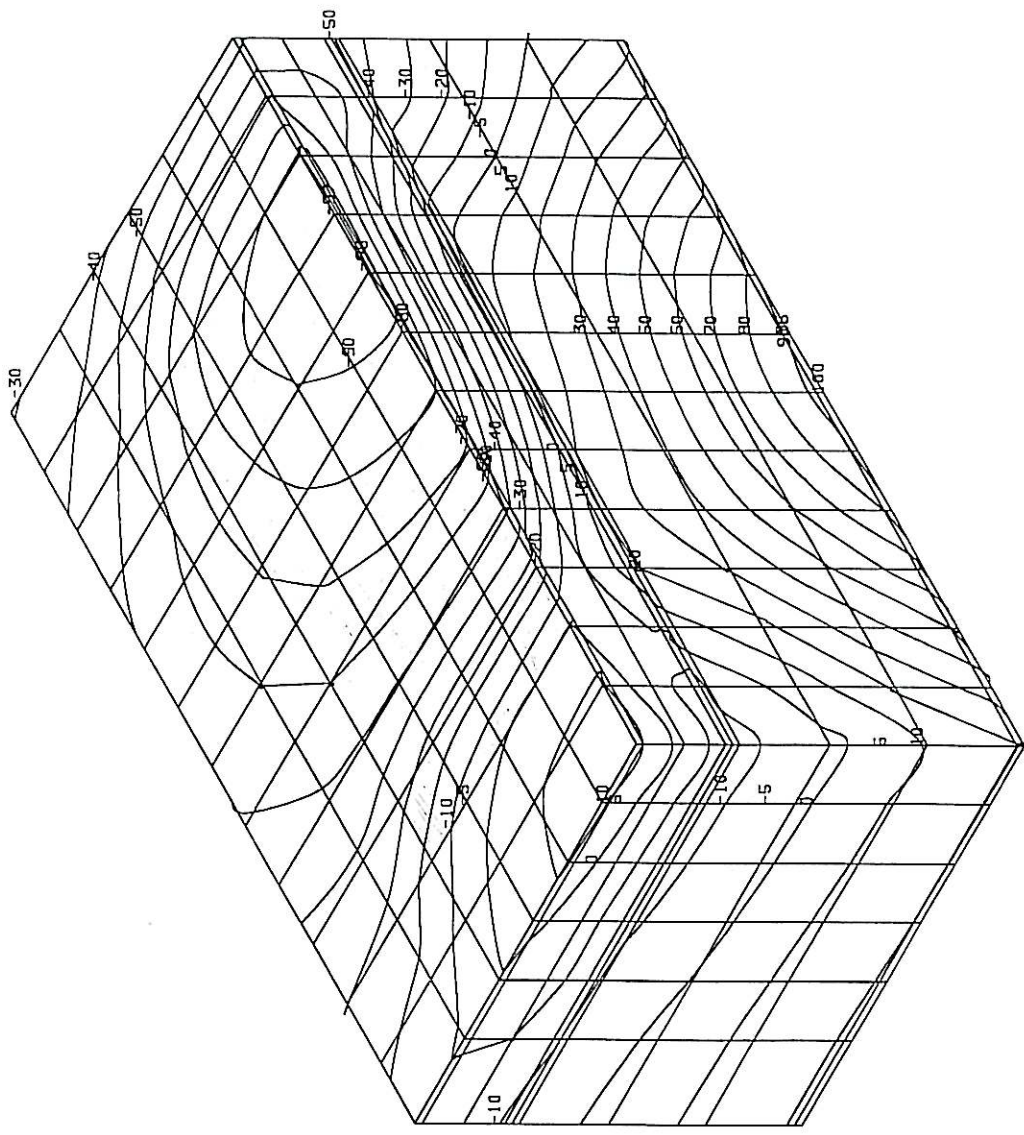
SCALE: 1/1

LENGTH
X #=2.1499cm
Y #=2.1499cm
Z #=2.1499cm

LOAD-STEP:
LS=2-1

PRESENTATION:
UNDEFORMED MESH
DETAIL

ARGUMENT:
STRAIN
Z -COMPONENT
SIGN CONSIDERED
100% =
0.000237

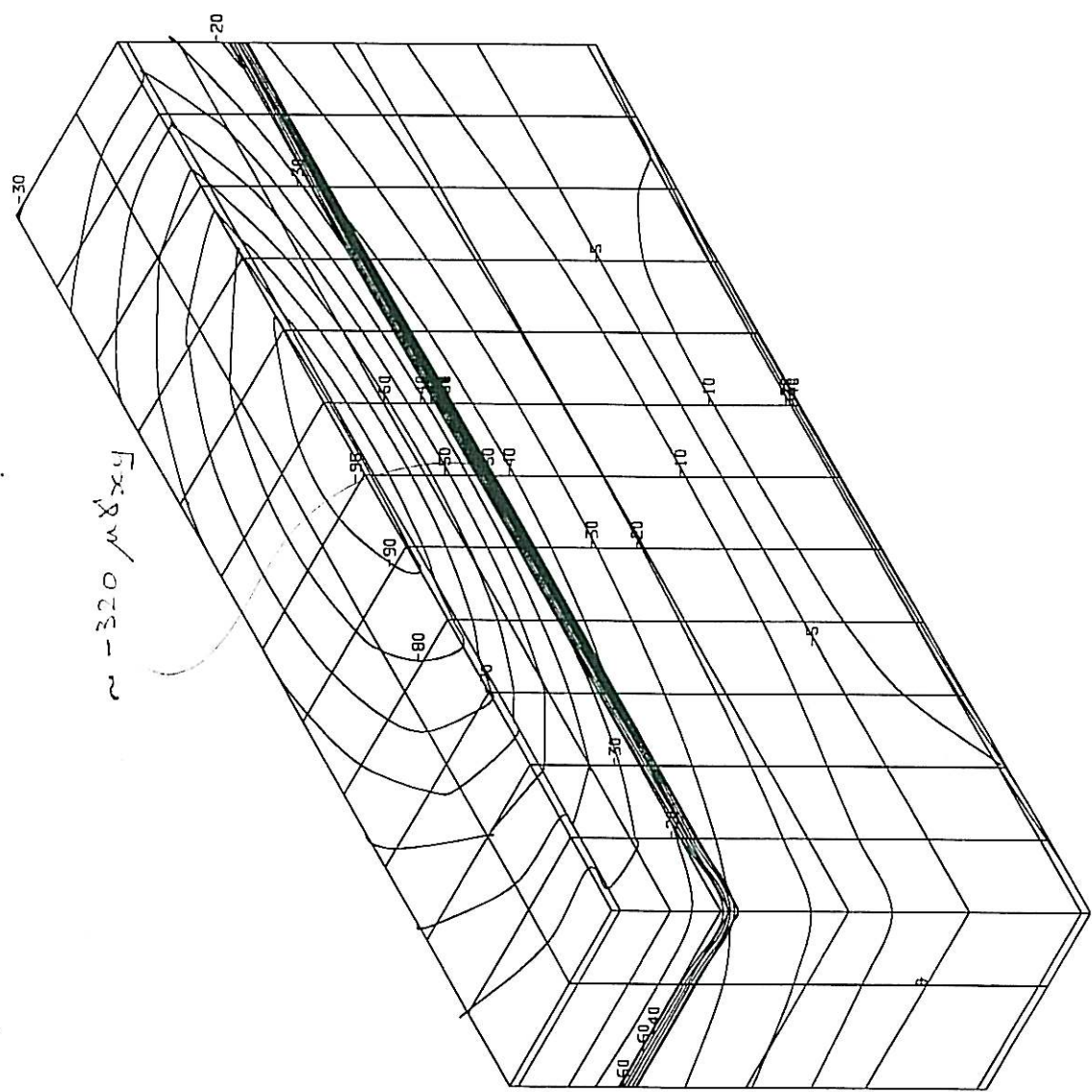


DESIGN BY SGG/901-lopaz geofe model MU 20.00-08
1998-10-15 9:53:10

STRUCTURE 2, MAX. DEFLECTION=0.36mm

Sheen F

SCALE: 1# = 1
 LENGTH # = 1.6833cm
 X # = 1.6833cm
 Y # = 1.6833cm
 Z # = 1.6833cm
 LOAD-STEP:
 LS=2-1
 PRESENTATION:
 UNDEFORMED MESH
 DETAIL
 ARGUMENT:
 STRAIN
 Gamma-XY
 SIGN CONSIDERED
 100% =
 0.000457



STRUCTURE 2, MAX. DEFLECTION=0.36mm

DESIGN BY 566/901-Lopez geofe model MU 20.00-08
 1998-10-15 10:16:22

Shear f

Shear F

SCALE: 1/10

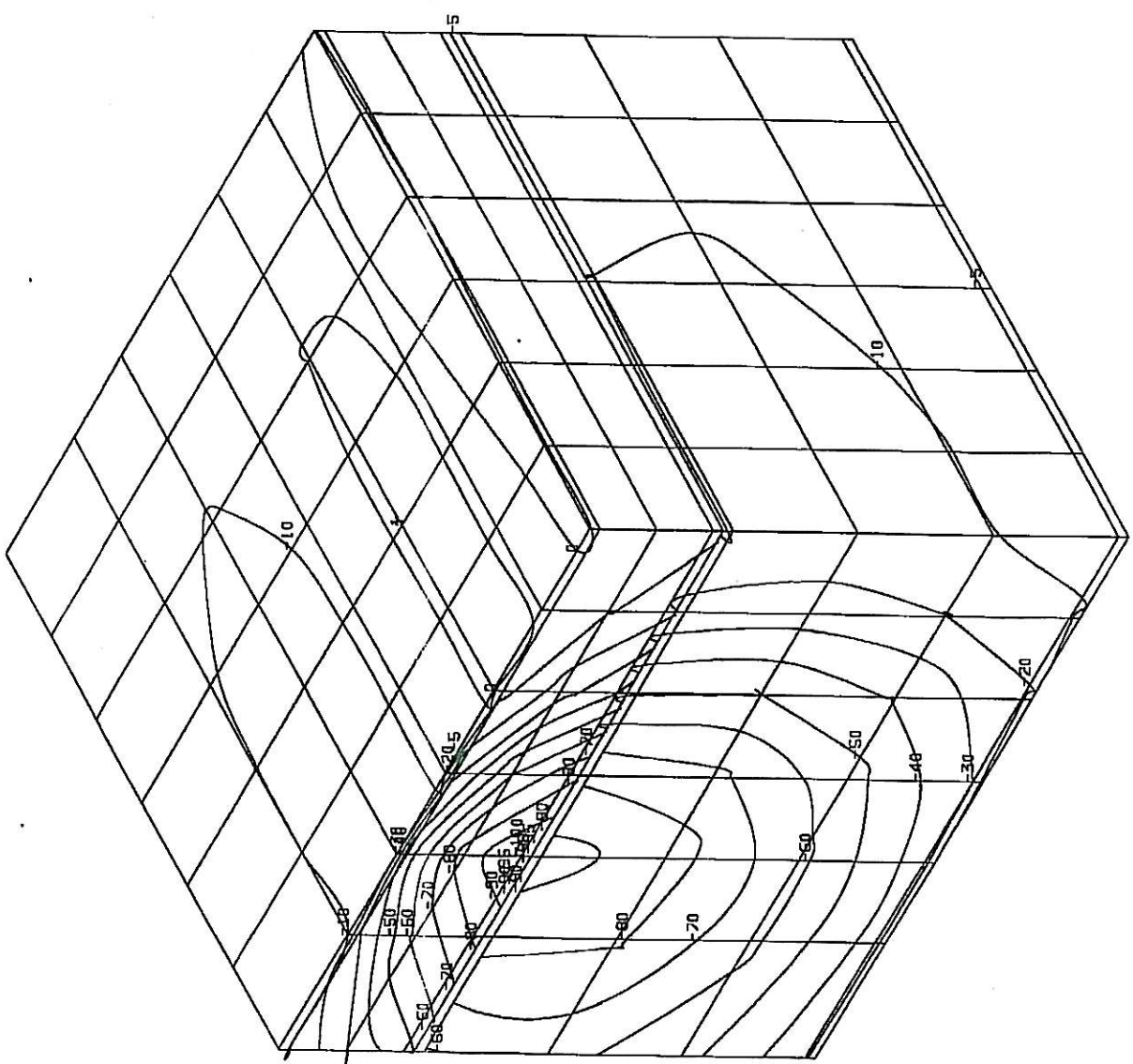
LENGTH
 X #=1.4521cm
 Y #=1.4521cm
 Z #=1.4521cm

LOAD-STEP:
 LS=2-1

PRESENTATION:
 UNDEFORMED MESH
 DETAIL

ARGUMENT:
 STRESS
 Tau-XY
 SIGN CONSIDERED
 100% = 299.256713kN/m2

DESIGN BY SGG/901-Lopez geofe model HU 20.00-08
 1998-10-15 10:21:0



STRUCTURE 2, MAX. DEFLECTION=0.36mm

APPENDIX D
ANALYSIS RESULTS: TEMPERATURE GRADIENT EFFECTS

- E1. The following pages contain influence lines for the maximum horizontal tensile strain and the octahedral shear stress, following from the results of the analysis of temperature and stiffness gradient effects. All of the figures show a comparison between the results obtained with the conventional layered elastic model and an axisymmetric finite element model.

It is strongly recommended that the reader study the analysis procedure as explained in Chapter 6 before trying to interpret the following figures. The top header of each graph contains a description of the structure that was analysed, the season to which the temperature data applies and whether the comparison was done for benchmarking purposes or for a comparison of temperature gradient effects. The second header of each graph indicates what stiffness modulus was used in the conventional layered elastic theory (LET) model. The following examples should illustrate the meaning of the figure headers.

Struc1 AC-TOP, SUMMER BENCH

LET model: E-ac = 2500

This header indicates that the comparison applies to Structure 1 (as defined in Chapter 6). The results are used for benchmarking purposes (to ensure that the FE and LET results compare well when no gradient is assumed). Results were calculated at the top of the asphalt surfacing. The LET model assumed a constant stiffness of 2500 MPa.

STRUC 2: AC-BASE-BOTT SUMMER 14H00

LET Model: E-ac = 830 MPa

This header indicates that the comparison applies to Structure 2 (as defined in Chapter 6). The results shown were calculated at the bottom of the base. The temperature gradient that was used to determine the stiffness gradient in the FE model was for 14h00 in summer (as defined in Chapter 6). The second header line indicates that the asphalt stiffness used in the LET model was 830 MPa.

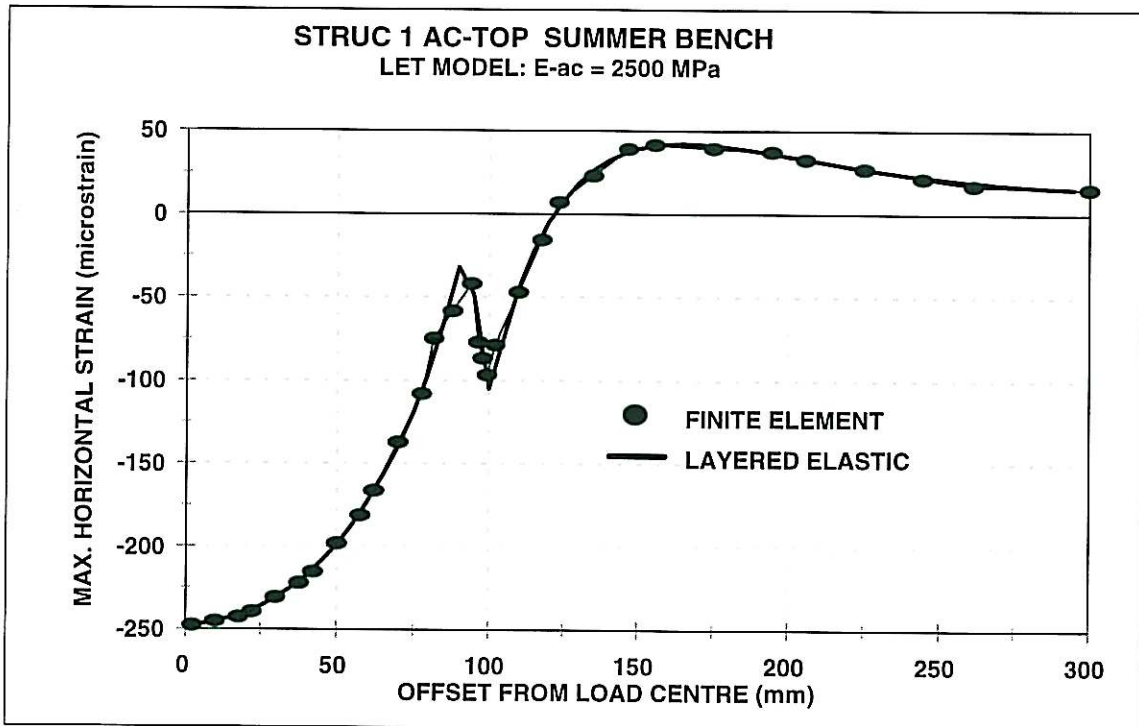


Figure E1. Finite Element and LET Benchmark

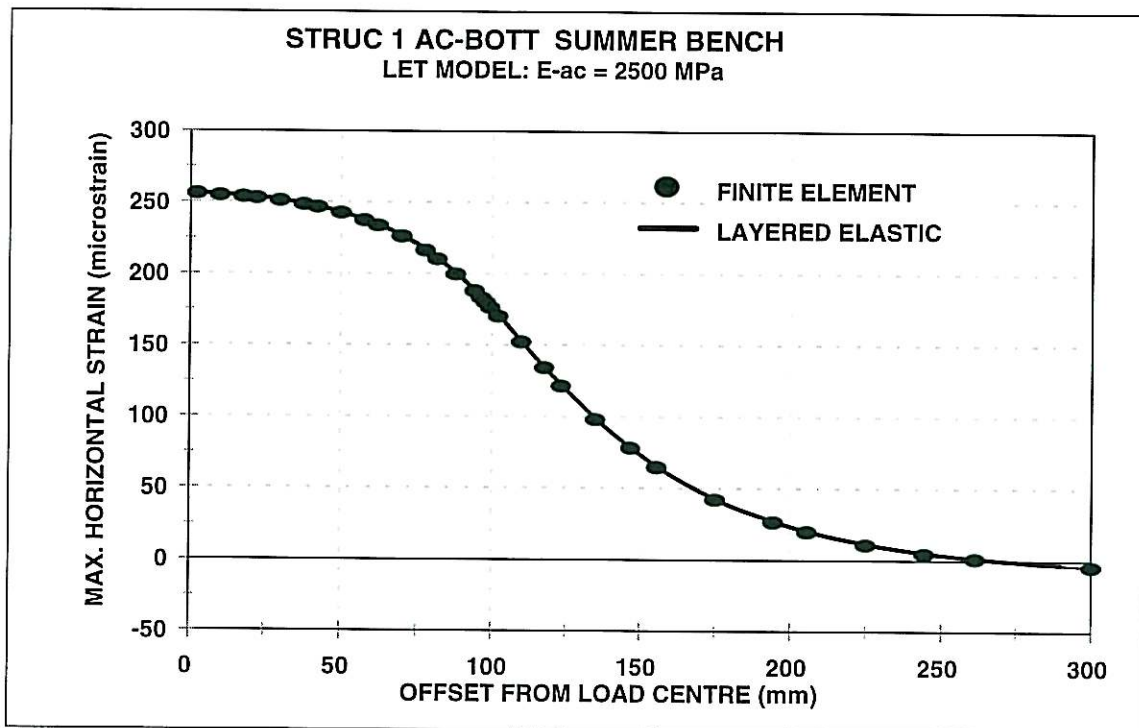


Figure E2. Finite Element and LET Benchmark

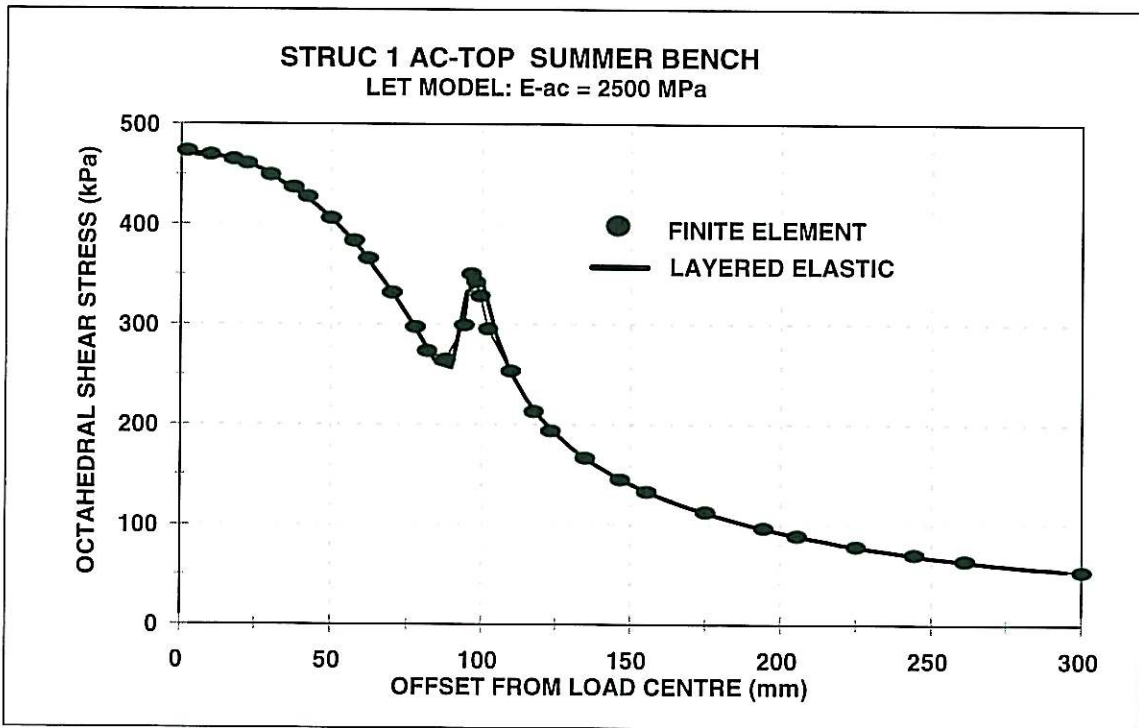


Figure E3. Finite Element and LET Benchmark

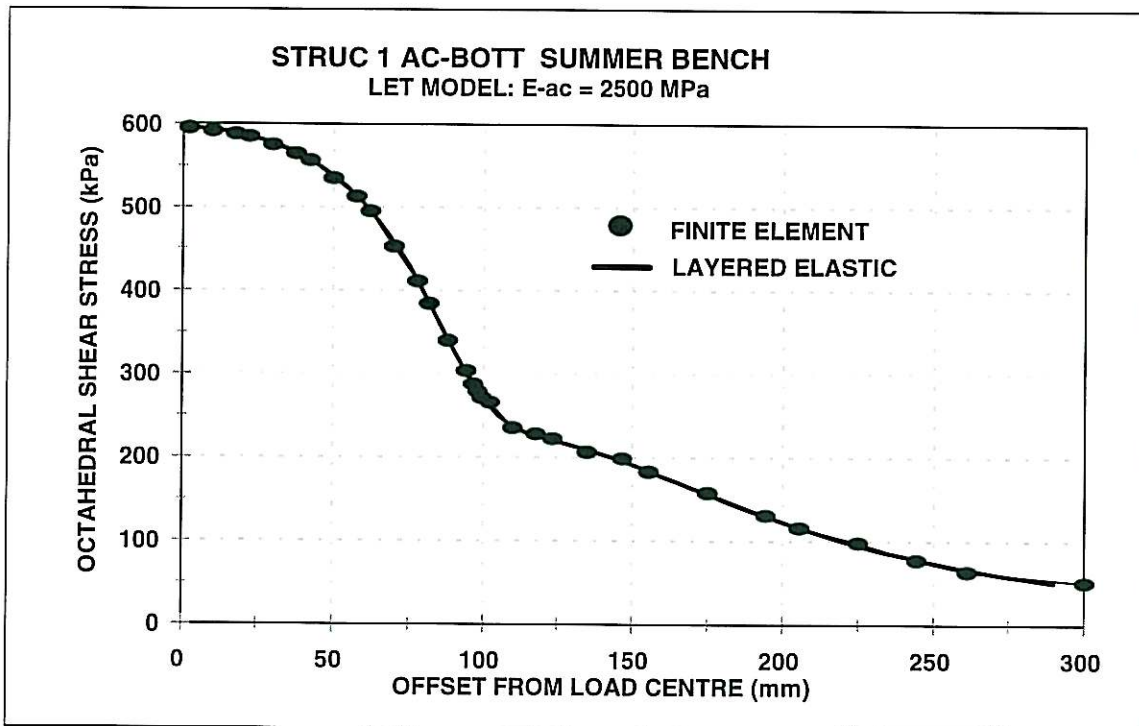


Figure E4. Finite Element and LET Benchmark

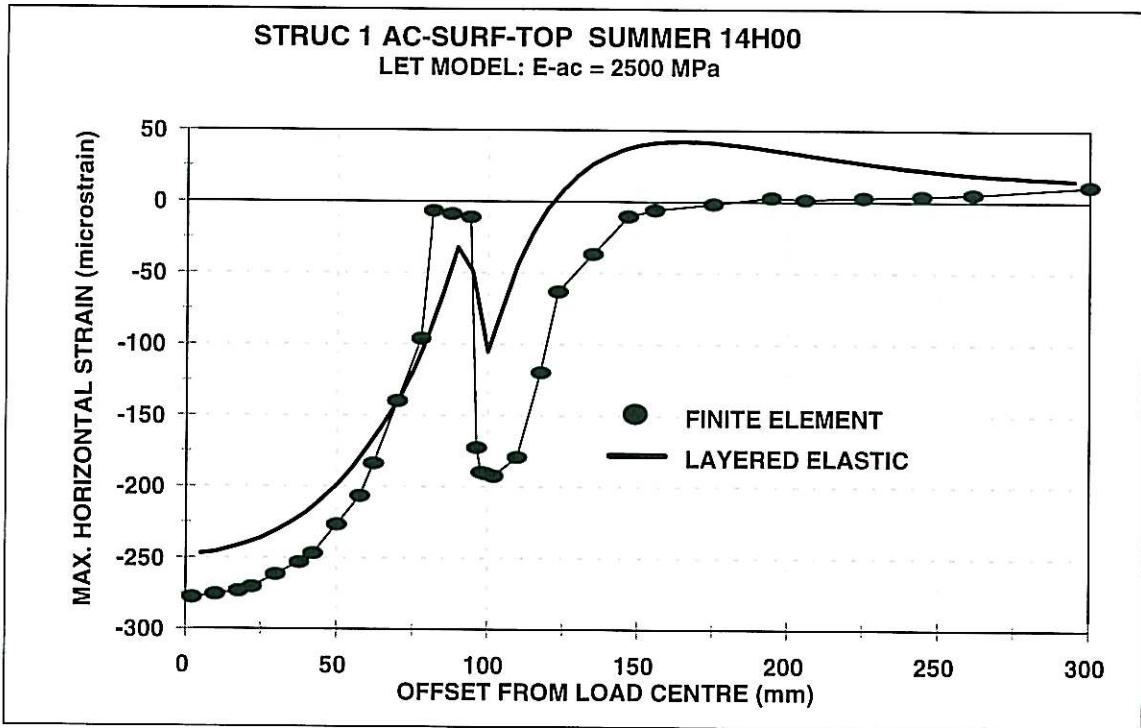


Figure E5. Finite Element and LET Comparison

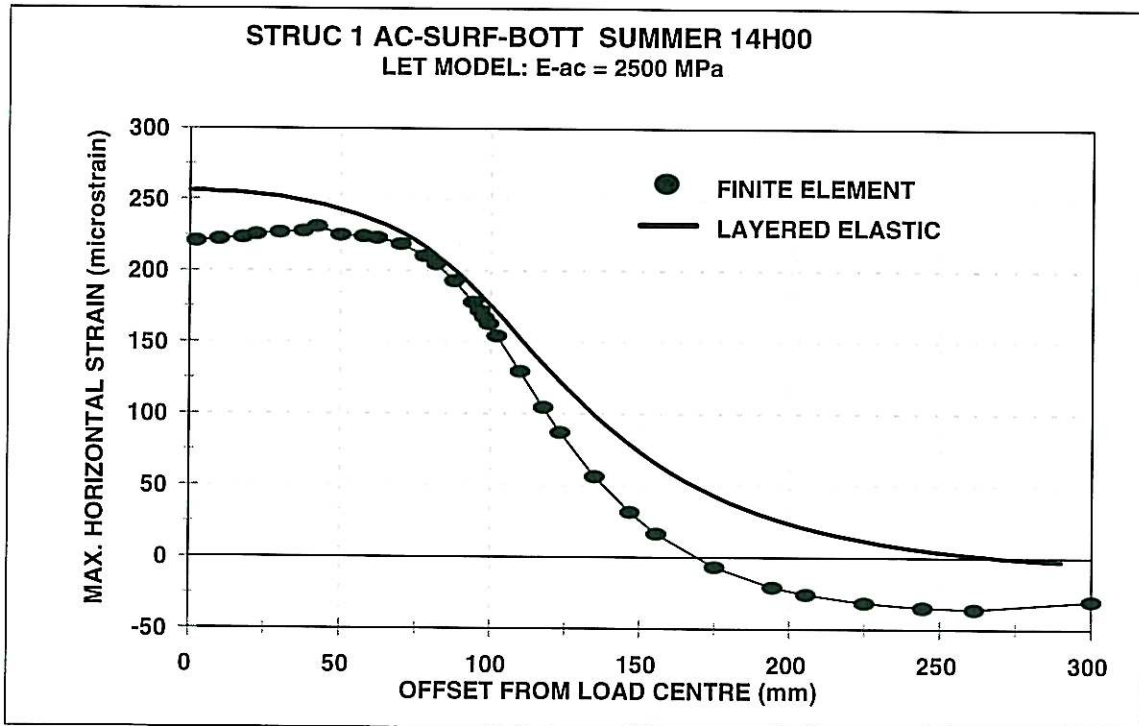


Figure E6. Finite Element and LET Comparison

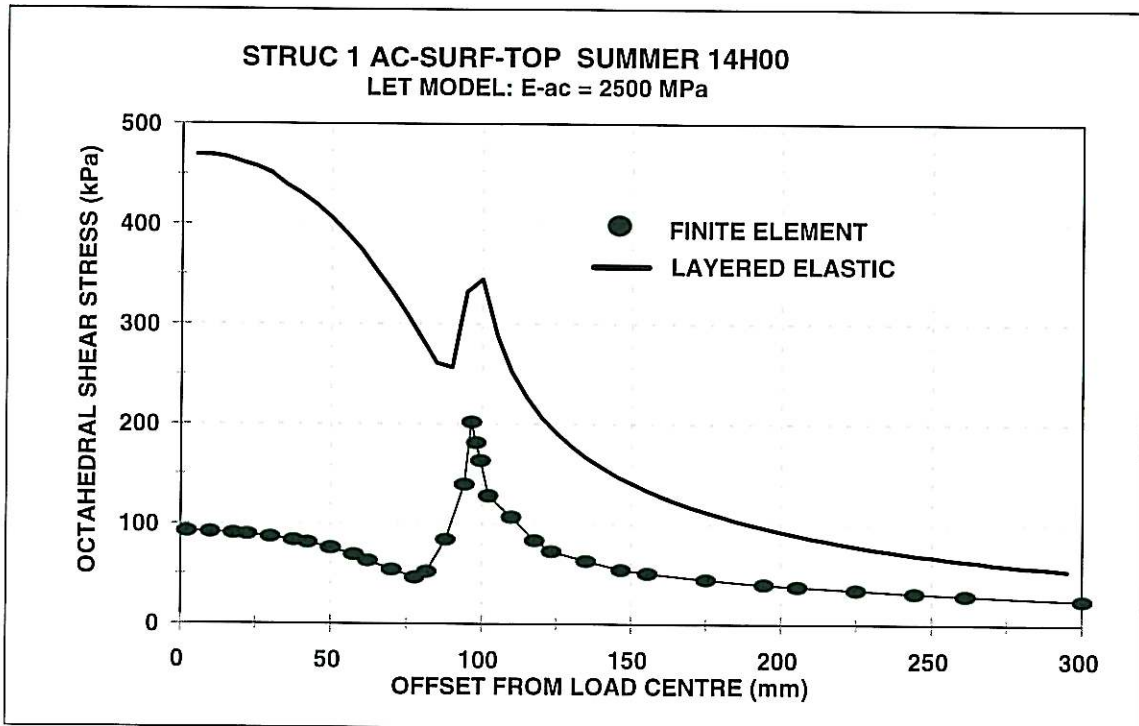


Figure E7. Finite Element and LET Comparison

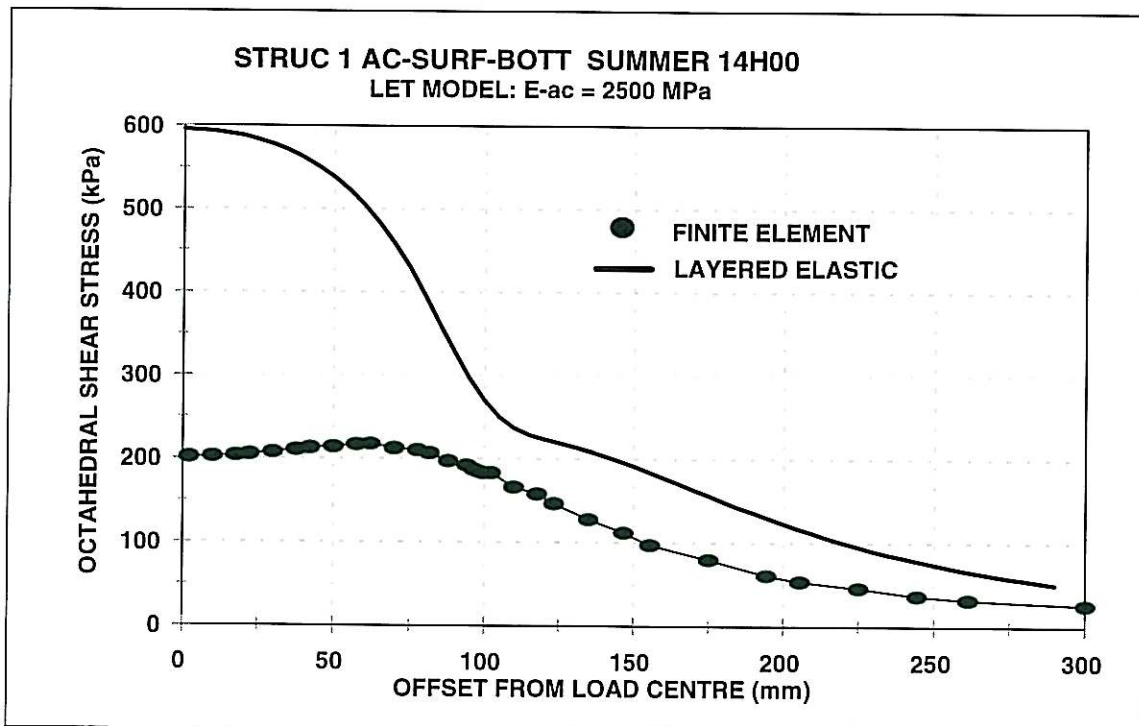


Figure E8. Finite Element and LET Comparison

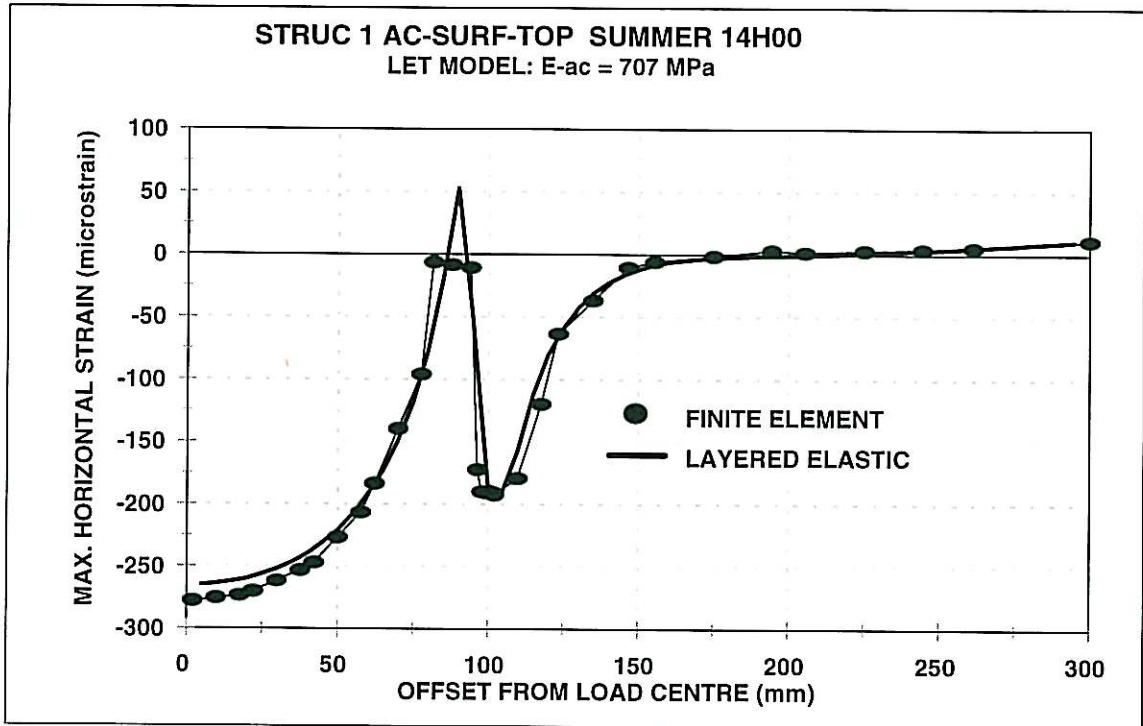


Figure E9. Finite Element and LET Comparison

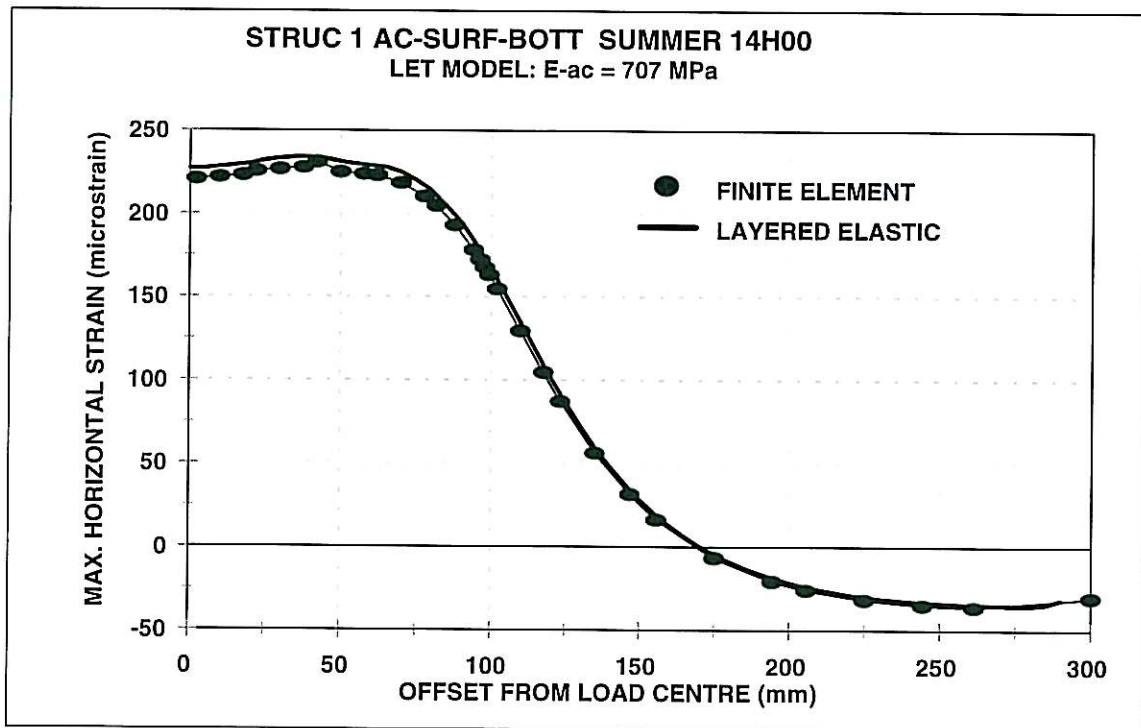


Figure E10. Finite Element and LET Comparison

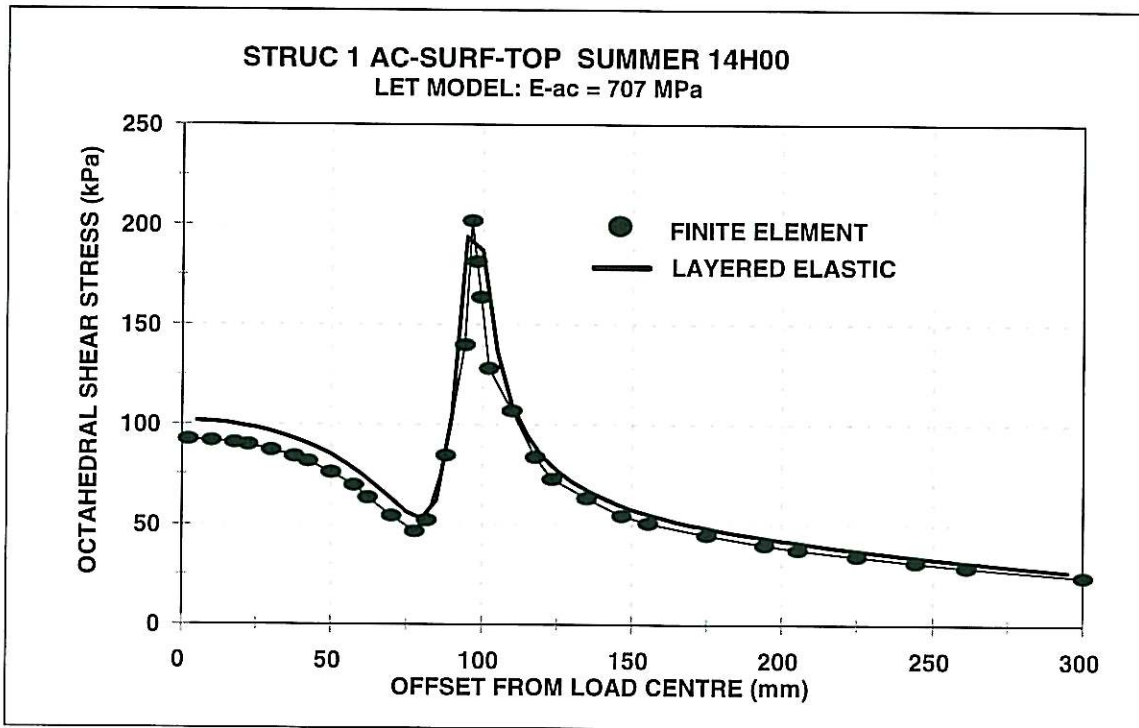


Figure E11. Finite Element and LET Comparison

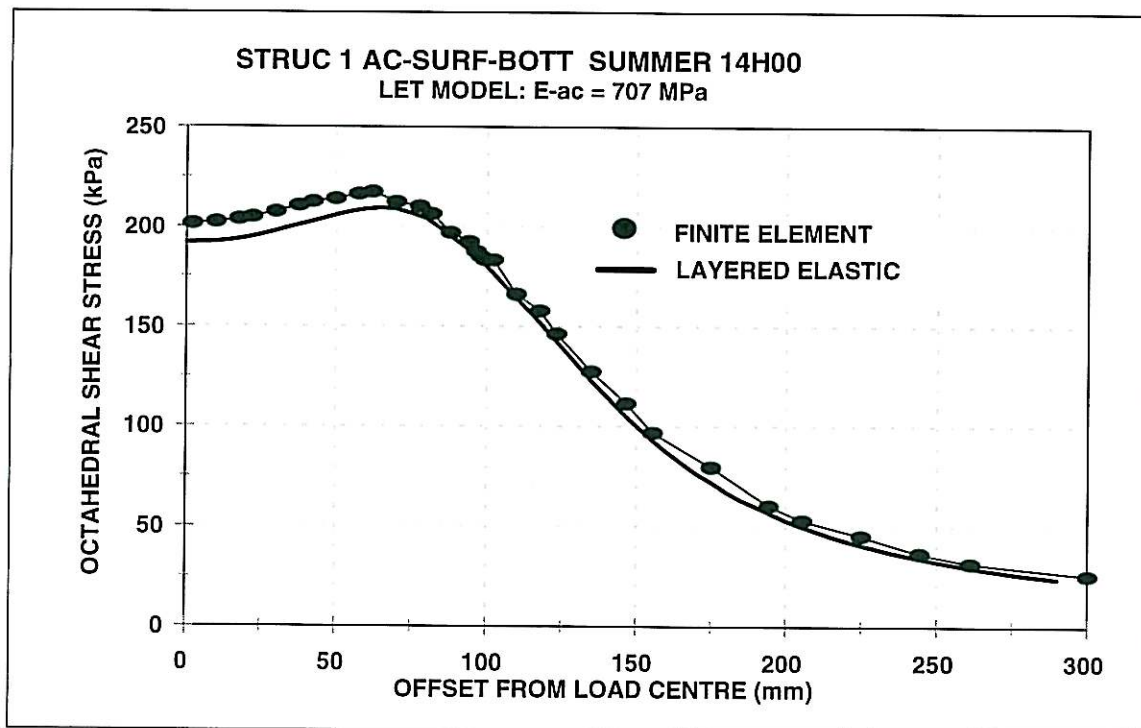


Figure E12. Finite Element and LET Comparison

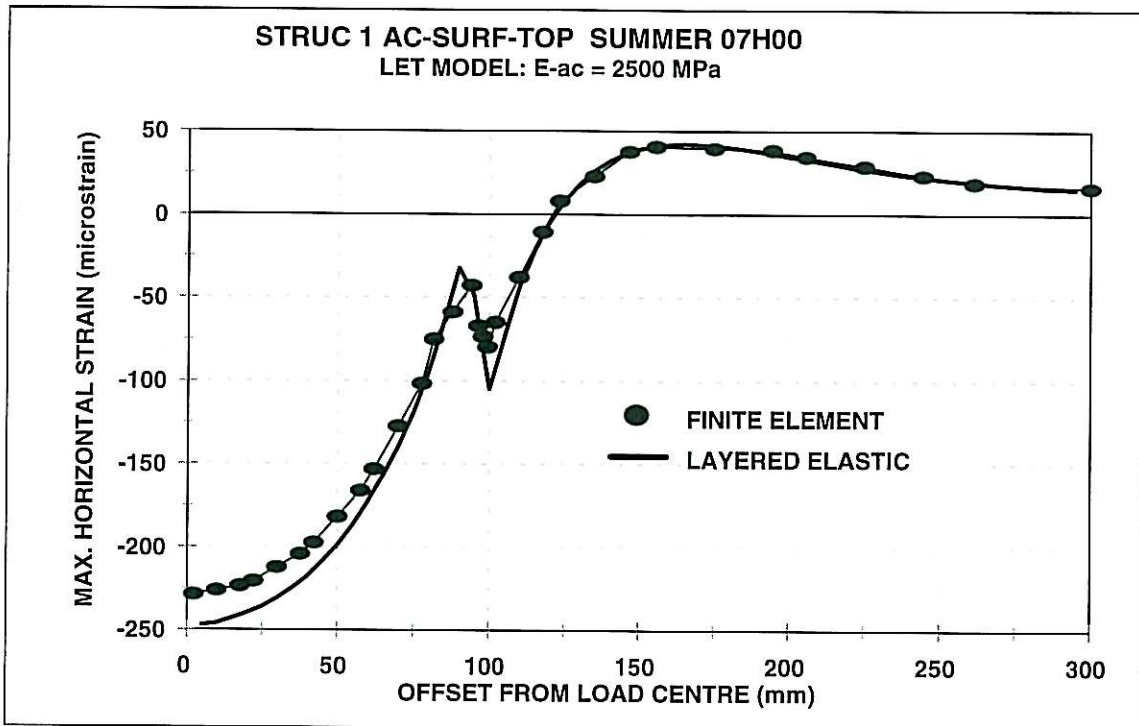


Figure E13. Finite Element and LET Comparison

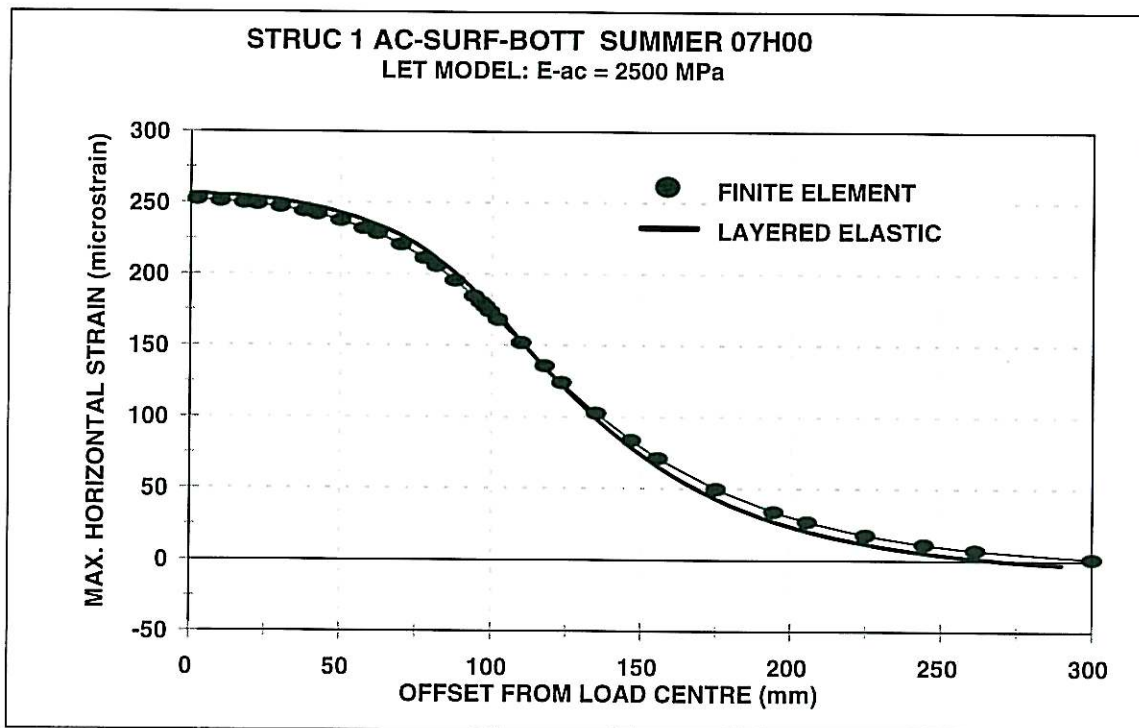


Figure E14. Finite Element and LET Comparison

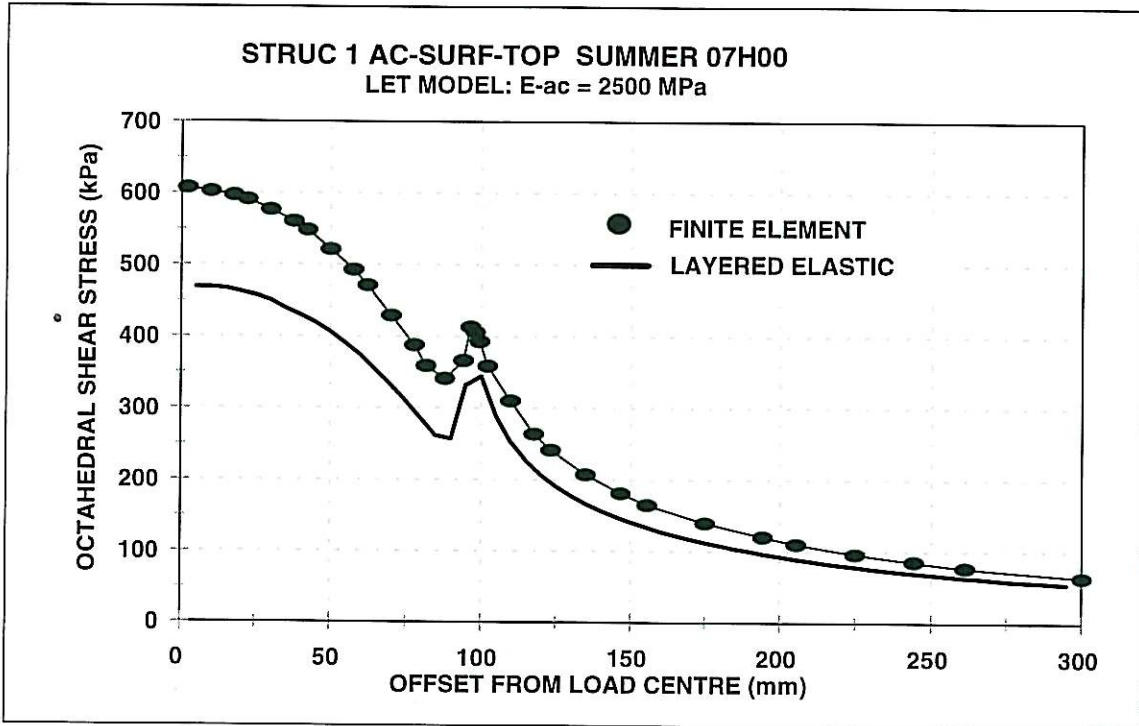


Figure E15. Finite Element and LET Comparison

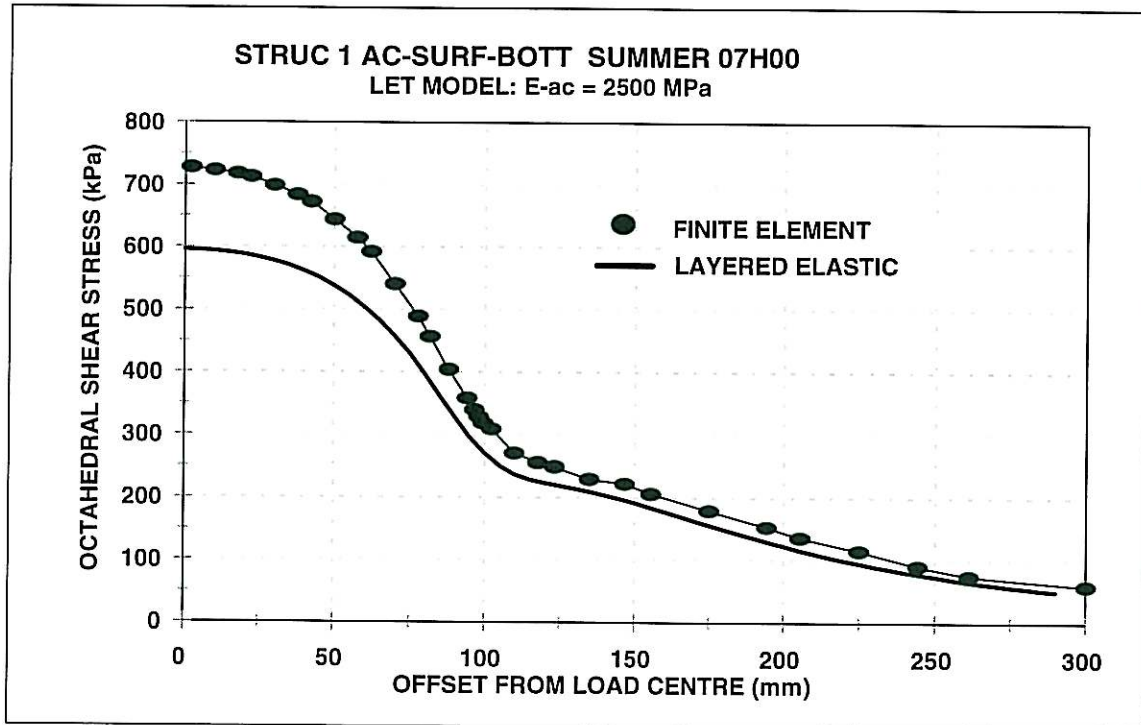


Figure E16. Finite Element and LET Comparison

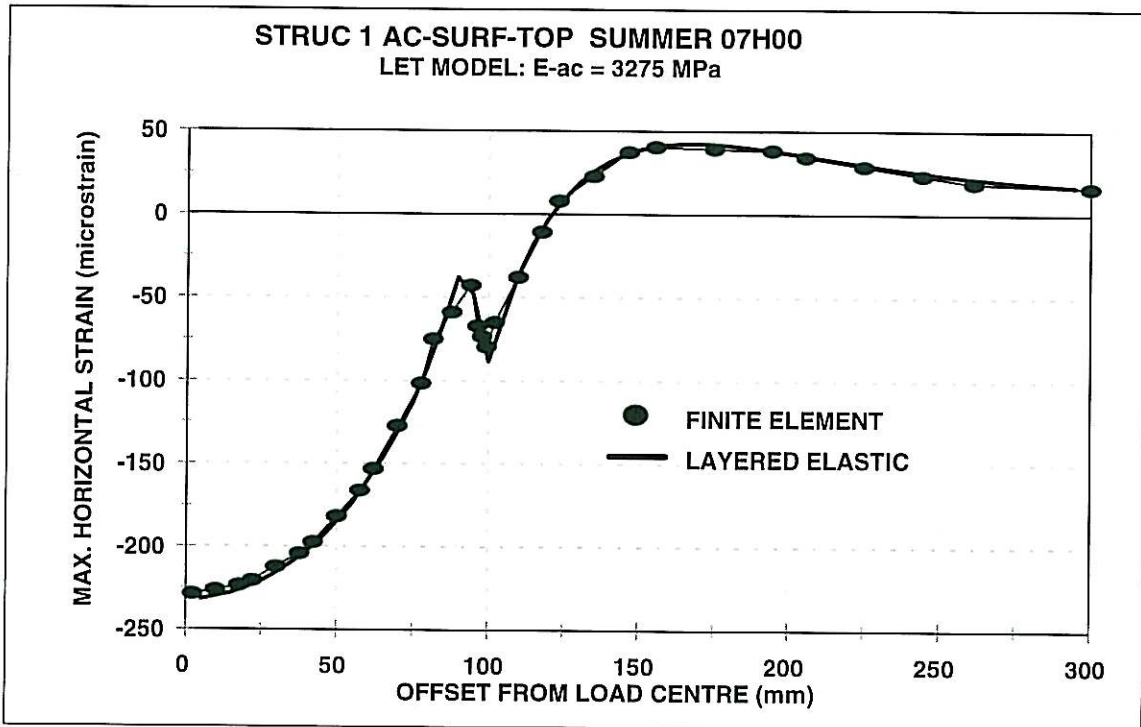


Figure E17. Finite Element and LET Comparison

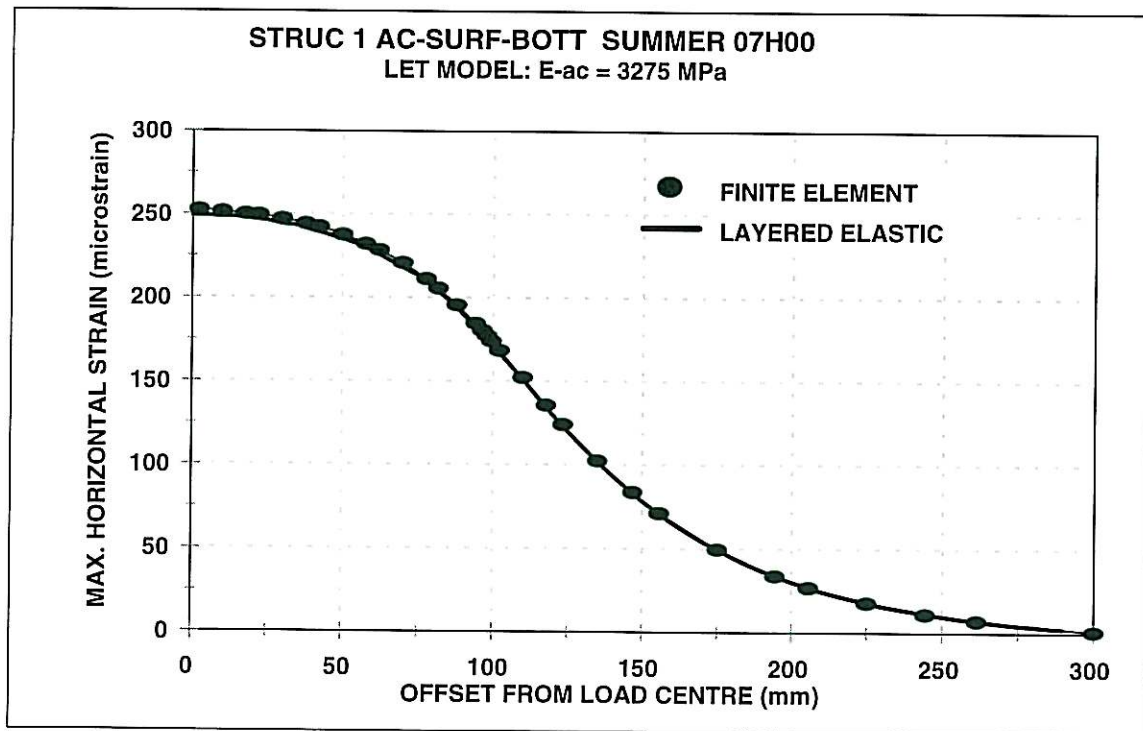


Figure E18. Finite Element and LET Comparison

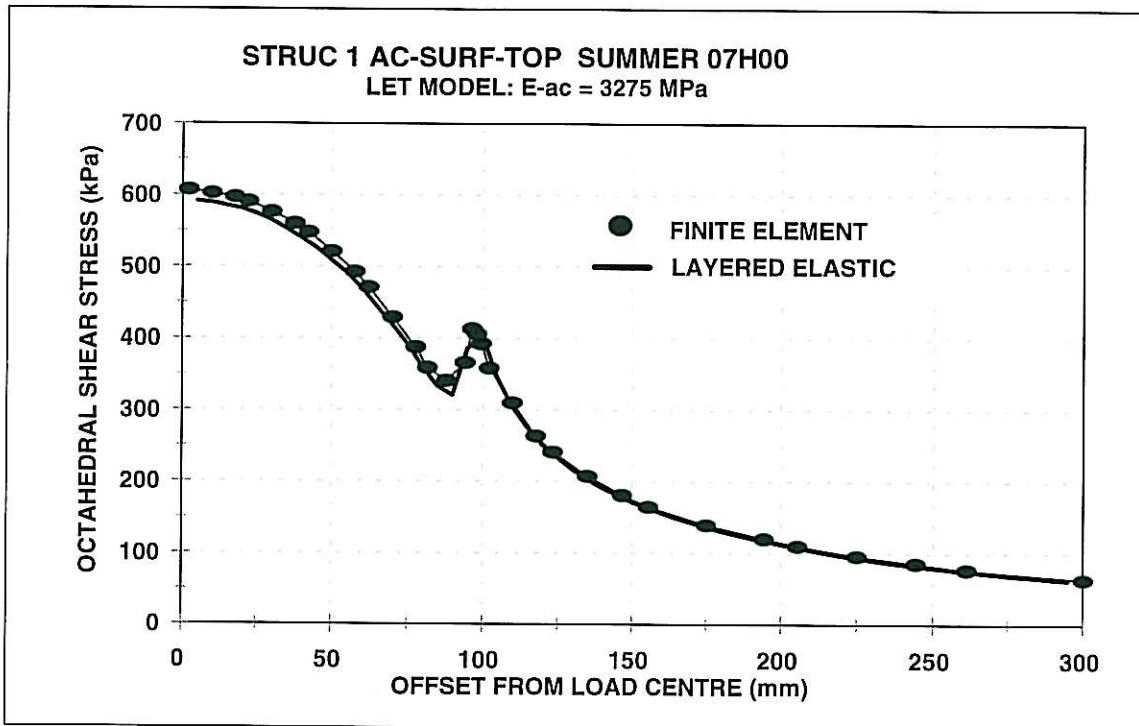


Figure E19. Finite Element and LET Comparison

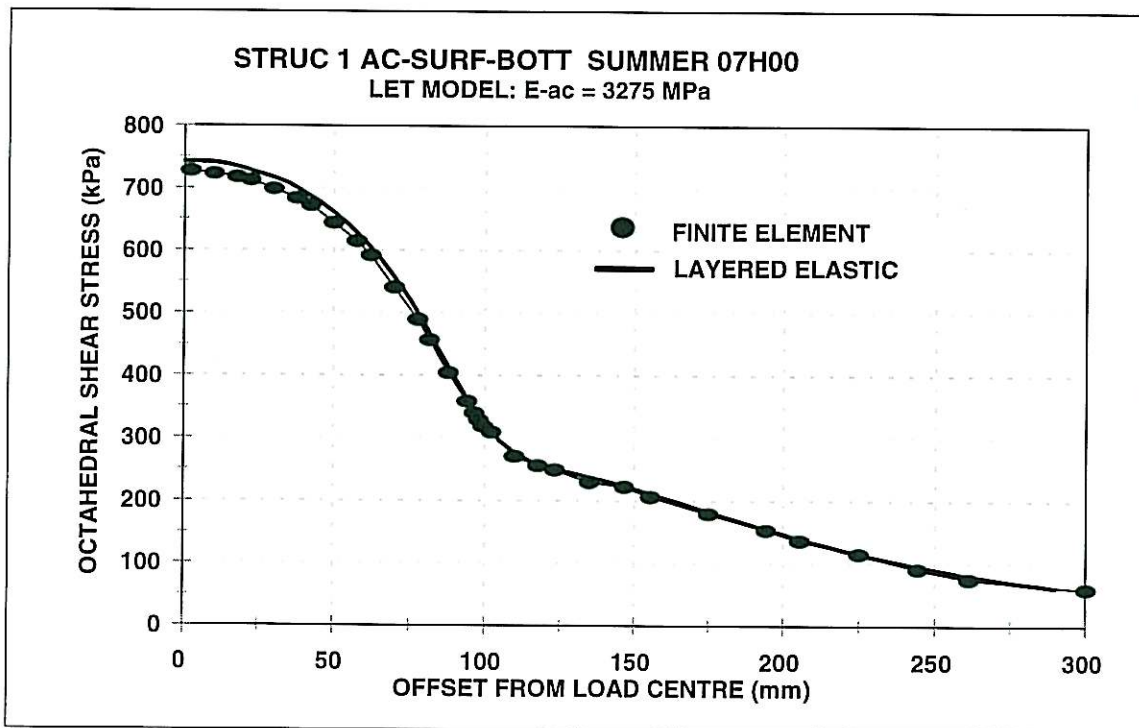


Figure E20. Finite Element and LET Comparison

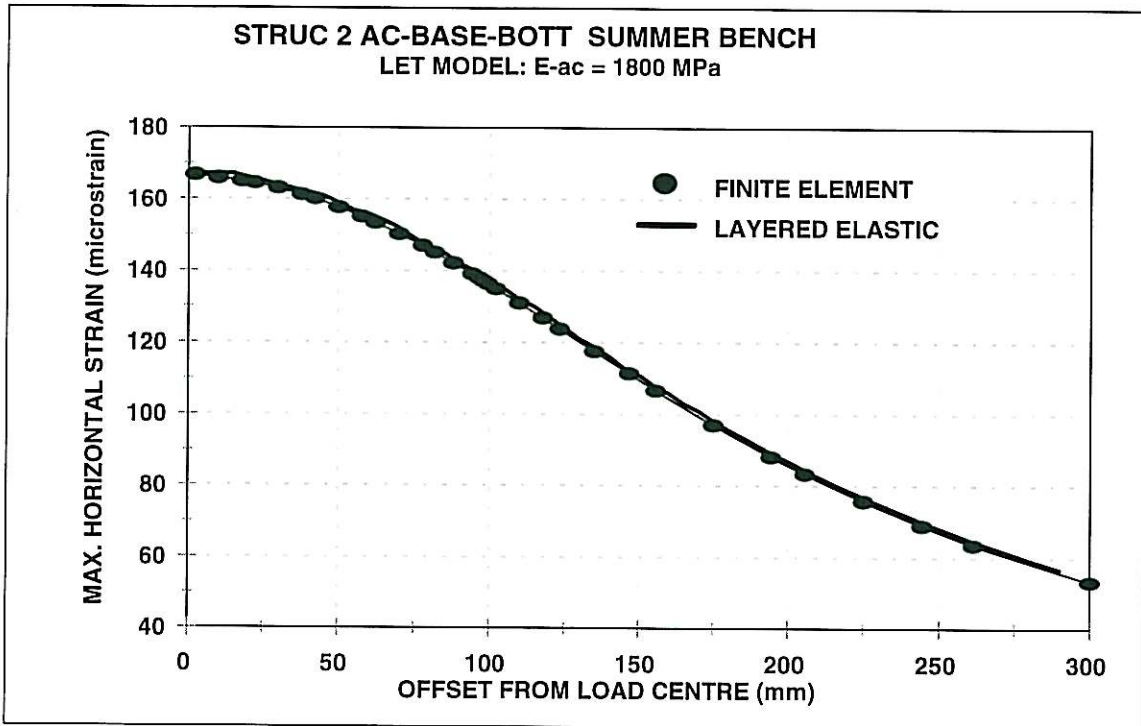


Figure E21: Finite Element and LET Benchmark

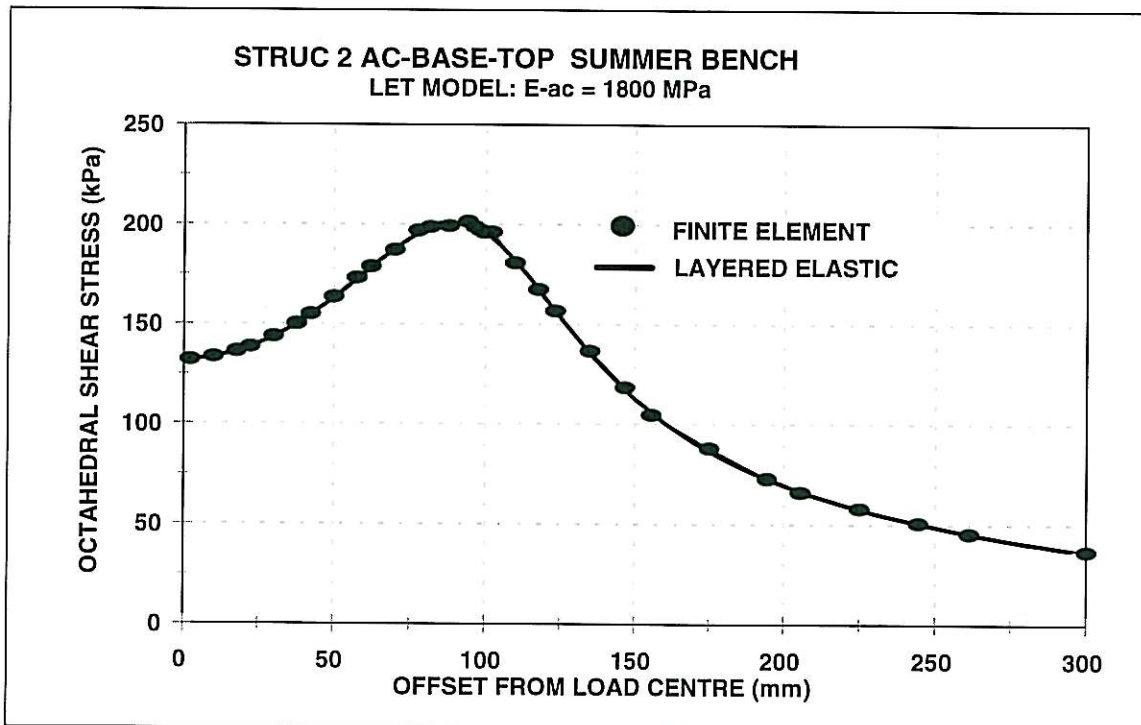


Figure E22: Finite Element and LET Benchmark

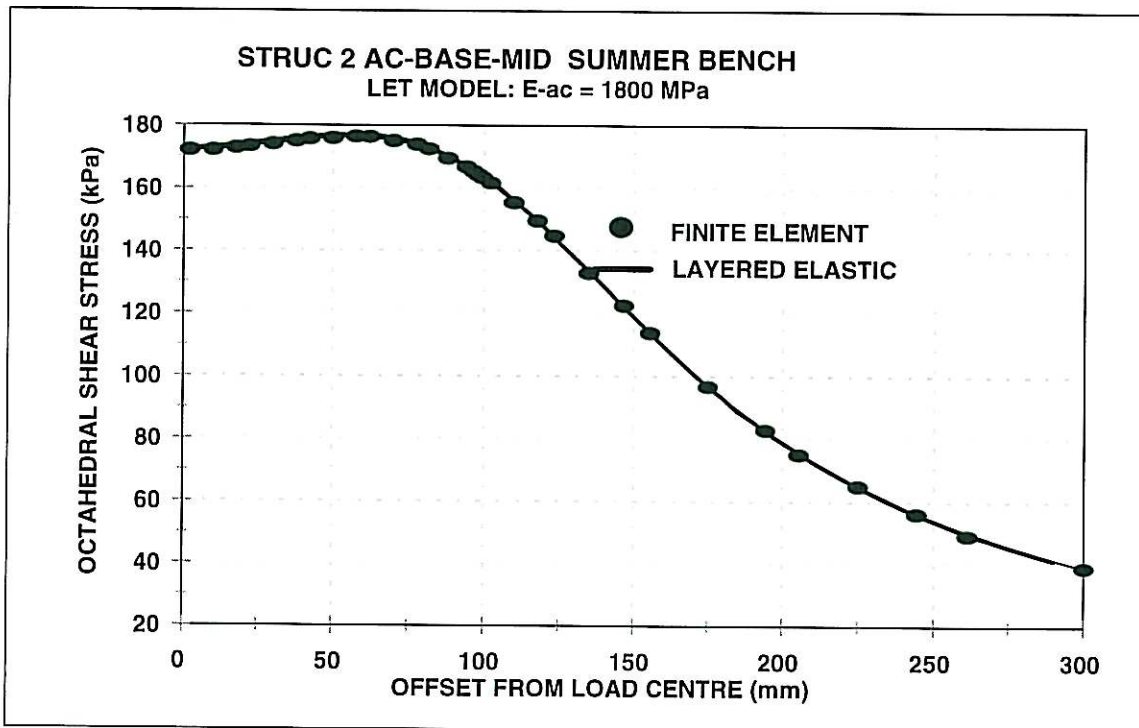


Figure E23: Finite Element and LET Benchmark

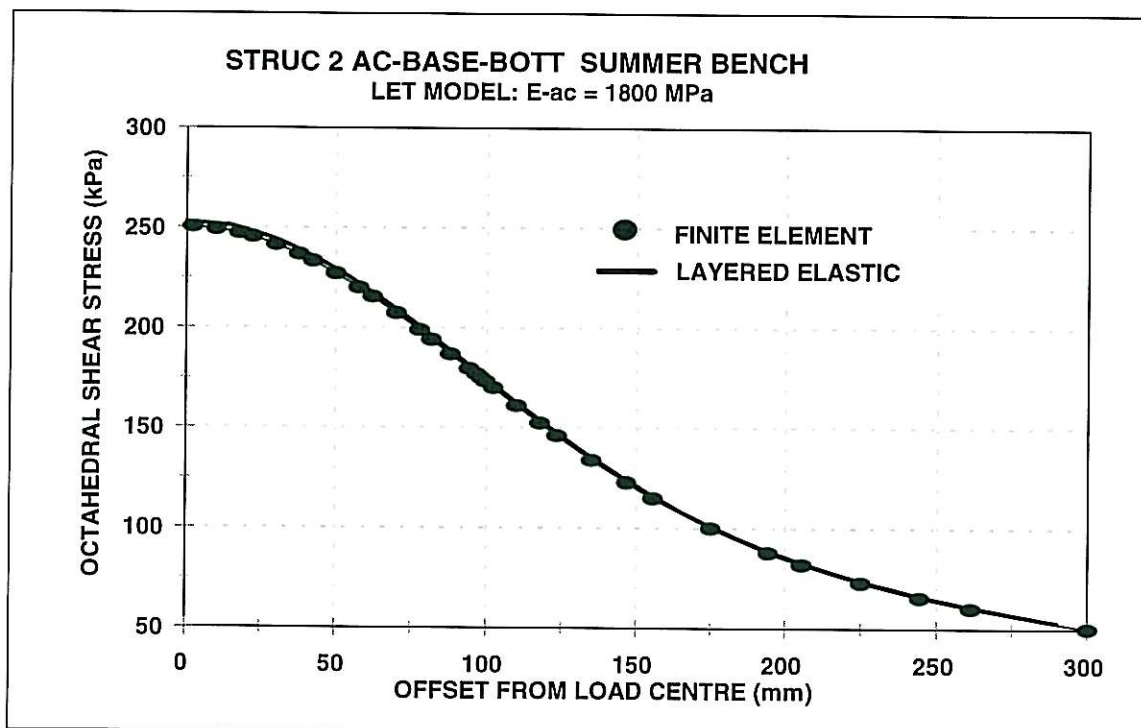


Figure E24: Finite Element and LET Benchmark

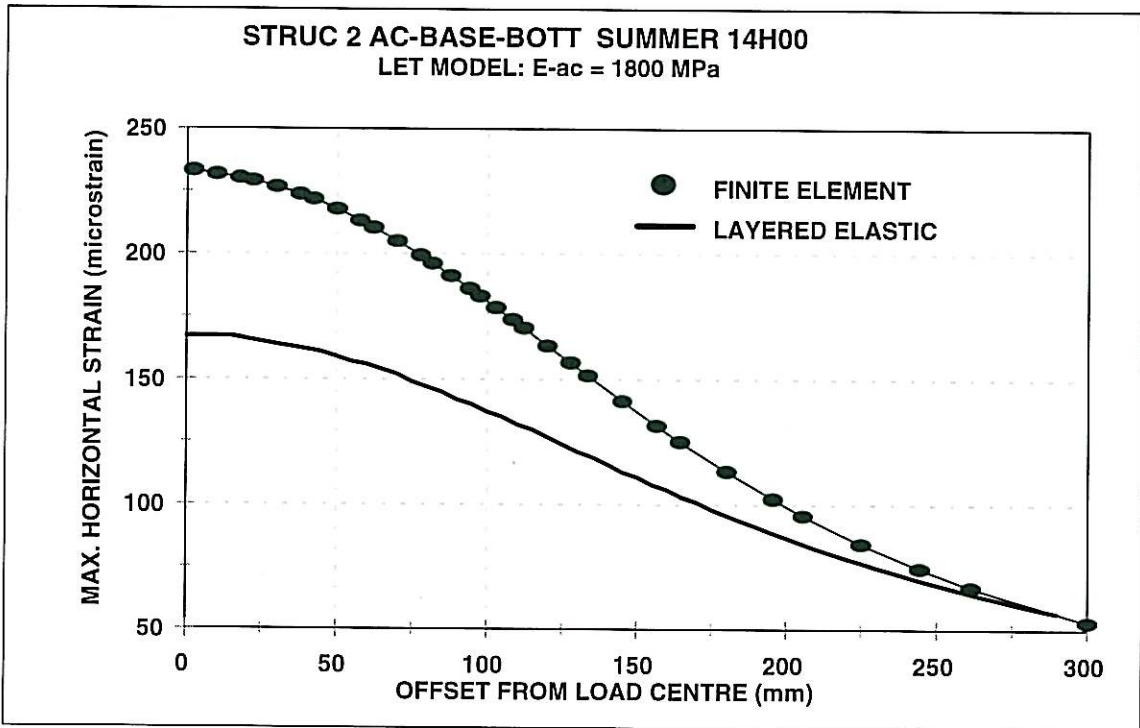


Figure E25: Finite Element and LET Comparison

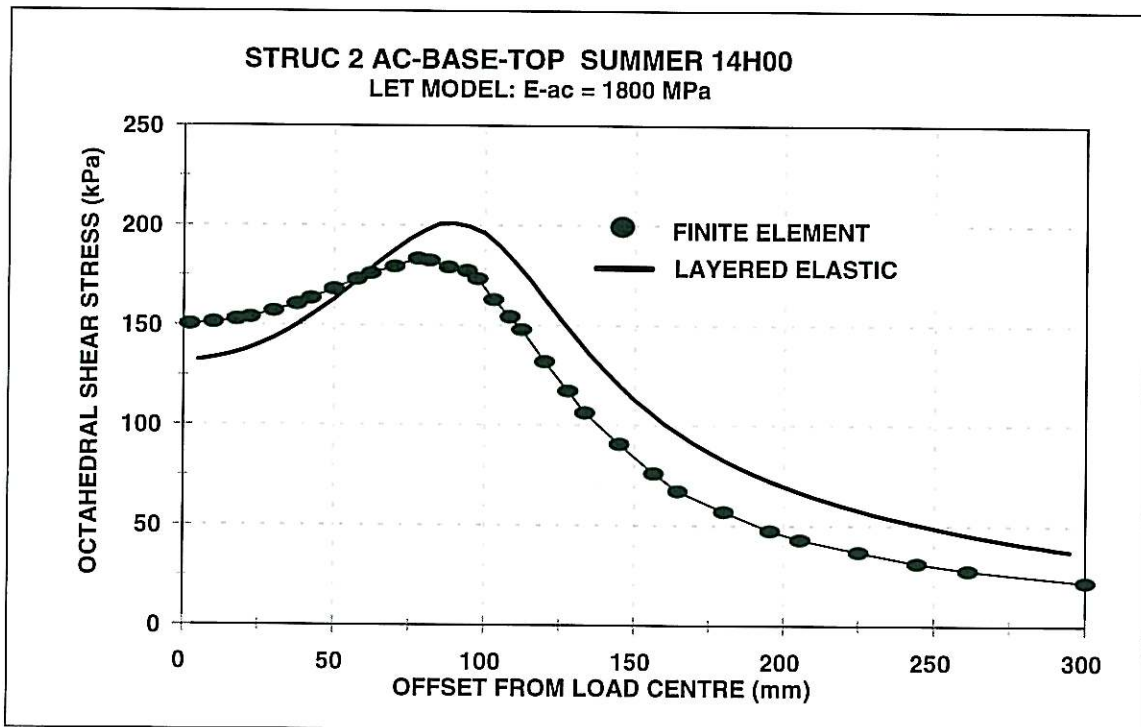


Figure E26: Finite Element and LET Comparison

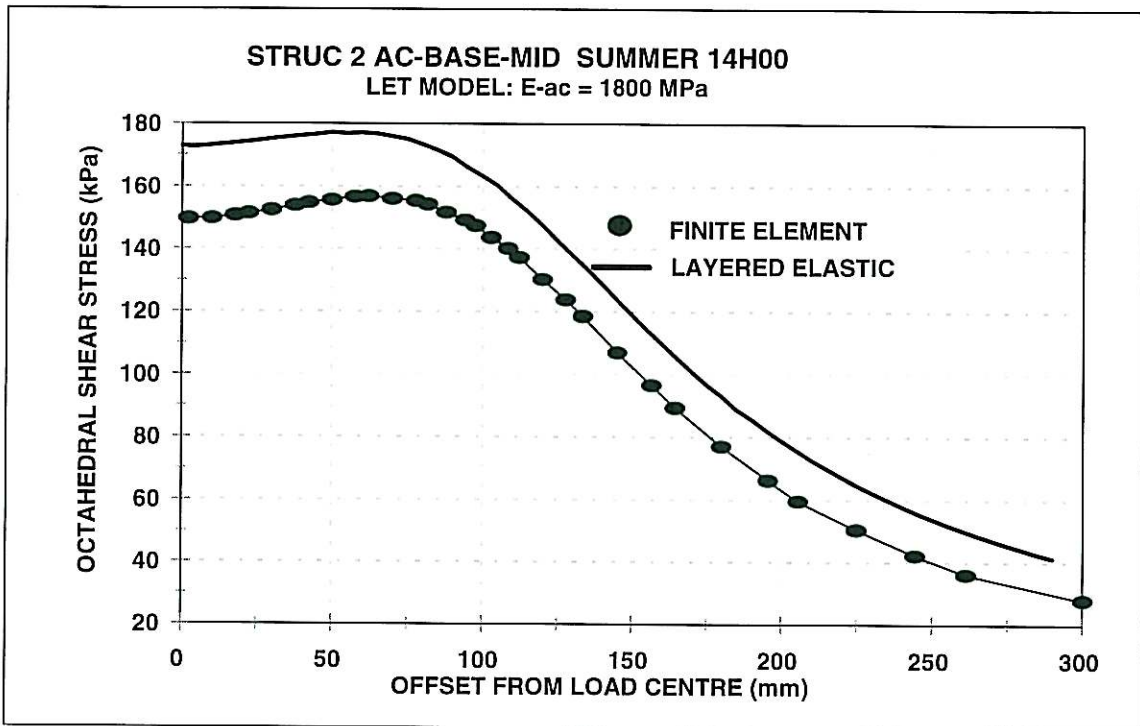


Figure E27: Finite Element and LET Comparison

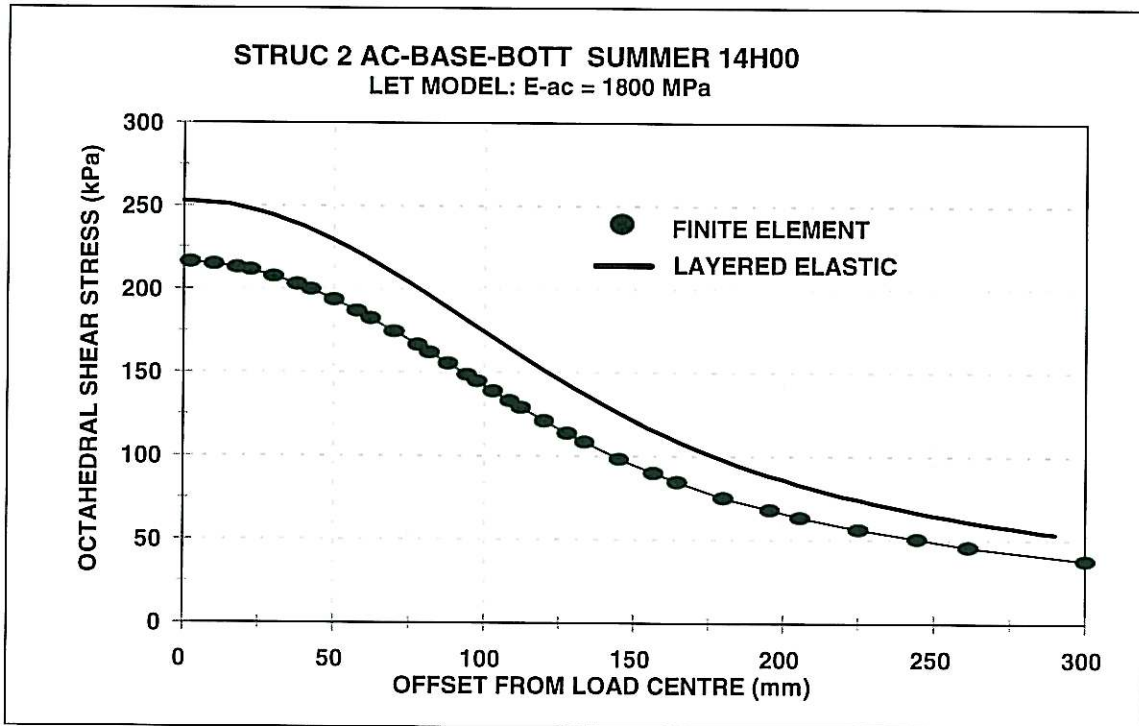


Figure E28: Finite Element and LET Comparison

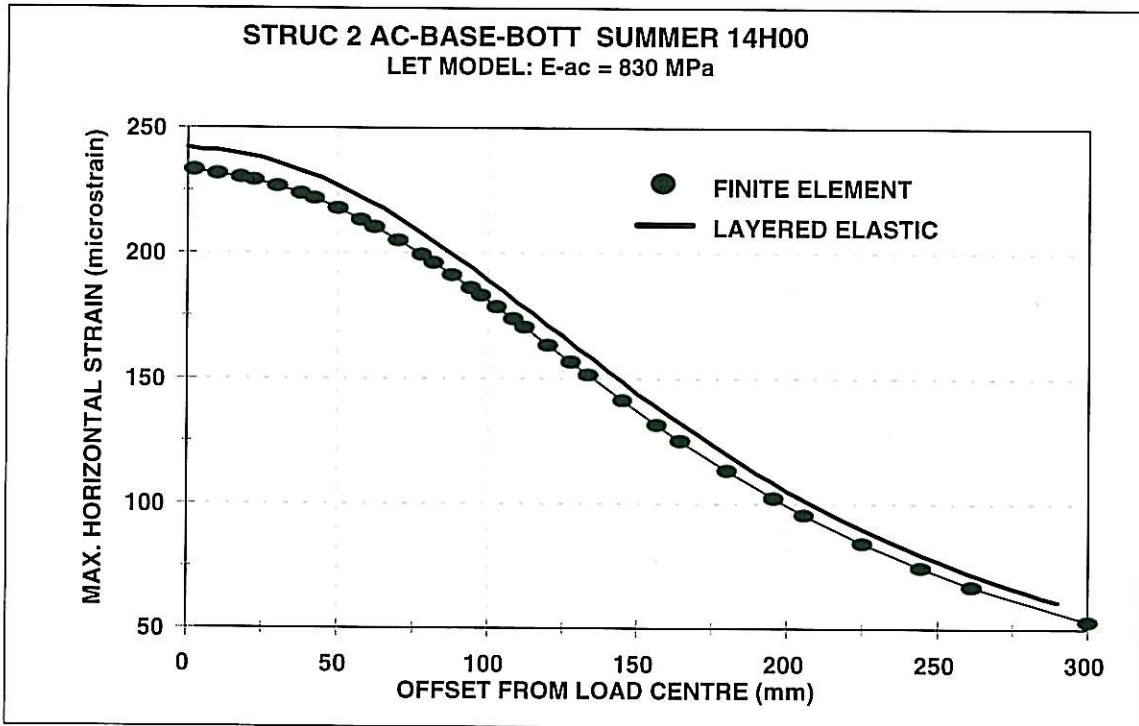


Figure E29: Finite Element and LET Comparison

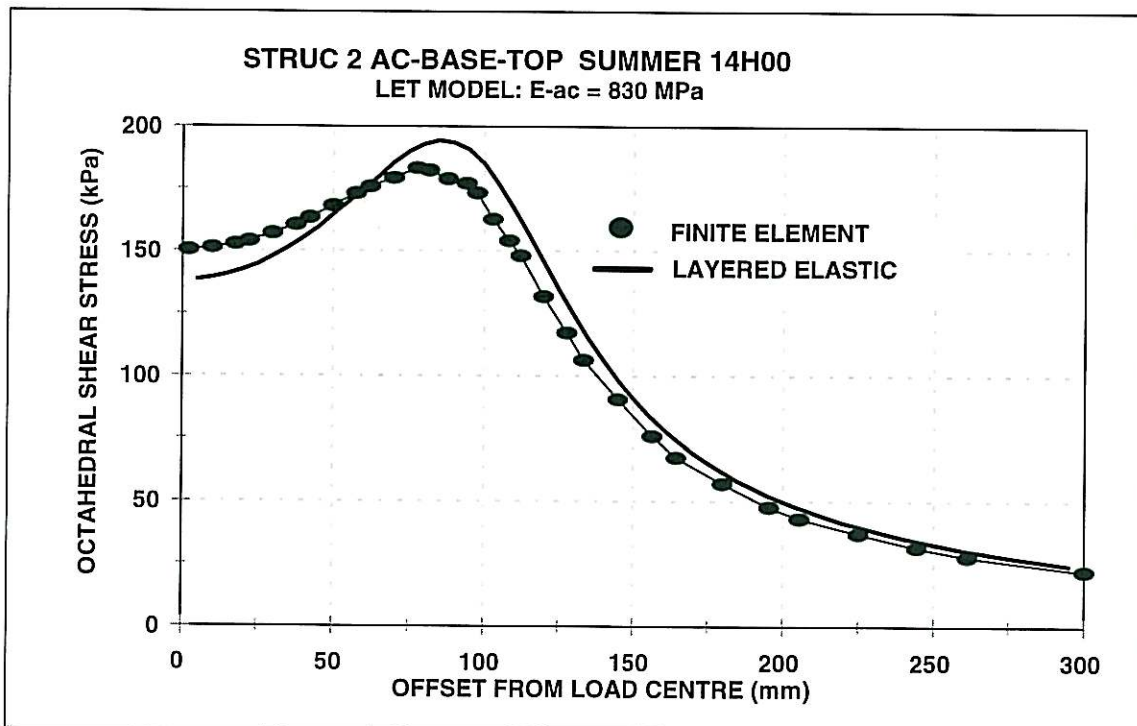


Figure E30: Finite Element and LET Comparison

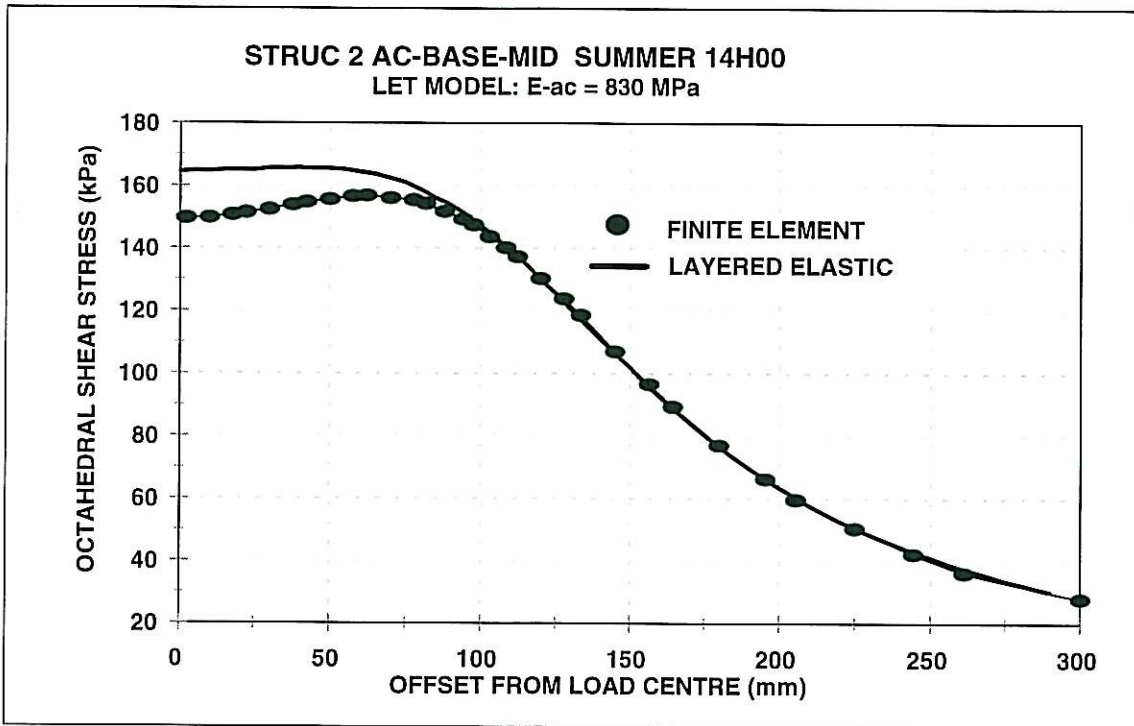


Figure E31: Finite Element and LET Comparison

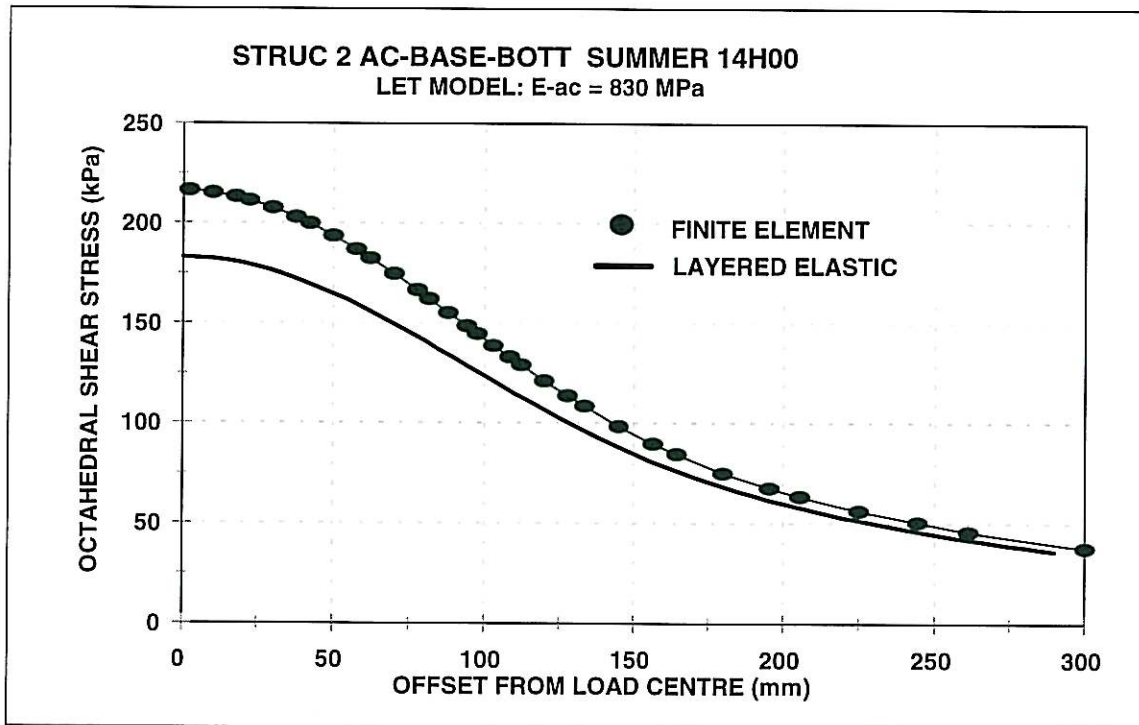


Figure E32: Finite Element and LET Comparison

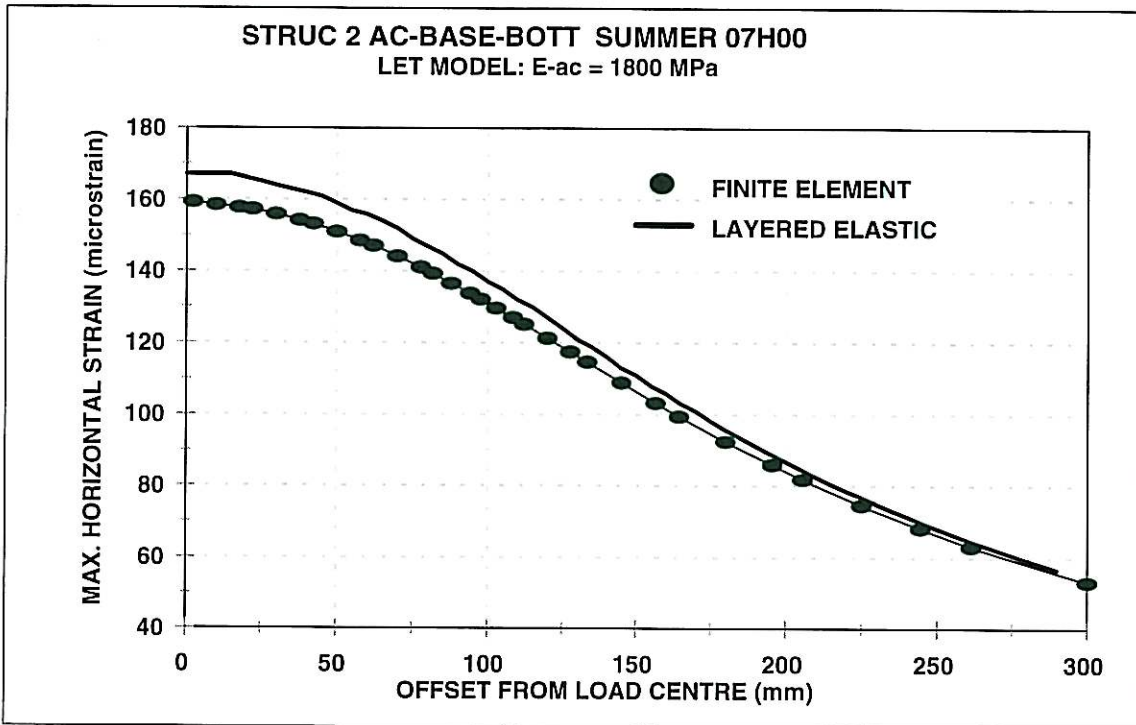


Figure E33: Finite Element and LET Comparison

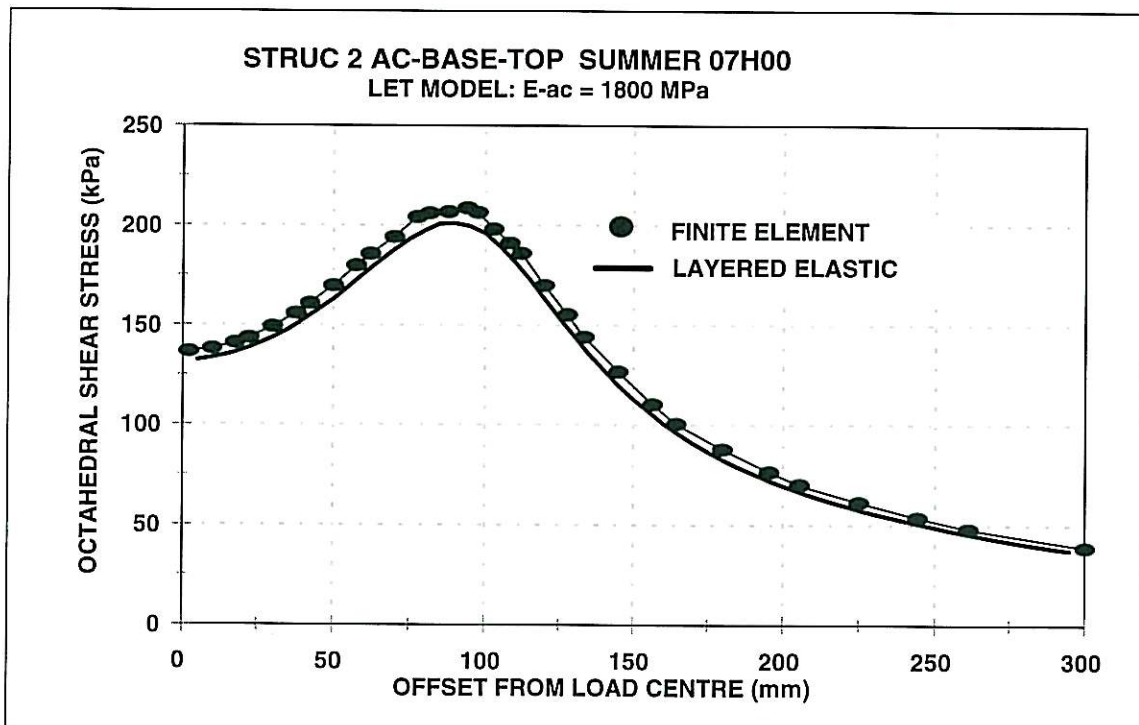


Figure E34: Finite Element and LET Comparison

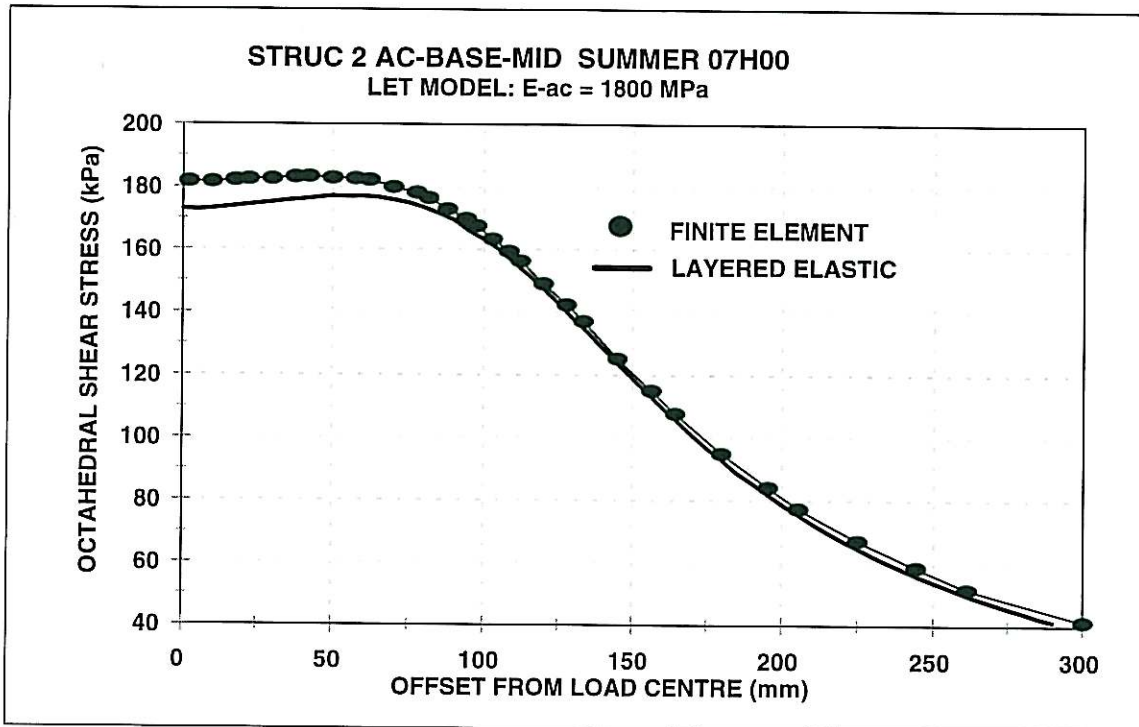


Figure E35: Finite Element and LET Comparison

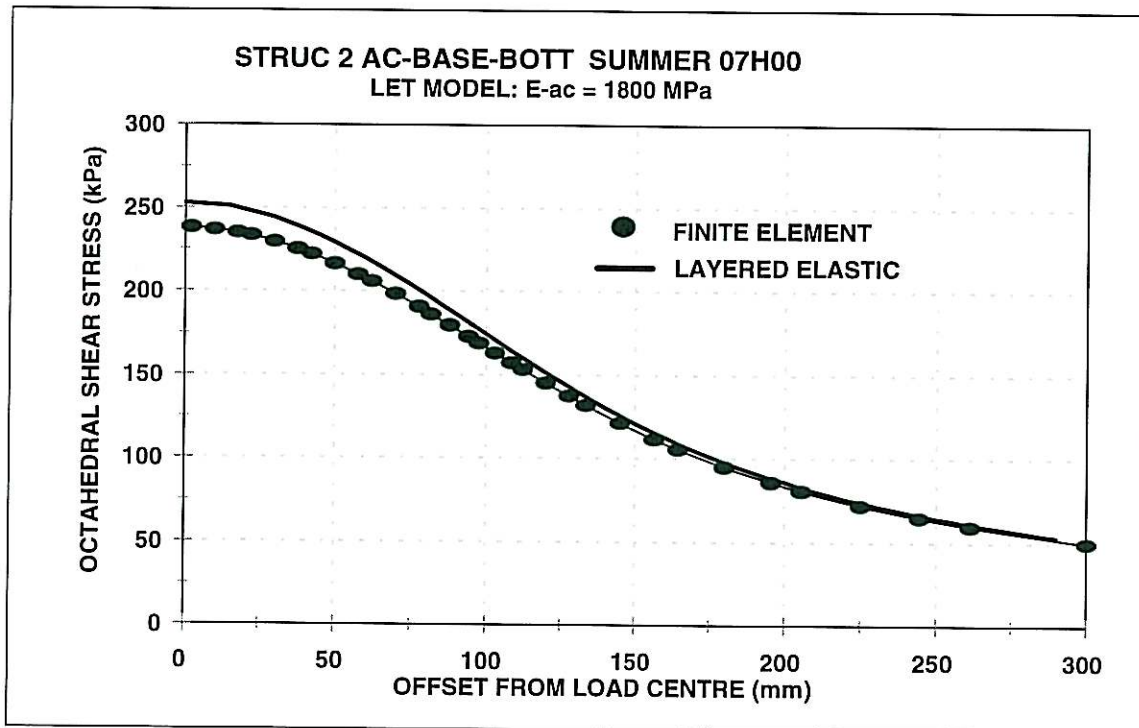


Figure E36: Finite Element and LET Comparison

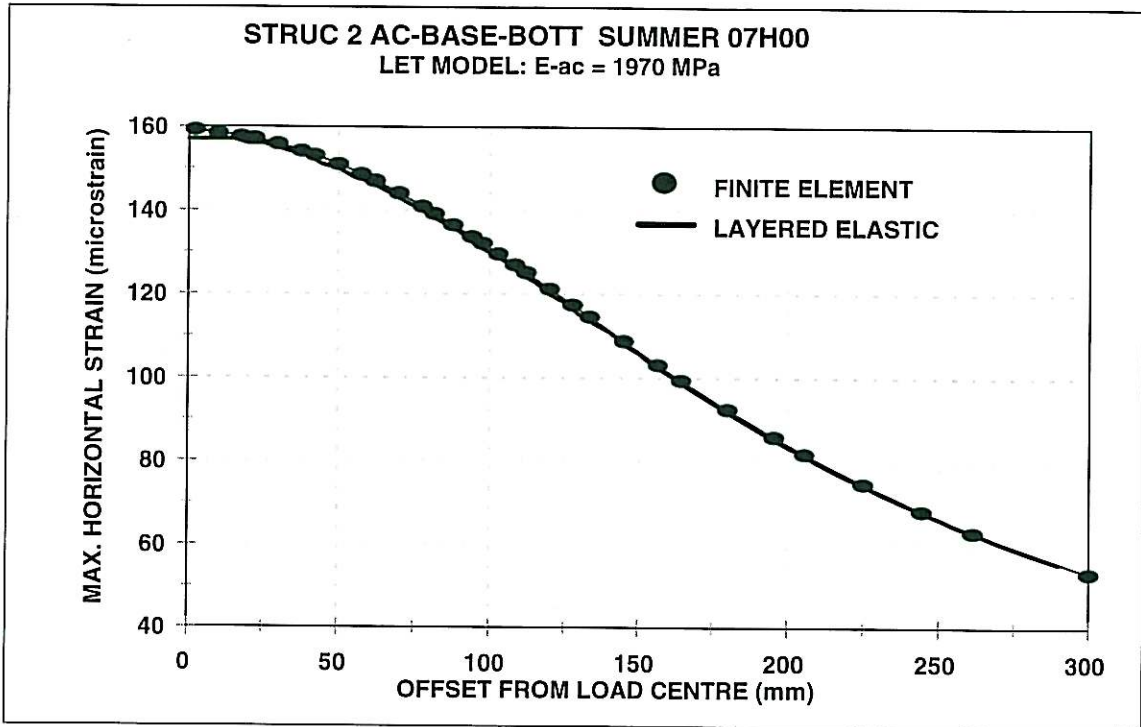


Figure E37: Finite Element and LET Comparison

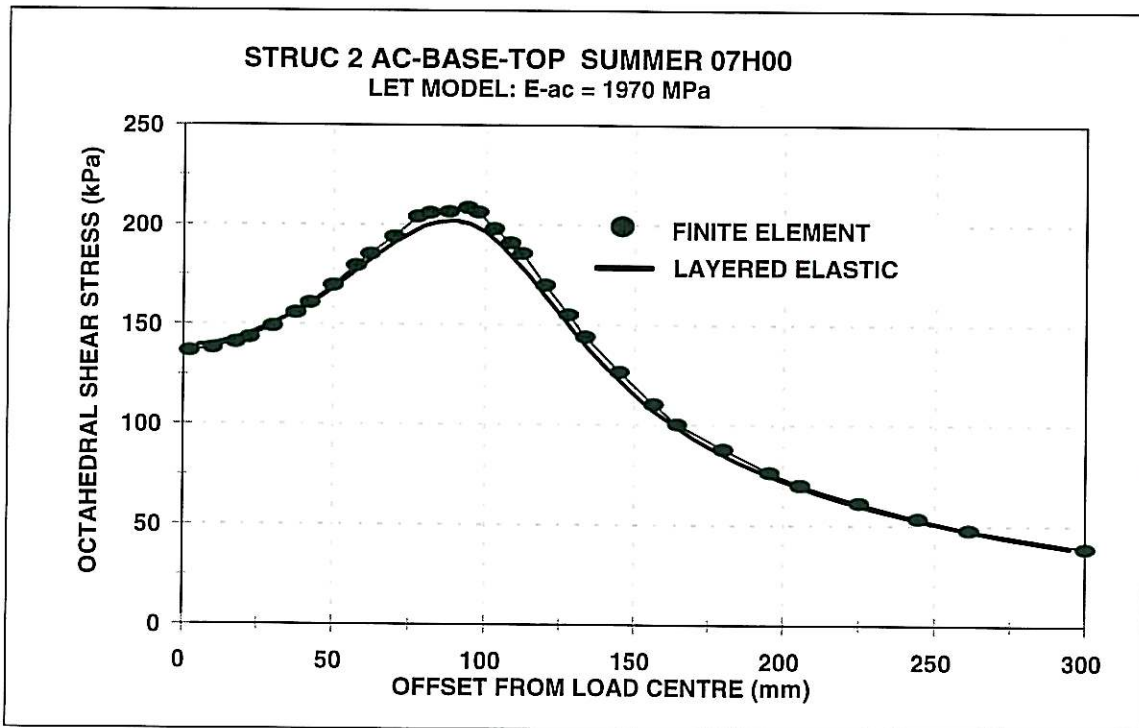


Figure E38: Finite Element and LET Comparison

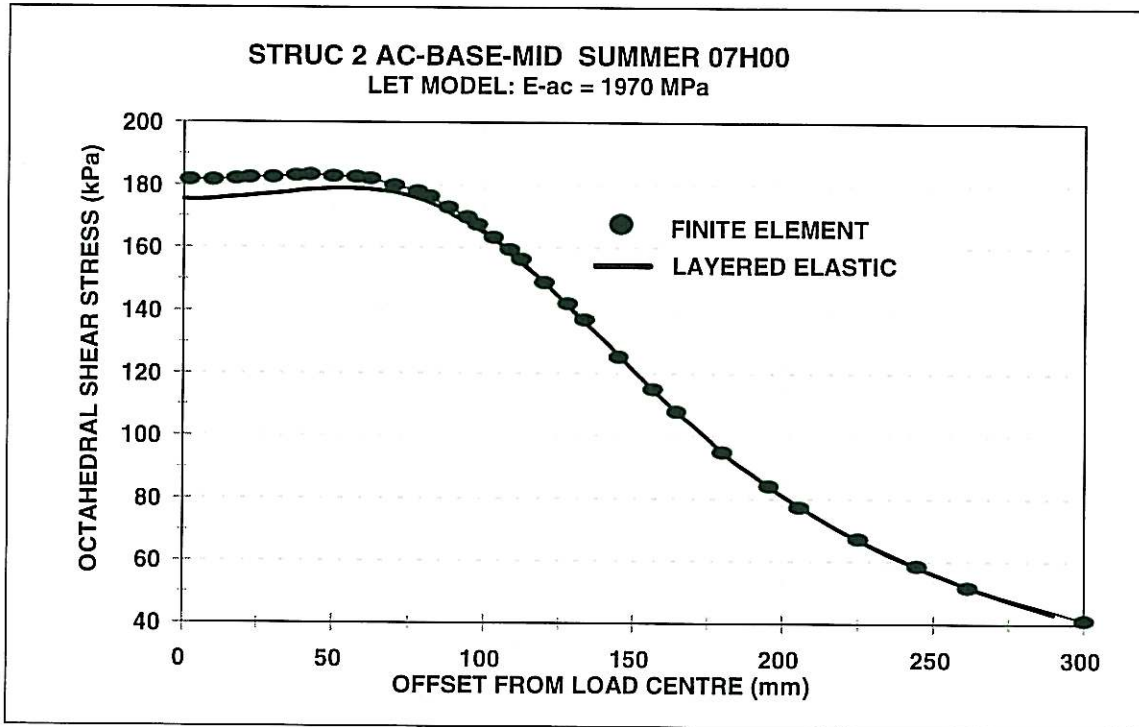


Figure E39: Finite Element and LET Comparison

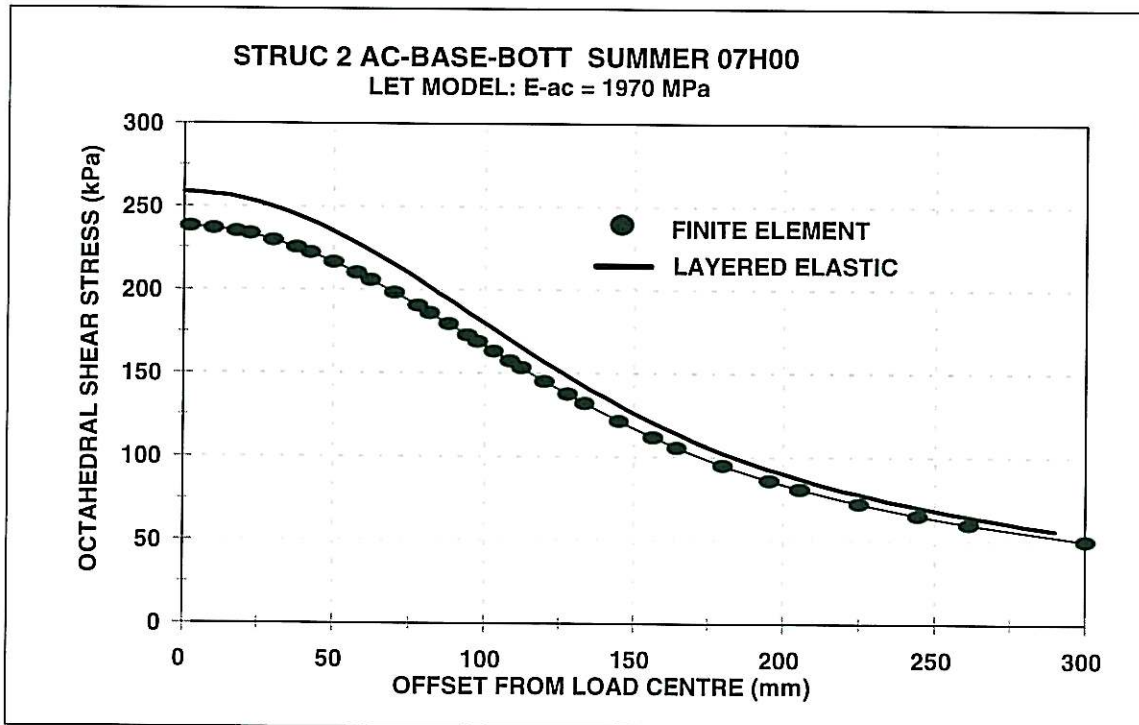


Figure E40: Finite Element and LET Comparison